2019 Synthesis and Processing Science Principal Investigators' Meeting

Gaithersburg Marriott Washingtonian Center, Gaithersburg, MD

July 17-19, 2019

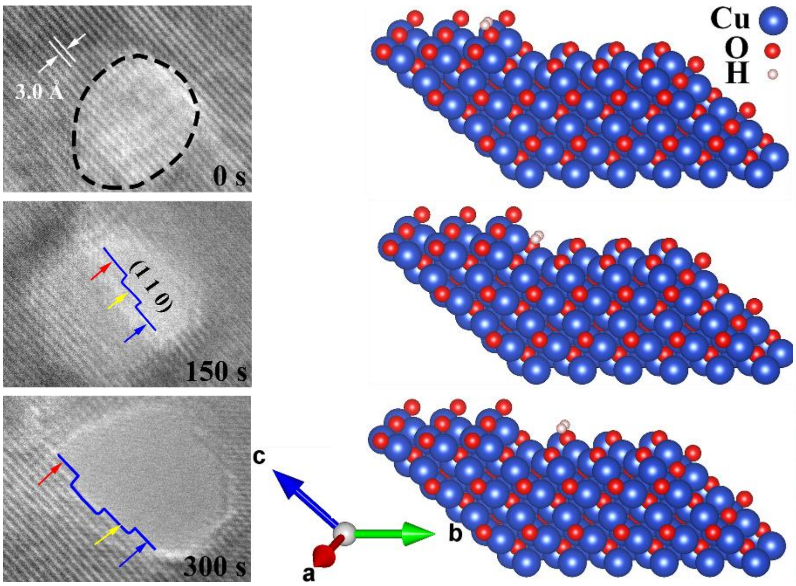

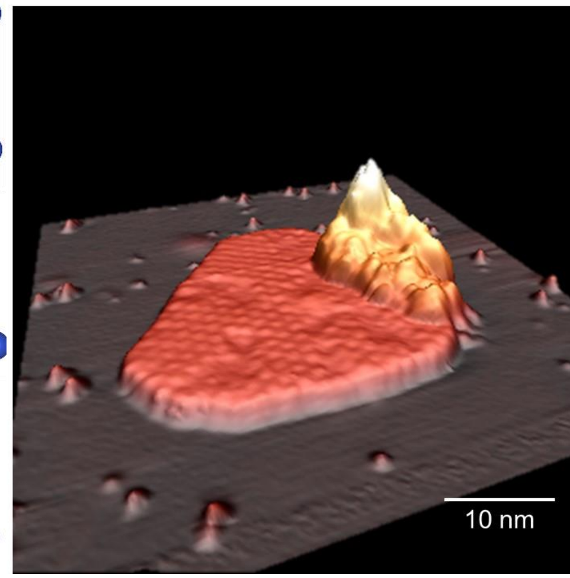

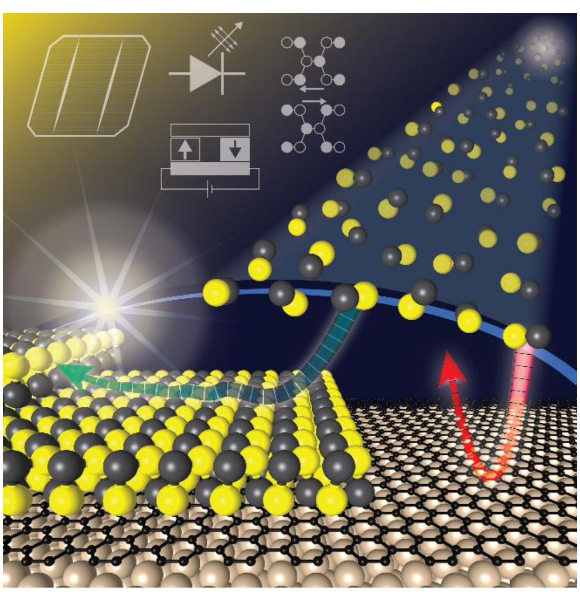

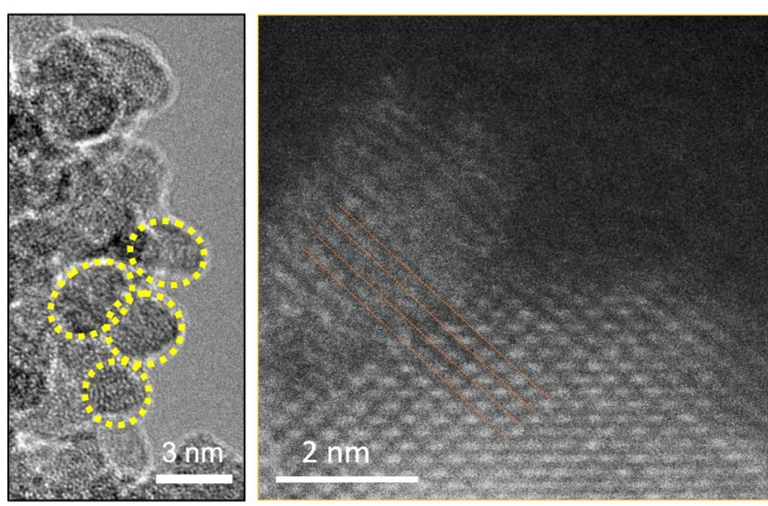

U.S. DEPARTMENT OF ENERGY | Office of Science

Office of Basic Energy Sciences
Materials Sciences and Engineering Division

On the Cover

Top Left: In situ high-resolution transmission electron microscopy snapshots show copper oxide as it reduces to copper in hydrogen gas at 350°C resulting in the formation of a hole that is nanometers in diameter. Top shows the inhomogeneous oxide reduction induced formation of a nanoscale hole at 0 seconds, 150 s and 300 s. Blue, red and yellow arrows show the formation and flow of multiple atomic steps during the oxide reduction process.
Top Middle: Pictorial illustration used for computational modeling of hydrogen adsorption at the different sites of the step edge. (Top) upper step edge; (Middle) (110) microfacet of the step edge; (Bottom) bottom step edge. Blue, red, and white spheres represent Cu, O, and H atoms, respectively. *Chemical Communication* **54**, 7342 (2018). (Courtesy: Guangwen Zhou, State University of New York, Binghamton)

Top Right: A scanning tunneling microscope image of a metal island of the rare-earth element dysprosium encapsulated at the surface of graphite. The metal was deposited at an elevated temperature of 577^{o}C after the graphite was bombarded with inert argon ions, generating entry portals for the metal to move below. Note that the metal island has a faceted footprint. The purple surface shows the graphite; the pink is the metal island under the first layer of graphite and the yellow shows the Dy cluster at the island top. *Carbon* **127** 305 (2018). (Courtesy: Pat A. Thiel and Michael C. Tringides, Ames Laboratory)

Bottom Left: This schematic depicts how a chalcogenide semiconductor, tin sulfide, grows on a graphene van der Waals substrate. SnS molecules in the gas phase prefer to adsorb on the evolving SnS crystal surface rather than stick to the graphene substrate, which explains a strong tendency toward vertical rather than lateral growth. Grey and yellow colored balls represent atoms of tin and sulfur, respectively. The hexagonal arrangement of black balls on top of a white balled surface represents a single graphite layer or graphene on a ruthenium metal support. *ACS Applied Nano Materials*, **1**, 6, 3026-3034 (2018). (Courtesy: Peter and Eli Sutter, University of Nebraska)

Bottom Middle and Right: By tuning the pulsed laser deposition process with *in situ* plasma diagnostics, amorphous nanoparticles of TiO_2 can be selectively deposited onto room temperature substrates to form mesoporous architectures (left). At higher substrate temperatures, these amorphous nanoparticles are sequentially deposited as "building blocks" to form crystalline TiO_2 nanostructures with different phases and morphologies. *Ex situ* Z-contrast scanning transmission electron microscope images (right) reveal how the particles crystallize by particle attachment to integrate into the evolving nanostructure. *Nano Letters* **17**, 4624 (2017). (Courtesy: David Geohegan, Oak Ridge National Laboratory)

This document was produced under contract number DE-SC0014664 between the U.S. Department of Energy and Oak Ridge Associated Universities.

The research grants and contracts described in this document are supported by the U.S. DOE Office of Science, Office of Basic Energy Sciences, Materials Sciences and Engineering Division.

Table of Contents

University Grants' Abstracts

FOREWORD

This abstract book comprises the scientific content of the 2019 Synthesis and Processing Science Principal Investigators' Meeting sponsored by the U.S. Department of Energy, Office of Science, Office of Basic Energy Sciences, Materials Sciences and Engineering (MSE) Division. The meeting, held on July 17–19, 2019, at the Marriott Washingtonian, Gaithersburg, Maryland, is the seventh principal investigators' meeting on this topic and is one among a series of research theme-based principal investigators' meetings being held by the MSE division.

The purpose of this principal investigators' meeting is to bring together all of the researchers funded in the Synthesis and Processing Science core research activity so they can get a firsthand look at the broad range of materials science research that is being supported in this important research area. The meeting will serve as a forum for the discussion of new results and research highlights, thus fostering a greater awareness of significant new advances in the field and the research of others in the program. The confidential and collegial meeting environment is intended to provide unique opportunities to develop new collaborations among PIs, and new ideas. In addition, the meeting affords BES program managers an opportunity to assess the state of the entire program at one time on a periodic basis, in order to chart future directions and identify new programmatic needs.

This year's meeting focuses on four topics within the Synthesis and Processing Science portfolio: Making 2D and quantum materials, field effects on synthesis, the role of organics in organizing materials, and understanding crystallization kinetics. Theory, computation, and in situ characterization remain crosscutting areas that will be incorporated into the four topics. While this is one way of organizing and presenting the research within this broad portfolio, there are many other synergies that could be highlighted and will be considered at future meetings.

Let me take this opportunity to express my thanks to all the meeting attendees for their active participation and sharing their ideas and new research results. Special thanks are given to the Meeting Chairs, James De Yoreo and Linda Schadler, for their dedicated efforts and invaluable assistance towards organizing this meeting. Finally, this meeting would not be possible without the logistical support from Teresa Crockett at DOE-BES-MSE as well as Linda Severs and staff at Oak Ridge Institute for Science and Education (ORISE).

Bonnie Gersten
Program Manager, Synthesis and Processing Science
Materials Sciences and Engineering Division
Office of Basic Energy Sciences
Office of Science
U.S. Department of Energy

This page is intentionally blank.

2019 DOE BES MSE Synthesis and Processing Science Principal Investigators' Meeting

This year's Synthesis and Processing Sciences Principle Investigators' Meeting addresses challenges and opportunities laid out in reports from recent BES-sponsored Basic Research Needs Workshops (BRNs) and Roundtables, that can take advantage of the scientific advances driven by this Core Research Area (CRA): "*developing new techniques to synthesize materials with desired structure, properties, or behavior; to understand the physical phenomena that underpin materials synthesis such as diffusion, nucleation, and phase transitions; and to develop* in situ *monitoring and diagnostic capabilities*." This program's research activities are complementary to the other core research activities of the Materials Discovery Design and Synthesis (MDDS) team of the Materials Sciences and Engineering Division (MSE) in the Office Basic Energy Sciences (BES). The Materials Chemistry CRA (MC) focuses on chemistry-based formation and control of new materials and morphologies and the Biomolecular Materials CRA emphasizes discovery and predictive assembly of materials and systems using concepts and principles of biology.

The passage of the National Quantum Initiative places a spotlight on the synthesis challenges associated with materials for quantum systems. These include obvious classes of materials such as 2D solids, topological insulators, and materials with atomic-scale defects that exhibit precise spatial distributions. Other less obvious classes were discussed in the report from the BES Roundtable on Opportunities for Basic Research for Next Generation Quantum Systems (QS). In particular, layered materials and hybrid organic-inorganic systems are seen as potential game-changers. Due to the paramount importance of establishing uniformity of local atomic environments of quantum states along with control over distance-dependent interactions between them, a central requirement in all of these materials systems is atomic or molecular precision. In many respects, the materials requirements of quantum information systems amplify long-standing challenges in synthesis and processing science such as directing synthetic outcomes to create novel materials architectures, manipulating the distribution of defects, and achieving atomic-scale perfection.

Commensurate with this pressing challenge, this year's meeting will place the topic of "Quantum and 2D Materials" front and center in the first two oral presentations sessions. Taking cues from both the Roundtable report and the earlier BRN workshop report on Quantum Materials for Energy Relevant Technologies, key questions that reflect opportunities for exploration in synthesis and processing science are: (1) Given the thermodynamic tendency towards heterogeneous distributions of defects in all materials, how can one harness defects and disorder to create uniform arrays of long-lived quantum states? (2) How does the juxtaposition of 2D solids and thin films in heterostructures create electronic and magnetic states that can be exploited for quantum systems? (3) How can we develop a fast, iterative synthesis technology that integrates in situ fabrication and characterization and is informed and/or directed by first principles theory and machine learning, thereby enabling rapid convergence toward a desired quantum-coherent property?

The use of external controls, either physical or chemical, has emerged as a vibrant field of research that has particular relevance to the challenge at hand and directly addresses one of the five priority research directions (PRDs) laid out in the BRN workshop report on Synthesis Science for Energy Relevant Technologies (SS): *"Accelerate materials discovery by exploiting extreme conditions,* *complex chemistries and molecules, and interfacial systems."* With that challenge in mind, this year's program includes two sessions that will explore recent advances and new opportunities in the use of physical and chemical controls to direct synthetic pathways and outcomes.

The first of these two sessions will address "Field Effects on Synthesis." The use of magnetic fields in high temperature bulk crystal growth, electric fields in electrodeposition of metals, and hydrostatic pressure in both hydrothermal and high-pressure crystallization are longstanding approaches to either enabling growth of materials that are not stable at ambient conditions or modifying mass transport and kinetics to achieve high quality films and bulk solids. More recently, the selective application of DC and AC electric fields in solution-based growth in ionic liquids, high shear stresses in re-solidification processes, and high ion beam fluxes during vapor-phase deposition has led to novel synthetic outcomes. Nearly all of these approaches create far-from-equilibrium conditions that violate foundational theories grounded in equilibrium thermodynamics. This session will explore the consequences of these violations and the novel synthetic outcomes they enable. Key questions include: How do high fields and fluxes alter the distribution and transport of reactants at interfaces and how are those changes reflected in the kinetics of synthetic processes? How does the interplay between the effect of fields on the kinetics of synthetic processes and the equilibria between phases alter the pathways to synthetic outcomes or provide access to otherwise un-accessible metastable or unstable states?

The second session will focus on "The Role of Organics in Organizing Materials." While this CRA focuses on physical aspects of assembly, often the physical and chemical controls are linked and must be discussed in tandem. For example, one important function of organics in modern synthesis science is to serve as ligands for the stabilization of nanoparticle systems. In addition to judicious choices for ligand chemistry, the more recent introduction of triggers such as stress or photons to exchange or transform ligands have revealed a rich vein for exploration of novel materials architectures based on physically directed organization of nanoparticle systems. The use of organics extends to thin film synthesis. While, the development of precursor chemistries for thin film growth techniques are not part of this CRA, the thin films grown from them by projects supported by this CRA serve alternately as precursors or surfactants in CVD/ALD growth. For bulk crystal growth, organics are used to modulate crystallization kinetics for habit control, rate enhancement, and modification of materials properties.

Progress in the use of organics to direct synthesis is limited by a number of scientific questions: (1) How does the presence of surface-bound organic molecules alter solvent and ion distributions near the interface, and how do those distributions result in directional forces between particles that lead to ordered assembly? (2) What is the impact of organic constituents on the formation of precursor particles that drive crystallization along non-classical pathways? (3) What are the dynamics of ligand rearrangement or exchange during crystallization, whether through ion-by-ion addition, cluster aggregation, or nanoparticle assembly? This session will provide an opportunity to explore the opportunities within the Program for addressing these questions and advancing the use of organics for synthetic control.

Crosscutting both the efforts in synthesis of quantum and 2D materials and the use of physical and chemical controls to direct synthesis, is the challenge of understanding crystallization kinetics. The problem of predicting and manipulating kinetics remains a vexing one and lies at the heart of multiple PRDs laid out in the Synthesis Science Basic Research Needs (SS BRN) workshop report. Success requires an understanding of the complexities in the energy landscape that separates reactants from products, as well as the sensitivity of both the minima and the barriers to synthesis conditions and external controls. Thus "Crystallization Kinetics" will comprise the focus of the fourth and final session of the meeting.

This topic lies at the heart of the first PRD from the BRN report: Achieve mechanistic control of synthesis to access new states of matter. As discussed in that report, the key knowledge gaps that prevent realization of this goal are: How can we develop a fundamental understanding of the processes by which reactants assemble into products and how they can be controlled? How can we use metastable ordered phases that are formed during synthesis but subsequently dissolve or transform before equilibrium is reached?

The opportunities to integrate both simulations and *in situ* characterization tools into research aimed at understanding kinetics and controlling the resulting materials have grown dramatically in the past decade. Measurement methods have reached spatial and temporal resolutions commensurate with computational approaches and relevant to the development of design rules. Indeed, the Quantum Systems Roundtable report highlighted "*the need for research that will lead to the development of new capabilities for real-time feedback and control of synthesis that are coupled with predictions and measurements of targeted quantum characteristics. This feedback would consist of both characterization and computation-based machine learning to optimize a material for the prescribed function*." This theme is also explicitly called out in the fourth PRDs from the SS Workshop report and is common to a number of the other BRN Workshop reports produced over the past three years. While not the focus of a session at this year's meeting, the Chairs urge speakers to integrate this theme into their presentation where sensible to give the Program's PIs a sense of progress and challenges in this endeavor.

Finally, we have asked two PIs who have been part of the S&PS program for many years to reflect on their careers as BES researchers, to tell us how their BES-supported research has shaped their careers and provided opportunities for intellectual growth, and to share their views on "best practices" for early and mid-career researchers who are trying to have the kind of impact in the future that these two individuals have achieved to date.

This page is intentionally blank.

Synthesis and Processing Science
Principal Investigators' Meeting Agenda

Meeting Chairs:
James De Yoreo, Pacific Northwest National Lab and **Linda Schadler,** University of Vermont

Wednesday, July 17, 2019

7:00 – 7:50am	****Breakfast****
7:50 – 8:00am	**Meeting Chairs: James De Yoreo and Linda Schadler** **Program Manager: Bonnie Gersten** *Introductory Remarks*
Session I	**Making 2D and Quantum Materials** **Session Chair: Chang-Beom Eom,** University of Wisconsin, Madison
8:00 – 8:20am	**Boris Yakobson**, Rice University *Predictive models for 2D materials synthesis, examples of practical relevance*
8:20 – 8:30am	Discussion
8:30 – 8:50am	**Ivan Božović,** Brookhaven National Laboratory *Molecular beam epitaxy of superconducting oxides*
8:50 – 9:00am	Discussion
9:00 – 9:15am	**Vlad Pribiag**, University of Minnesota *Integrated development of scalable materials platforms for topological quantum information devices*
9:15 – 9:20am	Discussion
9:20 – 9:50am	**Break**
9:50 – 10:05am	**Darrell Schlom**, Cornell University *Atomic engineering of ferroic layers to create a room-temperature magnetoelectric multiferroic*
10:05 – 10:10am	Discussion
10:10 – 10:30am	**Scott Chambers,** Pacific Northwest National Laboratory *MBE synthesis, structure and 2D electronic properties of $SrNiO_3/LaFeO_3$ superlattices*
10:30 – 10:40am	Discussion
10:40 – 10:55am	**Jacek Jasinski,** University of Louisville *Quantum phenomena and phase transitions in intercalated layered structures*

10:55 – 11:00am	Discussion
11:00 – 11:30am	**Poster Introductions for Session I**
11:30 – 1:00pm	****Working lunch**** **Introductory remarks:** **Linda Horton**, Division Director, Materials Science and Engineering Division **CRA Updates:** **Bonnie Gersten**, Program Manager, Synthesis and Processing Science (S&PS) CRA
1:00 – 2:30pm	**Poster Session 1**
Session 2:	**Session Chair: Zhiqiang Mao,** Pennsylvania State University *Making 2D and Quantum Materials*
2:30 - 2:50pm	**Michael Tringides,** Ames Laboratory *Tuning 2-d quantum material phases by metal intercalation of graphitic substrates*
2:50 – 3:00pm	Discussion
3:00 – 3:20pm	**David Geohegan,** Oak Ridge National Laboratory *Addressing the synthesis challenges for 2D materials with nonequilibrium processing and in situ diagnostics*
3:20 – 3:30pm	Discussion
3:30 – 4:00pm	****Break****
4:00 – 4:15pm	**Breakout Session I Introduction:** **Chang-Beom Eom**, University of Wisconsin *Challenges and opportunities in 2D and quantum materials research*
4:15 – 4:30pm	**Breakout session II Introduction:** **Alexandra Navrotsky**, University of California, Davis *Challenges and opportunities for controlling crystallization kinetics, understanding, predicting and controlling crystallization kinetics, mechanisms, and driving forces*
4:30 – 5:30pm	**Group break-outs:** See poster agenda for designated group leaders and break-out group assignments 1. **Leads: Mike Arnold**, Univ. of Wisconsin and **Eli Sutter**, Univ. of Nebraska Opportunities for S&PS brought out in the Roundtable Report on Quantum Materials 2. **Leads: Linda Schadler**, Univ. of Vermont and **Lynden Archer**, Cornell Univ. Opportunities for S&PS in predictive control of crystallization kinetics I 3. **Leads: Nancy Dudney**, ORNL and **Jim De Yoreo**, PNNL Opportunities for S&PS in predictive control of crystallization kinetics II

5:30 – 7:00pm	**Poster Session 1, continued**
7:00 – 8:30pm	****Working Dinner**** *General discussion on new opportunities, collaborative exchanges* *Reflections on a BES research career: Max Lagally, University of Wisconsin*

Thursday, July 18, 2019

7:00 – 8:00am	****Breakfast****
Session 3:	**Field Effects on Synthesis** **Session Chair: Himanshu Jain, Lehigh University**
8:00 – 8:20am	**Jun Liu,** Pacific Northwest National Laboratory *Electrochemically driven nanostructures: opportunities and challenges*
8:20 – 8:30am	Discussion
8:30 – 8:50am	**Nancy Dudney,** Oak Ridge National Laboratory *Ion transport and structural evolution of solid electrolytes*
8:50 – 9:00am	Discussion
9:00 – 9:15am	**Ming Tang,** Rice University *Development of morphological instability during electrodeposition of active metals*
9:15 – 9:20am	Discussion
9:20 – 9:50am	****Break****
Session 3	**Field Effects on Synthesis (continued)** **Session Chair: Peter Sutter,** University of Nebraska, Lincoln
9:50 – 10:10am	**Lynden Archer,** Cornell University *Electrodeposition in viscoelastic liquid electrolytes above the diffusion limit*
10:10 – 10:20am	Discussion
10:20 – 10:40am	**Jay Switzer,** Missouri University of Science and Technology *A new spin on epitaxy: spin coating semiconductors onto electrodeposited single-crystal-like substrates*
10:40 – 10:50am	Discussion
10:50 – 11:20am	**Poster Session 2 Introductions**
11:20 – 12:50pm	****Working Lunch**** *Discussions on new opportunities in synthesis science*
12:50 – 2:20pm	**Poster Session 2**

Session 3:	**Field Effects on Synthesis** (continued)
2:20 – 2:40pm	**Giovani Zangari,** University of Virginia *Prediction and control of atomic ordering in electrodeposited binary alloy films*
2:40 – 2:50pm	Discussion
2:50 – 3:10pm	**Andrei Fedorov** Georgia Tech University *Exploiting localized thermal and electric field gradients to control of nanomaterial phase and composition in far-from-equilibrium gas/liquid jet-assisted E-beam deposition*
3:10 – 3:20pm	Discussion
3:20 – 3:40pm	****Break****
Session 4:	**The Role of Organics in Organizing Materials** **Session Chair: Dongsheng Li,** Pacific Northwest National Laboratory
3:40 – 4:10pm	**Kristen Fichthorn,** Pennsylvania State University *Multi-scale simulations of nanowire growth in solution*
4:10 – 4:20pm	Discussion
4:20 – 4:35pm	**Tobias Hanrath,** Cornell University *The role of physicochemical solvent/subphase interactions in assembly and attachment at fluid-fluid interfaces*
4:35 – 4:40pm	Discussion
4:40– 4:55pm	**Scott Auerbach**, University of Massachusetts *Integrating experiment and modeling on zeolite formation: Role of organics in structure direction*
4:55 – 5:00pm	Discussion
5:00 – 7:00pm	**Poster Session 2,** continued
7:00 – 8:30pm	****Working Dinner**** General discussion on new opportunities, collaborative exchanges Reflections on a BES research career: Scott Chambers, PNNL

Friday, July 19, 2019

7:00 – 8:00am	****Breakfast****
8:00 – 8:45am	**Each Break-out group leader presents (7.5 min each)**
Session 5	**Understanding Crystallization Kinetics** **Session Chair: Stacey Bent,** Stanford University

8:45– 9:05am	**Linda Schadler**, University of Vermont *Using crystallization to control filler dispersion."*
9:05 – 9:15am	Discussion
9:15 – 9:35am	**Mark Ediger,** University of Wisconsin, Madison *Controlling the structure of vapor-deposited organic glasses and their crystalline products*
9:35 – 9:45am	Discussion
9:45 – 10:15am	****Break****
10:15 – 10:35am	**Guangwen Zhou,** The State University of New York, Binghamton *Atomic-scale mechanism of unidirectional oxide growth*
10:35 – 10:45am	Discussion
10:45 – 11:00am	**Ashwin Shahani,** University of Michigan *Probing the solidification of quasicrystals through joint experiment and simulation*
11:00 – 11:05am	Discussion
11:05 – 11:20am	**Timothy Weihs,** Johns Hopkins University *Exploring nucleation in composition gradients*
11:20 – 11:25am	Discussion
11:25 – 11:40am	**Meeting Chairs: James De Yoreo and Linda Schadler** **Program Manager: Bonnie Gersten** *Closing Remarks*
11:40am	Adjourn

This page is intentionally blank.

Synthesis and Processing Science Principal Investigators' Meeting

Breakout Group Assignments

Group: **Quantum I**

Lead: Michael Arnold

Team Members:

1. Ivan Božović
2. Scott Chambers
3. Francesca Cavallo
4. Paul Crowell
5. Yingge Du
6. Chang-Beom Eom
7. David Geohegan
8. Jacek Jasinski
9. Tiffany Kaspar
10. Max Lagally
11. Feng Liu
12. Peter Sutter

Group: **Quantum II**

Lead: Eli Sutter

Team Members:

1. Zhiquiang Mao
2. Ni Ni
3. Christopher Palmstrom
4. Vlad Priabig
5. Darrell Schlom
6. Peter Sushko
7. Jianwei Sun
8. Michael Tringides
9. Jiang Wei
10. Kia Xiao
11. Boris Yakobson
12. Ming Yu

Group: **Crystallization I**

Leads: Lynden Archer and Linda Schadler

Team Members:

1. Scott Auerbach
2. Paulette Clancy
3. Volkmar Dierolf
4. Mark Ediger
5. Michael Falk
6. Wei Fan
7. Andrei Fedorov
8. Kristen Fichthorn
9. Tobias Hanrath
10. Dongsheng Li
11. Jun Liu
12. Sanat Kumar
13. Maria Sushko

Group: **Crystallization II**

Leads: Nancy Dudney and James De Yoreo

Team Members:

1. Stacey Bent
2. Himanshu Jian
3. Maik Lang
4. Alexandra Navrotsky
5. Eugene Olevsky
6. Ashwin Shahani
7. Daniel Shoemaker
8. Jay Switzer
9. Ming Tang
10. Tim Weihs
11. Francesco Zaera
12. Giovanni Zangari
13. Gaungwen Zhou

Synthesis and Processing Science Principal Investigators' Meeting

POSTER SESSION 1
Wednesday, July 17, 2019

1. **Chang-Beom Eom**, University of Wisconsin, Madison
   Point defect control of oxide quantum heterostructures by chemical pulsed laser deposition

2. **Yingge Du**, Pacific Northwest National Laboratory
   Promoting diffusion across epitaxial interfaces for materials discovery

3. **Zhiqiang Mao**, Pennsylvania State University, **Jianwei Sun** and **Jiang Wei,** Tulane University
   Understanding the synthesis and new quantum phenomena of magnetic topological materials enabled by SCAN-based DFT calculations

4. **Feng Liu**, University of Utah
   Orbital design of 2D topological materials

5. Ksenia V. Bets, Nitant Gupta, and **Boris I. Yakobson**, Rice University
   Complementarity or epitaxy to enable 2D monocrystals growth

6. **Ivan Božović**, Brookhaven National Laboratory
   Molecular beam epitaxy of superconducting oxides

7. **Vlad Pribiag**, University of Minnesota, **Paul Crowell,** University of Minnesota, Sergey Frolov, University of Pittsburgh, Noa Marom, Carnegie Melon University
   Transport characterization and first-principles calculations of low-dimensional magnet-InSb structures

8. **Chris Palmstrom**, University of California, Santa Barbara
   Progress in metal/semiconductor heterostructures for scalable materials platforms for topological quantum information systems

9. **Scott Chambers, Peter Sushko** and **Tiffany Kaspar**, Pacific Northwest National Laboratory
   *Atomistic and electronic structure at epitaxial complex oxide heterojunction*s

10. **Jacek Jasinski**, Gamini Sumanasekera, and **MingYu**, University of Louisville
    Intercalation and high pressure of phosphorene – pathways to novel materials and physics

11. **Darrell Schlom**, Cornell University
    Unveiling hidden multipole order to create functional materials—by design

12. **Michael Tringides**, Ames Laboratory

    2-d quantum materials by metal intercalation and encapsulation under graphene/graphite

13. **David Geohegan** and **Kia Xiao**, Oak Ridge National Laboratory

    Nonequilibrium synthesis and processing approaches to tailor the functionality of 2D materials

14. **Eli Sutter** and **Peter Sutter**, University of Nebraska, Lincoln

    Synthesis and nanoscale optoelectronics of few-layer chalcogenide semiconductors and heterostructures

15. **Michael Arnold,** University of Wisconsin, Madison

    Atom-by-atom directional synthesis of semiconducting graphene

16. **Max Lagally**, University of Wisconsin, Madison, and **Francesca Cavallo**, University of New Mexico

    Semiconductor nanomembranes and sheets: compositions, geometries, and interfaces to access new functionalities

17. **Daniel Shoemaker**, University of Illinois, Urbana-Champaign

    New ternary semiconductors in shallow energy landscapes

18. **Stacey Bent,** Stanford University

    Understanding reaction mechanisms in atomic layer deposition of metal oxides and metal sulfides

19. **Francesco Zaera**, University of California, Riverside

    The role of the surface chemistry of precursors in growing thin solid films

20. **Michael Falk** and **Tim Weihs**, Johns Hopkins University

    Exploring nucleation in composition gradients

21. **Ashwin Shahani** and Sharon Glotzer, University of Michigan

    Probing the solidification of quasicrystals through joint experiment and simulation

22. **Guangwen Zhou**, The State University of New York, Binghamton

    Atomic-scale mechanism of unidirectional oxide growth

Synthesis and Processing Science Principal Investigators' Meeting

POSTER SESSION 2
Thursday, July 18, 2019

1. **Eugene Olevsky**, San Diego State University
   Field-assisted sintering: thermal and non-thermal factors of controlled nonequilibrium

2. **Maik Lang**, University of Tennessee, Knoxville
   Far-from-equilibrium processing of materials under extreme conditions

3. **Alexandra Navrotsky**, University of California, Davis
   Long versus short range order as driving forces for synthesis of complex oxides

4. **Himanshu Jian and Volkmar Dierolf**, Lehigh University
   Single crystal growth via solid→solid transformation (SCGST) of glass

5. **Ni Ni**, University of California, Los Angeles
   Exploring superconductivity at the edge of magnetic or structural instabilities

6. **Jun Liu** and **Maria Sushko**, Pacific Northwest National Laboratory
   Molecularly organized nanostructured materials

7. **James De Yoreo**, Pacific Northwest National Laboratory
   An in situ look at interfacial solution structure and its impact on particle nucleation and assembly

8. **Nancy Dudney**, Oak Ridge National Laboratory
   Ion transport and structural evolution of solid electrolytes

9. **Ming Tang**, Rice University
   Development of morphological instability during electrodeposition of active metals

10. **Lynden Archer** and Donald Koch, Cornell University
    Electrodeposition in viscoelastic liquid electrolytes above the diffusion limit

11. **Jay Switzer**, Missouri Science & Technology
    Spin coating epitaxial semiconductors

12. **Giovanni Zangari** and Leonid Zhegli, University of Virginia
    Prediction and control of atomic ordering in electrodeposited binary alloy films: direct synthesis of L10 magnetic phases

13. **Dongsheng Li**, Pacific Northwest National Laboratory

    Oriented attachment induces 5-fold twin formation via forming and decomposing high-energy grain boundaries

14. **Kristen Fichthorn**, Pennsylvania State University

    Multi-scale simulations of nanowire growth in solution

15. **Tobias Hanrath**, Cornell University, **Paulette Clancy**, Johns Hopkins University, and Lena Kourkoutis, Cornell University

    Synthesis and processing of large grain epitaxially fused quantum dot solids

16. **Scott Auerbach** and **Wei Fan**, University of Massachusetts, Amherst

    Integrating experiment and modeling on zeolite formation: on Raman spectra of silica zeolites

17. **Andrei Fedorov**, Georgia Institute of Technology

    Exploiting localized thermal and electric field gradients to control of nanomaterial phase and composition in far-from-equilibrium gas/liquid jet-assisted e-beam deposition

18. **Mark Ediger**, University of Wisconsin, Madison

    Controlling the structure of vapor-deposited organic glasses and their crystalline products

19. **Linda Schadler**, University of Vermont, **Sanat Kumar**, Columbia University, and Brian Benicewicz, University of South Carolina

    Understanding and controlling filler dispersion using PEO crystallization

20. **Linda Schadler**, University of Vermont, **Sanat Kumar**, Columbia University, and Brian Benicewicz, University of South Carolina

    Controlling filler dispersion using crystallization and vice versa in polyethylene based materials

21. **Linda Schadler**, University of Vermont, **Sanat Kumar**, Columbia University, and Brian Benicewicz, University of South Carolina

    Achieving nanofiller miscibility with polyolefin matrices

Laboratory Projects' Abstracts

This page is intentionally blank.

FWP Title: Molecular Beam Epitaxy of Superconducting Oxides

Ivan Božović (Lead PI), Jie Wu, Ilya Drozdov (PIs), Brookhaven National Laboratory

Program Scope

The mechanism of high-temperature superconductivity (HTS) is one of the most important problems in Condensed Matter Physics. Some basic facts - the spin and the charge of free carriers, the nature of superconducting transition, the effective interaction that causes electron pairing - are still unclear. Using a unique atomic-layer ('digital') molecular beam epitaxy (MBE) system, we synthesize single-crystal films of cuprates, nickelates, bismuthates, etc. We monitor the synthesis process *in situ* and in real time using advanced surface-science tools such as Low-energy electron microscopy and diffraction (LEEM/LEED) and Time-of-flight ion scattering and recoil spectroscopy (TOF-ISARS). This enables fabrication of multilayers and superlattices with atomically perfect interfaces, high-quality tunnel junctions, field-effect devices, and HTS nano-structures.

The program impact is twofold. First, our group is the source of unique samples, including the highest-quality HTS films and multilayer hetero-structures engineered down to a single atomic layer that are enabling breakthrough research of few dozen groups at national laboratories and leading universities in US and abroad. In-house experiments have also brought in several important results - discovery of HTS interface superconductivity, demonstration of Giant Proximity Effect, HTS in a single CuO_2 layer, the (de)localization of electron pairs at the superconductor-insulator quantum phase transition, an unusual demise of superfluid density with overdoping, and spontaneous breaking of rotational symmetry of the electron fluid. These and future experiments are hoped to provide clear-cut answers to at least some of the above questions, which would significantly impact research on HTS and more broadly on strongly-correlated materials. Most important, these new insights inform the quest to discover or engineer novel superconductors with superior properties such as a higher critical temperature or critical current. Thus, an increasing fraction of our future research will be aimed at testing these ideas directly by exploratory synthesis of novel candidate superconducting materials.

Recent Progress

Electron pairing in the pseudogap state revealed by shot noise in copper-oxide junctions. In the quest to understand high-temperature superconductivity in copper oxides, a vigorous debate has been focused on the pseudogap — a partial gap that opens over portions of the Fermi surface in the 'normal' state above the bulk critical temperature (T_c). The pseudogap has been attributed to precursor superconductivity, to the existence of preformed pairs, or to competing orders such as charge-density waves. A direct determination of the charge of carriers as a function of temperature and bias could help resolve among these alternatives.

With this motivation, we have synthesized a series of $La_{2-x}Sr_xCuO_4/La_2CuO_4/La_{2-x}Sr_xCuO_4$ (LSCO/LCO/LSCO) heterostructures using atomic-layer-by-layer molecular beam epitaxy, for several doping levels. The heterostructure schematics is shown in Fig. 1a. Scanning transmission electron microscopy (STEM) and high-resolution electron-energy-loss spectroscopy (HREELS) studies revealed atomically sharp interfaces and verified the high-quality of these devices (Fig 1b-1c). From such heterostructures, we fabricated tunnel-junction devices, schematically depicted in Fig. 1d, and performed detailed measurements of tunneling transport and shot-noise.

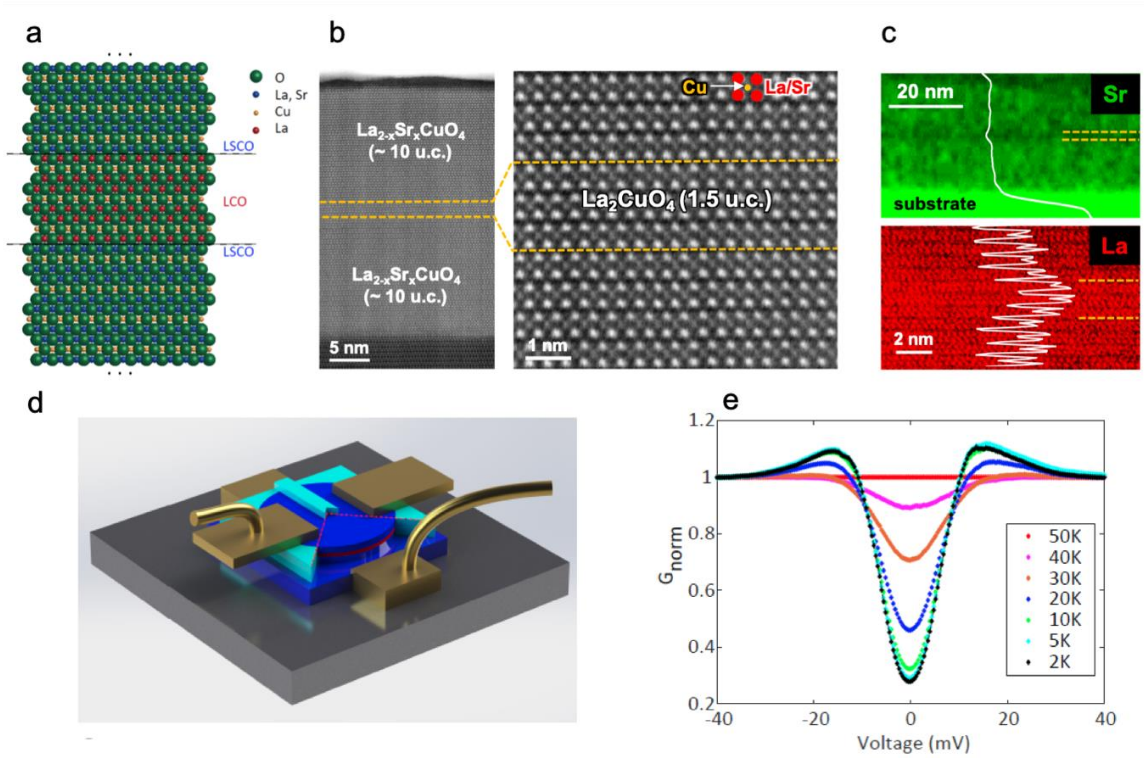

Figure 1. LSCO/LCO/LSCO tunneling structures synthesized by ALL-MBE. a, Film schematic: a tunneling barrier consisting of three molecular layers (1.5 unit cells) of undoped LCO is sandwiched between the bottom and the top superconducting LSCO electrodes. **b**, A high-resolution cross-section image of the actual device obtained by aberration-corrected scanning transmission electron microscopy (STEM) and high-angle annular dark-field imaging (HAADF). **c**, Elemental maps of Sr (green) and La (red) obtained by atomic-resolution energy dispersive x-ray spectroscopy (EDS) and electron-energy-loss spectroscopy (HREELS), respectively, with overlaid white lines showing averaged line profiles. Yellow dashed lines indicate the boundaries of the undoped LCO layers. **d**, Device schematic: photolithography and etching are used to prepare vertical tunneling devices, 10 or 20 μm in diameter. **e**, Tunneling differential conductance data normalized to those at T = 50 K, G_{norm} = (dI/dV)/(dI/dV)50K, as a function of the bias voltage, for a junction with nearly-optimally-doped (x = 0.15) LSCO electrodes. (After Ref. 1)

The differential conductance data (Fig. 1e) show a superconducting gap similar to what is seen in other tunneling experiments, including by point contact and scanning tunneling spectroscopy. The shot-noise data from the same devices delineate three distinct regions in the bias voltage-temperature (V-T) space. Well outside the superconducting gap region, the shot noise agrees quantitatively with independent tunneling of charge-e carriers. Deep within the gap, shot noise is greatly enhanced, reminiscent of multiple Andreev reflections. Starting above T_c and extending to biases much larger than the superconducting gap, there is a broad region in which the noise substantially exceeds the expectations of single-charge tunneling, indicating pairing of carriers. Pairs are detectable deep into the pseudogap region of temperature and bias. The same behavior was found for all doping levels in this study. This dramatic discovery repudiates much of the current thinking in the HTS field and has a potential to cause a paradigm shift in Condensed mater physics.

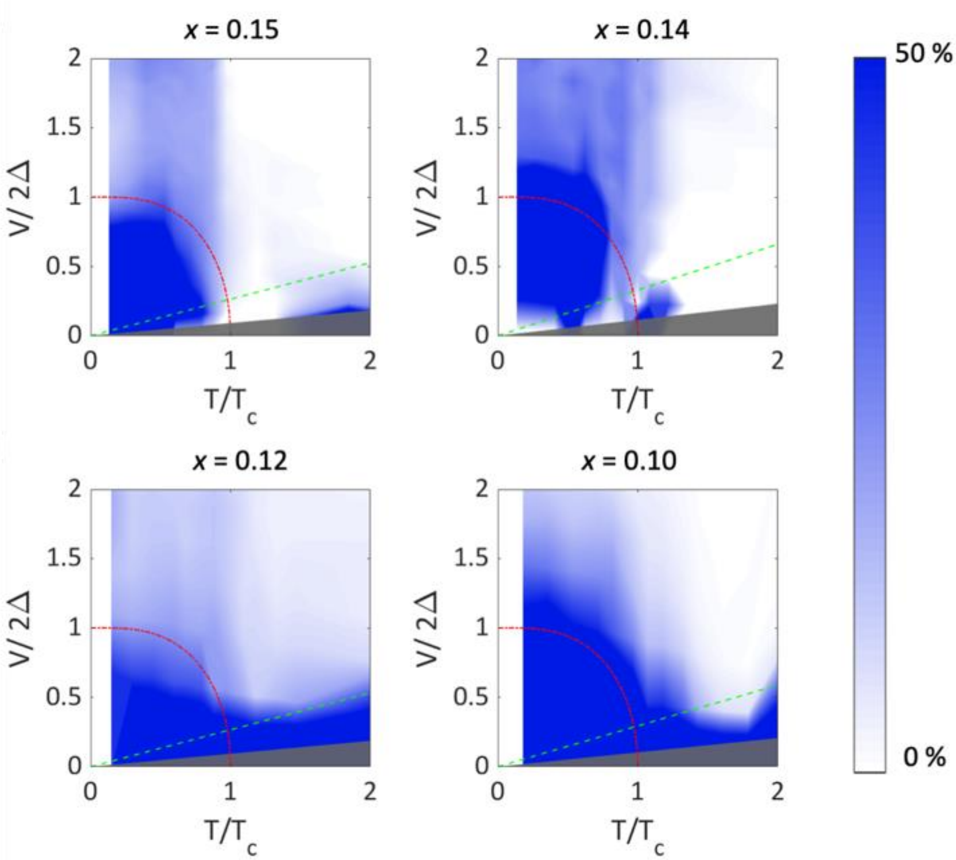

Figure 2. Evidence for preformed pairs in LSCO. The percentage of tunneling pairs inferred from shot-noise measurements on LSCO/LCO/LSCO tunnel junctions for doping levels x = 0.15, 0.14, 0.12, and 0.10, respectively. Red dash-dot lines: the superconducting gap region outside which z = 0 in BCS. Green dashed line: $V = k_B T/e$. Gray area: data inconclusive because of large error bar. (After Ref. 1)

Controlled synthesis and characterization of large-area single crystals of borophene. Borophene, a theoretically proposed two-dimensional boron allotrope with several of the predicted electronic or elastic properties rivalling those of graphene, has attracted much attention as a candidate material platform for high-speed, transparent, and flexible electronics, It has been recently synthesized, on Ag(111) substrates, and studied by tunneling and electron spectroscopy. The key open problems are that the exact crystal structure is still controversial, the nano-meter size single-crystal domains produced so far are too small for device fabrication, and the structural tunability via substrate-dependent epitaxy is yet to be proven. We have monitored synthesis of borophene *in situ* by low-energy electron microscopy, diffraction and scanning tunneling microscopy and modeled it by *ab initio* theory. We have resolved the crystal structure and phase diagram of borophene on Ag(111) but found that the domains remain nanoscale for all growth conditions. However, by growing borophene on Cu(111) surfaces, we obtain large single-crystal domains, up to 100 μm^2 in size. The crystal structure is a novel triangular network with η = 1/5 concentration of hexagonal vacancies. Our experimental data together with first principles calculations indicate charge-transfer coupling to substrate without significant covalent bonding. Our work demonstrates that the structure of borophene can be tuned by the choice of the substrate, sets the stage for fabricating borophene-based devices, and substantiates the idea of borophene as a model for artificial 2D materials development.

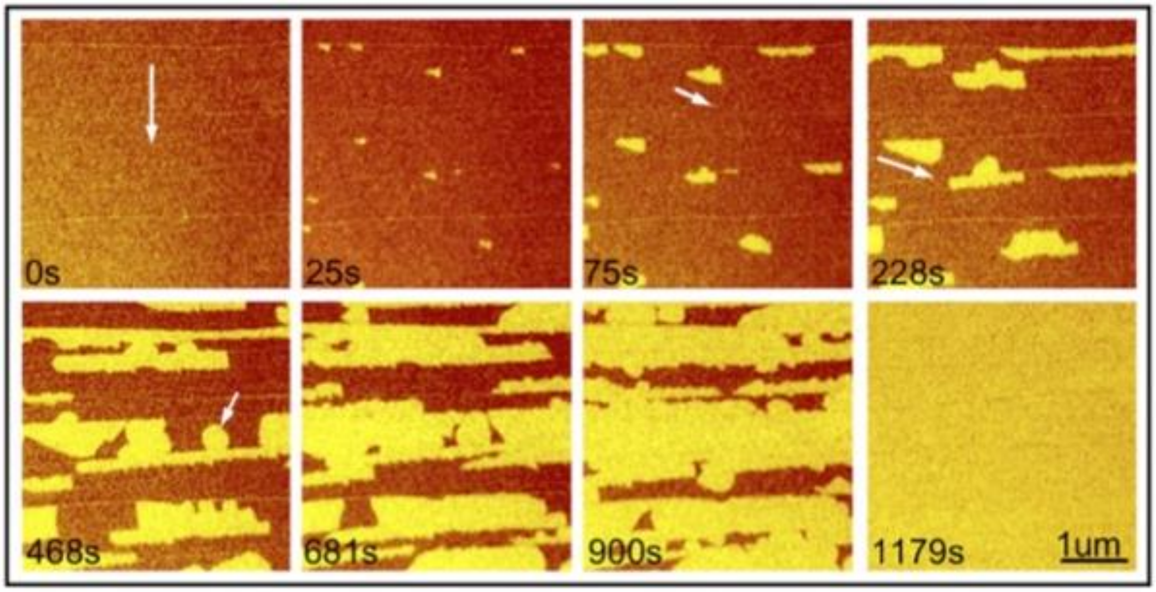

Figure 3. Growth dynamics of borophene on Cu(111) surface. Sequence of bright-field LEEM images at T = 770° K reveals that borophene islands prefer to nucleate from the down-step edge of Cu terraces (i.e. the direction marked by the arrow in the first, t = 0s, panel) and that growth proceeds faster along the step-edge direction. Snapshots taken at 75s and 228s illustrate that at this stage of growth borophene flakes display sharp edges along low-index directions of the substrate, as shown by the white arrows. These two panels along with the snapshot at 468s also show that down-step nucleation is followed by borophene growth across the upper step edge. In contrast to the down-step growth, up-step growth generates arc-shaped islands, indicating more isotropic growth kinetics, see the white arrow in the 468s panel. A continuous monolayer (ML) emerges reproducing faithfully the Cu(111) terrace structure. (After Ref. 2)

Future Plans

The key goal in FY2019 remains the formulation and release of the results of the comprehensive study of the key normal and superconducting properties of HTS cuprates that took over 12 years to complete, and included atomic-layer-by-layer synthesis of over 2,000 LaSrCuO films by MBE, and their characterization by a range of techniques. The first paper focused on the magnetic penetration depth (*Nature* 2016), the second on transverse resistivity (*Nature* 2017), and the third on longitudinal magneto-resistance (*Science* 2018). The next will focus on the temperature and doping dependence of the Hall Effect, the critical field and the coherence length.

Another important goal for FY2019 is ramping up the research using the new oxide MBE module of the OASIS system. The first *in-situ* ARPES spectra were recorded a year ago; these should be complemented in FY2019 by *in-situ* STM studies.

References

1. P. Zhou *et al.*, "Electron pairing in the pseudogap state revealed by shot noise in copper-oxide junctions", accepted for publication in *Nature* (2019).
2. R. Wu *et al.*, "Large-area single-crystal sheets of borophene on Cu(111) surfaces", *Nature Nanotechnology* 14, 44-49 (2019).

Publications supported by this FWP (2017-2019)

**bold face: high impact journals* (11)

1. P. Zhou, L. Chen, Y. Liu, I. Sochnikov, A. T. Bollinger, M.-G. Han, Y. Zhu, X. He, I. Božović and D. Natelson, "Electron pairing in the pseudogap state revealed by shot noise in copper-oxide junctions", accepted for publication in ***Nature*** (2019).
2. J. Wu, H. P. Nair, A. T. Bollinger, X. He, I. Robinson, J. P. Ruf, N. J. Schreiber, K. M. Shen, D. G. Schlom and I. Božović , "Electronic nematicity in Sr_2RuO_4", under revision in ***Nature Physics*** (2019).
3. R. Wu, A. Gozar and I. Božović, "Large-area single-crystal borophene islands on sacrificial Cu(111) film on sapphire", under revision in ***NPJ Quantum Materials*** (2019).
4. J. Wu, A. T. Bollinger, X. He, G. D. Gu, H. Miao, M. P. M. Dean, I. K. Robinson and I. Božović, "Angle-Resolved Transport Measurements Reveal Electronic Nematicity in Cuprate Superconductors", under review in *J. Supercond. Nov. Magn.* (2019).
5. R. Wu, I. K. Drozdov, S. Eltinge, P. Zahl, S. Ismail-Beigi, I. Božović and A. Gozar, "Large-area single-crystal sheets of borophene on Cu(111) surfaces", ***Nature Nanotechnology*** 14, 44-49 (2019).
6. I. K. Drozdov, I. Pletikosić, C.-K. Kim, K. Fujita, G. D. Gu, J. C. Séamus Davis, P. D. Johnson, I. Božović & T. Valla, "Phase diagram of $Bi_2Sr_2CaCu_2O_{8+\delta}$ revisited", ***Nature Communications*** 9, 5210 (2018).
7. F. Mahmood, X. He, I. Božović and N. P. Armitage, "Locating the missing superconducting electrons in overdoped cuprates", ***Phys. Rev. Lett.*** 122, 027003 (2019).
8. I. Božović, J. Wu, X. He and A. T. Bollinger, "What is really extraordinary in cuprate superconductors?", *Physica C* 558, 30-37 (2019).
9. P. Giraldo-Gallo, J. A. Galvis, Z. Stegen, K. A. Modic, F. F Balakirev, J. B. Betts, X.-J. Lian, C. Moir, S. C. Riggs, J. Wu, A. T. Bollinger, X. He, I. Bozovic, B. J. Ramshaw, R. D. McDonald, G. S. Boebinger and A. Shekhter, "Scale invariant magnetoresistance in the strange metal phase of a cuprate superconductor", ***Science*** 361, 479-481 (2018).
10. C. K. Kim, I. Drozdov, K. Fujita, J. C. Davis, I. Božović, T. Valla, "In-situ angle-resolved photoemission spectroscopy of copper-oxide thin films synthesized by molecular beam epitaxy", *Journal of Electron Spectroscopy and Related Phenomena* (2018) published online 09.08.2018.
11. I. Božović, X. He, J. Wu, and A. T. Bollinger, "The Vanishing Superfluid Density in Cuprates and Why It Matters", *J. Supercond. Nov. Magn.*, published online 07.13.2018. https://doi.org/10.1007/s10948-018-4792-7
12. I. Božović, J. Wu, X. He and A. T. Bollinger, "Can high-T_c superconductivity in cuprates be explained by the conventional BCS theory?", *Low Temperature Physics* 44, 674–683 (2018).
13. J. Wu, A. T. Bollinger, X. He and I. Božović, "Detecting electronic nematicity by the angle-resolved transverse resistivity measurements", *J. Supercond. Nov. Magn.* (2018) published online 10.3.2018. https://doi.org/10.1007/s10948-018-4885-3
14. J. Wu, A. T. Bollinger, X. He and I. Božović, "Pervasive electronic nematicity in a cuprate superconductor", *Physica C* 549, 95-98 (2018).
15. J. Wu, A.T. Bollinger, X. He and I. Božović, "Combinatorial synthesis and high-throughput characterization of copper-oxide superconductors", *Chin. Phys. B* 27, 118102 (2018).

16. I. Božović, J. Wu, X. He and A. T. Bollinger, "Is there a path from cuprates towards room-temperature superconductivity?", *Quantum Stud.: Math. Found.* 5, 55-63 (2018) https://doi.org/10.1007/s40509-017-0126-x

17. J. Wu, A. T. Bollinger, X. He and I. Božović, "Spontaneous breaking of rotational symmetry in copper oxide superconductors", ***Nature*** 547, 432-436 (2017).

18. X. Leng, J. Pereiro, J. Strle, G. Dubuis, A. T. Bollinger, A. Gozar, N. Litombe, D. Pavuna & I. Božović, "Insulator to Metal Transition in WO_3 Induced by Electrolyte Gating", ***NPJ Quantum Materials*** 2, 35 (2017).

19. A. Gozar, N. E. Litombe, J. E. Hoffman and I. Božović, "Optical Nanoscopy of High-T_c Cuprate Nano-Constriction Devices Patterned by Helium Ion Beams", ***Nano Letters*** 17, 1582-1586 (2017).

20. J. Wu, V. Lauter, H. Ambaye, X. He and I. Božović, "Search for ferromagnetic order in overdoped copper-oxide superconductors", ***Scientific Reports*** 7, 45896 (2017). I. Božović, X. He, J. Wu and A. T. Bollinger, "What is strange about high-temperature superconductivity in cuprates?", *Internat. J. Mod. Phys. B* 31, 1745005 (2017).

21. V. A. Gasparov, L. Drigo, A. Audouard, Xi He and I. Božović, "Study of high-T_c interface superconductivity in $La_{1.55}Sr_{0.45}CuO_4/La_2CuO_4$ heterostructures at high fields and frequencies", *Internat. J. Mod. Phys. B* 31, 1745016 (2017).

22. I. Božović, X. He, J. Wu and A. T. Bollinger, "On the origin of high-temperature superconductivity in cuprates", (invited keynote) in *Oxide-based Materials and Devices VIII*, edited by Ferechteh H. Teherani, David C. Look, David J. Rogers, Proc. of SPIE Vol. 10105, 1010502 (2017) doi: 10.1117/12.2261512.

23. S. Dietrich, W. Mayer, S. Byrnes, S. Vitkalov, A. Sergeev, A. T. Bollinger and I. Božović, "Microwave nonlinear response of oxide superconducting films in the Berezinskii-Kosterlitz-Thouless state", (invited) *in Oxide-based Materials and Devices VIII*, edited by Ferechteh H. Teherani, David C. Look, David J. Rogers, Proc. of SPIE Vol. 10105, 101051S (2017). doi: 10.1117/12.2264369

24. A. Gozar, P. Abbamonte and I. Božović, "Strong off-diagonal polarizability and electron-lattice coupling in high-temperature superconductors", (invited) In *Oxide-based Materials and Devices VIII*, edited by F. H. Teherani, D. C. Look and D. J. Rogers, Proc. of SPIE Vol. 10105, 101050B (2017). doi: 10.1117/12.2266052

25. D. Meyers, H. Miao, A. C. Walters, V. Bisogni, R. S. Springell, M. d'Astuto, M. Dantz, J. Pelliciari, H. Huang, J. Okamoto, D. J. Huang, J. P. Hill, X. He, I. Božović, T. Schmitt and M. P. M. Dean, "Doping dependence of the magnetic excitations in $La_{2-x}Sr_xCuO_4$", *Phys. Rev. B* 95, 075139 (2017).

26. I. Božović, X. He, J. Wu and A. T. Bollinger, "The demise of superfluid stiffness in overdoped $La_{2-x}Sr_xCuO_4$ films grown by molecular beam epitaxy", *J. Supercond. Nov. Magn.* 30, 1345-1348 (2017).

27. D. Pavuna, G. Dubuis, A.T. Bollinger, J. Wu, X. He and I. Božović, "On Local Pairs vs. BCS: Quo Vadis High-T_c Superconductivity?", *J. Supercond. Nov. Magn.* 30, 731-734 (2017). DOI 10.1007/s10948-016-3638-4

28. J. Wu, A. T. Bollinger, Y. Sun and I. Božović, "Ground State of Underdoped Cuprates in Vicinity of Superconductor-to-Insulator Transition", *J. Supercond. Nov. Magn.* 30, 1073-1076 (2017).

29. Z. Radović, M. Vanević, J. Wu, A. T. Bollinger and I. Božović, "Interface superconductivity in cuprates defies Fermi-Liquid description", *J. Supercond. Nov. Magn.* 30, 725-729 (2017). DOI 10.1007/s10948-016-3636-6

30. I. Božović, X. He, J. Wu and A. T. Bollinger, "What is strange about high-temperature superconductivity in cuprates?", *Internat. J. Mod. Phys. B* 31, 1745005 (2017).

Electronic, Magnetic and Optical Properties of Doped Metal Oxides Epitaxial Films and Interfaces

Scott A. Chambers, Peter V. Sushko, Yingge Du, Steven R. Spurgeon, Mark E. Bowden, Tiffany C. Kaspar, Timothy C. Droubay

Program Scope

Our current focus is on the synthesis and properties of epitaxial films, heterostructures and superlattices of complex oxides integrated with other complex oxides, and with Group IV semiconductors. Molecular beam epitaxy is our film growth method of choice because of the high source purity levels, low incident particle energies, and high degree of compositional control inherent in the method. We aim to deposit materials of the highest structural quality and compositional purity. However, we understand that apart from the existence of a growth window, multi-element materials rarely, if ever, condense from gas-phase atom beams incident on a substrate with precisely the targeted composition. Therefore, point defects in the form of anti-sites, vacancies, and interstitial atoms are typically present at some level. These defects can have a significant influence on the functional properties of the material system, even when present at concentrations below the detection limits of currently available analytical techniques. In addition, phases other than those that are desired can nucleate in the host lattice if they are more thermodynamically stable than the host. We strive to accurately characterize irregularities in our materials, and to understand how functional properties are influenced by these entities.

Recent Progress

In our oral presentation, we discuss new, unpublished results on the MBE synthesis and properties of 2D materials in the form of $[(LaFeO_3)_n / (SrNiO_3)_m]_k$ superlattices (SL) deposited on 10 u.c. buffer layers of $LaFeO_3$ on (001)-oriented $(La_{0.18}Sr_{0.82})(Al_{0.59}Ta_{0.41})O_3$ (LSAT) substrates. We denote this SL as $(LFO_n / SNO_m)_k$, where n and m are independently varied in different film sets, and k ranges from 5 to 20. This class of SLs has high tunability because the A and B site cations consist of different elements in the two phases. The bulk phases of the two constituent materials are distinct in that LFO is a stable, wide-gap (E_g = ~2.3 eV) antiferromagnetic insulator whereas SNO is unstable in the bulk, due largely to the instability of Ni^{4+}. Indeed, most naturally occurring Ni-based minerals contain formally divalent Ni^{2+}; only a few contain Ni^{3+} and, to the best of our knowledge, none contain Ni^{4+}. We hypothesize that SNO can be stabilized in $(LFO_n / SNO_m)_k$ by means of electron transfer from Fe to Ni at the internal interfaces. Such a system may exhibit unique and interesting properties, quite different from those of any bulk phase. The charge transfer process would result in formally Fe^{4+} and Ni^{3+}. We reason that since we have succeeded in stabilizing fully-oxidized $SrFeO_3$ as an epitaxial film [1,2] , Fe^{4+} would be more stable in a perovskite lattice than Ni^{4+}. We find that high-quality $(LFO_n / SNO_1)_k$ SLs with n = 1, 3, 5, and 8 u.c. are readily synthesized by MBE (Fig. 1). The primary imperfection we detect is cation intermixing over a length scale of ~1 u.c. at the internal interfaces. Core-level x-ray photoemission spectroscopy (XPS) reveals that indeed, electron transfer from Fe to Ni occurs at the internal interfaces (Fig 2). In-plane transport (ρ vs T) shows that the 1:1 SL exhibits very low-resistance semiconducting behavior, and that ρ rises at all T with increasing n (Fig. 3). The Ni 2p (Fig. 2) and 3p (not shown) line shapes remains characteristic of Ni^{3+}. Interestingly, ρ for the 1:1 SL increases

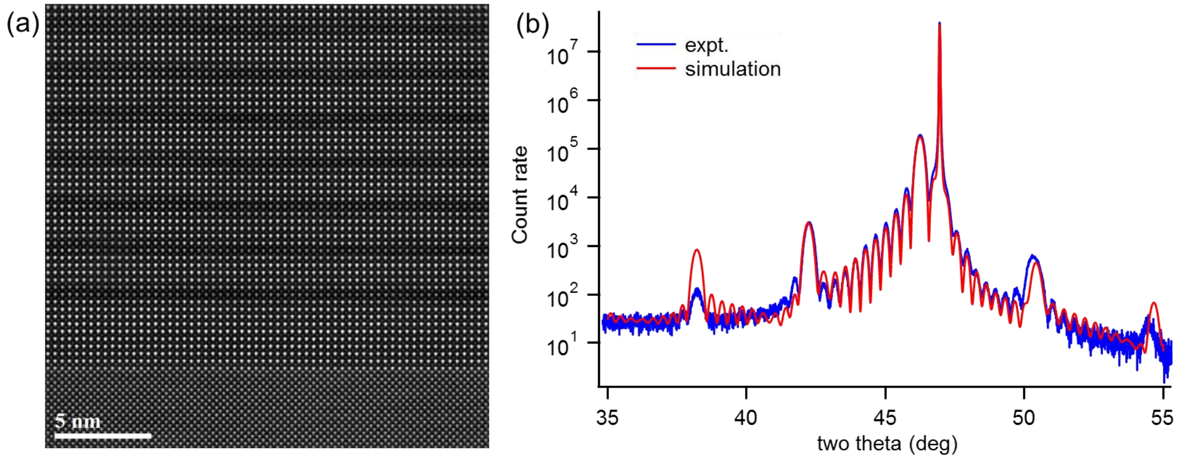

Fig. 1 STEM/HAADF image (a), and measured and simulated out-of-plane XRD scans (b) for a $(LFO_5 / SNO_1)_{10}$ superlattice grown on a 10 u.c. LFO buffer layer on LSAT(001).

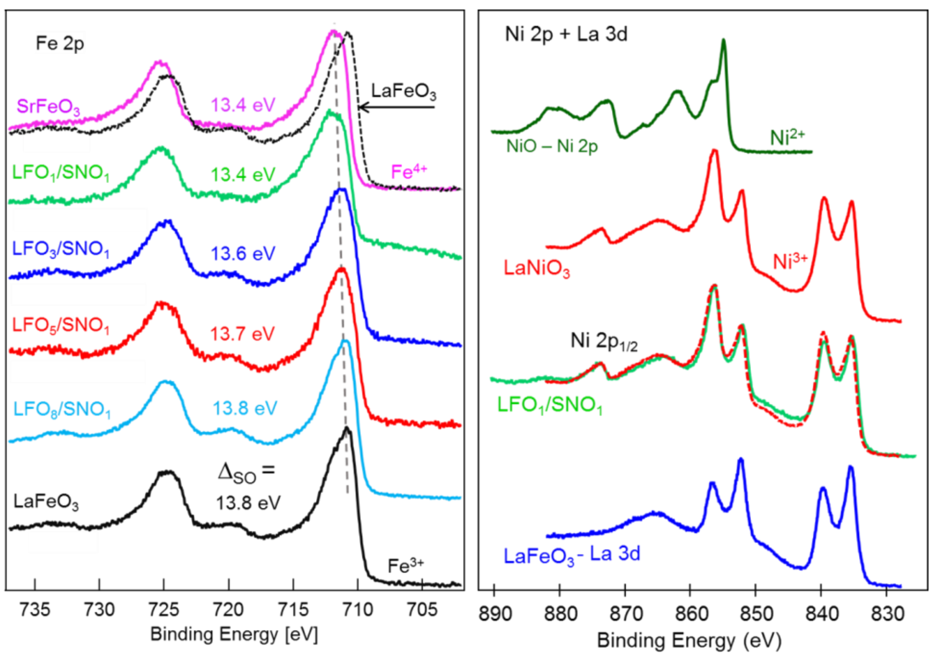

Fig. 2 Fe 2p and Ni 2p XPS for (LFO_n / SNO_1) SLs showing the evolution of the Fe and Ni valences with *n*. Comparison of the n = 1 spectra with those for epitaxial film standards of LFO and SFO reveals that all Fe is tetravalent due to electron transfer from Fe to Ni, and equal numbers of Fe and Ni *B*-site cations. As *n* increases, the fraction of tetravalent Fe drops as Fe in LFO layers not directly adjacent to the interface remains trivalent. There is strong overlap between the Ni 2p and the La 3d spectra; only the Ni $2p_{1/2}$ feature remaining unobscured, and that only for n = 1. However, comparison with a thick-film LNO standard makes it is clear that the Ni is trivalent for 1:1 SL. The broader Ni 3p spectra for all *n*:1 SLs (not shown) are consistent with Ni being trivalent in all SLs.

by several orders of magnitude when the SL is annealed in high vacuum at a modest temperature of 350°C for just 30 minutes. At the same time, the Fe 2p XPS line shape reverts from one characteristic of formally Fe^{4+} to one indicating Fe^{3+}, revealing that vacuum annealing generates O vacancies that compensate structural Fe^{4+}.

In contrast, $(LFO_5 / SNO_m)_k$ SLs with m = 1 to 5 u.c. exhibit a high degree of structural quality *only* for $m = 1$; the structural quality degrades rapidly with increasing m for $m \geq 2$. If we attempt to grow a thick epitaxial film of phase pure SNO, we find that the film nucleates in a bi-phasal fashion, with roughly equal proportions of $SrNi_2O_3$ and Sr_2NiO_3. STEM shows that the film consists of interlocked nanoscale crystallites of $SrNi_2O_3$ and Sr_2NiO_3. We conclude that the driver behind these two phenomena is that Ni in a spatially-extended, fully-oxidized SNO phase must be tetravalent, and this electron configuration is highly unstable. By phase separating to $SrNi_2O_3$ and Sr_2NiO_3, the material can stabilize Ni in the divalent state. Therefore, artificially-structured SNO can be realized in these SLs if the *B*-site Ni cation can draw an electron from a neighboring *B*-site Fe^{3+} cation in an adjacent layer and be stabilized as Ni^{3+}.

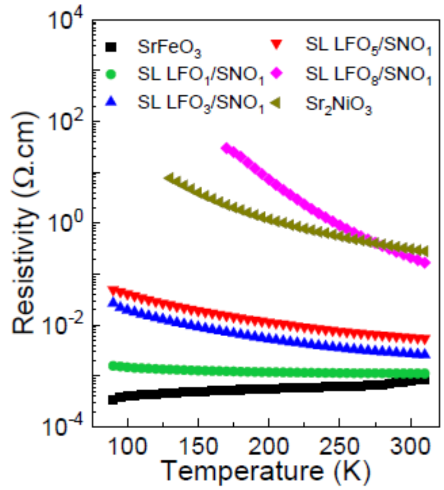

Fig. 3 $\rho(T)$ for (LFO_n / SNO_1) SLs with n = 1, 3, 5, and 8 u.c. The 1:1 SL is almost as conductive as thick-film, metallic SFO.

In our poster, we summarize three other areas of programmatic activity. First, we present on *hole-induced optical and electronic properties modification at p-*$Sr_xLa_{1-x}FeO_3$*/n-*$SrTiO_3$*(001)* heterojunctions prepared by MBE [1,3] . Core-level and valence-band XPS features monotonically shift to lower binding energy with increasing x, indicating downward movement of the Fermi level toward the valence band maximum. Combining valence band photoemission and O *K*-edge x-ray absorption data, we have mapped the evolution of the occupied and unoccupied bands and observe a narrowing of the gap, along with a transfer of state density from just below to just above the Fermi level as a result of hole doping. In-plane transport measurements confirm that the material becomes a *p*-type semiconductor at lower doping levels and exhibits a conversion from semiconducting to metallic behavior, but not until x = 1. Low-energy optical transitions revealed by spectroscopic ellipsometry are explained based on insights from first-principles density functional theory (DFT) calculations of densities of states and optical absorption spectra. At x = 0.12, a staggered, type-II band alignment occurs with a large built-in potential within the LSFO due to polar interface formation. This electronic structure facilitates charge transfer across the *p-n* junction and accounts for the strongly thickness-dependent extent of oxygen evolution reaction (OER) activity we observe.

Second, we illustrate *dynamical control of interface structure at the* $LaFeO_3/SrTiO_3$ *(001) heterojunction driven by flux-controlled nucleation chemistry* [4,5] . We find by STEM/EELS that *shuttered deposition* of La and Fe in an activated oxygen background on SrO-terminated $SrTiO_3$(001) leads to dissolution of the SrO monolayer whereas *co-evaporation* of La and Fe on the SrO-terminated substrate does not. These results are understood by employing DFT+*U* calculations of interface reaction energetics. In essence, deposition of the first monolayer of Fe in the absence of La forces formation of FeO_2 at the interface, and Fe^{4+} is unstable. The system responds by dissolution of the SrO at the interface and Sr diffusion into the film, allowing the more stable (…TiO_2/LaO…) interface structure to form.

Third, we demonstrate *2D hole gas formation at the $SrNb_xTi_{1-x}O_3$/Si(001) heterojunction understood by hard x-ray photoelectron spectroscopy (HAXPES)* [6] . MBE growth of 12 nm films of $SrNb_xTi_{1-x}O_{3-d}$ on intrinsic Si(001) unexpectedly leads to 2D hole gas (2DHG) formation on the Si side of the interface for x = 0, 0.08 and 0.20, and surface depletion of carriers in the SNTO. The hole gas does not form if x is too large (0.6), or if the film is too thick (20 nm). These results strongly suggest that the two electric fields are coupled. *But what is the physics?* To find out, we employed HAXPES to probe this deeply buried interface. Core-level line shapes are highly sensitive to the presence of built-in potentials in the vicinity of the heterojunction. However, extracting the detailed energy landscape from these spectra is nontrivial. In order to do so, we developed a novel algorithm that performs a comprehensive search over all possible binding energies in each layer within the probe depth, seeking a set of layer-resolved spectra which, when summed, generate a composite spectrum that matches experiment. By searching over both signs of the potential gradient in each material phase, a global minimum can be found for the cost function, defined by the quality of the spectral fit and the smoothness of the potential variations with depth. We have performed this analysis for SNTO/Si heterojunctions and have extracted band-edge profiles that explain in detail the observed transport properties, and are in quantitative agreement with potential profiles from Schrodinger-Poisson modeling. These results show how the surface and interface electric fields couple to generate the 2DHG in the Si.

Future Plans

We plan to explore other complex oxide heterostructures involving different metal cations, seeking to synthesize artificially-structured superlattices that allow formation of otherwise unstable or metastable forms of matter. We are also interested in further exploring the role of transient atom beam fluxes to open new synthetic pathways for novel materials. These pathways will open because particular 2D atom configurations can be realized via kinetic control of the arriving adatoms, thereby driving the system in advantageous directions. We remain interested in the MBE synthesis of spinels, having consistently found evidence for non-uniform cation distributions. Finally, we plan to use our new algorithm to interpret HAXPES data taken from other complex oxide/Si heterojunctions that exhibit novel and useful transport properties. Significantly, detailed band-edge profiles for buried heterojunctions and superlattices are not available from methods other than HAXPES and standing wave HAXPES, respectively.

References

[1] L. Wang, Y. Du, P. V. Sushko, M. E. Bowden, K. A. Stoerzinger, S. Heald, M. D. Scafetta, T. C. Kaspar, S. A. Chambers, Phys. Rev. Mater. **3**, 025401 (2019).

[2] L. Wang, Z. Yang, M. E. Bowden, Y. Du, Appl. Phys. Lett. **114**, 231602 (2019).

[3] L. Wang, Y. Du, L. Chang, K. A. Stoerzinger, M. E. Bowden, J. Wang, S. A. Chambers, Appl. Phys. Lett. **112**, 261601 (2018).

[4] R. Comes and S. Chambers, Phys. Rev. Lett. **117**, 226802 (2016).

[5] S. R. Spurgeon, P. V. Sushko, S. A. Chambers, R. B. Comes, Phys. Rev. Mater. **1**, 063401 (2017).

[6] Z. H. Lim, N. F. Quackenbush, A. Penn, M. Chrysler, M. Bowden, Z. Zhu, J. M. Ablett, T.-L. Lee, J. M. LeBeau, J. C. Woicik, P. V. Sushko, S. A. Chambers, J. H. Ngai, Phys. Rev. Lett., in press (2019).

Publications

<u>2018</u>

1. Steven R. Spurgeon, Peter V. Sushko, Arun Devaraj, Yingge Du, Timothy C. Droubay, Scott A. Chambers, "*Onset of Phase Separation in the Double Perovskite Oxide La_2MnNiO_6*", Phys. Rev. B **97**, 134110 (2018). DOI: 10.1103/PhysRevB.97.134110.
2. Kelsey A. Stoerzinger, Yingge Du, Kelvin H.L. Zhang, Jun Cai, J. Trey Diulus, Ryan T. Frederick, Gregory S. Herman, Ethan J. Crumlin, Scott A. Chambers, "*Impact of Sr-Incorporation on Cr Oxidation and Water Dissociation in $La_{(1-x)}Sr_xCrO_3$*", Adv. Mater. Int. 1701363 (2018). DOI 10.1002/admi.201701363.
3. Kelsey A. Stoerzinger, Yingge Du, Steven R. Spurgeon, Demie Kepaptsoglou, Quentin M. Ramasse, Ethan J. Crumlin, Scott A. Chambers, "*Chemical and Electronic Structure Analysis of a $SrTiO_3$ (001) / p-Ge (001) Hydrogen Evolution Photocathode*", MRS Comm. **8**, 46 (2018). DOI:10.1557/mrc.2018.38.
4. L. Wang, Y. Du, L. Chang, K. A. Stoerzinger, M. E. Bowden, J. Wang, S. A. Chambers, "*Interface Electronic Structure and Band Alignment at the p-n $La_{0.88}Sr_{0.12}FeO_3$ / $SrTiO_3$(001) Heterojunction*", Appl. Phys. Lett. **112**, 261601 (2018). DOI: 10.1063/1.5030897.
5. S.A. Chambers, Y. Du, Z. Zhu, J. Wang, M.J. Wahila, L.F.J. Piper, A. Prakash, J. Yue, B. Jalan, S.R. Spurgeon, D.M. Kepaptsoglou, Q. M. Ramasse, P.V. Sushko, "*Interconversion of intrinsic defects in $SrTiO_3$(001)* ", Phys. Rev. B **97**, 245204 (2018). DOI: 10.1103/PhysRevB.97.245204.
6. Le Wang, Kelsey A. Stoerzinger, Lei Chang, Jiali Zhao, Yangyang Li, Chi Sin Tang, Xinmao Yin, Mark E. Bowden, Zhenzhong Yang, Haizhong Guo, Lu You, Rui Guo, Jiaou Wang, Kurash Ibrahim, Jingsheng Chen, Andrivo Rusydi, Junling Wang, Scott A. Chambers, Yingge Du, "*Tuning Bifunctional Oxygen Electrocatalysts by Changing A-site Rare-Earth Element in Perovskite Nickelates*", Adv. Funct. Mater. **28**, 1803712 (2018). DOI: 10.1002/adfm.201803712.
7. Y. Du, P.V. Sushko, S.R. Spurgeon, M.E. Bowden, J.M. Ablett, T.-L. Lee, N.F. Quackenbush, J.C. Woicik, S.A. Chambers, "*Layer-resolved band bending at the n-$SrTiO_3$(001)/p-Ge(001) interface*", Phys. Rev. Mater. **2**, 094602 (2018). DOI: 10.1103/PhysRevMaterials.2.094602.
8. Kelsey A. Stoerzinger, Le Wang, Yifan Ye, Mark Bowden, Ethan J. Crumlin, Yingge Du, Scott A. Chambers, "*Linking surface chemistry to photovoltage in Sr-substituted $LaFeO_3$ for water oxidation*", J. Mater. Chem. A **6**, 22170 (2018). DOI: 10.1039/c8ta05741a.
9. Tiffany C. Kaspar, Peter V. Sushko, Steven R. Spurgeon, Mark E. Bowden, David J. Keavney, Ryan B. Comes, Sahar Saremi, Lane Martin, Scott A. Chambers, "*Electronic structure and band alignment of $LaMnO_3$ / $SrTiO_3$ polar / non-polar heterojunctions*", Adv. Mater. Int. 1801428 (2018). DOI: 10.1002/admi.201801428.
10. Tamas Varga, Timothy C. Droubay, Libor Kovarik, Dehong Hu, and Scott A. Chambers, "*Controlling the Structure and Ferroic Properties of Strained Epitaxial $NiTiO_3$/Al_2O_3 Thin Films by Post-Deposition Annealing*", Thin Solid Films **62**, 47 (2018). https://doi.org/10.1016/j.tsf.2018.07.030.
11. Shih-Chieh Lin, Cheng-Tai Kuo, Ryan Comes, Julien E. Rault, Jean-Pascal Rueff, Slavo Nemšák, Amina Taleb, Jeffrey B. Kortright, Julia Meyer-Ilse, Eric Gullikson, Peter Sushko, Steven R. Spurgeon, Matthias Gehlman, Lukasz Plucinski, Scott A. Chambers,

and Charles S Fadley, "*Interface composition and potential profile of $LaCrO_3/SrTiO_3$ determined by standing-wave excited photoemission spectroscopy*", Phys. Rev. B **98**, 165124 (2018). DOI: 10.1103/PhysRevB.98.165124.

12. J.C. Woicik, J.M. Ablett, N.F. Quackenbush, A.K. Rumaiz, C. Weiland, T.C. Droubay, S.A. Chambers, "*Charge-transfer excitations in the photo-ionization of NiO*", Phys. Rev. B. **97**, 245142 (2018). DOI: 10.1103/PhysRevB.97.245142/.
13. J. Debehets, P. Homm, M. Menghini, S.A. Chambers, C. Marchiori, M. Heyns, J.P. Locquet, J.W. Seo, "*Detecting Fermi-level shifts by Auger electron spectroscopy in Si and GaAs*", App. Surf. Sci. **440**, 386 (2018). DOI: https://doi.org/10.1016/j.apsusc.2018.01.079.
14. Dustin Gilbert, Peyton Murray, Alexandr Lonin, Steven R. Spurgeon, R. Chopdekar, Brian J. Kirby, Brian Maranville, Julie A. Borchers, A.T. N'Diaye, Kai Liu, Elke Arenholz, Yayoi Takamura, Alex J. Grutter. "*Ionic tuning of cobaltites at the nanoscale.*" Phys. Rev. Mater. **2**, 104402 (2018). DOI:10.1103/PhysRevMaterials.2.104402.

2019

1. Le Wang, Kelsey A. Stoerzinger, Lei Chang, Xinmao Yin, Yangyang Li, Chi Sin Tang, Endong Jia, Mark E. Bowden, Zhenzhong Yang, Amr Abdelsamie, Lu You, Rui Guo, Jingsheng Chen, Andrivo Rusydi, Junling Wang, Scott A. Chambers, Yingge Du, "*Strain Effect on Oxygen Evolution Reaction Activity of Epitaxial $NdNiO_3$ Thin Films*", ACS Adv. Mater. Int. **11**, 12941 (2019). DOI: 10.1021/acsami.8b21301.
2. Le Wang, Yingge Du, Peter V. Sushko, Mark E. Bowden, Kelsey A. Stoerzinger, Steven M. Heald, Mark. D. Scafetta, Tiffany C. Kaspar, Scott. A Chambers, "*Hole-Induced Electronic and Optical Transitions in $La_{1-x}Sr_xFeO_3$ Epitaxial Thin Films*", Phys. Rev. Mater. **3**, 025401 (2019). DOI: 10.1103/PhysRevMaterials.3.025401.
3. Mark D. Scafetta, Zhenzhong Yang , Steven R. Spurgeon, Tiffany C. Kaspar, Scott A. Chambers, "*Epitaxial growth and atomic arrangement in Fe_2CrO_4 on crystal symmetry matched (001) $MgAl_2O_4$*", J. Vac. Sci. Technol. A **37**, 031511 (2019). DOI: 10.1116/1.5093537.
4. Scott A. Chambers, "*X-ray Photoelectron Spectroscopy*", invited book chapter for Methods of Epitaxial Film and Heterostructure Characterization, eds. A.A. Demkov and S.A. Chambers, World Scientific, accepted (2019).
5. Tiffany C. Kaspar, "*Spectroscopy Ellipsometry*", invited book chapter for Methods of Epitaxial Film and Heterostructure Characterization, eds. A.A. Demkov and S.A. Chambers, World Scientific, accepted (2019).
6. Steven R. Spurgeon, "*Scanning Transmission Electron Microscopy of Oxide Interfaces and Heterostructures*", invited book chapter for Methods of Epitaxial Film and Heterostructure Characterization, eds. A.A. Demkov and S.A. Chambers, World Scientific, accepted (2019).
7. Paul S. Bagus, Connie J. Nelin, C. R. Brundle, Scott A. Chambers, "*A New Mechanism For XPS Line Broadening: The 2p-XPS of Ti(IV)*", J. Phys. Chem. C **123**, 7705 (2019). DOI: 10.1021/acs.jpcc.8b05576.
8. Lei Chang, Le Wang, Lu You, Zhenzhong Yang, Amr Abdelsamie, Qinghua Zhang, Yang Zhou, Lin Gu, Scott A. Chambers, and Junling Wang, "*Tuning Photovoltaic Performance of Perovskite Nickelates Heterostructures by Changing the A-Site Rare-Earth Element*", ACS Adv. Mater. Int., in press (2019).

9. Zheng Hui Lim, Nicholas F. Quackenbush, Aubrey Penn, Matthew Chrysler, Mark Bowden, Zihua Zhu, James M. Ablett, Tien-Lin Lee, James M. LeBeau, Joseph C. Woicik, Peter V. Sushko, Scott A. Chambers, Joseph H. Ngai, "*Charge Transfer and Built-in Electric Fields Between a Crystalline Oxide and Silicon*", Phys. Rev. Lett., in press (2019).

Nucleation and Self-Assembly of Hierarchical Materials: Predicting Pathways, Dynamics and Outcomes

Marcel D. Baer, Jaehun Chun, James J. De Yoreo, Karl T. Mueller, Christopher J. Mundy, Peter J. Pauzauskie

Physical and Computational Sciences Directorate, Pacific Northwest National Laboratory, Richland, WA 99352, USA

Program Scope

The long-term vision of this project is to develop a predictive understanding of the physical principles connecting atomic-scale interactions to the ensemble responses controlling the synthesis of hierarchical nanostructures via multi-step nucleation pathways and nanoparticle assembly. We pursue this vision through four scientific objectives that target key knowledge gaps: 1) What factors are responsible for the many complexities in the free energetics of cluster formation? 2) How do complex solution species and molecular clusters transition to the first ordered, stable nuclei? 3) How does interfacial solid and solution structure translate into forces that drive oriented particle attachment? 4) How and when does phase transformation occur in nanostructures assembled from primary particles of a distinct nanoscopic phase? Our approach combines synthesis of nanomaterials exhibiting non-classical pathways and representing distinct classes of structure and interactions, with characterization of synthetic pathways and dynamics using *in situ* methods including TEM, AFM, NMR, dynamic force spectroscopy and sum frequency generation, as well as theory and simulation. The outcome will be a predictive description of non-classical crystallization that crosses scales to connect atomistic details with ensemble outcomes based on models of reduced complexity.

Recent Progress

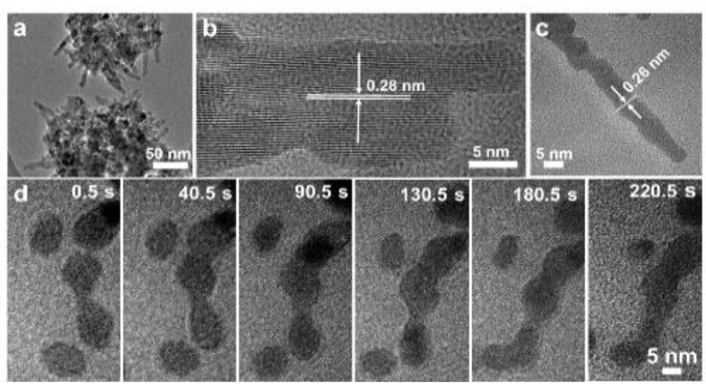

Figure 1. (a–c) *Ex situ* TEM images of ZnO grown in aqueous solution. (d) *In situ* TEM images of ZnO nanowire growth in methanol. Scale bar: 5 nm.

The interplay between crystal structure, solvent structure, interparticle forces and ensemble particle response dynamics governs the process of crystal growth by oriented attachment (OA),[1] yet quantitative relationships are lacking. Here we investigate those relationships during formation of ZnO nanostructures, which is widely attributed to OA (Fig. 1 a–c), [2, 3]. Previous work focused on static measurements of the orientational dependence of the binding energy between ZnO (001) surfaces, as well as hydration barriers created by structuring of water near the face [3]. Here we combine in situ liquid phase TEM (LP-TEM) observations of both single particle and ensemble assembly dynamics, with molecular simulations of interparticle forces to relate experimentally derived interparticle potentials to underlying fundamental interactions. We observed assembly of zinc oxide particles in methanol solutions (Fig. 1d) containing additional zinc acetate, which mitigated the problem of particle dissolution by the electron beam commonly observed for oxides. End-to-end attachments produced nanoparticle chains, confirming that individual nanoparticles can be the fundamental building blocks for the formation of ZnO nanowires by OA.

To determine whether particles attach with random orientations and subsequently rearrange into a single crystal, or whether they self-align prior to attachment, we tracked the trajectories during individual attachment events. For the example in Fig. 2, the relative orientation (θ_r) of the (002) faces decreased from θ_r = 43° to 15° at 54 s, and then to 4° at 63 s. As the two particles aligned to a perfect lattice match, OA was accomplished via a jump-to-contact across a final gap of ~ 1 nm. Attachment thus occurred along [001] by OA, leading to the formation of larger particles (Fig. 2f). This result was validated by Fourier transform analyses that visualize the rotational dynamics of the particles and confirmed their alignment prior to attachment (Fig. 2h).

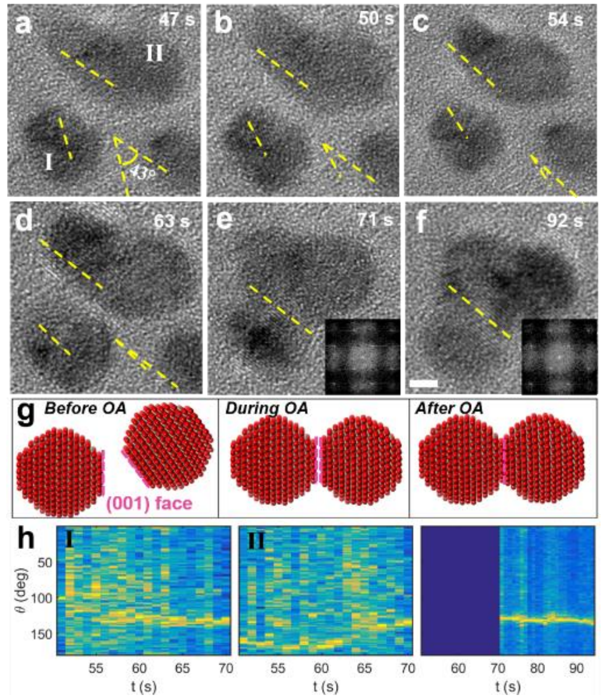

Figure 2. (a-f) LP-TEM image sequence showing OA of ZnO particles in methanol. Scale bar: 5 nm. (g) Scheme depicting OA. (h) 1D intensity profiles vs. time created from FFT of image sequence showing relative orientation of [002] direction for particles I, II, and coalesced particle.

Beyond individual cases of OA, we further examined the dynamics of particle ensembles, (Fig. 3). In the cases where particles attached, they all moved steadily towards each other with minor fluctuations in trajectories, before jumping to contact at separation h = 1.08 (± 0.33) nm (Fig. 4a). Moreover, the particles did not grow classically during the observation time, indicating that particle attachment was the dominant pathway of growth. We investigated the underlying free energy landscape by calculating the radial distribution probability function (RDF) for all particles according to $g(h) = \frac{1}{2\pi h\,\Delta h}\frac{N_h}{\rho}$, where N_h is the number of particles within [h-$\Delta h/2$, h+$\Delta h/2$] and ρ is the number of particles per area unit (Fig. 4b). The RDF was found to be relatively invariant during the course of the experiment, ensuring that it provides representative information about the particle interactions leading to attachment. We obtained a weak attractive potential $W(h)$ between

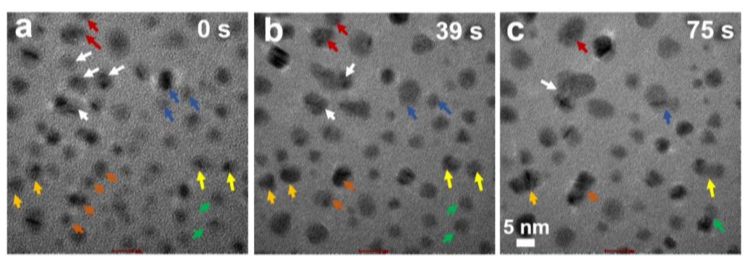

Figure 3. (a-c) three frames from an LP-TEM sequence illustrating evolution of particle ensembles used for subsequent analyses. Colored arrows mark groups of particles that eventually coalesce.

the particles over a relatively long range of several nanometers from the RDF (Fig. 4b inset). Importantly, no significant energy barrier was observed from the ensemble of particle behavior, suggesting a diffusion-limited process for particle attachment, in contrast to a reaction-limited process with a large energy barrier presumed in previous studies. [4]

This result was further validated by multiple independent calculations. We first measured a monomer-monomer attachment rate constant of k_{11} = 1.53 nm^2/s by assuming second order kinetics under a quasi-2D approximation (Fig. 4d). We then calculated mean squared displacements for multiple particles (Fig. 4c) and obtained an average diffusion coefficient for particles of radius a = 2.2 nm of 2.99 nm^2/s; which is ~10^6 times lower than expected from the Stokes-Einstein equation for bulk diffusion, but is consistent with previous LP-TEM observations. [5] Using these values, the preexisting reaction-limited hypothesis was tested based on an Arrhenius dependence and an insignificant attachment barrier of ~3kT was obtained, qualitatively consistent with the result from the RDF.

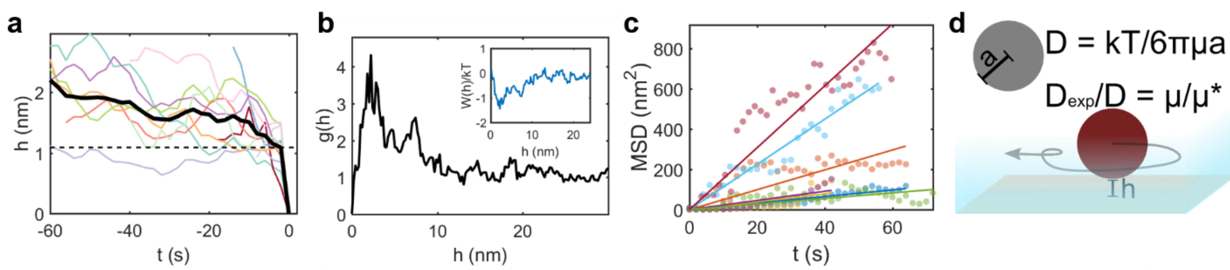

Figure 4. (a) Separation of two approaching particles showing jump to contact, (b) radial distribution function, inset plots $W(h)/kT = -\ln(g(h))$ (c) mean squared displacement of diffusing particles (d) Scheme depicting significantly reduced particle diffusivity at the TEM membrane surface.

Further physical insight into the dynamics of OA was obtained from a scaling analysis of rotational and translation motion. Considering the hydrodynamic mobility under torque with an effective viscosity due to 2D confinement, we find the timescale for rotation (~0.1 s) during jump-to-contact is significantly faster than for translation (~60 s). This drastic difference the two approaching particles to sample all possible angles and accomplish a specific orientation for OA, irrespective of the energetic considerations and the characteristics of W_{st}.

Finally, we studied the energetic drivers for OA in this system by considering the granularity of solvent and ions in the context of classical Density Functional Theory (cDFT). The calculated forces (per area) between two ZnO flat crystal faces showed a qualitative difference between OA and non-OA cases (Fig. 5a) owing to the patterned charge distributions of the specific crystallographic faces.

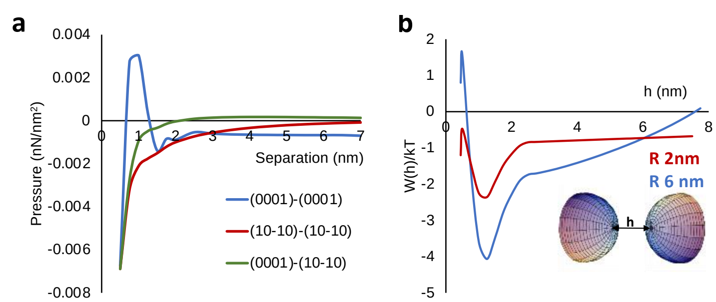

Figure 5. (a) Pressure between two (0001) facets (blue, OA), two (10-10) faces (red, OA) and (0001)-(10-10) faces (green, non-OA), in 10 mM zinc acetate dehydrate in methanol (b) Interaction potential between two spherical nano-particles with radii 2 nm (red line) and 6 nm (blue line) oriented along [001] direction.

Interestingly, a further calculation for 2 nm sized nanoparticles implementing the curvature effect indicates a barrier of ~ kT even for two like-charged (0001) faces of this polar crystal (Fig. 5b). The existence of negligible energy barriers and subtle energetic differences between OA and non-OA events implies that angular variations in *W(h)*, which would lead to interparticle torques, are crucial for attaining alignment, not the difference in the magnitude of *W*, as concluded in previously.[6, 7]

Amongst the most striking result of the experiments is that the attraction between particles is apparent already at h ~ 10 nm and torques begin to rotate particles at h > 5 nm (Fig. 3a-f). We are currently exploring physical rationales for the existence of such long-range forces and torques. Interaction of oppositely charged (0001) faces due to the intrinsic dipole nature of the ZnO crystal lattice in the presence of divalent salts and low dielectric media might lead to unique interactions due to electrostatics, as suggested previously.[8] However, from the viewpoint of electrodynamics, confinement of particles near the dielectric membrane of the TEM fluid cell is expected to produce an effective long-range dispersion interactions between the nanoparticles.[9] Finally, the electron beam may induce particle polarization, leading to dipolar interactions which scale as $1/h^3$ and therefore are expected to be long range.

Future Plans

Our future work on oriented attachment will tackle two important phenomena. The first is the source of the long range attractive forces and torques during ZnO OA. We expect a combination of cryo- and LP-TEM studies along with MD and cDFT studies at variable ionic strength to enable us to identify which source is responsible for the observed phenomenon. Cryo-TEM cannot capture the dynamics but can eliminate both the effects the electron beam and confinement near the TEM cell membrane. Moving to much higher ionic strength will dramatically alter the electrostatic interactions. The second is the process of alignment and transformation when nanoscopic and bulk phases differ. Here two systems — $NaYF_4$ and TiO_2 — for which we have, respectively, extensive data on particle evolution and interparticle forces, will provide the platform for the probing the dynamics and determining the mechanisms of those processes.

References

[1] J.J. De Yoreo, P.U.P.A. Gilbert, N.A.J.M. Sommerdijk et al., *Science*, **349** (2015) aaa6760.
[2] Pacholski, C.; Dipl.-Ing, A. K.; Weller, *Angew. Chem. Int. Ed.***, 41**,(2002**)** 1188.
[3] X. Zhang, Z. Shen, J. Liu et al., *Nature Comm.*, **8** (2017) 835.
[4] F. Caroleo, M. Stefanelli, G. Magna et al., *Org. Biomol. Chem.*, **17** (2019) 1113.
[5] H. Zheng, S.A. Claridge, A.M. Minor, A.P. Alivisatos, U. Dahmen, *Nano Lett.*, **9** (2009) 2460.
[6] D.A. Saville, J. Chun, J.L. Li et al., *Phys. Rev. Lett.*, **96** (2006) 018301.
[7] J. Chun, J.-L. Li, R. Car et al., *J. Phys. Chem. B*, **110** (2006) 16624.
[8] M. Trulsson, B. Jönsson, T. Åkesson et al. *Phys. Rev. Lett.*, **97** (2006) 068302.
[9] J. Lee, E. Nakouzi, D. Xiao et al., *Small*, e1901966.

Publications

Smeets P. J. M., Finney A. R., Habraken W., Nudelman F., Friedrich H., Laven J., De Yoreo J. J., Rodger P. M., and Sommerdijk N. (2017) A classical view on nonclassical nucleation. *Proceedings of the National Academy of Sciences of the United States of America* 114, (38) E7882-E7890. DOI. 10.1073/pnas.1700342114

Prakash A., Pfaendtner J., Chun J. H., and Mundy C. J. (2017) Quantifying the molecular-scale aqueous response to the mica surface. *Journal of Physical Chemistry C* 121, (34) 18496-18504. DOI. 10.1021/acs.jpcc.7b03229

Li, D. S., Wang H. L., Xiao D. D., Song M., Legg B., and Chun J. (2017) Investigating the magnitude and source of orientation-dependent interactions between TiO_2 crystal surfaces. *Nanoscale* 9, (29) 10173-10177. DOI. 10.1039/c7nr03535g

Li D. S., Chun J. H., Xiao D. D., Zhou W. J., Cai H. C., Zhang L., Rosso K. M., Mundy C. J., Schenter G. K., and De Yoreo J. J. (2017) Trends in mica-mica adhesion reflect the influence of molecular details on long-range dispersion forces underlying aggregation and coalignment. *Proceedings of the National Academy of Sciences of the United States of America* 114, (29) 7537-7542. DOI. 10.1073/pnas.1621186114

J. Lee, E. Nakouzi, M. Song, B. Wang, J. Chun and D. Li, (2018) "Mechanistic Understanding of the Growth Kinetics and Dynamics of Nanoparticle Superlattices by Coupling Interparticle Forces from Real-Time Measurements", *ACS Nano*, **12**, 12778–12787. DOI: 10.1021/acsnano.8b07880

Henzler K., Fetisov E. O., Galib M., Baer M. D., Legg B. A., Borca C., Xto J. M., Pin S., Fulton J. L., Schenter G. K., Govind N., Siepmann J. I., Mundy C. J., Huthwelker T., and De Yoreo J. J. (2018) Supersaturated calcium carbonate solutions are classical. *Science Advances* 4, (1) 11. DOI. 10.1126/sciadv.aao6283

D. Xiao, Z. Wu, M. Song, J. Chun, G.K. Schenter, and D. Li, (2018) "Silver Nanocube and Nanobar Growth via Anisotropic Monomer Addition and Particle Attachment Processes" *Langmuir*, **34**,1466–1472. DOI**:** 10.1021/acs.langmuir.7b02870

Liu L. L., Zhang S., Bowden M. E., Chaudhuri J., and De Yoreo J. J. (2018) In situ TEM and AFM investigation of morphological controls during the growth of single crystal $BaWO_4$. *Crystal Growth & Design* 18, (3) 1367-1375. DOI. 10.1021/acs.cgd.7b01216

Lim M. B., Hanson J. L., Vandsburger L., Roder P. B., Zhou X. Z., Smith B. E., Ohuchi F. S., and Pauzauskie P. J. (2018) Copper- and chloride-mediated synthesis and optoelectronic trapping of ultra-high aspect ratio palladium nanowires. *Journal of Materials Chemistry A* 6, (14) 5644-5651. DOI. 10.1039/c7ta07324k

Z. Shen , J. Chun, K.M. Rosso and C.J. Mundy, (2018) "Surface Chemistry Affects the Efficacy of the Hydration Force between Two ZnO($10\bar{1}0$) Surfaces" *J. Phys. Chem. C*, 122, 12259–12266. DOI: 10.1021/acs.jpcc.8b02421

Tao J. H., Nielsen M. H., and De Yoreo J. J. (2018) Nucleation and phase transformation pathways in electrolyte solutions investigated by in situ microscopy techniques. *Current Opinion in Colloid & Interface Science* 34, 74-88. DOI. 10.1016/j.cocis.2018.04.002

Lim, M.; Manandhar, S.; Pauzauskie, P.J.; "Patterning graphene oxide with optoelectronic tweezers." Applied Physics Letters, 113, 031106, (2018). DOI: 10.1063/1.5025225

Y. Chen, N. M. Washton, R. P. Young, A. Karkamkar, J. J. De Yoreo, K. T. Mueller, (2019) "Monitoring Ion Associations and Solvent Dynamics in the Formation of Cage-like Polyanions in Tetraalkylammonium Silicate Solutions" *Phys. Chem. Chem. Phys.* **21**, 4717-4720. DOI: 10.1039/c8cp07521b

A. Tuladhar, Z. A. Chase, M. D. Baer, B. A. Legg, A. D. Winkelman, J. Tao, S. Zhang, Z. Wang, C. Mundy, H-f. Wang, and J.J. De Yoreo, "Direct Observation of the Orientational Anisotropy of Interfacial –OH Groups at Muscovite Mica Surface" (2019) *J. Amer. Chem. Soc.* **141**, 2135−2142. DOI: 10.1021/jacs.8b12483

E.O. Fetisov , M. D. Baer, J. I. Siepmann, G.K. Schenter, S.M. Kathmann and C.J. Mundy, (2019) "The Statistical Mechanics of Solution-phase Nucleation: $CaCO_3$ Revisited", In: E. Maginn, Ed., Molecular Modeling Simulations: Applications and Perspectives.

M. Song J. Lee, B. Wang, B. A. Legg, S. Hu, J. Chun, D. Li, (2019) "In situ characterization of kinetics and mass transport of PbSe nanowire growth via LS and VLS mechanisms." *Nanoscale* **11**, 5874-5878. DOI: 10.1039/c9nr01200a

Zhou, X.; Xia, X.; Smith, B.E.; Lim, M.B.; Bard, A.; Pant, A.; Pauzauskie, P.J.; "Interface-dependent radiative lifetimes of single $NaYF_4$ up-conversion nanowires." *ACS Applied Materials & Interfaces*, 11, 22817-22823 (2019). DOI: 10.1021/acsami.8b17271

Lee, J.; Nakouzi, E.; Xiao, D.; Wu, Z.; Song, M.; Oplus, C.; Chun, J.; Li, D. (2019) "Interplay between short- and long-ranged forces leading to the formation of Ag nanoparticle superlattice," *Small* e1901966. DOI: 10.1002/smll.201901966

Controlling atomic scale ordering and phase transitions in oxide thin films

Yingge Du, Pacific Northwest National Laboratory

Program Scope

The overarching goal of this program is to *understand, predict, and ultimately control ion transport and topotactic phase transition processes occurring in structurally ordered transition metal oxide (TMO) thin films*. TMOs with interconnected, ordered vacant lattice sites enable facile, synchronous electron/ion intercalation reactions, and have been extensively investigated for energy conversion and storage applications, particularly for use as solid-state electrolytes, mixed electronic/ionic conductors, electrocatalysts, and electrodes in batteries and fuel cells. A topotactic phase transition (TPT), in which the final crystal lattice is closely related to that of the original material, may occur through the displacement and exchange of atoms as a result of intercalation. The fundamental questions we investigate are highly relevant to energy conversion and storage technologies, as such fundamental processes govern the mass-transport properties and failure mechanisms of widely used energy materials. TPTs occurring at the forefront of many catalytic reactions and electrode/electrolyte interfaces are often responsible for many of the challenges (e.g., safety concern due to volume expansion and capacity decrease after cycling due to loss of desired structure/phase) found in lithium ion batteries and solid oxide fuel cells.

We will investigate structurally and compositionally well-defined complex oxide films and thin-film based devices that will enable the facile intercalation of either small cations (e.g., Li^+, Na^+, and Ca^{2+}) or oxygen anions (O^{2-}). Our team will bring together 1) state-of-the-art synthesis of epitaxial oxide thin films and heterostructures; 2) detailed *in situ/in operando* characterization of the superstructures, film/substrate, film/film, film/vacuum, and film/solvent interfaces, and their evolution as a function of interfacial strain, doping level, and processing conditions; and 3) *ab initio* modeling of defect formation, structural ordering, and phase transition pathways and kinetics within the studied materials. The specific aims of this research are to: 1) correlate atomic-scale structural evolution, mesoscale topotactic phase transition, and macroscopic mass transport characteristics as TPTs occur; 2) understand how doping and interfacial strain can be used to modify the onset (e.g., temperature, electrochemical potential), dynamics, intermediate states, and trajectories of TPTs.

Recent Progress

The team was awarded another EMSL user proposal support (10/01/18-10/01/20). The needed instrument resources were granted, with an extra $46K in staff support. Postdocs currently supported by this program are Drs. Zhenzhong Yang (70%, on thin film growth and *in* *situ* TEM), Le Wang (50%, on thin film growth, characterization, and property measurement), and Linda Wangoh (50%, on thin films growth and synchrotron based materials characterization). We have developed collaborations with beamline scientists at Advanced Photon Source (APS/ANL), Advanced Light Source (ALS/LBNL), and Singapore Synchrotron Light Source (SSLS) to investigate the detailed structures of our samples.

Recent achievements led by this FWP are:

Epitaxial growth of $LiCoO_2$ (LCO) thin films with controlled orientations on $SrTiO_3$ substrates by pulsed laser deposition (PLD), and correlation of structural properties and atomic scale defects with substrate surface symmetry. $LiCoO_2$ is the most widely studied and used cathode material in lithium ion batteries with a layered structure. In its thin-film form, LCO can be integrated in novel all-solid-phase energy storage systems. However, an understanding of how Li ion transport is affected by atomistic details, such as interfacial defects and Li percolation network, which are still lacking. Through *ab initio* simulations, we reveal that antiphase boundary (APB) surfaces observed in well-defined LCO(001) thin films grown on $SrTiO_3$(111) (*JPCL* 9, 5515 (2018)) exhibit a rich structural variance due to their high susceptibility to defect formation. Some defect configurations have negligible or even negative formation energy and, hence, can occur spontaneously under experimental conditions. It is found that Li ion diffusion along APBs can proceed in a correlated mode, which leads to a dramatic decrease in activation energy with respect to their uncorrelated diffusion. Such a mechanism enables APBs to function as a viable ion transfer channel that couples in-plane Li ion diffusion pathways, thus facilitating Li transfer from one two-dimensional basin to another, potentially enabling new energy storage architectures.

We further investigated the redox chemistry and phase transitions in epitaxial $LiCoO_2$ thin films upon Li metal contact. Li dendrites are known to cause deleterious and, in many cases, catastrophic effects in the performance of Li rechargeable batteries. Using in situ transmission electron microscopy, we directly observe at the atomic scale the interaction of Li metal with well-defined, epitaxial thin films of $LiCoO_2$ (Fig. 1). A fast, spontaneous chemical reaction can be triggered once Li contact is made, leading to expansion and pulverization of $LiCoO_2$ and yielding Li_2O and Co metal as the final reaction products. A topotactic phase transition is identified close to the reaction front, resulting in the formation of CoO as a metastable intermediate. *In situ* TEM, in combination with *ab initio* simulations, reveal that a high density of grain and antiphase boundaries are formed at the reaction front. These are critical for enabling short-range topotactic phase transitions to form CoO and enable long-range Li propagation. This study provides insights into mitigating Li dendrites and guiding the design of more robust energy materials.

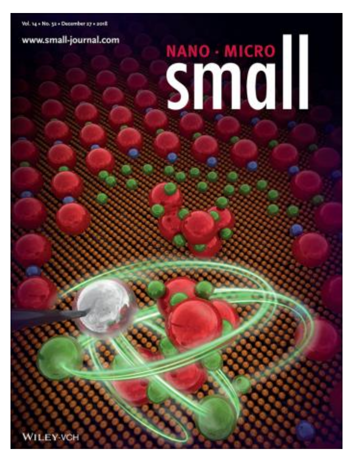

Fig. 1. Direct visualization of Li dendrite effect on $LiCoO_2$ cathode by in situ TEM. (*Small* 14, 1803108, 2018)

Being able to control the orientation of LCO enables a novel two-step synthesis approach for the epitaxial growth of Li-containing compounds. This approach involves the deposition of transition metal oxides (Li-free, e.g., WO_3 and TiO_2) directly on oriented epitaxial $LiCoO_2$ thin films to form stable Li-containing compounds as a result of Li out-diffusion from the LCO cathode layers. Li out diffusion results in the lithiation of WO_3 to form Li_2WO_4, a known solid state electrolyte, as confirmed by XRD and STEM. The epitaxial interface between $LiCoO_2$ and Li_2WO_4 is an ideal test bed for fundamental ion transport studies. By tuning the growth parameters, many stable intermediate compounds (e.g., Li_2WO_4, $LiMn_2O_4$, and $Li_4Ti_5O_{12}$) can be synthesized through this method. In addition, the structural and chemical evolution due to (de)lithiation in $LiCoO_2$ can provide atomistic insights into the failure mechanisms for cathodes during the charge/discharge processes. (Manuscript in preparation)

We also studied oxygen diffusion in model $SrFeO_{2.5+\delta}$ ($0 \leqslant \delta \leqslant 0.5$, SFO) systems. By tuning the synthesis and processing conditions, we were able to control the orientation of oxygen vacancy channels (OVCs) in Brownmillerite (BM) structured $SrFeO_{2.5}$ as well as tuning the oxygen stoichiometry. We show OVCs of BM-SFO thin films can be oriented differently on a $LaAlO_3$(001) substrate by controlling the oxygen partial pressure during growth and subsequent annealing conditions. The dynamic BM structure formation and evolution processes yield distinctively different optical and electronic properties, owing to the difference in both the oxygen stoichiometry and OVC configuration in the resultant films. With the established recipe, we generated semiconducting $SrFeO_{2.5}$ with vertically aligned OVCs and metallic, perovskite $SrFeO_3$ (P-SFO) standards so that the other intermediate states can be directly compared and understood as shown in Fig. 2. Our results offer further insight into the phase stability and oxygen-diffusion mechanisms, which is important for the predictive synthesis of novel functional materials. (*APL* 114, 231602 (2019)) Using *in situ* and environmental transmission electron microscopy, we also directly observed the phase transition from BM-$SrFeO_{2.5}$ to P-$SrFeO_3$. The directional migration of oxygen from $SrTiO_3$ substrate to $SrFeO_{2.5}$ is driven by an internal electric field generated by electron beam illumination during TEM imaging. Time-dependent *in situ* TEM studies reveal the reaction front, dynamics, and intermediate of the oxidation process. With the aid from DFT calculations, we provide atomic level understanding of the redox chemistry (Manuscript in preparation).

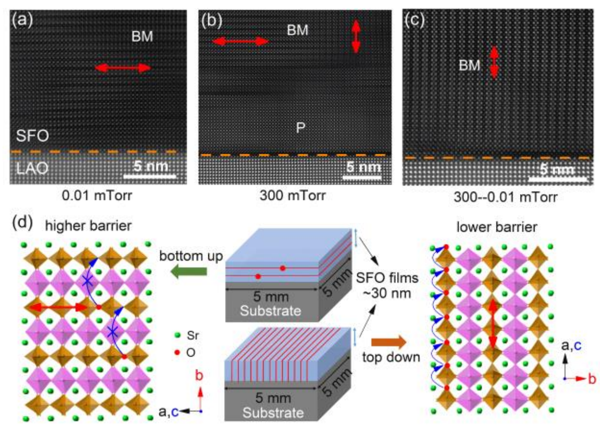

Fig. 2. STEM images and structural models showing that by varying the synthesis and processing conditions, $SrFeO_{2.5}$ can be grown with the OVCs either parallel or perpendicular to the $LaAlO_3$(001) substrate. (*APL* 114, 231602 (2019))

Future Plans

We are currently preparing three journal articles initiated by the Early Career program, reporting oxygen diffusion induced phase transition in $SrFeO_{2.5}$, delithiation induced topotactic phase transition in $LiCoO_2$, and lithiation induced phase transitions in transition metal oxides (e.g., WO_3 and TiO_2), respectively. Going forward, we will investigate ion diffusion and interface evolution processes occurring at the solid-solid interfaces (e.g., $SrFeO_{2.5}/SrTiO_3$, and Solid state electrolyte/$LiCoO_2$ deposited by PLD). In addition, we will be pursuing *in situ* study of multi-valent ion (e.g., Zn^{2+} and Mg^{2+}) diffusion induced topotactic phase transitions in oxides by ETEM and STEM.

Publications

1. L. Wang, Z. Yang, M. E. Bowden, and Y. Du*, Brownmillerite Phase Formation and Evolution in Epitaxial Strontium Ferrite Heterostructures, *Applied Physics Letters* 114, 231602 (2019).

2. Y. X. Qin, Z. Z. Yang, J. J. Wang, Z. Y. Xie, M. Y. Cui, C. M. Tian, Y. Du, and K. H. L. Zhang, Epitaxial Growth and Band Alignment of *p*-NiO/*n*-Fe_2O_3 Heterojunction on Al_2O_3(0001), Applied Surface Science 464, 488 (2019).

3. G. Li, Q. Shen, Z. Yang, S. Kou, F. Zhang, W. Zhang, H. Guo, and Y. Du*, Photocatalytic Behaviors of Epitaxial $BiVO_4$ (010) Thin Films, Applied Catalysis B: Environmental 248, 115 (2019).

4. L. Wang, K. A. Stoerzinger, L. Chang, X. Yin, Y. Li, C. S. Tang, E. Jia, M. E. Bowden, Z. Yang, and A. Abdelsamie, L. You, R. Guo, J. Chen, A. Rusydi, J. Wang, S. A. Chambers, and Y. Du*, Strain Effect on Oxygen Evolution Reaction Activity of Epitaxial $NdNiO_3$ Thin Films, ACS applied materials & interfaces 11 (13), 12941 (2019).

5. Z. Z. Yang, P. V. Ong, Y. He, L. Wang, M. E. Bowden, W. Xu, T. C. Droubay, C. Wang, P. V. Sushko, and Y. Du*, Direct Visualization of Li Dendrite Effect on $LiCoO_2$ Cathode by *In Situ* TEM, *Small* 14 (52) (2018).

6. P. V. Ong, Z. Z. Yang, P. V. Sushko, and Y. Du*, Formation, Structural Variety, and Impact of Antiphase Boundaries on Li Diffusion in $LiCoO_2$ Thin-Film Cathodes, *Journal of Physical Chemistry Letters* 9 (18), 5515 (2018).

7. L. Guo, Z. Yang, K. Marcus, Z. Li, B. Luo, L. Zhou, X. Wang, Y. Du*, and Y. Yang, MoS_2/TiO_2 heterostructures as nonmetal plasmonic photocatalysts for highly efficient hydrogen evolution, *Energy & Environmental Science* 11 (1), 106 (2018).

8. Y. He, J. C. Liu, L. L. Luo, Y. G. Wang, J. F. Zhu, Y. Du, J. Li, S. X. Mao, and C. M. Wang, Size-dependent dynamic structures of supported gold nanoparticles in CO oxidation

reaction condition, *Proceedings of the National Academy of Sciences of the United States of America* 115 (30), 7700 (2018).

9. X. Li, K. J. Zhang, D. Mitlin, E. Paek, M. S. Wang, F. Jiang, Y. Huang, Z. Z. Yang, Y. Gong, L. Gu, W. G. Zhao, Y. Du, and J. M. Zheng, Li-Rich LFNMO Cathodes: Atomic Scale Insight on the Mechanisms of Cycling Decay and of the Improvement due to Cobalt Phosphate Surface Modification, *Small* 14 (40), 1870014 (2018).

10. X. Chen, M. Vörös, J. C. Garcia, T. T Fister, D. B. Buchholz, J. Franklin, Y. Du, T. C. Droubay, Z. Feng, H. Iddir, L. A. Curtiss, M. J. Bedzyk, and P. Fenter, Strain-Driven Mn-Reorganization in Overlithiated $Li_xMn_2O_4$ Epitaxial Thin-Film Electrodes, *ACS Applied Energy Materials* 1 (6), 2526 (2018).

11. X. Li, K. J. Zhang, D. Mitlin, Z. Z. Yang, M. S. Wang, Y. Tang, F. Jiang, Y. Du*, and J. M. Zheng, Fundamental Insight into Zr Modification of Li- and Mn-Rich Cathodes: Combined Transmission Electron Microscopy and Electrochemical Impedance Spectroscopy Study, *Chemistry of Materials* 30 (8), 2566 (2018).

12. J. Y. Zhang, W. W. Li, R. L. Z. Hoye, J. L. MacManus-Driscoll, M. Budde, O. Bierwagen, L. Wang, Y. Du, M. J. Wahila, L. F. J. Piper, T. L. Lee, H. J. Edwards, V. R. Dhanak, and K. H. L. Zhang, Electronic and Transport Properties of Li-doped NiO Epitaxial Thin Films, Journal of Materials Chemistry C 6 (9), 2275 (2018).

13. K. H. L. Zhang, G. Q. Li, S. R. Spurgeon, L. Wang, P. F. Yan, Z. Y. Wang, M. Gu, T. Varga, M. E. Bowden, Z. H. Zhu, C. M. Wang, and Y. Du*, Creation and Ordering of Oxygen Vacancies at $WO_{3-\delta}$ and Perovskite Interfaces, ACS applied materials & interfaces 10 (20), 17480 (2018).

14. L. Wang, K. A. Stoerzinger, L. Chang, J. L. Zhao, Y. Y. Li, C. S. Tang, X. M. Yin, M. E. Bowden, Z. Z. Yang, H. Z. Guo, L. You, R. Guo, J. Wang, K. Ibrahim, J. S. Chen, A. Rusydi, J. L. Wang, S. A. Chambers, and Y. Du*, Tuning Bifunctional Oxygen Electrocatalysts by Changing the A-Site Rare-Earth Element in Perovskite Nickelates, *Advanced Functional Materials* 28 (39) (2018).

Ion transport and Structural Evolution of Solid Electrolytes: Ionic transport as a tool to monitor /direct processing of solid electrolytes

Nancy J. Dudney[1], Robert L. Sacci[1], Miaofang Chi[2], Xiaoming Liu[2], X. Chelsea Chen[1], Gabriel M. Veith[1], Thomas Malkowski[1]
[1]Chemical Sciences Division and [2]Center for Nanophase Materials Sciences, Oak Ridge National Laboratory, Oak Ridge, TN 37831

Program Scope

The overarching goal of this program is to address the challenges inherent in controlling the synthesis and fabrication of stable or metastable solid electrolyte phases with high room temperature ionic conductivity. Success in achieving our overarching goal we will be attained through three specific aims:

1) Understand intermediate structures or phases that will enable new synthesis routes.
2) Use ion transport and other in situ measurements to *monitor* the formation and evolution of grain, domain and defect structures during processing.
3) Understand reactions of the solid electrolytes with air, electrodes, or other electrolytes and assess if these can be used to direct synthesis of new metastable or multiphase structures.

Follow-on to the 2nd aim is the ultimate, and high-risk, goal to identify effective ways to use the ionic current or polarization to *direct* the defect and microstructure for the ionic materials.

To accomplish these goals, the program integrates synthesis investigations with advanced Li sensitive characterization methods such as neutron scattering/spectroscopy, ion transport measurements during synthesis, and low energy electron microscopy, along with the collaboration for different theoretical tools to probe/predict processes at different length and time scales. The focus on the identification, synthesis, and processing of ionically conducting solid state materials, of both inorganic and polymeric materials, is critical for next generation energy storage, as identified in several DOE Basic Research Needs reports. The ability to use synthesis to direct and control ionic conduction is challenging due to the intrinsic diffusivity of the mobile alkali ions. When successful, we will enable the development of new controlled synthesis approaches to direct solid-state electrochemistry and reactivity.

Recent Progress

1. **Ionic transport as a tool to *monitor* processing of solid electrolytes.** Corresponding to Specific Aim 2, impedance spectroscopy is implemented as a tool to monitor the structural change during the synthesis and processing of solid electrolytes. The synthesis/processing of three representative solid-state electrolytes is being monitored:

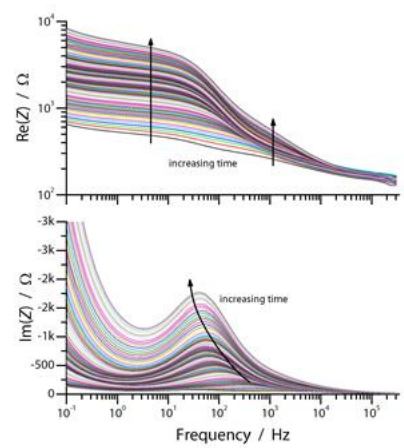

Figure 1. Grain boundary resistance of Li_3OBr gradually changes when under 100 psi pressure.

1) *The grain boundary resistance of Li rich antiperovskite under pressure*. Li_3OBr was synthesized through an organic metathesis reaction to be phase pure and proton-free. The resulting product was pressed into a pellet and placed into a custom-made impedance cell where 100 psi of pressure was

applied and held for one week. Being relatively soft, the pellet was dense; yet the grain boundary resistance, extracted from the impedance (Figure 1), increased over time under the constant pressure (Figure 1). We are also using dynamic impedance spectroscopy to follow the kinetics of structural changes during quenching with < 1 s time resolution. Analysis is underway to determine the physical process leading to the increasing resistance.

2) *Crystallization of $Li_{0.33}La_{0.56}TiO_3$ (LLTO) film*. The crystallization of a sol-gel coated amorphous LLTO film on STO single crystal was monitored in situ with transmission electron microscopy. As shown in Figure 2, at 500℃ crystalline LLTO formed epitaxially at the interface. At 700℃, nucleation of bulk grains was observed with the formation of grain boundaries.[1] An impedance spectroscopy study is underway to monitor the crystal growth kinetics of the same system to correlate transport properties with the different stages with crystal growth.

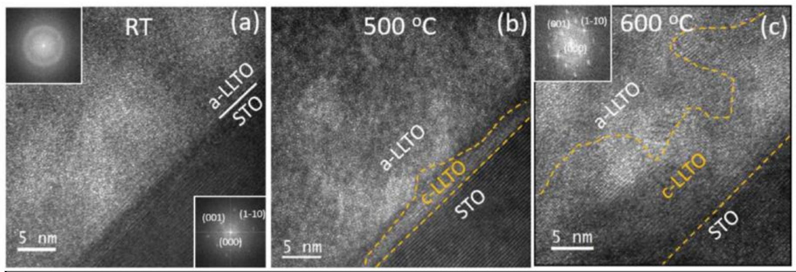

Figure 2. Amorphous LLTO crystallization on STO single crystal.

3) *Crystallization of polymer electrolytes.* The conductivity of polymer electrolyte is quite sensitive to its crystalline structure below the melting temperature (50 to 65℃). Using quasi-elastic neutron scattering (QENS), the segmental relaxation of poly(ethylene oxide) + lithium salt was examined. We discovered one order of magnitude decrease in the structural relaxation time of the polymer electrolyte when the sample just cooled down to 30℃ compared to the same temperature equilibrated for one week. This corresponded to a 3-fold increase in the ionic conductivity. In a collaboration with Prof. Sanat Kumar group from Columbia University, a polymer electrolyte consisting of poly(ethylene oxide) (PEO), lithium bis(trifluoromethanesulfonyl)imide (LiTFSI) and silica nanoparticles with poly(methyl methacrylate) surface functionalization was monitored by impedance spectroscopy. The higher the nanoparticle loading, the slower conductivity reached equilibrium value (Figure 3).

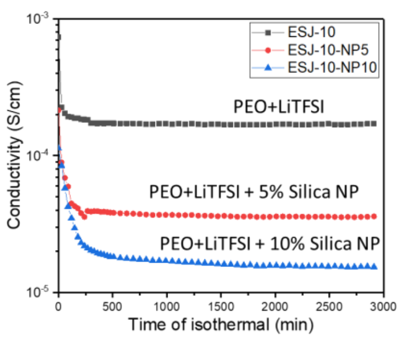

Figure 3. Conductivity during the crystallization of PEO polymer electrolytes with the presence of silica nanoparticles at 54℃.

2. **Ionic transport as a tool to *direct* processing of solid electrolytes.** Using an AC or DC field to drive ions through materials and interfaces is a new approach in material synthesis and processing of ion conducting materials. We have explored several new routes to influence and perhaps improve the solid electrolyte processing by forcing the electric field (and resulting current) through the material.

1) *Phonon softening of lattice dynamics.* We observed that exciting the ion motion at resonance can lead to a softening of the phonon modes at much higher frequency for the Li_3OBr antiperovskite (Figure 4). Here the complex impedance is used to find the resonance frequency

of bulk ion conduction, which relates to ion motion at an excited state. An outcome of the electric field oscillating at ion hopping resonance is that phonons related to the motion of the mobile ions should soften, i.e. decrease in intensity. The phonons that are expected to undergo softening are zone-boundary ones, which are only detectable using inelastic neutron scattering. Our preliminary tests are showing that this is indeed the case for several different lithium solid electrolytes.

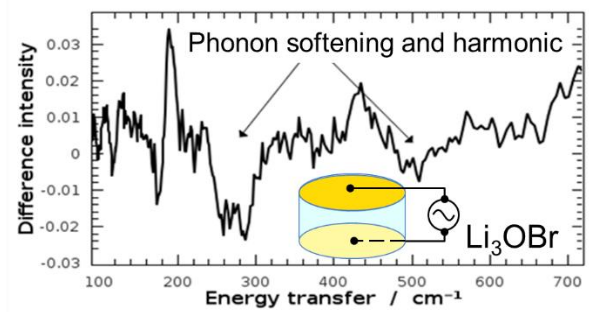

Figure 4. Observed phonon-softening of Li_3OBr. Intensity difference is for AC frequency "on" minus "off" resonance.

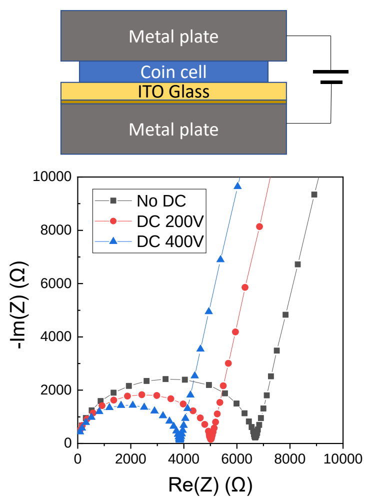

Figure 5. Using DC electric field to align ion conducting path in polymer electrolytes.

2) *Using DC electric field to align ion conducting path in polymer electrolytes.* When a polymer electrolyte PEO + lithium triflate is in the semi-crystalline state, the crystalline domains do not contribute to ion conduction as they exclude the lithium salts. The conductivity of the polymer electrolyte in the amorphous phase is greatly decreased due to the confinement by the randomly oriented crystalline domains. Here we use a DC electric field to direct the ion-conducting path through alignment of crystalline domains during crystallization. A piece of polymer electrolyte was placed in between two metal plates with a glass insulator to prevent breakdown (Figure 5). A DC voltage of 200V to 400V was applied during the isothermal crystallization of the polymer electrolyte at 54 °C and held for 16 hours. The resistance of the polymer electrolyte decreased with increasing DC field. Investigations are underway to discover the underpinnings of the effect of the DC field.

3. **Fabricating composites of ion-conducting polymer and ceramic: identifying and minimizing ion-transport barrier at the interface.** In a polymer-ceramic composite where both components are ion conductors, the interface plays a difficult role. Recently, we discovered that there is a large interfacial resistance for ion transport between a model polymer and ceramic electrolyte.[2,3] Currently there are no design principles to guide materials choice and processing to reduce a barrier that may result from polarization, reduced mobility or concentration of the mobile ions, or barriers related to solvation. Ideally with better knowledge of ion motion across interfaces these effects can be anticipated and alleviated by materials design. The 3rd specific aim is directed to the underlying mechanisms and reaction processes that impact such ionically active interfaces.

Recently, we used quasi-elastic neutron scattering to identify ion transport barrier between a model polymer electrolyte, PEO with dissolved LiTFSI salt, and a model ceramic electrolyte, doped $Li_xAl_yTi_2(PO_4)_3$-type ceramic from Ohara corporation (Ohara ceramic). The composite was fabricated by simply mixing the polymer and untreated ceramic powder in water followed by drying. We discovered that in the absence of LiTFSI, Ohara ceramic posed negligible change in the segmental dynamics of PEO. In contrast, with the presence of LiTFSI, Ohara ceramic slowed down the segmental motion of PEO chains by ~60% compared to neat PEO + LiTFSI. The intrinsic ionic conductivity of the polymer phase in the composite decreased by ~30% compared to the neat polymer electrolyte. The underpinnings of these results may be that polymer chains in the vicinity of the ceramic surface are less mobile due to coordination with surface bound lithium ions (Figure 6).

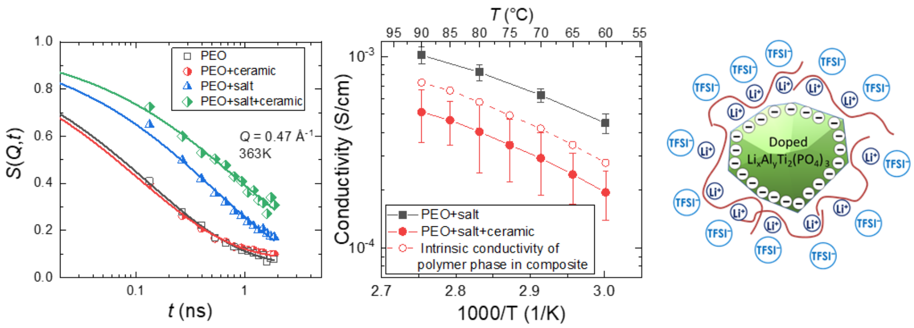

Figure 6. Affinity at ceramic surfaces and Li^+ causes the polymer PEO chains near the ceramic surface to become less mobile through coordination with bound Li^+, which leads to a decrease in segmental mobility and ion conductivity.

Accordingly, we explored two approaches to minimize interfacial ion-transport barrier when forming the composite electrolyte. The first approach was to graft a layer of short PEO chains onto the surface of the ceramic. The hypothesis is that the effect of ceramic on the segmental motion of the polymer electrolyte will be eliminated by creating a charge-neutral surface. Another approach was to covalently bound the $TFSI^-$ anion onto the backbone of the polymer electrolyte. The hypothesis is that this will minimize the space charge layer near the polymer-ceramic electrolyte interface. The details of these approaches will be presented in the poster.

Future Plans

We will continue to explore multiple ways that ionic transport can be used to study processing pathways and kinetics, and ultimately how the current or polarization act to direct the formation of lattice defects and microstructural features. Further we find that interface reactions between ionic solids or when a solid electrolyte is equilibrated with gases or solvents also play key roles in controlling the synthesis. Our studies will coordinate a suite of in situ methods and theoretical calculations to elucidate the generalized rules that direct synthesis of ionic materials. The impact of this work will enable new and better solid electrolytes that may lead to safer, lower cost and higher energy dense batteries. More broadly many materials have mobile ions that may influence synthesis and processing routes, so we anticipate these will be impacted by the research addressed in this work. Further, functional solid-state ionic materials and devices impact a wide range of technologies beyond energy storage.

References

1. Xiaoming Liu, Qiang Zheng, Michael Zachman, Yan Wang, Nancy Dudney, Ming Tang, Miaofang Chi, “ Real-time observation of atomic-scale eutectoid solid-state crystallization,” in preparation.

2. Chen, X. C.; Liu, X.; Pandian, A. S.; Lou, K.; Delnick, F. M.; Dudney, N. J., *ACS Energy Letters* **2019**, 4, 1080-1085.

3. Pandian, A. S.; Chen, X. C.; Chen, J.; Lokitz, B. S.; Ruther, R. E.; Yang, G.; Lou, K.; Nanda, J.; Delnick, F. M.; Dudney, N. J., *Journal of Power Sources* **2018**, 390, 153-164.

Publications

Xiaoming Liu, Yan Chen, Zachary D. Hood, Cheng Ma, Seungho Yu, Asma Sharafi, Hui Wang, Ke An, Jeff Sakamoto, Donald J. Siegel, Yongqiang Cheng, Niina H. Jalarvo, and Miaofang Chi, "Elucidating the mobility of H^+ and Li^+ ions in $(Li_{6.25-x}H_xAl_{0.25})La_3Zr_2O_{12}$ *via* correlative neutron and electron spectroscopy" *Energy Environ. Sci*., DOI: 10.1039/c8ee02981d

X. Chelsea Chen, Robert L. Sacci, Naresh C. Osti, Madhusudan Tyagi, Beth Armstrong, Yangyang Wang, Max J. Palmer and Nancy J. Dudney, "Study of Segmental Dynamics and Ion Transport in Polymer-Ceramic Composite Electrolytes by Quasi-elastic Neutron Scattering", Themed collection of Charge Transporting Nanostructured Polymers for Electrochemical Systems, *Molecular Systems Design and Engineering*, 2019, **4**, 379-385

Z. D. Hood, H. Wang, A. S. Pandian, R. Peng, K. D. Gilroy, M. Chi, C. Liang, Y. Xia, "Fabrication of Submicron-thick Solid Electrolyte Membranes of β-Li_3PS_4 via Tiled Assembly of Nanoscale, Plate-like Building Blocks," *Adv. Energy Mater*. 2018, 1800014.

B. H. Shen, G. M. Veith, B. L. Armstrong, W. E. Tenhaeff, R. L. Sacci, "Predictive design of shear-thickening electrolytes for safety considerations" *J. Electrochem. Soc*. **164**, 12, A2547-2551 (2017).

Yin, K., Zhang, M., Hood, Z. D., Pan, J., Meng, Y. S., and Chi, M. F., "Self-Assembled Framework Formed During Lithiation of SnS_2 Nanoplates Revealed by in Situ Electron Microscopy" *Accounts of Chemical Research* **50** 1513 (2017).

N. Dudney, "Evolution of the lithium morphology from cycling of thin film solid state batteries" *J. Electroceram*. **38**, 222 (2017). Invited article for issue on Solid State Batteries

B. H. Shen, G. M. Veith, W. E. Tenhaeff, "Silicon surface tethered polymer as artificial solid electrolyte interface" *Sci. Rep*. **8**, 11549 (2018).

T. Aytug, M. S. Rager, W. Higgins, F.G. Brown, G. M. Veith, C. M. Rouleau, H. Wang, Z. D. Hood, S. M. Mahurin, R. T. Mayes, P. C. Joshi, T. Kuruganti, "Vacuum-Assisted Low-Temperature Synthesis of Reduced Graphene Oxide Thin-Film Electrodes for High-Performance Transparent and Flexible All-Solid-State Supercapacitors" *ACS Materials and Interfaces* **10**(13), 11008-11017 (2018).

W. Li, X. Liu, H. Celio, P.Smith, A. Dolocan, M. Chi, A. Manthiram, "Mn versus Al in Layered Oxide Cathodes in Lithium-Ion Batteries: A Comprehensive Evaluation on Long-Term Cyclability" *Advanced Energy Materials* **8**(15), 1703154 (2018).

Windmüller, C.A. Bridges, C.-L. Tsai, S. Lobe, C. Dellen, G. M. Veith, M. Finsterbusch, S. Uhlenbruck, O. Guillon, "Impact of Fluorination on Phase Stability, Crystal Chemistry, and

Capacity of $LiCoMnO_4$ High Voltage Spinels" *ACS Applied Energy Materials*, **1,** 715-724 (2018).

M. H. Zhang, K. B. Yin, Z. D. Hood, Z. Bi, C. A. Bridges, S. Dai, Y. S. Meng, M. P. Paranthaman, and M. F. Chi, "In situ TEM observation of the electrochemical lithiation of N-doped anatase TiO_2 nanotubes as anodes for lithium-ion batteries" *J. Mater. Chem. A*, **5** 20651-20657 (2017).

Robert L Sacci, Michelle L Lehmann, Souleymane O Diallo, Yongqiang Q Cheng, Luke L Daemen, James F Browning, Mathieu Doucet, Nancy J Dudney, Gabriel M Veith, "Lithium Transport in an Amorphous Li_xSi Anode Investigated by Quasi-elastic Neutron Scattering" *The Journal of Physical Chemistry C*, **121**, 21, 11083-11088

Growth Mechanisms and Controlled Synthesis of Nanomaterials (ERKCS81): Addressing the synthesis challenges for 2D materials with nonequilibrium processing and in situ diagnostics

David B. Geohegan,[1] Kai Xiao,[1] Alex Puretzky,[1] Gyula Eres,[2] Mina Yoon,[1]
Gerd Duscher,[2,3] Christopher M. Rouleau,[1]
Postdocs: Yu-Chuan Lin,[1] Yiling Yu[3] Students: Chenze Liu[3] and Yiyi Gu[3]
[1]Center for Nanophase Materials Sciences and [2]Materials Science and Technology Division, Oak Ridge National Laboratory, Oak Ridge, TN 37831
[3]Dept. of Materials Science and Engineering, Univ. of Tennessee, Knoxville, 37996

Program Scope

This program addresses a critical research need in synthesis science to understand, predict, and ultimately direct the synthesis of novel quantum nanomaterials, especially atomically-thin 2D materials, and hierarchically assembled oxide nanostructures that are crucial to DOE's energy mission. The remarkable properties of such quantum nanomaterials result from confinement, interfacial interactions, and dimensionality effects at the same length scales where fundamental synthesis questions arise. The research approach therefore integrates real-time diagnostic synthesis environments with theoretical and computational methods to understand the mechanisms of formation and assembly of the "building blocks" of nanomaterials, coupled with the development of new synthetic platforms that will permit their controllable assembly into quantum nanomaterials with desired properties. In order to access novel metastable states, the program emphasizes the development of synthesis methods and real-time diagnostics to both induce and probe chemical and physical transformations away from thermodynamic equilibrium, combining laser driven synthesis and processing with laser spectroscopic diagnostic techniques, along with *in situ* electron microscopy, and neutron scattering. By revealing the kinetics, energetics, and interactions governing the assembly of nanostructures from well-defined "building blocks" the program endeavors to develop methods for nanomaterial synthesis integrating new approaches coupling theory/computation and experiment for adaptive real-time control with feedback over multiple length scales.

Recent Progress

Addressing the crosscutting challenges in the controllable synthesis of nanostructures and thin films requires identification of the reaction pathways, key precursors, and assembly kinetics on different time and length scales. We use the nonequilibrium features of pulsed laser deposition (PLD) to address this problem by tuning the ablation process to modify the kinetic energies and fluxes of species to study non-equilibrium processes, such as defect creation and substitution of atoms within existing crystals to effect the formation of alloys, or phase transformations. On the other hand, we have learned how to tune the pulsed laser ablation process to produce and selectively "soft-land" fluxes of ultrasmall (3-5 nm) amorphous nanoparticles to substrates by PLD using *in situ*, time-resolved intensified CCD-array imaging and plasma diagnostics, a regime we call "nanoparticle PLD".[1] We have shown previously that these amorphous, ultrasmall nanoparticles (UNPs) serve as "building blocks" in the assembly of nanostructures, thin films, and 2D crystals that occur by the non-classical mechanisms of crystallization by particle attachment (CPA).[1] To better understand these phenomena, and understand how 2D layers grow from such precursors, we have recently developed new laser processing environments to provide controllable, stepwise processing at both the microscale (using optical imaging and spectroscopy) and within the TEM (using electron imaging and spectroscopy). In this talk, we will present our recent progress in these areas.

PLD provides a rather unique, digital pulsed plasma that, with energies of ~100 eV can drive the formation of metastable phases of novel materials during synthesis, such as amorphous diamond.[2] Recently, as shown in **Figure 1**, we have employed PLD of pure Se to understand the thresholds for the creation of S vacancies and the replacement of S within monolayers and bilayers of single-crystalline WS_2 (that we had previously grown by VTE and transferred to TEM grids). The rather unique Se plasma plume was characterized by ion probe measurements and intensified gated CCD imaging, and could be slowed using collisions with background Ar from kinetic energies of 25 eV/atom in vacuum to 1.7 eV/atom over a distance of 10 cm in 50 mTorr Ar. Atomic resolution TEM imaging, XPS, and Raman spectroscopy were used to reveal the thresholds for partial substitution in the topmost S atoms within the ML WS_2, as well as the threshold for the bottom S atoms, permitting full conversion of the monolayer. These thresholds agree with theoretical predictions of Komsa, et al.[3] These results, essentially developing the techniques for ion implantation and defect control in monolayers and bilayers, demonstrate regimes for the controlled synthesis and processing of 2D materials to form alloys, implant dopant atoms, and explore phase conversion processes using arbitrary source atoms in the < 20 eV range.

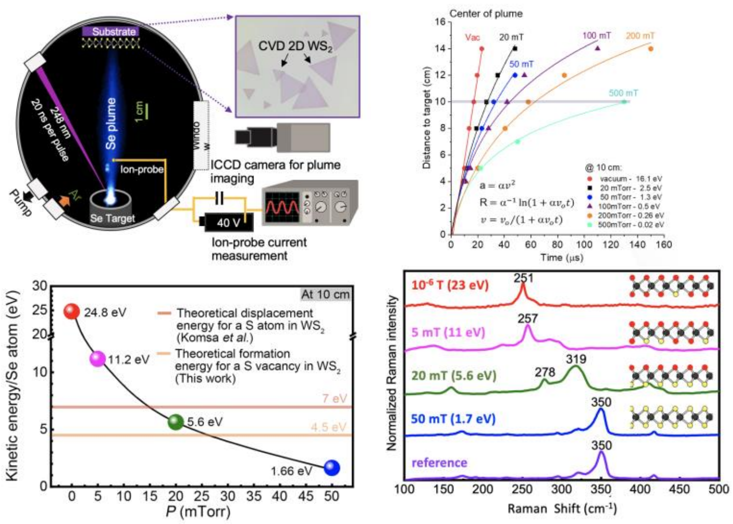

Figure 1. In situ diagnostics of 2D materials synthesis by PLD: Selenization of WS_2 with controlled kinetic energy beams of Se. (top) Gated ICCD imaging and ion probe current measurements are used to record and adjust the kinetic energy and flux of species arriving at existing, freestanding 2D WS_2 crystals through the use of inert background gas (Ar) collisions. The maximum kinetic energies per Se atom can be tuned to reveal thresholds in the <20 eV range for the formation of defects and substitution of atoms for S atoms in the top and bottom of a WS_2 monolayer crystal as evidenced in TEM, XPS, and Raman spectra (shown at lower right, 600 shots, 250°C). (*in preparation)***.**

These low ion energy regimes influence approaches for direct PLD of 2D materials. Recently, we developed simple optical reflectivity diagnostics to monitor and control

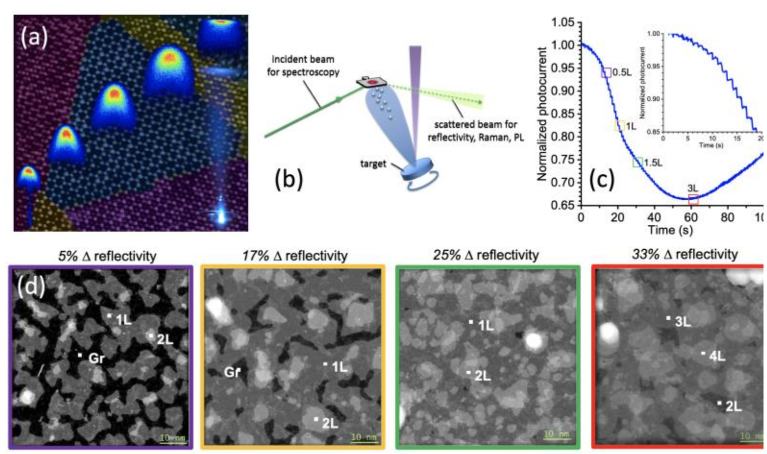

Figure 2. PLD of 2D $MoSe_2$ controlled by *in situ* optical reflectivity. (a) Gated-ICCD imaging record gas-phase (~<100 μs) dynamics of plasma plume deposition processes. (b,c) In situ optical reflectivity record the shot-to-shot deposition of $MoSe_2$ on SiO_2/Si substrates, allowing controllable deposition of nominal monolayers, in accordance with model predictions. (d) HAADF-AR-Z-STEM of $MoSe_2$ deposited onto graphene TEM grids at 600°C for different changes in optical reflectivity show the partial layer coverage for comparison. These diagnostics allow deposition rates to be controlled in real time. (*in preparation*)

the nucleation and growth of 2D materials by PLD, as shown in **Figure 2**. By tuning the thickness of SiO_2 layers on Si substrates, we were able to achieve large changes in optical reflectivity per nominal monolayer when 2D crystals such as $MoSe_2$ or WSe_2 were deposited by PLD. These *in situ* diagnostics, once calibrated with *ex situ* TEM and AFM morphological analysis, allow an understanding and control of nucleation and growth processes. The steps evident in Fig. 2c reflect the digital deposition corresponding to each laser pulse. The timescales for this deposition can be compared with the ICCD imaging of the pulsed plasma propagation schematically illustrated in Fig. 2a. Processes such as subsequent desorption (e.g., of Se at higher temperatures) can also be observed. Such diagnostics, coupled with the aforementioned control of the PLD flux and kinetic energy, will allow the exploration of 2D materials nucleation and growth kinetics. The same optical reflectivity diagnostics should be implemented for CVD chambers as well.

The formation of thin films and nanostructures involving the stepwise incorporation of different "building block" precursors, from atoms and molecules to ultrasmall amorphous nanoparticles, is difficult to capture in real-time at the nanoscale. To explore these phenomena, we are employing laser-driven synthesis and processing of precursors within two reactors. The first is a high vacuum optical microchamber that is positioned underneath an optical microscope that is coupled with a small excimer laser and other laser sources to allow pulsed-to-CW laser processing of microns-sized regions of specimens (either existing crystals, or precursor materials) with *in situ* Raman, photoluminescence, and second-harmonic generation spectroscopy. The second is a 200mW laser (two wavelengths 985nm, and 415 nm) that is nanopositioned within the Libra 200 TEM at the University of Tennessee (at JIAM, with Profs. Duscher and Rack) to provide chopped pulses (or CW) of illumination to ~5 μm regions of TEM grids during *in situ* TEM imaging, SAED, and EELS.

As shown in **Figure 3**, we are exploring how amorphous precursors undergo crystallization on a variety of TEM-grid substrates, both amorphous and crystalline. In general, we find that the amorphous precursors crystallize in a stepwise fashion with increasing laser energy, in accordance with the Ostwald-Lussac law of stages and can be trapped in metastable states. We observe the convergence and flattening of the precursor material into two-dimensions, and orientational alignment driven by lattice matching to the substrate. By comparison to the excellent alignment to the $MoSe_2$ substrate of Figure 3, for example, only polycrystalline films with random

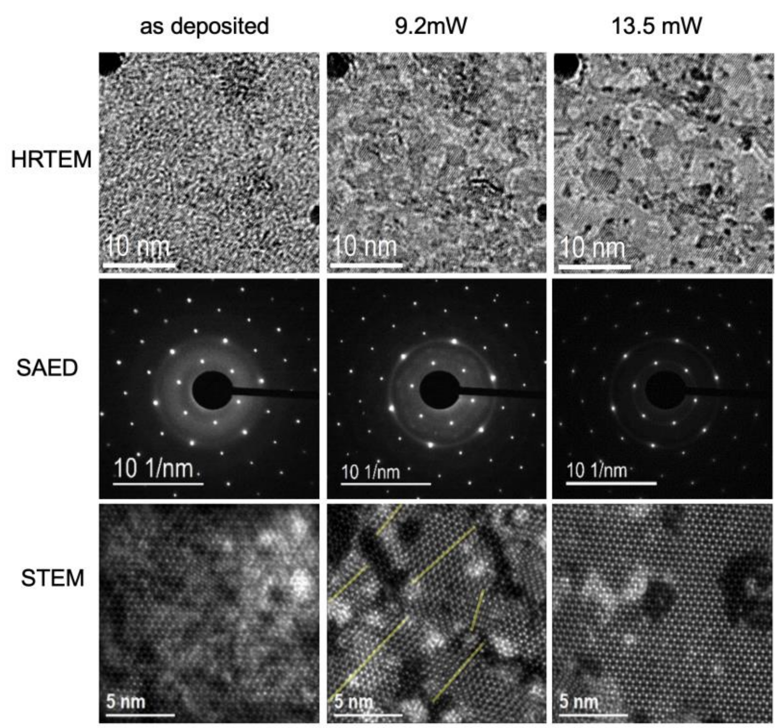

Figure 3. *in situ* TEM, SAED, and EELS of the laser processing assembly of amorphous WSe_2 'building blocks' into 2D crystals on $MoSe_2$ substrates. Using a 985nm laser within a HRTEM, PLD-deposited amorphous-TMDC precursors are processed shot-by-shot at different laser powers to induce and understand different crystallization and assembly pathways on different substrates, such as freestanding graphene or (as shown here) $MoSe_2$. SAED reveals the progression of amorphous, to polycrystalline, and finally epitaxial crystalline WSe_2 on $MoSe_2$. Corresponding atomic-resolution Z-STEM images reveal the guiding role of the lattice-matched substrate in guiding crystallization by particle attachment and merging of islands. (*in preparation)*

crystal orientation can be obtained on graphene, and different kinetics and metastable states are observed. Dewetting of the 2D film can be induced, and a variety of crystallization by particle attachment phenomena have been observed involving both 3D nanoparticles and 2D flakes. This platform, utilizing laser-driven thermal and photolytic processes of predeposited precursors, provides insight on the processes involved during typical growth. However, this approach differs from the stepwise delivery and crystallization of precursor species during typical growth by PLD or VTE. By adjusting the precursor species and annealing procedure, both pathways can result in strikingly similar epitaxial WSe_2 crystals on $MoSe_2$.

Future Plans

Using *in situ* time-resolved reflectivity (Fig. 2) as a diagnostic technique, we will explore the effects of control over nucleation and growth rates on the crystallite size and film quality during the direct synthesis of 2D TMDC crystals by PLD. We are implementing *in situ* Raman spectroscopy during PLD at elevated temperatures to assess crystalline quality and layer number, and will target individual crystals spectroscopically using remote microscopy. Using our time-resolved plasma diagnostics we will explore the effects of tuning the precursor species (from atoms to nanoparticles) and associated kinetic energies via background gas collisions (a) directly in PLD film growth at high temperatures, and (b) for the deposition of convertible amorphous precursors at low temperature. Through the use of existing 2D TMDC single crystals as witness plates to be analyzed by *in situ* diagnostics and *ex situ* atomic-resolution STEM, we will continue to explore the thresholds for atomic displacements and ion implantation on monolayers and few-layers using PLD plumes (as demonstrated in Fig. 1). The synthesis of novel heterostructures by atomic replacement (as shown in Fig. 1), as well as doped layers and alloys, will be explored using KE's in this ~ < 20 eV/atom range. Conversely, by "soft-landing" amorphous material with very low KE, principally clusters and nanoparticles via 'nanoparticle-PLD,' we have the unique opportunity to explore the mechanisms of crystallization by particle attachment by controllably post-processing these precursors. We seek to understand pathways to crystallization and novel metastable nanophases both at the *individual* particle level and in *ensembles*. These mechanisms will be investigated for different systems, including TiO_2 and transparent conducting oxides, TiN – a plasmonic refractory material, as well as the TMDC precursors for 2D crystals. We develop stepwise, pulsed laser processing techniques in several environments: first, in a vacuum microchamber with *in situ* optical micro-spectroscopy techniques on TEM-grid-based substrates, second, directly in the HRTEM (as shown in Fig. 3) using imaging, EELS, and SAED, and third, at larger ~mm scale. These platforms permit multiple experiments with rapid feedback control, consistent with the priority research directions for synthesis to "*integrate…in situ characterization tools to achieve directed synthesis with real-time adaptive control*". A novel nanoparticle PLD system employing 2 lasers will explore the synthesis of novel mixed phase nanoparticle-based coatings using multiple targets and photolytic processing to incorporate nanoparticle building blocks on a variety of practical substrates, with relevance to additive manufacturing of energy-relevant coatings.

References

1. M. Mahjouri-Samani, M.Tian, A. A. Puretzky, M. F. Chi, K. Wang, G. Duscher, C. M. Rouleau, G. Eres, M. Yoon, J. Lasseter, K. Xiao, and D. B. Geohegan, "Nonequilibrium Synthesis of TiO_2 Nanoparticle "Building Blocks" for Crystal Growth by Sequential Attachment in Pulsed Laser Deposition," *Nano Letters* **17**(8), 4624-4633 (2017).
2. D. H. Lowndes, D.B. Geohegan, A.A. Puretzky, D.P. Norton, C.M. Rouleau, "Synthesis of novel thin-film materials by pulsed laser deposition," *Science* **273**, 898 (1996).
3. H.-P. Komsa, J. Kotakoski, S. Kurasch, O. Lehtinen, U. Kaiser, and A. V. Krasheninnikov, "Two-Dimensional Transition Metal Dichalcogenides under Electron Irradiation: Defect Production and Doping," *Phys. Rev. Lett.* **109**, 035503 (2012).

DOE Sponsored Publications in the Last Two Years

1. K. Wang, A. A. Puretzky, Z. Hu, B. R. Srijanto, X. Li, N. Gupta, H.Yu, M. Tian, M. Mahjouri-Samani, X. Gao, A. Oyedele, C. M. Rouleau, G. Eres, B. I. Yakobson, M. Yoon, K. Xiao, and D. B. Geohegan "Strain tolerance of two-dimensional crystal growth on curved surfaces," *Science Advances* **5** (5), eaav4028 (2019).
2. X. Sang, X. Li, A.A. Puretzky, D.B. Geohegan, K. Xiao, R.R .Unocic, "Atomic Insight into Thermolysis-Driven Growth of 2D MoS_2," *Adv. Funct. Mater.* 1902149 (2019).
3. A. D. Oyedele, S. Z. Yang, T. Feng, A. V. Haglund, Y. Gu, A. A. Puretzky, D. Briggs, ... "Defect-mediated phase transformation in anisotropic 2D $PdSe_2$ crystals for seamless electrical contacts," *J. Am. Chem. Soc. DOI:* 10.1021/jacs.9b02593 (2019).
4. D. B. Brown, W. Shen, X. Li, K. Xiao, D. B. Geohegan, S. Kumar "Spatial mapping of thermal boundary conductance at metal-molybdenum diselenide interfaces," *ACS Appl. Mater. Interfaces* **11**, 14418 (2019).
5. E. Inclan, M. Yoon "Performance of biologically inspired algorithms tuned on TiO2 nanoparticle benchmark system," *Computational Materials Science* **165**, 63 (2019).
6. N. Briggs, S. Subramanian, Z. Lin, X. Li, X. Zhang, K. Zhang, K. Xiao, D. Geohegan, R. Wallace, L.-Q. Chen, M. Terrones, A. Ebrahimi, S. Das, J. Redwing, C. Hinkle, K. Momeni, A. van Duin, V. Crespi, S. Kar, J. A. Robinson, "A Roadmap for Electronic Grade 2D Materials," *2D Materials* **6**, 022001 (2019).
7. X. Li, J. Zhang, A. A. Puretzky, A. Yoshimura, X. Sang, Q. Cui, Y. Li, L. Liang, A. W. Ghosh, H. Zhao, R. R. Unocic, V. Meunier, C. M. Rouleau, B. G. Sumpter, D. B. Geohegan, and K. Xiao, "Isotope-Engineering the Thermal Conductivity of Two-Dimensional MoS_2" *ACS Nano* **13**, 2481–2489 (2019).
8. M. G. Stanford, Y.-C. Lin, M. G. Sales, A. N. Hoffman, C. T. Nelson, K. Xiao, S. McDonnell, P. D. Rack, "Lithographically patterned metallic conduction in single-layer MoS_2 via plasma processing," *npj 2D Materials and Applications* **3**, 13 (2019).
9. O. Maksov, O. Dyck, K. Wang, K. Xiao, D. B. Geohegan, B. G. Sumpter, R. K. Vasudevan, S. Jesse, S. V Kalinin, M. Ziatdinov, "Deep learning analysis of defect and phase evolution during electron beam-induced transformations in WS_2," *npj Computational Materials* **5**, 12 (2019).
10. M. Tian, C. Liu, J. Ge, D. Geohegan, G. Duscher, G. Eres, "Recent progress in characterization of the core–shell structure of black titania," *Journal of Materials Research*, **34**, 1138 (2019).
11. R.Rao, C. L. Pint, A. E. Islam, R. S. Weatherup, S. Hofmann, E. R Meshot, F. Wu, C. Zhou, N. Dee, P.B. Amama, J. Carpena-Nuñez, W. Shi, D. L Plata, E. S. Penev, B. I. Yakobson, P. B. Balbuena, C. Bichara, D. N. Futaba, S. Noda, H. Shin, K. Su Kim, B. Simard, F. Mirri, M. Pasquali, F. Fornasiero, E. I Kauppinen, M. Arnold, B. A. Cola, P. Nikolaev, S. Arepalli, H.-M. Cheng, D. N. Zakharov, E. A. Stach, J. Zhang, F. Wei, M. Terrones, D. B. Geohegan, Be. Maruyama, S. Maruyama, Y. Li, W. W. Adams, A J. Hart, "Carbon Nanotubes and Related Nanomaterials: Critical Advances and Challenges for Synthesis toward Mainstream Commercial Applications", *ACS Nano* **12**, 11756 (2018).
12. J. Bauer, L. S.Quintanar, K.Wang, A. A. Puretzky, K. Xiao, D. B. Geohegan, and A. Boulesbaa, "Ultrafast Exciton Dissociation at the 2D-WS2 Monolayer/Perovskite Interface," *J. Phys. Chem. C* **122,** 28910 **(**2018).
13. R. K. Vasudevan, N. Laanait, E. M. Ferragut, K. Wang, D. B. Geohegan, K. Xiao, M. Ziatdinov, S. Jesse, O. Dyck & S.V. Kalinin, "Mapping mesoscopic phase evolution during E-beam induced transformations via deep learning of atomically resolved images," *npj Computational Materials*, **4**, 30 (2018).

14. Y. Xie, T. Wang, B. Zhu, C. Yan, P. Zhang, X. Wang, G. Eres, "19-Fold thermal conductivity increase of carbon nanotube bundles toward high-end thermal design applications," *Carbon* **139**, 445 (2018).
15. G. Eres, C. M. Rouleau, A. A. Puretzky, D. B. Geohegan, and H. Wang "Cooperative behavior in the evolution of alignment and structure in carbon-nanotube arrays grown using chemical vapor deposition," *Phys. Rev. Applied* **10**, 024010 (2018).
16. Z.-J. Wang, F. Ding, G. Eres, M. Antonietti, R. Schloegl, M. G. Willinger, "Formation Mechanism, Growth Kinetics, and Stability Limits of Graphene Adlayers in Metal-Catalyzed CVD Growth," *Adv. Mat. Interfaces* **5**, 1800255 (2018).
17. M. Z. Bellus, M. Mahjouri-Samani, S. D. Lane, A. D. Oyedele, X. Li, A. A. Puretzky, D. Geohegan, K. Xiao, and H. Zhao, "Photocarrier Transfer across Monolayer MoS_2−$MoSe_2$ Lateral Heterojunctions," *ACS Nano*,**12**, 7086 (2018).
18. X. Sang, X. Li, W. Zhao, J. Dong, C. M. Rouleau, D. B. Geohegan, F. Ding, K.Xiao, R. R. Unocic, "In situ edge engineering in two-dimensional transition metal dichalcogenides," *Nat. Comm.* **9**, 2051 (2018).
19. C. Park, S. W. Kim, M. Yoon, "First-Principles Prediction of New Electrides with Nontrivial Band Topology Based on One-Dimensional Building Blocks," *Phys. Rev. Lett.* **120**, 026401 (2018).
20. E. Inclan, D. Geohegan, M. Yoon, "A hybrid optimization algorithm to explore atomic configurations of TiO_2 nanoparticles," *Computational Materials Science* **141,** 1 (2018).
21. Oyedele, C. Rouleau, D. Geohegan, K. Xiao, "The growth and assembly of organic molecules and inorganic 2D materials on graphene for van der Waals heterostructures," *Carbon* **131**, 246-257 (2018).
22. M. Mahjouri-Samani, M. K. Tian, A. A. Puretzky, M. F. Chi, K. Wang, G. Duscher, C. M. Rouleau, G. Eres, M. Yoon, J. Lasseter, K. Xiao, and D. B. Geohegan, "Nonequilibrium Synthesis of TiO_2 Nanoparticle "Building Blocks" for Crystal Growth by Sequential Attachment in Pulsed Laser Deposition," *Nano Letters* **17** (8), 4624-4633 (2017).
23. W. D. Tennyson, M. Tian, A. B. Papandrew, C. M. Rouleau, A. A. Puretzky, B. T. Sneed, K. L. More, G. M. Veith, G. Duscher, T. A. Zawodzinski, D. B. Geohegan, "Bottom up synthesis of boron-doped graphene for stable intermediate temperature fuel cell electrodes," *Carbon*, **123**, 605 (2017).
24. H. Yu, N. Gupta, Z. Hu, K. Wang, B. R. Srijanto, K. Xiao, D. B Geohegan, B. I Yakobson, "Tilt Grain Boundary Topology Induced by Substrate Topography" *ACS Nano* **11**, 8612 (2017).
25. M. G. Stanford, P. R. Pudasaini, E. T. Gallmeier, L. Liang, N. Cross, A. Oyedele, G. Duscher, M. Mahjouri-Samani; K. Wang; K. Xiao; D. B. Geohegan; A. Belianinov, B. G. Sumpter, P. D. Rack, "High conduction hopping behavior induced in transition metal dichalcogenides by percolating defect networks: toward atomically thin circuits," *Adv. Funct. Mat.* **27**, 1702829 (2017).
26. H-J. Qian, G. Eres & S. Irle, "Quantum chemical molecular dynamics simulation of carbon nanotube–graphene fusion," *Molecular Simulation* **43**, 1269 (2017).

Growth Mechanisms and Controlled Synthesis of Nanomaterials (ERKCS81):
Nonequilibrium synthesis and processing approaches to tailor the functionality of 2D materials

Kai Xiao,[1] Alex Puretzky,[1] Gyula Eres,[2] Mina Yoon,[1]
Gerd Duscher,[2,3] Christopher M. Rouleau,[1] David B. Geohegan[1]
Postdocs: Yu-Chuan Lin,[1] Yiling Yu[3] Students: Chenze Liu[3] and Yiyi Gu[3]
[1]Center for Nanophase Materials Sciences and [2]Materials Science and Technology Division, Oak Ridge National Laboratory, Oak Ridge, TN 37831
[3]Dept. of Materials Science and Engineering, Univ. of Tennessee, Knoxville, 37996

Program Scope

This program addresses a critical research need in synthesis science to understand, predict, and ultimately direct the synthesis of novel quantum nanomaterials, especially atomically-thin 2D materials, and hierarchically assembled oxide nanostructures that are crucial to DOE's energy mission. The remarkable properties of such quantum nanomaterials result from confinement, interfacial interactions, and dimensionality effects at the same length scales where fundamental synthesis questions arise. The research approach therefore integrates real-time diagnostic synthesis environments with theoretical and computational methods to understand the mechanisms of formation and assembly of the "building blocks" of nanomaterials, coupled with the development of new synthetic platforms that will permit their controllable assembly into quantum nanomaterials with desired properties. In order to access novel metastable states, the program emphasizes the development of synthesis methods and real-time diagnostics to both induce and probe chemical and physical transformations away from thermodynamic equilibrium, combining laser driven synthesis and processing with laser spectroscopic diagnostic techniques, along with *in situ* electron microscopy, and neutron scattering. By revealing the kinetics, energetics, and interactions governing the assembly of nanostructures from well-defined "building blocks" the program endeavors to develop methods for nanomaterial synthesis integrating new approaches coupling theory/computation and experiment for adaptive real-time control with feedback over multiple length scales.

Recent Progress

Atomically thin two-dimensional (2D) layered materials and their heterostructures form an almost infinite palette of new candidate quantum materials. Quantum confinement within individual monolayers, bilayers, etc. and their heterostructures endow unique quantum properties that are typically far different than their parent bulk compounds. In addition, heterogeneities in 2D materials such as defects, substitutional dopants, edges, layer stacking, and strain offer tremendous opportunity to tailor quantum states. For example, specific defects in 2D materials can localize excitons to create robust quantum emitters in 2D materials such as WSe_2 or hBN that are envisioned for quantum information applications. By tailoring the stacking of the same or different component layer "building blocks" various artificially-structured phases and heterostructures can be formed to explore emergent quantum properties. However, there are still significant challenges to tailor the functionality of 2D materials for quantum information applications which require fundamental understanding and control of heterogeneity during synthesis and processing. To better understand the evolution of heterogeneities in 2D crystals during synthesis and processing, including strain, phase, and edge structures and their emergent functionalities, we have recently developed in situ diagnostics both the microscale using optical imaging and laser spectroscopy, and at the atomic scale using electron microscopy and spectroscopy. In this talk, we will present our recent progress in these areas.

Defects in 2D materials are not only crucial to enable new optical and electronic properties or localized quantum emitters, but also to drive structural phase transitions for the formation of new metastable phases for quantum materials (e.g., phase transformations from 2H to 1T, or 1T'). Recently, as shown in **Figure 1**, we have revealed a defect-mediated phase transformation in 2D $PdSe_2$ layers under the Ar-plasma irradiation. When exposed to the Ar-plasma many defects were formed in the few-layer $PdSe_2$ crystals, however instead of increasing disorder and amorphizing the crystal, the defects helped to self-assemble a new crystalline phase with different stoichiometry, $Pd_{17}Se_{15}$, that formed seamless contact with the layered $PdSe_2$. DFT calculations were performed to understand this defect-mediated phase transformation process. This new phase is metallic and provided a seamless contact to significantly reduce the contact resistance down to ~0.75 kΩ µm for ohmic contacts in $PdSe_2$ transistors, resulting in a 20-fold improvement of the carrier mobility. The results illustrate the importance of understanding and controlling defect generation and evolution pathways to enable new phases with modulated properties, not only for next-generation 2D electronic devices, but for the exploration of lateral 2D heterostructures with emerging quantum states such as Weyl and Dirac semimetals and topological superconductivity.

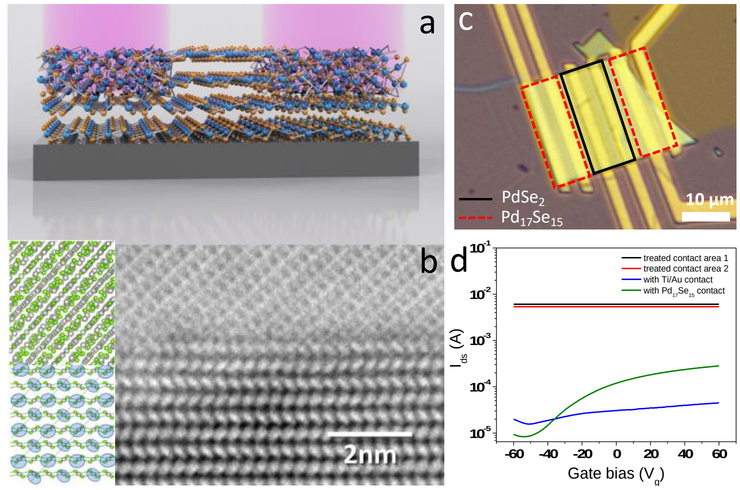

Figure 1. Defect-mediated phase transformation by plasma exposure in highly anisotropic 2D $PdSe_2$. (a) a schematic image shows the selective plasma irradiation of 2D semiconducting $PdSe_2$, inducing a phase transition to metallic nonlayered $Pd_{17}Se_{15}$ phase, and forming atomically shape interface as seamless contact in $PdSe_2$ transistors. (b) a STEM image of formed $PdSe_2/Pd_{17}Se_{15}$ junction shows the atomic sharp interface. Inset of figure (b) shows the DFT calculation illustrating the transformation pathway from layered $PdSe_2$ to cubic $Pd_{17}Se_{15}$ through the loss of Se atoms. (c) Optical image of a $PdSe_2$ device, with irradiated contact area used to obtain the transport properties of irradiated area, pristine channel with traditional Ti/Au contact, and pristine channel with $Pd_{17}Se_{15}$ contacts. (d) Transfer curves of the irradiated region, $PdSe_2$ channel with Ti/Au contact, and $PdSe_2$ channel with $Pd_{17}Se_{15}$ contact. (A. D. Oyedele, *et al., J. Am. Chem. Soc.* **141**, 8928 (2019)).

Strain can not only can tune the optoelectronic properties in 2D materials (e.g., to localize excitons for single photon emitters) but can stabilize metastable phases for emerging quantum states. In order to understand how atomically thin 2D crystals accommodate strain as they grow over curved surfaces, and how this strain changes their growth habits and optoelectronic properties, we developed a synthetic way to control the strain in 2D crystals. As shown in Figure 2, monolayer WS_2 crystals were grown by chemical vapor deposition on substrates that had been lithographically patterned with features differing in Gaussian curvature (K_G). The crystals were triangular and grew without strain up and down linear steps and trenches as deep as 180 nm (where K_G = 0), which is important for vertical integration strategies of 2D materials. However, features that incorporated positive and negative curvature, such as donuts (see figure), induced biaxial strains within single crystals that could be tolerated up to 1.5%. Taller features exerted strains sufficient to induce defects which fractured the crystals. Importantly, instead of hindering the growth, obstacles with nonzero Gaussian curvature were shown to *accelerate* the growth rate of crystal facets in the strain-tolerant regime. This acceleration was explained by a simple model that included multiplication of nucleation sites induced by the strain caused by these obstacles. Phase-field simulations were performed to understand the shape evolution of the crystals. The results provide a synthetic strategy to engineer the strain of 2D materials in three dimensions to achieve predetermined optoelectronic properties, phase transformations, and other effects important for quantum information

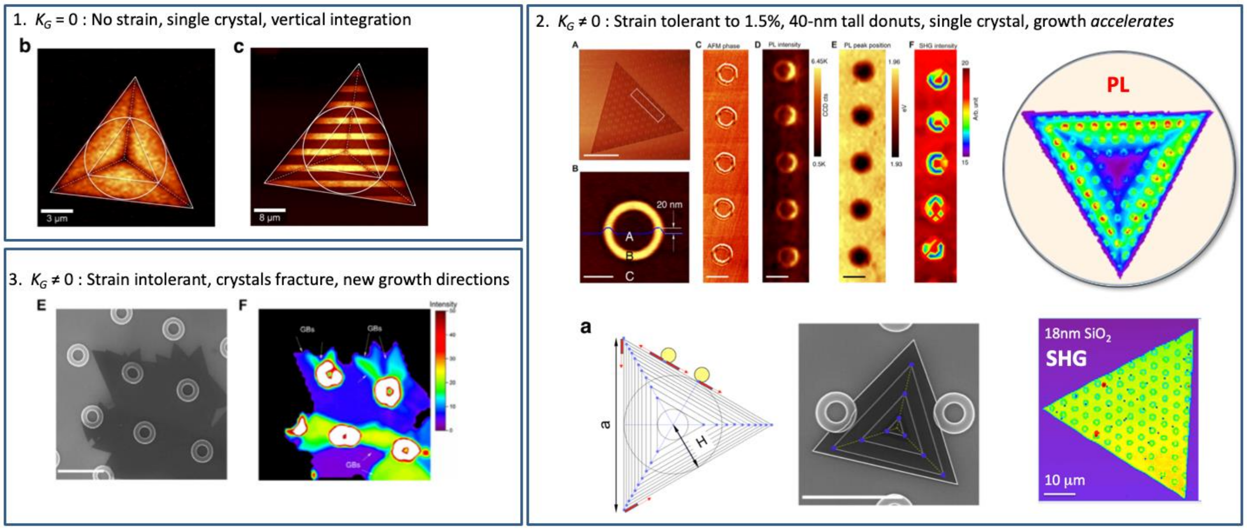

Figure 2. Effects of strain on the growth of 2D crystals. Triangular 2D crystals of WS_2 were grown on lithographic features to induce strain via Gaussian curvature K_G. (1) Features such as trenches with $K_G = 0$ induce no strain and growth rate is constant, as shown by PL imaging. (2) Features such as donuts with $K_G \neq 0$ induce strain, as revealed by shifts in the PL and Raman spectra. The crystals can stretch to tolerate strains up to 1.5% while remaining single crystals (shown by SHG mapping). Interestingly, the strained facets increase their growth rate. (3) Above this strain, defects form, and the crystal essentially fractures to grow in different directions, as SEM and SHG mapping shows. K. Wang, *et al.*, *Sci. Adv.* **5** (5), eaav4028 (2019).

science and other applications.

Strain also plays a key role in the growth of 2D crystals on flat substrates when two monolayer triangular single crystals collide, or when domains of fractured monolayer crystals (such as shown in the third panel of Figure 2) interact. This situation is of key relevance since understanding how multiple randomly-oriented crystals converge into monolayer films and form grain boundaries is crucially important to macroscale electrical transport and other properties. We (and other groups) have reported the existence of twisted bilayer overlap regions during some interactions between triangular crystallites where one material appears to grow up and over the other, resulting in a thin bilayer ribbon growing at the mismatch angle, such as those shown in **Figure 3**. Alternatively, nucleation of a misoriented grain at the boundary is possible, followed by second-layer vdW heteroepitaxy. The process is poorly understood, however if it can be controlled it allows the direct synthesis of a much wider variety of bilayers with unusual twist angles and properties. Like the collision between two tectonic plates at the macroscale, understanding the energetics of strain developed during the collision of atomically-thin crystals, and the vdW interactions between the crystals and the substrate for different twist angles, form an important fundamental problem which we are currently investigating with spectroscopic diagnostics, imaging, theory, and atomic-scale electron microscopy.

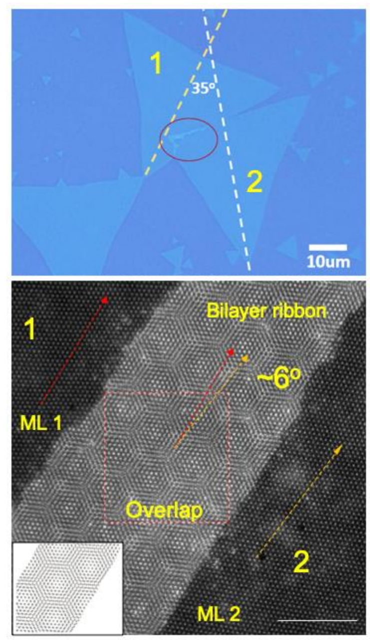

Figure 3. Twisted bilayer ribbon grain boundaries from two 2D monolayer crystals. (top) The formation of twisted bilayers sometimes occurs when two 2D MoS_2 crystals meet during growth. (bottom) Moiré lattices reveal the twist angle (here for WS_2). Preferred angles and theoretical simulations are investigating the driving forces for this effect (*in preparation*).)

The edge structure and chemistry of 2D materials are crucially important for tailoring their magnetic, optical, electrical, and catalytic properties for specific applications. In order to understand this edge evolution and reconstruction at the atomic scale, we performed in situ heating experiments using aberration-corrected scanning transmission electron microscopy (STEM) to track the edge evolution and transformation in $Mo_{1-x}W_xSe_2$ (x = 0.05) monolayers that we had synthesized by VTE growth. As shown in **Figure 4**a, varying the local chemical potential during heating triggers the formation of nano-pores that become terminated by different stable reconstructed edge configurations that possess different metallic and/or magnetic properties. Our density functional theory calculations and *ab initio* molecular dynamics simulations explained how the local chemical potential induced the observed thermally-induced structural evolution and the exceptional stability of the four most commonly observed edges. As shown in **Figure 4b**, the atomistic dynamics of defects during the elimination of a grain boundary can also be understood during thermolysis-driven growth of MoS_2 crystals by mimicking growth conditions within the TEM. This coupling of computational modeling and *in situ* atomistic STEM imaging in changing chemical environments demonstrated here provides a pathway to explore the controlled atomic scale manipulation of matter for the directed predictive synthesis of edge configurations and phases of 2D materials with desired functionality.

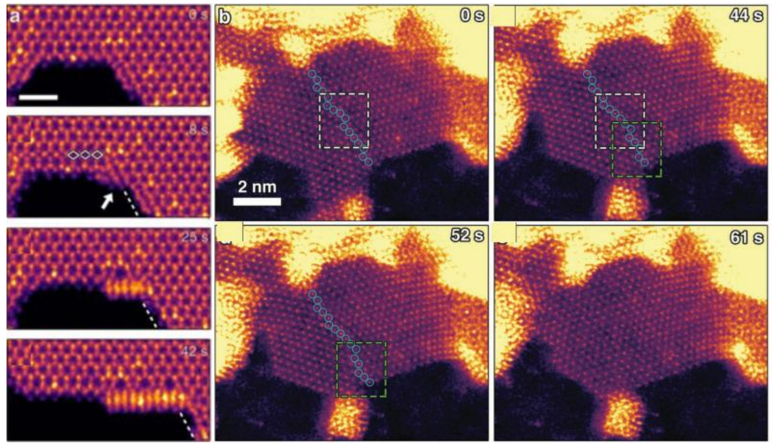

Figure 4. *in situ* STEM observation of the atomistic edge reconstruction dynamics and grain coalescence process induced by heating. (a) Atomic resolution HAADF-STEM image frames showing typical states in the process of edge reconstruction from a ZZSe-Se to ZZSe-Mo-NW30. Scale bar is 1 nm. (b) STEM images acquired at different times show the reorientation of two grains initially exhibiting different orientations at 600 °C. Atoms from the right grain at the grain boundary are marked by blue circles. ((a) X. Sang, et al., *Nat. Comm*. **9**, 2051 (2018); (b) X. Sang, et al., *Adv. Funct. Mater*. 1902149 (2019)).

Future Plans

We will continue to explore the fundamental role of strain in the growth of 2D crystals during the CVD synthesis process by employing lithographically-defined substrates and materials with layer-dependent optical properties, such as $PdSe_2$ and WSe_2. Through a synthetic strain-engineering approach, we will attempt to stabilize new metastable phases in 2D $PdSe_2$ for emerging quantum states (e.g., Weyl semimetals and superconductors) and to localize excitons for single photon emitters in other 2D materials (e.g., WSe_2). Understanding the growth sequence of bilayer crystals is very important to construct heterostructures and bilayer crystals with well-defined stacking. Therefore, using our recently-developed laser thinning approach combined with our ability to grow isotopically pure 2D materials in sequenced fashion, such as $^{92}MoS_2$ and $^{100}MoS_2$, we will undertake studies to identify the growth sequence of bilayer crystals with different stacking angles, with relevance to the synthesis of twisted bilayers with long-range ordered Moiré superlattices. We will also explore the rich opportunities for defect-mediated phase transformations and dynamics in $PdSe_2$ and other layered 2D materials employing laser-driven, thermal, and plasma-driven processes using the *in situ* time-resolved laser spectroscopic platform in our custom-designed microchamber. STEM/EELS will provide atomistic information on how defects form, aggregate and finally induce the structural reconstructions that form new phases. Each of these approaches address priority research directions for synthesis to "*integrate…in situ characterization tools to achieve directed synthesis with real-time adaptive control*".

DOE Sponsored Publications in the Last Two Years

1. K. Wang, A. A. Puretzky, Z. Hu, B. R. Srijanto, X. Li, N. Gupta, H.Yu, M. Tian, M. Mahjouri-Samani, X. Gao, A. Oyedele, C. M. Rouleau, G. Eres, B. I. Yakobson, M. Yoon, K. Xiao, and D. B. Geohegan "Strain tolerance of two-dimensional crystal growth on curved surfaces," *Science Advances* **5** (5), eaav4028 (2019).
2. X. Sang, X. Li, A.A. Puretzky, D.B. Geohegan, K. Xiao, R.R .Unocic, "Atomic Insight into Thermolysis-Driven Growth of 2D MoS_2," *Adv. Funct. Mater.* 1902149 (2019).
3. A. D. Oyedele, S. Z. Yang, T. Feng, A. V. Haglund, Y. Gu, A. A. Puretzky, D. Briggs, ... "Defect-mediated phase transformation in anisotropic 2D $PdSe_2$ crystals for seamless electrical contacts," *J. Am. Chem. Soc. DOI:* 10.1021/jacs.9b02593 (2019).
4. D. B. Brown, W. Shen, X. Li, K. Xiao, D. B. Geohegan, S. Kumar "Spatial mapping of thermal boundary conductance at metal-molybdenum diselenide interfaces," *ACS Appl. Mater. Interfaces* **11**, 14418 (2019).
5. E. Inclan, M. Yoon "Performance of biologically inspired algorithms tuned on TiO2 nanoparticle benchmark system," *Computational Materials Science* **165**, 63 (2019).
6. N. Briggs, S. Subramanian, Z. Lin, X. Li, X. Zhang, K. Zhang, K. Xiao, D. Geohegan, R. Wallace, L.-Q. Chen, M. Terrones, A. Ebrahimi, S. Das, J. Redwing, C. Hinkle, K. Momeni, A. van Duin, V. Crespi, S. Kar, J. A. Robinson, "A Roadmap for Electronic Grade 2D Materials," *2D Materials* **6**, 022001 (2019).
7. X. Li, J. Zhang, A. A. Puretzky, A. Yoshimura, X. Sang, Q. Cui, Y. Li, L. Liang, A. W. Ghosh, H. Zhao, R. R. Unocic, V. Meunier, C. M. Rouleau, B. G. Sumpter, D. B. Geohegan, and K. Xiao, "Isotope-Engineering the Thermal Conductivity of Two-Dimensional MoS_2" *ACS Nano* **13**, 2481–2489 (2019).
8. M. G. Stanford, Y.-C. Lin, M. G. Sales, A. N. Hoffman, C. T. Nelson, K. Xiao, S. McDonnell, P. D. Rack, "Lithographically patterned metallic conduction in single-layer MoS_2 via plasma processing," *npj 2D Materials and Applications* **3**, 13 (2019).
9. O. Maksov, O. Dyck, K. Wang, K. Xiao, D. B. Geohegan, B. G. Sumpter, R. K. Vasudevan, S. Jesse, S. V Kalinin, M. Ziatdinov, "Deep learning analysis of defect and phase evolution during electron beam-induced transformations in WS_2," *npj Computational Materials* **5**, 12 (2019).
10. M. Tian, C. Liu, J. Ge, D. Geohegan, G. Duscher, G. Eres, "Recent progress in characterization of the core–shell structure of black titania," *Journal of Materials Research*, **34**, 1138 (2019).
11. R. Rao, C. L. Pint, A. E. Islam, R. S. Weatherup, S. Hofmann, E. R Meshot, F. Wu, C. Zhou, N. Dee, P.B. Amama, J. Carpena-Nuñez, W. Shi, D. L Plata, E. S. Penev, B. I. Yakobson, P. B. Balbuena, C. Bichara, D. N. Futaba, S. Noda, H. Shin, K. Su Kim, B. Simard, F. Mirri, M. Pasquali, F. Fornasiero, E. I Kauppinen, M. Arnold, B. A. Cola, P. Nikolaev, S. Arepalli, H.-M. Cheng, D. N. Zakharov, E. A. Stach, J. Zhang, F. Wei, M. Terrones, D. B. Geohegan, Be. Maruyama, S. Maruyama, Y. Li, W. W. Adams, A J. Hart, "Carbon Nanotubes and Related Nanomaterials: Critical Advances and Challenges for Synthesis toward Mainstream Commercial Applications", *ACS Nano* **12**, 11756 (2018).
12. J. Bauer, L. S.Quintanar, K.Wang, A. A. Puretzky, K. Xiao, D. B. Geohegan, and A. Boulesbaa, "Ultrafast Exciton Dissociation at the 2D-WS2 Monolayer/Perovskite Interface," *J. Phys. Chem. C* **122,** 28910 **(**2018).
13. R. K. Vasudevan, N. Laanait, E. M. Ferragut, K. Wang, D. B. Geohegan, K. Xiao, M. Ziatdinov, S. Jesse, O. Dyck & S.V. Kalinin, "Mapping mesoscopic phase evolution during E-beam induced transformations via deep learning of atomically resolved images," *npj Computational Materials*, **4**, 30 (2018).

14. Y. Xie, T. Wang, B. Zhu, C. Yan, P. Zhang, X. Wang, G. Eres, “19-Fold thermal conductivity increase of carbon nanotube bundles toward high-end thermal design applications,” *Carbon* **139**, 445 (2018).
15. G. Eres, C. M. Rouleau, A. A. Puretzky, D. B. Geohegan, and H. Wang “Cooperative behavior in the evolution of alignment and structure in carbon-nanotube arrays grown using chemical vapor deposition,” *Phys. Rev. Applied* **10**, 024010 (2018).
16. Z.-J. Wang, F. Ding, G. Eres, M. Antonietti, R. Schloegl, M. G. Willinger, “Formation Mechanism, Growth Kinetics, and Stability Limits of Graphene Adlayers in Metal-Catalyzed CVD Growth,” *Adv. Mat. Interfaces* **5**, 1800255 (2018).
17. M. Z. Bellus, M. Mahjouri-Samani, S. D. Lane, A. D. Oyedele, X. Li, A. A. Puretzky, D. Geohegan, K. Xiao, and H. Zhao, “Photocarrier Transfer across Monolayer MoS_2−$MoSe_2$ Lateral Heterojunctions,” *ACS Nano*,**12**, 7086 (2018).
18. X. Sang, X. Li, W. Zhao, J. Dong, C. M. Rouleau, D. B. Geohegan, F. Ding, K.Xiao, R. R. Unocic, “In situ edge engineering in two-dimensional transition metal dichalcogenides,” *Nat. Comm.* **9**, 2051 (2018).
19. C. Park, S. W. Kim, M. Yoon, “First-Principles Prediction of New Electrides with Nontrivial Band Topology Based on One-Dimensional Building Blocks,” *Phys. Rev. Lett.* **120**, 026401 (2018).
20. E. Inclan, D. Geohegan, M. Yoon, “A hybrid optimization algorithm to explore atomic configurations of TiO_2 nanoparticles,” *Computational Materials Science* **141,** 1 (2018).
21. Oyedele, C. Rouleau, D. Geohegan, K. Xiao, “The growth and assembly of organic molecules and inorganic 2D materials on graphene for van der Waals heterostructures,” *Carbon* **131**, 246-257 (2018).
22. M. Mahjouri-Samani, M. K. Tian, A. A. Puretzky, M. F. Chi, K. Wang, G. Duscher, C. M. Rouleau, G. Eres, M. Yoon, J. Lasseter, K. Xiao, and D. B. Geohegan, "Nonequilibrium Synthesis of TiO_2 Nanoparticle "Building Blocks" for Crystal Growth by Sequential Attachment in Pulsed Laser Deposition," *Nano Letters* **17** (8), 4624-4633 (2017).
23. W. D. Tennyson, M. Tian, A. B. Papandrew, C. M. Rouleau, A. A. Puretzky, B. T. Sneed, K. L. More, G. M. Veith, G. Duscher, T. A. Zawodzinski, D. B. Geohegan, “Bottom up synthesis of boron-doped graphene for stable intermediate temperature fuel cell electrodes,” *Carbon*, **123**, 605 (2017).
24. H. Yu, N. Gupta, Z. Hu, K. Wang, B. R. Srijanto, K. Xiao, D. B Geohegan, B. I Yakobson, “Tilt Grain Boundary Topology Induced by Substrate Topography” *ACS Nano* **11**, 8612 (2017).
25. M. G. Stanford, P. R. Pudasaini, E. T. Gallmeier, L. Liang, N. Cross, A. Oyedele, G. Duscher, M. Mahjouri-Samani; K. Wang; K. Xiao; D. B. Geohegan; A. Belianinov, B. G. Sumpter, P. D. Rack, “High conduction hopping behavior induced in transition metal dichalcogenides by percolating defect networks: toward atomically thin circuits,” *Adv. Funct. Mat.* **27**, 1702829 (2017).
26. H-J. Qian, G. Eres & S. Irle, “Quantum chemical molecular dynamics simulation of carbon nanotube–graphene fusion,” *Molecular Simulation* **43**, 1269 (2017).

Oriented Attachment Induces 5-Fold Twin Formation via Forming and Decomposing High-Energy Grain Boundaries

PI: Dongsheng Li, Pacific Northwest National Laboratory

Program Scope

The vision of this Does Basic Energy Sciences (BES) Early Career project is to reveal the unknown molecular mechanisms of mass transport and structural evolution during classical and nonclassical nanocrystal synthesis to enable the design of nanostructures with controlled size and morphology and tailored properties. Specifically, the research investigates two types of growth mechanisms of branched structure formation: (1) particle-based growth, particularly oriented attachment (OA), and (2) vapor-liquid-solid (VLS) growth. Representative examples of metal[1,2] (Au, Ag, Pd), oxide[3,4] (TiO_2, Ag_3PO_4, OA), and semiconductor[5] (PbSe, VLS) material systems are under investigation.

My specific objectives are the following:

Objective 1. Establish the source of the driving force for OA, the barriers to OA, and the factors that control them, including surface charge, solvent exclusion, and interface hydration.

Objective 2. Understand the source of hierarchical organization—i.e., branching at many length scales—during OA and VLS growth and the correlation between branching rate and trunk extension.

Objective 3. Use the knowledge gained from Objectives 1 and 2 to direct growth of nanostructures for tailored properties.

Currently, we are working on Objectives 1, 2, and 3.

Recent Progress

Over the past year, I made significant progress in understanding crystal growth mechanisms and thus designing/controlling their structures, which are closely tied to their functional applications. Specifically, (**1**) We revealed that OA induced fivefold twin formation via forming and decomposing high-energy grain boundaries. (**2**) We established the mechanisms of particle interactions, the interplay of forces driving particle aggregation, and the factors controlling the assembly process and final structure, such as solvent, particle shape, and ligands. (**3**) We determined the mechanism of branched PbSe nanowire growth via VLS and studied the factors controlling branch density and branched wire size. (**4**) In previous work, I identified the mechanisms of phase transition from anatase to rutile and confirmed that this phase transition correlates to the OA, which results in branched rutile nanowire growth. Building on this discovery, we further identified the structure-function relationship of the transitional phases, whose presence improves the photocatalytic activity of TiO_2. (**5**) We investigated the role of edge dislocations, induced via OA, in improving photocatalytic activity of TiO_2.

Here, we present the details of OA induced fivefold twin formation via forming and decomposing high-energy grain boundaries (Figure 1). The occurrence of fivefold twinned nanoparticles, commonly observed in both natural and synthetic crystalline materials, leads to unique properties. However, nearly 200 years after their discovery, the formation mechanism is still ambiguous. Using in situ high-resolution transmission electron microscopy (TEM) combined with molecular dynamics simulations, we demonstrate that fivefold twinning occurs via repeated OA of ~3 nm Au nanoparticles. These OA events create high-energy grain boundaries, which accumulate strain during atomic rearrangement and consequently decompose via nucleation and growth of a special class of twins whose net strain is zero, inducing the fivefold twin structures. The results provide a quantitative understanding of the fivefold twinning process; this knowledge provides guidance for interpreting and controlling twin structures and morphologies of a wide range of materials.

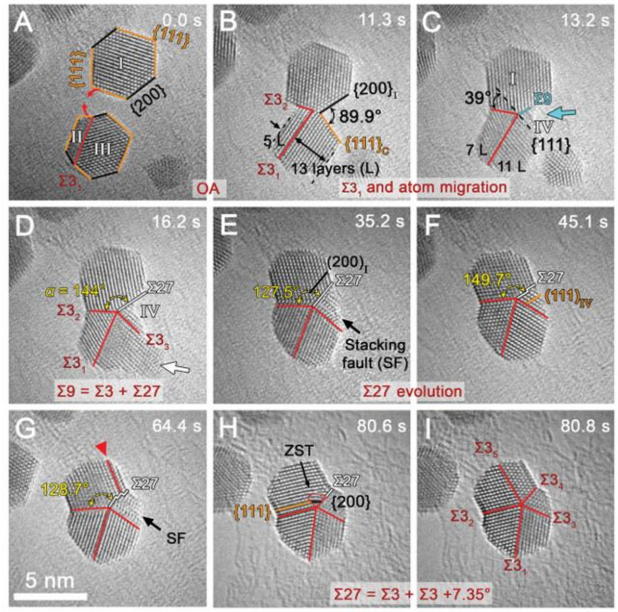

Figure. 1. (A-B) Formation of $\Sigma 3_2$ and ~90° concave surfaces after the OA process. (C) Migration of atoms to the concave surface region (cyan arrow) with the formation of the Σ9 GB and $\Sigma 3_2$ migration of two atomic layers toward region III from II. (D-G) Oscillation between $\Sigma 27\text{-}(200)_{I}$ and $\Sigma 27\text{-}(111)_{IV}$ configurations and corresponding angle of α between $\Sigma 3_2$ and Σ27. (H) Nucleation of zero strain twin (ZST)on Σ27 near twin pole. (I) Formation of fivefold twin. The red arrow in (G) denotes one layer of twin interface through partial dislocation slipping.

Future Plans

I will continue to perform force measurements via atomic force microscopy and dynamic force spectroscopy on TiO_2 systems to investigate the factors that control OA, such as temperature, salts, pH, etc. TEM experiments will be carried out for imaging under in situ heating conditions to achieve a quantitative understanding of (1) crystal growth via nonclassical pathways, such as OA (TiO_2, Ag_3PO_4, and ZnO), (2) screw-dislocation–driven VLS growth (PbSe branched nanowires), and (3) the source of hierarchical organization and direct hierarchical growth..

References

1 Song, M., Wu, Z., Lu, N. & Li, D. Strain Relaxation-Induced Twin Interface Migration and Morphology Evolution of Silver Nanoparticles. *Chemistry of Materials* **31**, 842-850, doi:10.1021/acs.chemmater.8b03984 (2019).

2 Lee, J. *et al.* Mechanistic Understanding of the Growth Kinetics and Dynamics of Nanoparticle Superlattices by Coupling Interparticle Forces from Real-Time Measurements. *ACS Nano* **12**, 12778-12787, doi:10.1021/acsnano.8b07880 (2018).
3 Li, D. *et al.* Investigating the magnitude and source of orientation-dependent interactions between TiO_2 crystal surfaces. *Nanoscale* **9**, 10173-10177 (2017).
4 Li, D. *et al.* Trends in mica–mica adhesion reflect the influence of molecular details on long-range dispersion forces underlying aggregation and coalignment. *Proceedings of the National Academy of Sciences* **114**, 7537-7542 (2017).
5 Song, M. *et al.* In situ characterization of kinetics and mass transport of PbSe nanowire growth via LS and VLS mechanisms. *Nanoscale* **11**, 5874-5878, doi:10.1039/C9NR01200A (2019).

Publications (2017–2018)

1. Song, M.; Wu, Z.; Lu, N.; Li, D., Strain Relaxation-Induced Twin Interface Migration and Morphology Evolution of Silver Nanoparticles. *Chemistry of Materials* 2019, 31 (3), 842-850.
2. Song, M.; Lee, J.; Wang, B.; Legg, B. A.; Hu, S.; Chun, J.; Li, D., In situ characterization of kinetics and mass transport of PbSe nanowire growth via LS and VLS mechanisms. *Nanoscale* 2019, 11, 5874-5878.
3. Jaewon Lee, Elias Nakouzi, Dongdong Xiao, Zhigang Wu, Miao Song, Jaehun Chun, and Dongsheng Li, Interplay between Short- and Long-ranged Forces Leading to the Formation of Ag Nanoparticle Superlattice, *Small*, 2019, 1901966
4. Wu, Z.; Xiao, D.; Lee, J.; Ren, P.; Song, M.; Li, D., Palladium nanostructures with well-controlled morphologies obtained by one-pot and one-step polyol method. *Journal of Crystal Growth* 2019, 521, 34-40
5. Li, Y.; Wang, C.; Song, M.; Li, D.; Zhang, X.; Liu, Y., TiO_2-x/CoOx photocatalyst sparkles in photothermocatalytic reduction of CO_2 with H_2O steam. *Applied Catalysis B: Environmental* 2019, 243, 760-770.
6. Lee, J.; Nakouzi, E.; Song, M.; Wang, B.; Chun, J.; Li, D., Mechanistic Understanding of the Growth Kinetics and Dynamics of Nanoparticle Superlattices by Coupling Interparticle Forces from Real-Time Measurements. *ACS Nano* 2018, 12 (12), 12778-12787.
7. Wang, B.; Cai, H.; Zhao, D.; Song, M.; Guo, P.; Shen, S.; Li, D.; Yang, S., Enhanced Photocatalytic Hydrogen Evolution by Partially Replaced Corner-site C Atom with P in g-C_3N_4. *Applied Catalysis B: Environmental* 2018.
8. Dongsheng Li, Jaehun Chun, Dongdong Xiao, Weijiang Zhou, Huacheng Cai, Lei Zhang, Kevin M. Rosso, Christopher J. Mundy, Gregory K. Schenter, James J. De Yoreo, Trends in mica–mica adhesion reflect the influence of molecular details on long-range dispersion forces underlying aggregation and coalignment. *Proceedings of the National Academy of Sciences* 2017*, 114* (29), 7537-7542.
9. Dongsheng Li, Hailong Wang, Dongdong Xiao, Miao Song, Benjamin Legg, Jaehun Chun (2017), Investigating the magnitude and source of orientation-dependent interactions between TiO_2 crystal surfaces. *Nanoscale* 2017, *9*, 10173-10177.
10. Zhigang Wu, Jaehun Chun, Sayandev Chatterjee, Dongsheng Li, Fabrication of oriented crystals as force measurement tips via focused ion beam and microlithography methods. *Surf. Interface Anal.* 2018, *50* (1), 117-122.
11. Dongdong Xiao, Zhigang Wu, Miao Song, Dongsheng Li, Silver Nanocube and Nanobar Growth via Anisotropic Monomer Addition and Particle Attachment Processes. *Langmuir* 2018, 34, 1466-1472.

Electrochemically Driven Nanostructures: Opportunities and Challenges

Jun Liu, Pacific Northwest National Laboratory, Richland, WA 99352

Program Scope

The objective of this program is to develop general principles for the synthesis of nanocomposite materials with multiscale structural control. In particular, the program will focus on role of the solvation and interfacial structures and interactions on local nucleation, secondary nucleation and assembly, and the effect of an external field on the interfacial interactions. The program will be based on four integrated elements, model experimental systems will well-defined interfacial structures, extensive tools to characterize the interfaces, in-situ and ex-situ methods to monitor the nucleation and growth processes, and theory to incorporate the effects of interfacial structures and predict nucleation and synthesis. The knowledge gained will be used to understand and control nucleation and assembly of materials with both atomic and longer length-scale ordering, and furthermore, to develop principles for synthesizing hierarchical structures assisted by external fields. The results from such studies have implications for energy storage and conversion. State-of-the-art characterization techniques, in particular transmission electron microscopy (TEM), atomic force microscopy (AFM), will be used to probe the early-stage nucleation processes with unprecedented time and spatial resolution. Extensive molecular and mesoscale computer modeling will also be used to elucidate fundamental mechanisms of interfacial binding, nucleation, and self-assembly, and guide the materials synthesis efforts.

Electrochemically Driven Nanostructures

External fields provide an effective method for controlling local environment around the nucleation sites and interfaces and another method for controlling the pathways of heterogeneous crystal growth and affect the reaction mechanisms and outcomes. One hand, electrochemical deposition is widely studied to prepare nanomaterials and oriented nanowires. On the other hand, electrochemical deposition is also a very important problem in the properties of energy storage materials. Example include lithium dendrite formation in batteries which is a large safety concern. This program focuses on the early stages of nucleation under mild electrochemical deposition conditions.

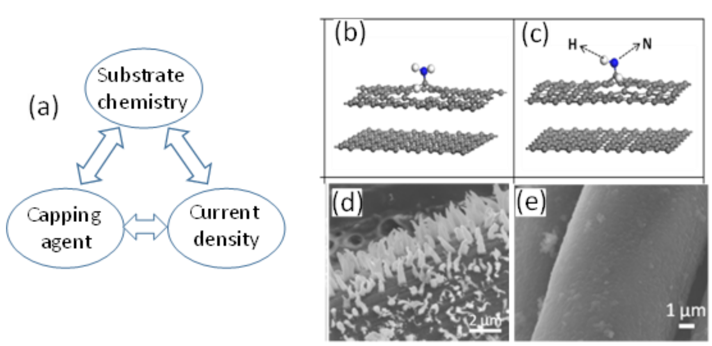

Figure 1. Approaches to understand nucleation in electrochemical deposition. (a) The interplay between substrate chemistry, surface absorption and capping and the electrochemical driving forces. (b) and (c) Examples of different functional groups on carbon. (d) different morphologies of Li metal deposited on different carbon surfaces from needle-like structures to smooth deposition (PNNL unpublished).

Under mild electrochemical depositions, the role electrochemical driving force can be similar to thermodynamic driving force under hydrothermal conditions. Under hydrothermal conditions, the nucleation is induced by changing temperature so that the concentration of the precursors is higher than the solubility (super saturated solutions) and the thermodynamic driving force is related to the degree of supersaturation. Under electrochemical deposition, the available reaction species is related to the current density. Therefore, the opportunities and challenges depends on the knowledge and ability to systematically vary the electrochemical driven force to derive the desired outcomes. Figure 2 shows examples of electrochemical deposited nanowires. Under normal conditions polymer films were produced. The nanowires were obtained by modulating the current density. The hypothesis is that the nucleation and growth can be separately manipulated. However, similar phenomena should be avoided on the anode of an electrochemical battery cell (Figure 1) to prevent dendrite formation.

Figure 2. Electrochemically deposition of oriented conducting polymers on conducting and semiconducting substrates. The polymers chains are also molecularly aligned. The polymer seeds were first deposited with a large current density, followed by slow growth of polymer nanowires at a low current density.[1]

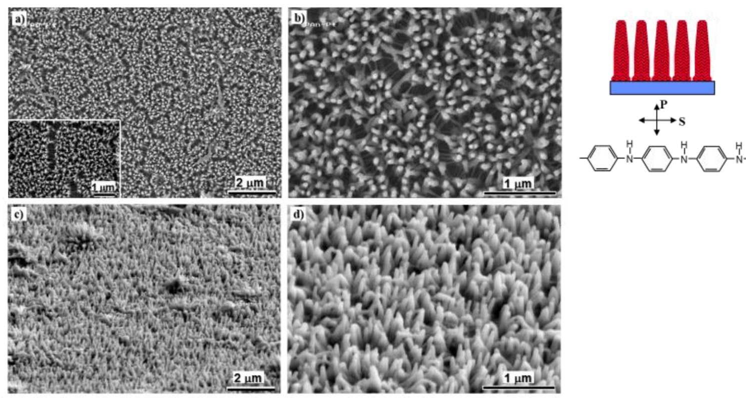

The microstructures of the electrochemically deposited film are also related to the interfacial reactions between the surface of the substrate and the solvent molecules. For example, in most cases all solvent molecules react with Li metal and such reactions promote the formation of Li dendrites. We have developed a general mechanism to stabilize the interface based on the choice of salt-to-solvent molar ratios. We find that with a high salt-to-solvent molar ratio (1:2), the solvent molecules are mostly coordinated in the solvation shell of the Li+ ions, which effectively suppresses the reactivity of solvents toward graphite or Li-metal anode. The new solvent is successfully deployed in commercial Li-ion cells as a non-flammable electrolytes, demonstrating good electrochemical performance comparable traditional electrolytes. Non-dendritic Li plating/stripping with high coulombic efficiency (CE) (>99%) is achieved in Li/Cu half-cells showing the potential of employing nonflammable electrolytes in Li-metal batteries.

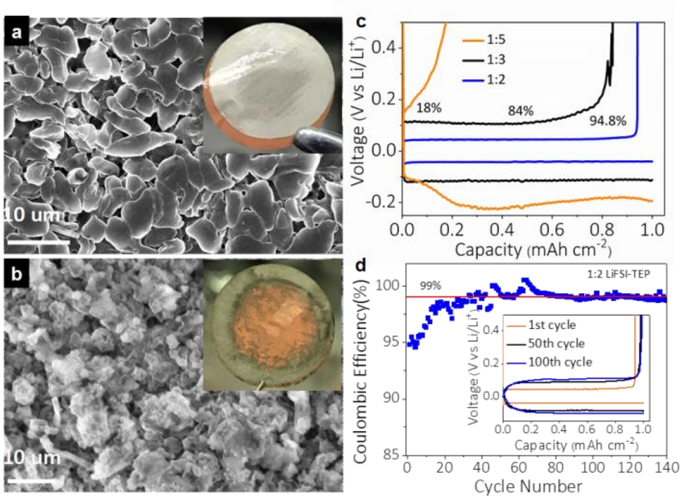

Figure 3. Morphologies of electrochemically deposited Li films. (a) Non-dendritic Li deposition of large Li particles when the Li-solvent interactions are suppressed. (b) Deposition of high surface area Li dendrites. (c) Stripping and deposition of Li in stabilized solvents. (c) Columbic efficiency of Li deposition.[2]

Acknowledgement

This research is supported by the U.S. Department of Energy, Office of Science, Basic Energy Sciences, Division of Materials Sciences and Engineering, under Award KC020105-FWP12152 “Molecularly Organized Nanostructures.”

References

1. L. Liang, J. Liu, CF Windisch, GJ Exarhos, and YH Lin. "Direct Assembly of Large Arrays of Oriented Conducting Polymer Nanowires." Angewandte Chemie-International Edition 41(19):3665-68, 2002.

2. Z. Zeng, V. Murugesan, K. S. Han, X.Jiang, L. Xiao, X. Ai, H. Yang, J-G. Zhang, M. L. Sushko, J. Liu, Y. Cao, “Suppressing Reactivity of Nonflammable Electrolytes for Li-Ion and Li-Metal Batteries,” Nature Energy, 2018.

Molecularly organized nanostructured materials

Jun Liu, Maria Sushko, James De Yoreo, Praveen Thallapally, Jinhui Tao

Pacific Northwest National Laboratory, Richland, WA

Program Scope

The goal of this project is to develop innovative approaches employing molecularly directed interfacial reactions to control crystallization and self-assembly of functional nanocomposites for energy applications. Synthesis of these materials has been extensively studied, but a unifying theory underlying such synthesis processes is lacking. The central challenge is to develop principles to predict the synthesis of ordered, hierarchical materials with structural ordering across scales from atomic to nanoscale and beyond. We hypothesize that a general principle of interface-controlled nucleation and self-assembly can be developed to predict and control the synthesis of nanocomposite materials with multiscale structural ordering. This project will focus on interfacially controlled nucleation in synthesizing carbon-metal-metal oxide nanocomposite materials. The knowledge gained will be extended to understand and control self-assembly of materials with both atomic and longer length-scale ordering, and furthermore, to develop principles for synthesizing hierarchical structures through multi-generation homoepitaxial nucleation processes. The results from such studies have implications for many energy applications, including batteries, supercapacitors, fuel cells, and H storage and generation. State-of-the-art transmission electron microscopy (TEM), atomic force microscopy (AFM), nuclear magnetic resonance (NMR), and other spectroscopy techniques will be used to probe the early-stage nucleation processes with unprecedented time and spatial resolution. Extensive molecular and mesoscale computer modeling will also be used to elucidate fundamental mechanisms of interfacial binding, nucleation, and self-assembly, and guide the materials synthesis efforts. This research addresses the BES grand challenge of developing "*...atom-precise and energy-efficient synthesis of revolutionary new forms of matter with tailored properties.*"

Recent Progress

This project is demonstrating the potential of a general synthetic approach for multiscale structural control by manipulating the interfacial nucleation and self-assembly of nanoscale building blocks, developing an integrated theoretical and experimental approach, and developing and applying new in situ characterization tools. We developed a theoretical framework for modeling interfacially directed crystallization pathways and a suite of in situ scanning probe and

TEM characterization techniques for monitoring nucleation and crystal growth processes. Through a combination of theoretical and experimental research, we have shown that the interfacial solvent structure, ion distributions in the double layer and on the surface are critical controls for surface-directed nucleation and growth. Using a model system of ZnO nanoparticles, we have shown that the correlated fluctuation dynamics of growth solutions in the interfacial region largely dictates the morphology of hierarchical architectures (Fig. 1).[1] The project also demonstrated that face specific ion and ligand adsorption onto nanoparticle surface and surface defects directs particle growth and heterogeneous nucleation by modifying surface strain, surface energy[2] and surface reactivity,[3] respectively. Finally, the project has demonstrated that the electrochemical properties of electrode materials can be manipulated using electrolyte-dependent reaction mechanism.[4]

1. *Mechanisms of formation of highly-branched wurtzite ZnO nanostructures*. Initial stages of branched structure formation were captured to delineate between two possible growth pathways: oriented attachment of nanoparticles, as is often surmised, or a process of repeated secondary nucleation.[1] Using a range of precursor concentrations, we systematically vary hierarchical organization of ZnO architectures and investigate their formation by liquid phase scanning electron microscopy (SEM) and high-resolution transmission electron microscopy interpreted via classical Density Functional Theory (cDFT). At low [Zn^{2+}], ZnO "flowers" with stocky branches elongated along [0001] form, with stems and branches exhibiting a unique crystallographic relationship attributable to minimization of lattice mismatch. At intermediate [Zn^{2+}], a more complex structure of thin, intergrown platelets appears, growing fastest along the [-1-1 2 0]. At still higher [Zn^{2+}], hedgehog-like structures emerge with branches again elongated along [0001]. *In situ* liquid phase SEM demonstrates that all branches form through secondary nucleation and grow by classical processes. cDFT results imply the morphological evolution with increasing [Zn^{2+}] arises from an interplay between rising thermodynamic driving force, which promotes branch number and variability of orientation, and increasing barriers to interfacial transport due to ion correlation forces that alter the anisotropic kinetics of growth. These findings provide a quantitative picture of branching that sets to rest past controversies and advances efforts to decipher growth mechanisms of hierarchical structures in real solution environments.

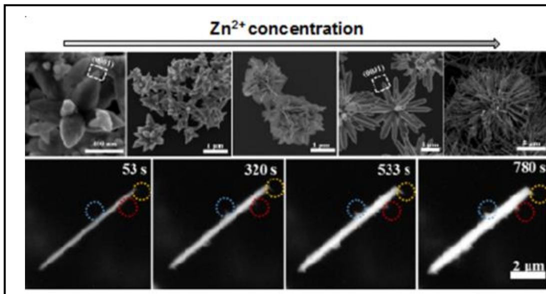

Figure 1. Hierarchical organization of ZnO can be systematically varied by varying precursor concentration. This study conclusively proves that all branches form through secondary nucleation and grow by classical processes.

2. *Morphology control of anisotropic nanocrystals.* We investigated the formation of Au penta-twinned nanorod by liquid cell transmission electron microscopy (LC-TEM).[2] It is found that a truncated-decahedron forms in the absence of cetyl-trimethyl ammonium bromide (CTAB), whereas in the presence of CTAB a penta-twinned nanorod forms by producing {100} facets via

reentrant groove and selectively inhibiting atom addition to {100} facets. Density functional theory (DFT) simulations predicted that partial relieve of strain energy of decahedral nanoparticle by Br^- ions adsorption causes the {100} facets to appear possibly via reentrant groove at smaller size. The asymmetric selective adsorption of CTAB onto the Au {100} facets results in the decrease in the surface energy of {100} facets below that of the {111} facets and drives the formation and anisotropic growth of penta-twinned nanorod. Strain and surface energy-tuning strategies are proposed to play a key role in regulating penta-twinned nanostructure, providing a new insight for controlled synthesis of metallic nanorods. Our work points out the importance of the synergy of strain and surface energy, which provides an in-depth insight into the anisotropic growth of nanorods and lays foundations for controlled synthesis of nanomaterials.

3. *Mechanism for growth of supported porous materials*. New mechanism is discovered that utilizes an active substrate to provide control over the nucleation sites and kinetics of growth of a porous overlayer.[3] A combined *in situ* atomic force microscopy and *ab initio* molecular dynamics study of a benchmark metal organic framework (MOF), ZIF-8 growing at the ZnO/H_2O interface in the presence of the MOF linker molecule, 2-methyl-imidazole (2-MIM) revealed that MOF formation is controlled by dissolution of surface Zn^{2+} ions, which, in turn, is controlled by multiple roles of 2-MIM as a “step-pinner” and “dissolution-promoter” at the distinct step edges and terraces of the ZnO substrate. This synergy between metal oxide dissolution and linker adsorption provides a new avenue for designing synthetic processes of porous heterostructures.

Our findings point towards an approach to synthesis of heterostructures that goes beyond simple principles of lattice matching. Instead, the results highlight the possibility of utilizing organic-substrate interactions to manipulate the substrate surface chemistry, dissolution kinetics and geometry, and the chemical potential of desired products to define the nucleation and growth characteristics of the overgrown layer. Such an approach may provide a general strategy for controlling heterostructure orientation, composition and formation kinetics. As an example of an application of this approach, we synthesized ZIF-8 with dual porosity using ZnO nanorods and spherical nanoparticles as an active substrate. The size and shape of ZnO nanostructures, which are completely consumed during synthesis, defines the larger-scale porosity, while fine-scale porosity is defined by the intrinsic pore size of ZIF-8 framework.

4. *Atomistic insight into particle coalescence*. By using *in situ* liquid-cell transmission electron microscopy, we reveal the initial contact of Au nanocrystals over their hydration layers, which is achieved via the newly formed nanobridge between the nanocrystals.[5] Classical density functional theory calculations and *ab initio* molecular dynamics simulations suggest that the formation of nanobridge is attributed to the accumulation of auric ions and higher local supersaturation in the gap. The resulted nanobridge can promote the dehydration, contact and fusion of the Au nanocrystals and this mechanism can be used for a controllable aggregation. Our finding provides an indepth understanding of the role of solution ions/atoms in nanoparticle coalescence process.

5. *Charge storage mechanism in aqueous rechargeable zinc–manganese dioxide batteries*. We demonstrated a new charge storage mechanism in δ-MnO_2 for designing high-rate performance Zn-MnO_2 batteries.[4] A joint nondiffusion controlled Zn^{2+} intercalation in bulk δ-MnO_2 and H^+ conversion reaction pathway was identified in δ-MnO_2 cathode during charge and discharge, in which the charge storage mechanisms could be tailored through electrolytes, especially via the anion of zinc salt. Fast reaction kinetics not limited by ion diffusion was realized for Zn-δ-MnO_2 batteries in $Zn(TFSI)_2$-based mild aqueous electrolyte in a wide C-rate range. This mixed energy storage mechanism contributes to superior high rate electrochemical performance of 136.9 mAh g^{-1} discharge capacity at 20 C and 93% capacity retention after 4000 cycles. This study opens a new gateway to the design of high-rate electrode materials by manipulating the effective redox reactions in electrode materials for rechargeable batteries.

Future Plans

Future work will focus on fundamental understanding of the role of solvent and electric field in nucleation on well-defined nanostructured substrates. The emphasis will be on the impact of interfacial solvent properties and solution composition on early stages of heterogeneous nucleation, phase evolution and branch formation and on the role of electric field in manipulating these processes. Future research will be based on four integrated elements: modeling experimental systems with well-defined interfacial structures, extensive characterization of interfaces, *in situ* and *ex situ* methods to monitor nucleation and growth processes, and theory to incorporate the effects of interfacial structures and predict nucleation and assembly. This project will focus on four key tasks.

1. In-depth study of physico-chemical processes taking place during metal nucleation on graphitic surfaces in electric field.
2. Using newly developed AFM-based technique for measuring interfacial solvent structuring with sub-nanometer spatial resolution to explore solvent structure evolution during heterogeneous nucleation.
3. Explore and apply principles of interface- controlled crystallization in simple solvents and in ionic liquids and self-assembly to control the pathways leading to complex higher-order architectures.
4. Expanding the materials systems to include two dimensional crystalline and quantum materials,

References

1. Lili Liu, Maria L. Sushko, Edgar C. Buck[2], Xin Zhang, Libor Kovarik, Zhizhang Shen, Elias Nakouzi, Jinhui Tao, James J. De Yoreo, Jun. Liu· "Mechanism of branch formation during the growth of hierarchical ZnO nanostructures" (submitted)
2. Jin B., Sushko M.L., Liu Z/, Cao X., Jin C., Tang R. (2019) Understanding anisotropic growth of Au penta-twinned nanorods by liquid cell transmission electron microscopy. *J. Phys. Chem. Letters* 10 (7):1443–1449. DOI 10.1021/acs.nanolett.8b03139
3. Jinhui Tao, Mal-Soon Lee, Zhisen Zhang, Susrut Akkineni, Debasis Banerjee Mark Bowden, Praveen K. Thallapally, Yongsoon Shin, Maria L. Sushko, James J. De Yoreo, Jun Liu· "Step-specific ligand interactions control crystallization of metal-organic framework heterostructures" (submitted).
4. Jin, Y., Zou, L., Liu, L., Engelhard, M. H., Patel, R. L., Nie, Z., Han, K. S., Shao, Y., Wang, C., Zhu, J., Pan, H., Liu, J., (2019) Joint Charge Storage for High-Rate Aqueous Zinc–Manganese Dioxide Batteries. *Advanced Materials* 1900567. DOI: 10.1002/adma.201900567
5. Jin B., Sushko M.L., Liu Z, Jin C, Tang R (2018) In situ liquid cell TEM reveals bridge-induced contact and fusion of Au nanocrystals in aqueous solution. *Nano Letters* 18 (10), 6551-6556. DOI: 10.1021/acs.nanolett.8b0313

Publications

6. Jin, Y., Zou, L., Liu, L., Engelhard, M. H., Patel, R. L., Nie, Z., Han, K. S., Shao, Y., Wang, C., Zhu, J., Pan, H., Liu, J., (2019) Joint Charge Storage for High-Rate Aqueous Zinc–Manganese Dioxide Batteries. *Advanced Materials* 1900567. DOI: 10.1002/adma.201900567
7. Jin B., Sushko M.L., Liu Z/, Cao X., Jin C., Tang R. (2019) Understanding anisotropic growth of Au penta-twinned nanorods by liquid cell transmission electron microscopy. *J. Phys. Chem. Letters* 10 (7):1443–1449. DOI 10.1021/acs.nanolett.8b03139
8. Tao J., Nielsen M.H., De Yoreo J.J. (2018) Nucleation and phase transformation pathways in electrolyte solutions investigated by *in situ* microscopy techniques. *Current Opinion in Colloid & Interface Science* 34, 74-88. DOI: 10.1016/j.cocis.2018.04.002
9. Han Y., Sinnwell M.A., Sun L., Teat S.J., Sushko M.L., Bowden M.E., Miller Q.R.S., Schaef H.T., Liu L., Nie Z., Liu. J., Thallapally P.K. (2019) Desulfurization Efficiency Preserved in a Heterometallic MOF: Synthesis and Thermodynamically-Controlled Phase Transition *Advanced Science* 6 (7), 1802056. DOI 10.1002/advs.201802056
10. Zeng Z, Murugesan V, Han K.S., Jiang X, Cao Y, Xiao L, Ai X, Yang H, Zhang JG, Sushko M.L., and Liu J. (2018) Non-flammable electrolytes with high salt-to-solvent ratios for Li-ion and Li-metal batteries. *Nature Energy*, **3**, 674–681 DOI. 10.1038/s41560-018-0196-y

11. Jin B., Sushko M.L., Liu Z, Jin C, Tang R (2018) In situ liquid cell TEM reveals bridge-induced contact and fusion of Au nanocrystals in aqueous solution. *Nano Letters* 18 (10), 6551-6556. DOI: 10.1021/acs.nanolett.8b0313

12. Tao J., Nielsen M.H., De Yoreo J.J. (2018) Nucleation and phase transformation pathways in electrolyte solutions investigated by *in situ* microscopy techniques. *Current Opinion in Colloid & Interface Science* 34, 74-88. DOI: 10.1016/j.cocis.2018.04.002

13. Cheng Y.W., Tao J., Zhu G.M., Soltis J.A., Legg B. A., Nakouzi E., De Yoreo J. J., Sushko M.L., and Liu J. (2018) Near surface nucleation and particle mediated growth of colloidal Au nanocrystals. *Nanoscale* 10, (25) 11907-11912. DOI. 10.1039/c8nr03408g

14. Terban M.W., Banerjee D., Ghose S., Medasani B., Shukla A., Legg B. A., Zhou Y. F., Zhu Z. H., Sushko M.L., De Yoreo J.J., Liu J., Thallapally P.K., and Billinge S. J. L. (2018) Early stage structural development of prototypical zeolitic imidazolate framework (ZIF) in solution. *Nanoscale* 10, (9) 4291-4300. DOI. 10.1039/c7nr07949d

15. Sinnwell M. A., Atwood J. L., and Thallapally P.K. (2018) Sorption of CO_2 in a hydrogen-bonded diamondoid network of sulfonylcalix 4 arene. *Supramolecular Chemistry* 30, (5-6) 540-544. DOI. 10.1080/10610278.2018.1436709

16. Xiao L., Lu X., Fang Y., Sushko M.L., Cao Y., Ai X., Yang H., and Liu J. (2018). Low-Defect and Low-Porosity Hard Carbon with High Coulombic Efficiency and High Capacity for Practical Sodium Ion Battery Anode. *Advanced Energy Materials*. 8, (20) 1703238. DOI: 10.1002/aenm.201703238

17. Kim S. J., Mahmood J., Kim C., Han G. F., Kim S. W., Jung S. M., Zhu G. M., De Yoreo J. J., Kim G., and Baek J. B. (2018) Defect-free encapsulation of Fe^0 in 2D fused organic networks as a durable oxygen reduction electrocatalyst. *Journal of the American Chemical Society* 140, (5) 1737-1742. DOI. 10.1021/jacs.7b10663

18. Banerjee. D., Chen. X., Lobanov. S. S., Plonka. A. M., Chan, X., Daly, J. A., Kim, T., Thallapally. P. K., Parise. J. B., (2018) Iodine adsorption in metal organic frameworks in the presence of humidity *ACS. Appl. Mater. Interfaces.*, 10, 10622-10626.

19. Lucero. J., Elsaidi. S. K., Anderson. R., Wu. W., Gomez-Gualdron. D. A., Thallapally. P. K., Carreon. C. A., (2018); Time Dependent Structural Evolution of Porous Organic Cage CC3. *Cryst. Growth. Des.*, 18, 921 – 927.

20. Elsaidi. S. K., Mohamed. M. H. Banerjee. D., Thallapally. P. K., (2018) Flexibility in Metal Organic Frameworks: A fundamental understanding " *Coord. Chem. Rev.*, 358, 125 – 152.

21. Wang X. F., Zhang M. H., Alvarado J., Wang S., Sina M., Lu B. Y., Bouwer J., Xu W., Xiao J., Zhang J. G., Liu J., and Meng Y. S. (2017) New insights on the structure of electrochemically deposited lithium metal and its solid electrolyte interphases via cryogenic TEM. *Nano Letters* 17, (12) 7606-7612. DOI. 10.1021/acs.nanolett.7b03606

22. Medasani B. K., Liu J., and Sushko M. L. (2017) Stable Pt clusters anchored to monovacancies on graphene sheets. *MRS Communications* 7, (4) 891-895. DOI. 10.1557/mrc.2017.112

23. Elsaidi S. K., Sinnwell M. A., Banerjee D., Devaraj A., Kukkadapu R. K., Droubay T. C., Nie Z., Kovarik L., Vijayakumar M., Manandhar S., Nandasiri M., McGrail B. P., and Thallapally P. K. (2017) Reduced magnetism in core-shell magnetite@MOF composites. *Nano Letters* 17, (11) 6968-6973. DOI. 10.1021/acs.nanolett.7b03451

24. Cao X. X., Pan A. Q., Liu S. N., Zhou J., Li S. T., Cao G. Z., Liu J., and Liang S. Q. (2017) Chemical synthesis of 3D graphene-like cages for sodium-ion batteries applications. *Advanced Energy Materials* 7, (20) 10. DOI. 10.1002/aenm.201700797

25. Pan H., Li B., Mei D., Nie Z., Shao Y., Li G., Li X. S., Han K. S., Mueller K. T., Sprenkle V., and Liu J. (2017) Controlling solid–liquid conversion reactions for a highly reversible aqueous zinc–iodine battery. *ACS Energy Letters*, 2674-2680. DOI. 10.1021/acsenergylett.7b00851

26. Lu D., Tao J., Yan P., Henderson W., Li Q., Shao Y., Helm M., Borodin O., Graff G., Polzin B. , Wang C., Engelhard M. Zhang , J-G. , De Yoreo J.J. , Liu J. , Xiao J.. (2017). "Formation of Reversible Solid Electrolyte Interface on Graphite Surface from Concentrated Electrolytes" *Nano Lett. 17*, 1602-1609 DOI 10.1021/acs.nanolett.6b04766

27. Li W.Z., Kovarik L., Cheng Y., Nie L., Bowden M.E., Liu J., and Wang Y. (2017). Stabilization and transformation of Pt nanocrystals supported on $ZnAl_2O_4$ spinel, *RSC Advances*, 7, 3282-3286, DOI: 10.1039/C6RA26159K

2-d quantum materials by metal intercalation of graphene/graphite

M.C.Tringides[1,2] K.M. Ho[1,2] , M.Hupalo[1] , P. A. Thiel[1,3] , C. Z. Wang[1]
[1] Ames Laboratory, [2] Department of Physics-ISU, [3] Department of Chemistry-ISU Ames IA 50011

I. Program Scope

Graphene and other 2-d layered materials have been in mainstream research because of their unusual electronic and magnetic properties [1-3]. These properties can be tuned by finding ways to control further their band structure. One way to accomplish this target is by metal intercalation of graphene or graphite. Besides tuning graphene properties the intercalated metal is chemically well protected by graphene on top. Intercalation is a very promising and unexploited process with large potential for synthesis of 2-d heterostructures that is poorly understood. One FWP goal is for a given metal to identify the key thermodynamic processes and kinetic barriers that control intercalation [5]. Essential processes (adatom diffusion, lattice incorporation, adatom transfer to lower layers, de-intercalation) have not been yet clarified. Depending on the kinetic pathways chosen, different intercalated phases can form, which can be used to build metal/graphene heterostructures. For these heterostructures it is important to determine their formation energies, their thermal stability and temperature range of operation.

Another FWP goal is to use electronic interactions across the interfaces in metal/graphene heterostructures to modify the potential experienced by the graphene electrons, to generate novel topological phases and to synthesize quantum materials. Layered heterostructures are commonly fabricated via mechanical stacking of exfoliated layers of 2-d materials, but this has limitations because of interface contamination. Using metal intercalation on graphitic substrates offers a new synthesis method to grow stacked quantum materials with tunable properties. The grown heterostructures X1-G or X1-G-X2 will consist of the intercalated metal X1 below; of graphene G; and a different metal X2.

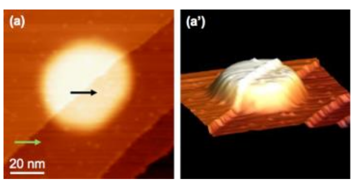

Fig. 1.Encapsulated Cu islands across graphite steps separating different terraces. The step height at the top (black arrow) is the same as the step height at of the terrace (green arrow) 0.33nm, the step of graphite. This indicates bilayer graphene is covering the upper part of the island.

Because interfaces are critical in layered materials they require the use of complementary techniques for structure (high resolution LEED and STM) and band structure (ARPES) characterization. These experimental efforts will be carried out in parallel with theoretical efforts to define the optimal systems, the growth "window" to fabricate the heterostructures and their energetic stability.

II. Previous work

Defect-mediated intercalation of metals in graphite. **Dy island encapsulation** Metal intercalation experiments were carried on graphite[5]. We found that 3 metals--Dy, Ru, and Cu--can be encapsulated at the graphite (0001) surface if two specific conditions are met: Defects are present in the graphite surface to act as entry portals for the deposited atoms, and the deposition temperature is well above ambient. Focusing on Dy as a prototype, we have shown that surface intercalation is much different than bulk intercalation (commonly performed under liquid environment) because the intercalated metal takes the form of bulk-like Dy rafts, rather than the $(\sqrt{3}\times\sqrt{3})R30^{\circ}$ structure known for the bulk compound. For each metal a specific temperature "window" applies when the kinetic processes become sufficiently fast. Since this type of nucleation is new modeling has been performed to understand what controls the nucleation time and location. Theory and stochastic lattice-gas modeling were developed to understand the formation of intercalated islands between the top and underlying layer at the surface of layered materials[6].

Cu island encapsulation When the substrate is held at 800 K during deposition, conditions are optimal for the formation of encapsulated multilayer Cu islands[7]. Deposition temperatures below 600 K favor adsorbed Cu clusters on top, while deposition temperatures above 800 K favors single-layer intercalated Cu islands. The multilayer Cu islands are characterized in detail with respect to size and shape, thickness and continuity of the graphitic overlayer, relationship to graphite steps, and stability in air. The experimental techniques used are STM and X-ray photoelectron spectroscopy. We also use DFT to compare stabilities of a wide variety of Cu atom distributions on/under graphite.

Modeling of encapsulated Cu island shapes We develop a continuum elasticity (CE) model for the equilibrium shape of these islands, and compare its predictions with experimental data[8]. The CE model incorporates appropriate surface energies, adhesion energies, and strain energy. The agreement between the CE model and the data is—with one exception—excellent, both qualitatively and quantitatively. The model predicts that the embedded island shape is invariant with size, manifest both by constant side slope and by constant aspect ratio. The aspect ratio of an embedded Cu island is much larger than that of a supported but non-embedded Cu island, due to resistance of the graphene membrane to deformation. Experimental data diverge from the model predictions only in the case of the aspect ratio of small islands, below a critical height of ~10 nm. Strong support for the CE model and its interpretation is provided by additional data for embedded Fe islands.

Encapsulation of Ru islands Using STM and XPS we show that Ru can form metallic nanoislands on graphite [9]. These islands are air-stable, contain 2 to 4 single-atom layers of Ru, and have diameters on the order of 10 nm. The graphite surface must first be ion-bombarded, then held at elevated temperature (1000 to 1180 K) during Ru deposition. A coincidence lattice forms between graphene and the Ru island top. Its characteristics closely resemble the well-established characteristics of single-layer graphene on the (0001) surface of bulk Ru. The embedded Ru islands are energetically favored over on-top (adsorbed) islands, based on DFT calculations for Ru films.

Manipulation of Dirac cones in intercalated graphene We have theoretically investigated the electronic band structure of epitaxial graphene on SiC with intercalation of rare earth metal ions (e.g., Yb and Dy) [4]. The intercalation can be used to control the coupling of the constituent components (buffer layer, graphene, and substrate), resulting in strong modification of the graphene band structure. It is demonstrated that the metal-intercalated epitaxial graphene has tunable band structure by controlling the position of the Dirac cones, the shape of the band dispersion (whether linear or quadratic); and the intercalation layer the metal adatoms are bonded to (i.e. whether between buffer layer and substrate or between graphene and buffer layer).

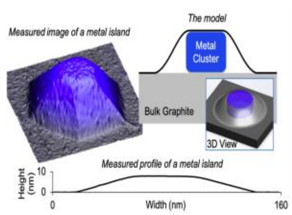

Fig.2 STM image of encapsulated Cu island on graphite with low height to diameter ratio. An analytic model that includes graphene's elastic energy and graphene graphite adhesion energy can account for these "squeezed"shapes.

Interface modification of the potential of graphene electrons. We have studied the structural and electronic properties of graphene grown on SiC, using low energy electron diffraction (SPA-LEED), STM and angle resolved photoemission spectroscopy (ARPES) [10]. We find in the ARPES spectra several new replicas of Dirac cones in the Brillouin zone (BZ), which have not been seen in previous graphene work because of the low quality graphene-SiC interface. The location of the replica cones are only at 3 wavevectors of the $6\sqrt{3} \times 6\sqrt{3}$ unit cell of the Moire (out of 169 possible wavevectors) at the buffer layer–SiC interface. Since the same wavevectors are also seen in the SPA-LEED diffraction this confirms that these wavevectors are intrinsic to the interaction Hamiltonian the electrons experienced oat the interface.

III. Future Plans

Encapsulated metal islands under graphite. In addition to Dy, Cu, Ru, we have observed similar encapsulated islands with Pt and Gd. In all cases, the graphitic lattice can be clearly resolved atop the metal island and on the sides. The good crystalline quality of the metal is evidenced by the faceted shape and, in the case of Ru and Dy, by the presence of a Moiré pattern which reflects long-range coincidence between the periodicities of the metal and the graphitic overlayer lattices.

There are a number of important, open questions about these structures, even for the elemental metals. One major topic is their mechanism of formation. From the experiments, it is clear that defects induced by ion bombardment are necessary [5] but the ratio of encapsulated islands to defects is very small, suggesting that only a small fraction of defects serve as effective entry portals. Theoretical work planned in this FWP will help to clarify the nature of the active portals (i.e., size, and decoration of the perimeter with metal atoms), which may be different for different metals. Also from the experiments, it is clear that deposition at elevated temperature is necessary, implying the existence of a key activated process that is mainly accessible during deposition, since annealing post-deposition is ineffective at producing intercalated islands. Again, theoretical work planned in this FWP will help to clarify the nature of various activated processes, particularly the activation barrier for metal atoms to pass through portals and the factors that influence this barrier, such as size, configuration, and decoration by affixed metal atoms.

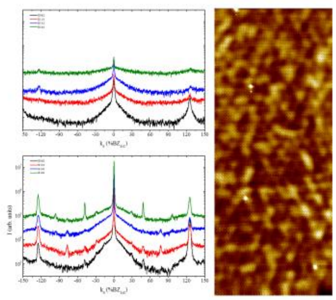

Fig.3 SPALEED profiles as a function of energy for clean graphene (left bottom) and intercalated graphene (left top). The intensity distribution can be used to deduce the location of Dy. STM showing intercalated Dy. without the 6x6 modulation (right).

The identification of intercalation mechanisms on the nanoscale poses open questions. We will perform first-principles calculations and atomistic simulations to investigate the optimal conditions and pathways for bare metals or metal/alloys, especially rare earth, intercalation of graphene and graphite. For the experiments on graphite which introduce defects as portals, calculations of the relevant barriers will be useful. The knowledge of the barriers will be crucial information to determine the annealing procedure for bare metal or for metal co-deposition. It was overlooked in the literature that defects can also be traps for the intercalants and slow diffusion because the attachment energy for most metal at the defect sites is usually very large. We will investigate how to avoid the defect trapping and promote the passage of metal intercalants through and away from the defects. While defects on graphene may help accelerate metal intercalation, defect-free graphene would be more desirable for applications. We therefore will also investigate the mechanism and process of defect healing on graphene and graphite, after island encapsulation, to propose a successful experimental procedure. We will check theoretically how the graphene layer can be restored to its initial uniform form by balancing the detachment of metal atoms from the defect perimeter with the attachment of carbon atoms to fill in the defects (which can arrive from low coordination graphene edges.) Moreover, electronic structures of the intercalated graphene and graphite surfaces will be further characterized by comparing simulated STS spectra for atoms on top vs atoms below graphene, to help the interpretation of the experimental spectra.

While metal encapsulation beneath graphene has been partially studied, to date mainly 2-d intercalation layers have been identified, i.e. [12]. Thus, the metal islands that are encapsulated beneath graphite are special in terms of their preferred multilayer (3-d) geometry. These islands can be grown with heights of a few metal layers to several tens of metal layers, depending on the metal and on the experimental conditions. A natural extension of our studies would be to synthesize multi-component alloy islands, and the 3-d aspect opens opportunities for multi-component synthesis of nanoscale films including intermetallics.

Quantum materials by intercalation Intercalation studies will be continued for graphene grown on SiC. QWe will search for intercalation phases for single metals and metal combinations under graphitic surfaces. These phases will provide a wide range of choices to build binary or ternary heterostructures with tunable electronic interactions mediated by the interfaces, with promising topological properties. These possibilities already gained add new routes in the synthesis of 2-d quantum phases. For example Ca intercalated in graphene was shown to be a 2-d superconductor with T_c ~4K (reminiscent of earlier studies of superconductivity in intercalated graphite [13]). Pb intercalated below graphene was shown to induce magnetism to graphene because of the large Spin Orbit (SO) coupling of Pb [14].

Intercalation of 2-d materials will be investigated both on graphene and graphite. It is an uncharted area requiring systematic search to identify the correct parameter “window”. The newly discovered method of graphite intercalation through defects is a fast and efficient procedure to identify quickly the intercalation “window”. By reducing the sputtered defect density the encapsulated islands will have large lateral sizes and will be candidate systems for novel quantum materials. More importantly the electronic and magnetic properties of the intercalated metal can differ from its corresponding bulk properties, both because of the reduced dimensions and difference in the bonding configuration of the metal in the graphite galleries.

Open questions about the kinetics of intercalation The importance of kinetics for intercalation can be seen from studies in the literature. One of the most widely studied systems is Au on graphene on SiC. with different phases observed depending on the intercalation conditions. When Au was deposited only on the buffer layer the Au intercalant forms two ordered Au phases. The low coverage (1/3ML) phase has holes while the high coverage (1ML) phase has electrons [15]. Guided by theory we will map out the 2-d phases of intercalated Dy on buffer layer and monolayer graphene as a function of growth conditions using STM, SPA-LEED, XPS, DFT. Both low and high coverage phases will be identified. More importantly the location of the Dy atoms will be determined whether between SiC-buffer or between buffer-graphene or a mixture of the two [4]. The distribution of the metal atoms will be determined from the variation of the SPA-LEED spots as a function of electron energy. As already noted this information can be used so the physical properties of intercalated layer can be selectively tuned. For example the band gap can be tuned continuously by varying the relative occupation of the SiC-buffer and buffer-monolayer galleries [4]. Intercalation of Pb in graphene on Ir(111) transforms the graphene electrons into a 2-d electron gas in the presence of a large effective magnetic field because of the SO coupling, seen in very well resolved Landau levels with STS spectra[14]. Similar studies will be carried out for graphene on SiC with more possibilities since graphene of different thickness (single-, bi-, and tri-layer) can be grown.

Modeling metal intercalation on graphitic substrates. There is a need for better characterization of the intercalation processes and for better comparison between experimental results and calculations, because currently there are systems where the results of experiments are not consistent with results in the theoretical literature. Despite the high barriers calculated for H and Li it was found with well-designed experiments that intercalation was successful on defect-free substrates. In addition the initial substrate morphology most likely will be a mixture of graphene of different thickness (i.e. a fraction can be buffer and the rest monolayer) and also plays a role. The boundaries between domains of the different thicknesses is a good place for the diffusing atoms to intercalate [16]. In most theoretical studies a small unit cell is assumed, which implies periodic arrangement on the surface; but steps or domain boundaries involve mesoscale non-periodic structures with a distribution of atom configurations. We will extend theoretical calculations beyond periodic structures to examine the role of boundaries in graphene flakes: how atoms can move towards the interior of the flake after they diffuse underneath at the edges. Effects of the substrate on such intercalation pathways and barriers will be calculated. Other issues include whether the intercalated material is ordered or disordered, laterally dense or dilute, single- or multi-layer, and how the conditions of preparation affect these characteristics.

References

[1]A.H.Castro Neto et al *Rev. Mod. Phys.* 81, 109 (2009).
[2] Z. K. Liu et al *Nature* **499**, 419–425 (2013).
[3] C. Berger et al *J. Phys. Chem. B*, 108, 19912 **(**2004)
[4] M. Kim et al *Carbon* 123 93 (2017)
[5] Y. Zhou et al *Carbon* 127 (2018) 305 311
[6] Y. Han et al *Phys. Rev. Mat*. **1**, 053403 (2017)
7. A. Lii-Rosales et al J. Phys. Chem. C 2018, 122, 4454 (journal cover)
[8] S. E. Julien et al *Nanoscale* 11, 6445 (2019).
[9] A. Lii-Rosales, et al *Nanotechnology* 29 (2018) 505601 (14pp)
[10].L. Huang et al *Phys. Rev. B, 96, 035411 (2017)*
[11]M. Büttner et al *Carbon* **49**, 3937 (2011).
[12]M. Batzill et al *Surf. Sci. Rep*. **67**, 83 (2012).
[13] S. Ichinokura et al ACS Nano 10, 2761 (2016)
[14]. F. Calleja et al Nature Physics | 11 2015 43
[15] I. Gierz et al Phys. Rev. B 81, 235408 (2010)
[16] L. Jin et al *Phys. Chem. Chem. Phys.* 13 (2011) 16655-16660.

Surface Structure FWP FY17-19 Publications

1. N. Anderson et al. *J. Appl. Phys*. 121 , 014310 (2017);
2. N. A. Anderson et al. Vaknin *Journal of Magnetism and Magnetic Materials* 435 212 (2017)
3 .L. Huang et al. *Phys. Rev. B, 96, 035411 (2017)*
4. M. Kim et al. *Carbon* 123 93 (2017)
5.C. Brand et al., *Phys. Rev. B* 96, 035432 (2017)
6. A. Lii-Rosales et al., *Physical Review Materials* 1, 026002 (2017)
7. D. Appy et al. *Journal of Vacuum Science & Technology A: Vacuum, Surfaces, and Films* **35**, 061401 (2017)
8 Y. Han et al., *Phys. Rev. Mat*. **1**, 053403 (2017)

9. N.A. Anderson et al. *Phys. Rev. Mate*. 1, 054005 (2017)
10.A. Lii-Rosales et al. *J. Phys. Chem.* C 2018, 122, 4454 (journal cover)
11Y. Zhou et al., A *Carbon* 127 (2018) 305 311
12 A. Lii-Rosales *Nanotechnology* 29 (2018) 505601
13 N. Anderson et al. *JMMM* 474 666 (2019)
14 Y. Han et al. *Phys. Rev. B 99*, 115415 (2019)
15 Y. Han et al. *Surface Science* 685, 48 (2019).
16 S. E. Julien et al. *Nanoscale* 11, 6445 (2019).
17 K. Idczak et al. *Appl. Surf. Sci.* 487 (2019) 1348
18 T. Jaroch et al. , *Journal of Crystal. Growth (in press)*
19 "Tuning Pb intercalation under graphene on SiC" S. Chen, C.-C. Kuo, P. A. Thiel. E. Conrad and M. C.Tringides *2d Materials* (under review).

This page is intentionally blank.

University Grants' Abstracts

This page is intentionally blank.

Electrodeposition of metals in viscoelastic liquid electrolytes

Lynden A. Archer and Donald L. Koch, School of Chemical & Bimolecular Engineering, Cornell University

Program Scope

Electrodeposition is used in manufacturing processes for creating metal, colloid, and polymer coatings on conductive substrates. The process also plays an important role in electrochemical storage technologies based on batteries, where it must be carefully managed to facilitate stable and safe operations at low operating temperatures, high rates and over many cycles of charge and discharge. In all currently used electrolytes deposition is subject to a variety of hydrodynamic and morphological instabilities at both low and high current densities, which lead to complex transport phenomena in the electrolyte and unstable deposition, including formation of ramified structures known as dendrites. These instabilities were first studied in the context of electroplating, where it was found to be remarkably difficult to achieve uniform deposition of many metals. They have received renewed interest due to the role unstable electrodeposition plays in creating metallic dendrites implicated in the failure of microcircuits and in the failure of high-energy lithium and emerging sodium-metal batteries by internal short circuits. The ~~proposed~~ research employs experiment, theory, and numerical approaches to understand the effect of elasticity in liquid electrolytes on the stability of electrodeposition. A related goal of the study is to develop design principles for viscoelastic liquid electrolytes that are able to stabilize electrodeposition at low and high current densities. The project is designed to evaluate the hypothesis that liquid electrolytes comprised of semi-dilute, entangled solutions of high molecular weight polymers ($M_w > 1 \times 10^6$ g/mol) with high, liquid-like ion mobilities should be able to stabilize electrodeposition by multiple processes (Figure 1), including fundamental changes in convective flow produced by polymer stresses, polymer adsorbtion at and retardation of ion transport to dendrite nucleates, osmotic resistance to ion concentration at dendrite tips, and polymer drag on a bulk electrolyte. All of these effects originate from the assumption that polymer chains move more slowly than solvent molecules or ions in solution.

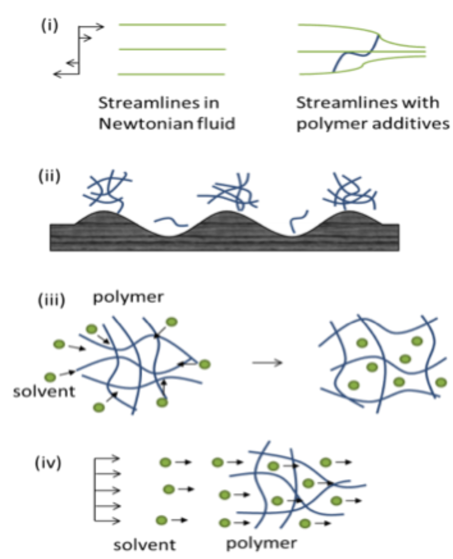

Fig. 1 Possible stabilizing mechanisms introduced by high molar mass polymer additives in a liquid electrolyte.

Recent Progress

I. Polymer elasticity completely suppresses electroconvection

To evaluate the hypothetical stabilization mechanisms in **Figure 1**, we previously created viscoelastic electrolytes in which high molecular weight poly(ethylene oxide), M_w = 8.1 x10^6 g/mol, or poly(methyl methacrylate), M_w = 2 x 10^6 g/mol, were added to conventional protic and aprotic liquid electrolytes. By means of direct optical visualization and tracer particle velocimetry experiments of metal electrodeposition in such electrolytes, we discovered that at concentrations above the entanglement threshold, electroconvection and over-limiting conductance is suppressed by polymer elasticity. These experiments also revealed that soft metals such as Na and Li deposit in more compact morphologies in a viscoelastic electrolyte.[1]

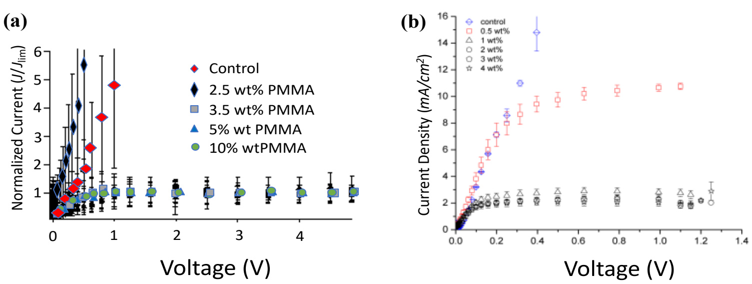

Fig. 2 (a) Current density (*J*) versus voltage (*V*) plot for Li||Nafion||Li cells containing EC-PC 1M LiTFSI electrolyte and PMMA (*M*w=0.9 x 10^{6}g/mol) at various concentrations. (b) *J*-V plot Cu||Nafion||Cu cells containing 0.05M $CuCl_2$ aqueous electrolyte and PEO (*M*w=8.1 x 10^{6}g/mol).[2]

To determine root causes, we recently designed electrochemical cells in which the electrolyte is bounded on one side by a cation-selective Nafion^{TM} membrane. By interrogating the current-voltage (*J*-V) profile and tracer particle motions near the membrane-electrolyte interface, it is possible to isolate and study the effect of electrolyte viscoelasticity on the hydrodynamic instability. The results reported in **Fig. 2** show that under these conditions over-limiting conductance is completely suppressed, and the diffusion-limited transport regime extended indefinitely, over a narrow range of polymer concentration close to the entanglement threshold.

We used 10µm and 3µm uncharged polystyrene tracer particles to interrogate the velocity profile in aqueous electrolytes at voltages well above the threshold for onset of hydrodynamic instability in the polymer-free electrolytes. The results reported in **Fig. 3a** reveal that there are substantial velocity components both parallel < **u** > and normal < **v** > to the membrane surface in the closed

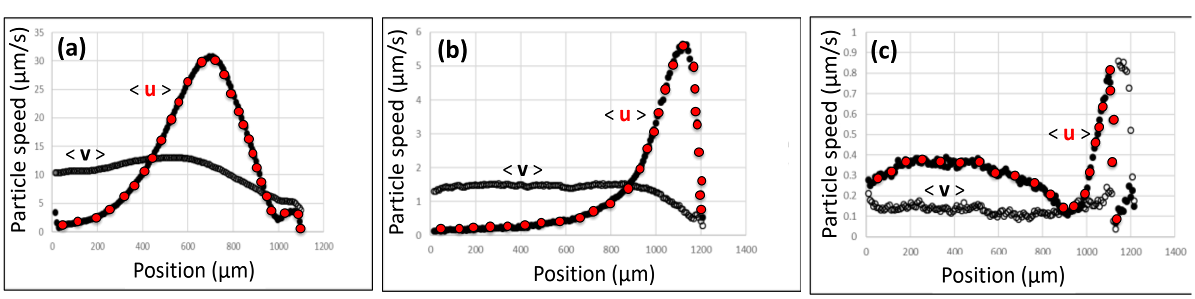

Fig. 3 Lateral and vertical components of the root-mean square average velocity as a function of distance from a cation selective membrane for Cu||Nafion||Cu cells at *V* = 80RT/F, $\kappa^{-1} \approx$ 10nm, and membrane-electrolyte interface located at a position of 1200 µm). **(a)** Control $CuCl_2$ aqueous electrolyte without polymer; **(b)** Same as (a), but with 0.5 wt% PEO (*M*w = 8.1 x 10^6 g/mol); **(c)** same as (a) with 1 wt% PEO (*M*w = 8.1 x 10^6 g/mol).

cell, and that these velocities are strong functions of position normal to the membrane surface up to distances several hundred micrometers away from the membrane/electrolyte interface and well into the electrolyte bulk. The position at which the maximum in $<\mathbf{u}>$ is observed is related to the thickness of the extended space charge layer Λ created by ion depletion at the cation selective membrane and the maximum value of $<\mathbf{u}>$ provides a rough estimate for the slip velocity, u_s, at the edge of the space charge layer. Comparing these profiles with the corresponding ones measured in electrolytes with PEO concentrations bracketing where over-limiting conductance is suppressed, reveals the mechanisms through which an entangled electrolyte suppresses over-limiting conductance: electrolyte viscoelasticity reduces the strength of the underlying convective flow and also lowers the value of Λ. We note also that the values of Λ and $u_{s,V}$ deduced from the experiments in electrolytes with/without polymer are orders of magnitude larger than those predicted by any current theory. Understanding the source of this behavior is the subject of our future experimental and theoretical studies.

II. Numerical simulations reveal that polymer elasticity favors uniform deposition

To elucidate the microscopic processes responsible for the observations from our *J*-V (**Fig. 2**) and tracer velocimetry (**Fig. 3**) experiments, we recently performed numerical simulations of electroconvection in a viscoelastic fluid.[3] In the numerical simulations, we use the FENE-CR model to capture the effects of polymer elasticity in a Newtonian fluid medium. The results summarized in Fig. 4 reveal that polymers alter electroconvection and the over-limiting current in two desirable ways. At a moderate dimensionless voltage (V = 20RT/F), the polymer destabilizes steady electroconvection leading to a time dependent flow with more uniform ion flux (**Fig. 4a, b**). At a higher dimensionless voltage V = 80, the convection becomes chaotic even in a Newtonian fluid (**Fig. 4c**). Polymer elasticity reduces the size of low salt concentration blobs and suppresses high-ion flux events (**Fig. 4d**).

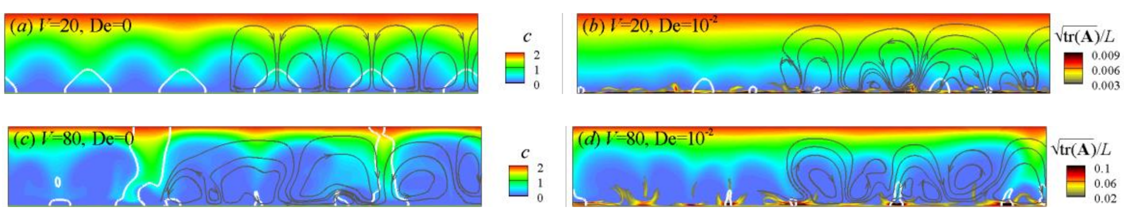

Fig. 4 Salt concentration and stress distribution near an ion-selective electrode for: (**a**) V = 20; De=0, **(b)** V =20; De=10^{-2}, **(c)** V=20; De=0, **(d)** V = 80; De=10^{-2}; double layer thickness $\delta=10^{-3}$. Contour plots show salt concentration c and polymer extension tr($\mathbf{A}$)$^{-1/2}/L$, gray lines are streamlines, and the white contour lines indicate high flux regions with i^{+}_{y}=-3 in (a, b) and -10 in (**c**, **d**), respectively.[3]

We also computed the ionic current and magnitude of the relative tangential (slip) velocity as a function of the Weissenberg number, which characterizes the strength of the polymer stretching in the locally high shear rate in the space charge layer. The results show that the polymer elasticity reduces the current substantially,[3] explaining the strong effect on over-limiting conductance observed experimentally.

Future Plans

Values of Λ and u_s deduced from our tracer particle studies are orders of magnitude larger than expected from any current theory. The results show further that over the range of voltages studied, u_s and Λ are weaker functions of voltage than expected from theory. Our future studies will utilize strictly neutral molecular and carbogenic fluorophores as tracer particles to more fully resolve the electroconvective flow profile in the ESCL. An advantage of these tracers is that they are substantially smaller than those used in our current studies and do not aggregate, which will make it possible to interrogate electroconvective flow near cation selective interfaces in more detail and over a wider range of *V* than possible in our earlier experiments. We will also use the method to study electroconvection in electrolytes with a wider range of salt concentration (μM to M), and optionally in which the electrolyte viscosity is adjusted using polymer additives with molar masses well below the entanglement threshold in the melt.

References

[1] Wei, S., Cheng, Z., Nath, P., Tikekar, M.D., Li, G. and Archer, L.A. (2018) Stabilizing electrochemical interfaces in viscoelastic liquid electrolytes. *Science Advances* **4**, 6243

[2] Warren, A., Zhang, D., Choudhury, S. and Archer, L.A. (2019) Electrokinetics in viscoelastic liquid electrolytes above the diffusion limit. *Macromolecules*, DOI: *10.1021/acs.macromol.9b00536*

[3] Li, G., Archer, L.A. and Koch, D.L. (2019) Electroconvection in a viscoelastic electrolyte. *Phys. Rev. Lett.* **122**, 124501

Publications

[1] Wei, S., Cheng, Z., Nath, P., Tikekar, M.D., Li, G. and Archer, L.A. (2018) Stabilizing electrochemical interfaces in viscoelastic liquid electrolytes. *Science Advances* **4**, 6243

[2] Tikekar, M. D., Li, G., Archer, L.A. and Koch, D.L. (2018) Electroconvection and morphological instabilities in potentiostatic electrodeposition across liquid electrolytes with polymer additives. *J. Electrochemical Society* **165**, A3697-A3713

[3] Warren, A., Zhang, D., Choudhury, S. and Archer, L.A. (2019) Electrokinetics in viscoelastic liquid electrolytes above the diffusion limit. *Macromolecules*, DOI: *10.1021/acs.macromol.9b00536*

[4] Li, G., Archer, L.A. and Koch, D.L. (2019) Electroconvection in a viscoelastic electrolyte. *Phys. Rev. Lett.* **122**, 124501

[5] Zhao, Q., Liu, X., Stalin, S., Khan, K. and Archer, L.A. (2019) Solid-state polymer electrolytes with in-built fast interfacial transport for secondary lithium batteries. *Nature Energy* **4**, 365-373

[6] Zhao, Q., Tu, Z., Wei, S., Zhang, K., Choudhury, S., Liu, X. and Archer, L.A. (2018) Building organic-inorganic hybrid interphases for fast interfacial transport in rechargeable metal batteries. *Angewandte Chemie* **57**, 992-996

[7] Zhao, Q., Zachman, M.J., AlSadat, W.I., Zheng, J., Kourkoutis, L.F. and Archer, L.A. (2018) Solid electrolyte interphases for high-energy aqueous aluminum electrochemical cells. *Science Advances* **4**, eaau8131

Atom-by-Atom Directional Synthesis of Semiconducting Graphene

Michael S. Arnold, University of Wisconsin-Madison, Department of Materials Science and Engineering, michael.arnold@wisc.edu

Program Scope

Graphene is an atomically thin crystal of carbon atoms that are arranged in a flat honeycomb lattice, with exceptional charge and energy transport properties. This project focuses on advancing the synthesis of graphene in the form of narrow, long, and oriented nanoribbons and organized arrays of nanoribbons. Whereas continuous sheets of graphene conduct charge similar to *metals*, narrow nanoribbons with smooth edges can behave as *semiconductors* with promise for advancing next-generation electronics and energy technologies. Other spin, magnetic, catalytic, and transport phenomena can also be derived by structuring graphene in the form of nanoribbons, depending on crystal orientation and the structure of the edges.

Semiconducting nanoribbons must be especially narrow (less than 10 nanometers) and have a particular structure of edges (armchair). The rational and organized synthesis of graphene nanoribbons with these characteristics has been challenging. Arnold has recently discovered a promising route for overcoming these challenges by driving graphene crystal growth via chemical vapor deposition with a giant crystal shape anisotropy and armchair edge faceting on single crystal germanium substrates. Measurements have shown that the nanoribbons are semiconducting with state-of-the-art electrical properties compared to nanoribbons grown by other methods. Recent research has moreover revealed that interactions between the substrate and the nanoribbon edges drive the formation of the nanoribbons and that the location of nanoribbons can be controlled by initiating their growth using lithographically patterned seed crystals.

Recent Progress

Over the last two years, we have:

- **Learned to use seeds to decouple nucleation and growth [1]**

We have discovered how to seed graphene crystal growth by lithographically patterning monolayers of graphene into nanoscale (25 – 100 nm in diameter) discs, transferring them to a Ge substrate, and then initiating growth from their edges. Without seeds, the orientation of graphene's lattice with respect to the Ge lattice is set during nucleation. For example, without seeds, about 45% of crystals evolve into high aspect ratio nanoribbons with armchair lattice orientations roughly pointed along Ge$[110]$, another 45% of the crystals evolve into high aspect ratio nanoribbons with armchair lattice orientations roughly pointed along Ge$[1\bar{1}0]$, and the remaining 10% of the crystals evolve into low aspect ratio rhombus-like structures with armchair lattice orientations rotated away from both Ge$[110]$ and Ge$[1\bar{1}0]$. By using seeds, any arbitrary relative lattice orientation can be created on-demand, thereby separating nucleation and growth processes.

This capability has been exploited to elucidate the dramatic effect of relative crystallographic orientation on growth kinetics. High aspect ratio nanoribbons form when the armchair crystallographic direction of the seeds is parallel to Ge[110]; however, low-aspect ratio structures form when the seeds are rotated away from Ge[110]. The structure and bonding between the edges of the seeds and the Ge surface are the only factors that change as the seeds are rotated. Thus, we have learned that it is indeed edge-substrate interactions that control growth kinetics and the anisotropy of these kinetics on Ge(001), as opposed to anisotropic diffusion, for example. It is these edge-substrate interactions that are the secret to coaxing graphene crystal growth processes to anisotropically and directly yield nanoribbons.

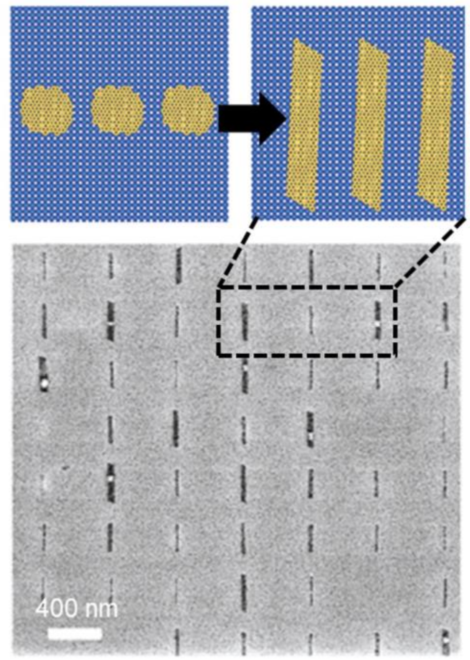

Figure 1. (Top) Schematic and (bottom) scanning electron micrograph of nanoribbon synthesis from seeds, via chemical vapor deposition on germanium.

- **Demonstrated synthesis of unidirectionally aligned nanoribbon arrays with controlled positioning and reduced polydispersity via seeding [1]**

We have exploited seeding to create arrays of parallel nanoribbons that are unidirectionally aligned, for the first time (Fig. 1). Seeding also reduces size polydispersity, because all ribbons begin growing at the same time.

- **Achieved nanoribbon synthesis from sub-5 nm seeds at variable pitches on Ge [2]**

We have demonstrated that nanoribbons can successfully grow from sub-5 nm seeds, in arrays with periods of 50 nm or smaller, without changes in kinetics arising from crowding effects. The viability of initiating nanoribbon synthesis from sub-5 nm seeds is important because it indicates that seed-mediated nanoribbon synthesis is compatible with the vanishingly small seed sizes that will be needed to seed the growth of sub-5 nm nanoribbons in the future. The viability of initiating nanoribbon synthesis from tightly pitched seeds is important because arrays of parallel nanoribbons will be needed for future applications.

- **Discovered that small graphene crystals rotate and "lock-in" to energetically favorable orientations [manuscript in preparation]**

To learn more about processes that occur during nucleation and/or shortly after nucleation, we have reduced the size of our lithographically patterned seeds by etching. We have discovered that once seeds become smaller than 15 nm in diameter, they begin to freely rotate on the Ge(001) surface at growth temperature and then lock into favorable configurations with armchair lattice orientation parallel to either Ge[110] or Ge$[1\bar{1}0]$. Thus, nanoribbons form on Ge(001) even without seeds because small crystals that form from spontaneously generated nuclei adopt favorable orientations that happen to coincide with the crystallographic orientations that produce the largest growth rate anisotropy.

- **Studied nanoribbon synthesis on vicinal Ge(001) surfaces [3]**

We have investigated nanoribbon synthesis on vicinal Ge(001) surfaces in order to ascertain the role of steps on nanoribbon synthesis and drive unidirectional alignment without seeds. The seeding data, discussed above, indicate that if the lattice of graphene nuclei that naturally form can be globally aligned, it may be possible to orient ribbons in one direction without seeding. However, two perpendicular orientations of nuclei spontaneously form on Ge(001) due to the symmetry of this surface. We have studied growth on vicinal surfaces with a miscut of 0, 6, and 9° towards Ge[110]. LEEM, TEM, and SAED characterization show that > 90% of the ribbons grown on Ge(001)-9° are aligned within ± 1.5º perpendicular to the miscut and have armchair edges (Fig. 2). Aligned ribbons with sub-10 nm widths and smooth edges are achieved.

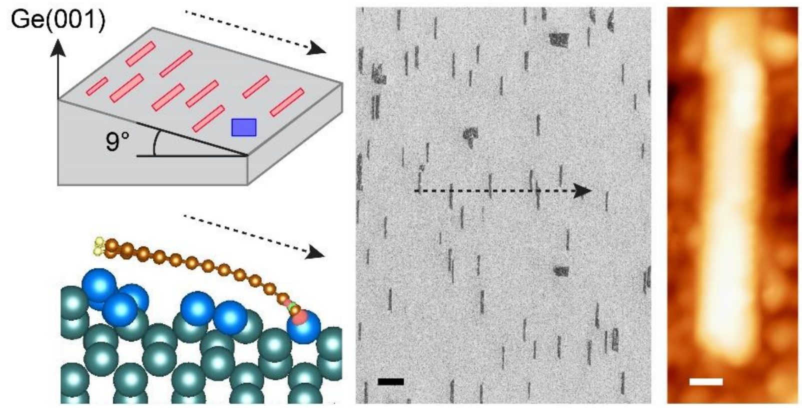

Figure 2. Nanoribbons on Ge(001) miscut 9° towards Ge[110] (left). Scanning electron (center, scalebar = 200 nm) and scanning tunneling microscopy (right, scalebar = 2 nm) images of ribbons with smooth armchair edges and narrow, uniform widths. Arrows point downhill.

- **Demonstrated for the first time the growth of graphene nanoribbons on Si wafer platforms [4]**

We have succeeded in growing nanoribbons on Si platforms by using epilayers of Ge (Fig. 3). This is a significant result because it provides a viable route for integrating carbon-based electronic materials onto conventional silicon platforms. Nanoribbons nucleate and grow on epilayers of Ge on Si in the same way as they do on Ge(001) single crystal substrates – with similar densities, kinetics, and aspect ratios – without interference from Si that diffuses from the bulk to the Ge surface or from threading dislocations inherent in the Ge epilayer due to the Si/Ge lattice mismatch.

- **Other [5,6,7]**

We have also collaborated with O. Moutanabbir on the heteroepitaxy of 2D Sb (antimonene) on Ge [5]; M. Bedzyk at Northwestern on characterization via STM, XRD, and XRR of novel surface reconstructions on Ge(110) stabilized by graphene, not previously observed on group-IV surfaces [6]; and M. Lagally at Wisconsin on controlling the defect and pinhole density of continuous graphene films designed to passivate the Ge surface [7].

Future Plans

Moving forward, this project will (1) study the fundamental science underpinning the substrate-nanoribbon interactions that control the anisotropic synthesis and engineer the synthesis with the goal of growing higher aspect ratio ribbons; (2) advance the growth of nanoribbons from seeds to improve their monodispersity and better control their properties; and (3) learn how to go beyond the synthesis of individual nanoribbons to synthesize organized assemblies of many nanoribbons.

The research of semiconducting graphene materials is motivated by the promise of these materials to impact next-generation high-performance energy-efficient semiconductor logic, energy-efficient RF communications, and sensing technologies. The project additionally promises to yield materials with electronic structures and bandgaps tailored for capturing solar, infrared, and THz electromagnetic energy for photovoltaic and photodetector applications, plasmonics, and optoelectronics. The detailed understanding of nanoribbon synthesis and processing gained could also impact the development of nanoribbons for applications including batteries, spintronics, thermoelectrics, and quantum information technologies.

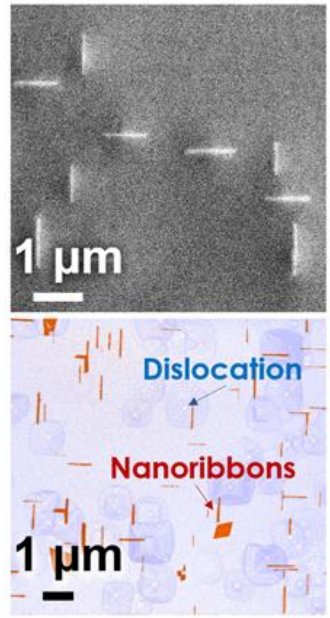

Figure 3. (Top) SEM demonstrating ribbon growth on Ge epilayers on Si. (Bottom) Superposition of two SEM images showing ribbon positions (before Secco etch) and etch pits that reveal the location of the dislocations (after Secco etch), demonstrating ribbon synthesis unaffected by threading dislocations.

References

1. A. J. Way, R. M. Jacobberger, M. S. Arnold, Seed-Initiated Anisotropic Growth of Unidirectional Armchair Graphene Nanoribbon Arrays on Germanium. ***Nano Letters*** 18, 898 (2018).

2. A. J. Way, E. Murray, F. Goeltl, R. M. Jacobberger, M. Mavrikakis, M. S. Arnold, Anisotropic synthesis of armchair graphene nanoribbon arrays from sub-5 nm seeds at variable pitches on germanium. ***Submitted*** (2019).

3. R. M. Jacobberger, E. Murray, M. Fortin-Deschenes, F. Goeltl, W. A. Behn, Z. J. Krebs, P. L. Levesque, D. Savage, C. Smooth, M. G. Lagally, P. Desjardins, R. Martel, V. Brar, O. Moutanabbir, M. Mavrikakis, M. S. Arnold, Alignment of semiconducting graphene nanoribbons on vicinal Ge(001). ***Nanoscale*** 11, 4864-4875 (2019).

4. V. Saraswat, Y. Yamamoto, H. J. Kim, R. M. Jacobberger, K. R. Jinkins, A. J. Way, N. P. Guisinger, and M. S. Arnold**,** Synthesis of armchair graphene nanoribbons on germanium-on-silicon, ***Submitted*** (2019).

5. M. Fortin-Deschenes, R. M. Jacobberger, C.-A. Deslauriers, O. Waller, E. Bouthillier, M. S. Arnold, O. Moutanabbir, Dynamics of Antimonene-Graphene van der Waals Growth ***Advanced Materials*** 10.1002/adma.201900569 (2019).

6. G. P. Campbell, B. Kiraly, R. M. Jacobberger, A. J. Mannix, M. S. Arnold, M. C. Hersam, N. P. Guisinger, M. J. Bedzyk, Epitaxial graphene-encapsulated surface reconstruction of Ge(110). ***Physical Review Materials*** **2**, 044004 (2018).

7. R. M. Jacobberger, M. J. Dodd, M. Zamiri, A. J. Way, M. S. Arnold, M. G. Lagally, Effect of Surface Facet and H_2:CH_4 Ratio on Passivation of Germanium by Graphene. ***Submitted*** (2019).

Publications (and patents)

Publication dates after 7/15/2017

R. M. Jacobberger, M. S. Arnold, High Performance Charge Transport in Semiconducting Armchair Graphene Nanoribbons Grown Directly on Germanium. ***ACS Nano***, 11, 9 (September 7, 2017).

M. S. Arnold, A. J. Way, R. M. Jacobberger, Seed-mediated growth of patterned graphene nanoribbon arrays. ***U.S. Patent 9,761,669*** (Application filed July 18, 2016; Granted September 12, 2017).

S. Mukherjee, N. Nateghi, R. M. Jacobberger, E. Bouthillier, M. de la Mata, J. Arbiol, T. Coenen, D. Cardinal, P. Levesque, P. Desjardins, R. Martel, M. S. Arnold, O. Moutanabbir, Growth and Luminescence of Polytypic InP on Epitaxial Graphene. ***Advanced Functional Materials*** 28, 1705592 (December 20, 2017).

F. Anwar, C. R. Carlos, V. Saraswat, V. S. Mangu, M. S. Arnold, F. Cavallo, Nanoscale graphene/Ge wigglers as building blocks for THz sources. ***AIP Advances* 7**, 115015 (November 13, 2017).

A. J. Way, R. M. Jacobberger, M. S. Arnold, Seed-Initiated Anisotropic Growth of Unidirectional Armchair Graphene Nanoribbon Arrays on Germanium. ***Nano Letters*** 18, 898 (January 30, 2018).

P. F. Nealey, T.-H. Chang, S. Xiong, Z. Ma, M. S. Arnold, R. Jacobberger, Atomic layer chemical patterns for block copolymer assembly. ***U.S. Patent. 9,927,706*** (Application filed July 20, 2016; Granted March 7, 2018).

G. P. Campbell, B. Kiraly, R. M. Jacobberger, A. J. Mannix, M. S. Arnold, M. C. Hersam, N. P. Guisinger, M. J. Bedzyk, Epitaxial graphene-encapsulated surface reconstruction of Ge(110). ***Physical Review Materials* 2**, 044004 (April 13, 2018).

V. Saraswat, R. M. Jacobberger, J. S. Ostrander, C. L. Hummell, A. J. Way, J. Wang, M. T. Zanni, M. S. Arnold, Invariance of Water Permeance through Size-Differentiated Graphene Oxide Laminates. ***ACS Nano*** 12, 7855 (July 11, 2018).

B. Kiraly, A. J. Mannix, R. M. Jacobberger, B. L. Fisher, M. S. Arnold, M. C. Hersam, N. P. Guisinger, Driving Chemical Interactions at Graphene-Germanium van der Waals Interfaces via Thermal Annealing. ***Applied Physics Letters*** 113, 213103 (November 20, 2018).

R. M. Jacobberger, E. Murray, M. Fortin-Deschenes, F. Goeltl, W. A. Behn, Z. J. Krebs, P. L. Levesque, D. Savage, C. Smooth, M. G. Lagally, P. Desjardins, R. Martel, V. Brar, O. Moutanabbir, M. Mavrikakis, M. S. Arnold, Alignment of semiconducting graphene nanoribbons on vicinal Ge(001). ***Nanoscale*** 11, 4864-4875 (Februrary 22, 2019).

M. Fortin-Deschenes, R. M. Jacobberger, C.-A. Deslauriers, O. Waller, E. Bouthillier, M. S. Arnold, O. Moutanabbir, Dynamics of Antimonene-Graphene van der Waals Growth ***Advanced Materials*** 10.1002/adma.201900569 (April 10, 2019).

R. M. Jacobberger, M. J. Dodd, M. Zamiri, A. J. Way, M. S. Arnold, M. G. Lagally, Effect of Surface Facet and H_2:CH_4 Ratio on Passivation of Germanium by Graphene. ***Submitted*** (2019).

A. J. Way, E. Murray, F. Goeltl, R. M. Jacobberger, M. Mavrikakis, M. S. Arnold, Anisotropic synthesis of armchair graphene nanoribbon arrays from sub-5 nm seeds at variable pitches on germanium. ***Submitted*** (2019).

V. Saraswat, Y. Yamamoto, H. J. Kim, R. M. Jacobberger, K. R. Jinkins, A. J. Way, N. P. Guisinger, and M. S. Arnold**,** Synthesis of armchair graphene nanoribbons on germanium-on-silicon, ***Submitted*** (2019).

Title: Integrating Experiment and Modeling of Zeolite Formation: On Raman Spectra of Silica Zeolites

PIs: Scott M. Auerbach[1,2] and Wei Fan[2]

[1]Department of Chemistry and [2]Department of Chemical Engineering, UMass Amherst

Program Scope

We are investigating structures and stages leading to zeolite formation. Zeolites are the most used catalysts by weight on planet earth, used as shape-selective acid catalysts in fluid catalytic cracking and other chemical catalysis applications.[1] Zeolites also show promise for new applications such as biofuel production[2] and carbon dioxide capture.[3] Synthesizing new zeolites that are tailor made for these promising applications remains a grand challenge in synthesis and processing science, because we know precious little at the atomic scale about how zeolites crystallize in solution.[4] In the present project, we are creating a novel integration of experiment and modeling to identify key steps in the formation of zeolitic order.

Heteroatoms and OSDAs: In particular, we wish to understand the effects of heteroatoms such as Al, Ge, and Zn, and of organic structure directing agents (OSDAs) such as alkyl ammonium species, on zeolite formation, particularly their impact on structures in the pre-crystalline synthesis gel. We think of this pre-crystalline gel as the "black box" of zeolite synthesis. We're curious if rings and cages that form in the gel correlate with those in the eventual zeolite. We hypothesize that the heteroatom/OSDA pair influences structures that form in the precursor gel by stabilizing particular rings and cages. Testing this hypothesis by looking inside the "black box" will provide an evidence-based foundation to a new way of thinking about and controlling zeolite synthesis.

Integrating Experiment and Modeling: We are tackling this problem by integrating synthesis, spectroscopy, and modeling of structures and spectra to shed light on amorphous structures. The key spectroscopic techniques we are applying are total scattering and Raman spectroscopy – both capable of providing information on medium length scales – scales larger than individual Si-O bonds but shorter than zeolite unit cells (Fig. 1). The key challenge of this approach is reliably interpreting the structural information locked in total scattering data and Raman spectra, requiring

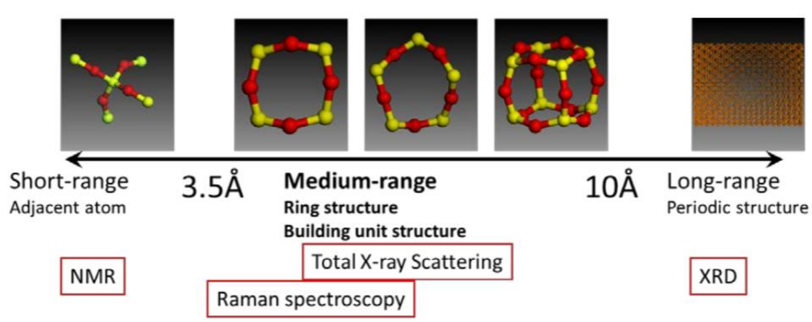

Fig 1. Length scales and characterization methods for understanding zeolite formation.

benchmarking on known structures, and tight collaboration between experiment and theory. The experiment benchmarks the theory, while the theory interprets the experiment; theory suggests an experiment through prediction, and experiments test the theory.

Year 1: We have launched this project through a Raman spectroscopy study on all-silica zeolites, to establish assignments useful in analyzing Raman spectra of pre-crystalline synthesis gels. There are many spectral-assignment approaches reported in the literature; we have sought a single, consistent approach that can be used for both zeolites and precursor, amorphous gels. We have synthesized and modeled all-silica zeolites to answer the questions: What are the zeolite sub-structures responsible for Raman peaks? Rings or other structures? How much does a Raman spectral signature depend on the environment? Answering these questions can propel Raman spectroscopy to a new level of diagnostic power in shedding light on how zeolites form.

Recent Progress

Executive Summary: We found that the conventional wisdom in the Raman spectroscopy of zeolites – that one can assign peaks in Raman spectra to individual rings – to be false. Instead, we identified that Raman spectral features could be associated with "ring junctions" in zeolite frameworks connecting three adjacent zeolite rings. Furthermore, we found that specific Raman frequencies were found to anti-correlate with the relevant edge-junction Si-O-Si angles.

Interpreting Raman Spectra: The first and perhaps most appealing method for interpreting Raman spectra is to assign peaks to specific rings, such as the 480 cm^{-1} feature assigned to the 4-ring in silica-chabazite (CHA).[5] A second approach is to assign Raman peaks to Si-O-Si bridges such as the 500 cm^{-1} feature in zeolite A (LTA).[6] A third method is to assign Raman peaks to "composite building units" such as the double-4-ring, present in both CHA and LTA. Because zeolites LTA and CHA both contain 4-rings, 6-rings, and 8-rings, we would expect that the Raman spectra of these two zeolites would be very similar *if* the ring-assignment method were valid. Previous data, and our own new data, for these systems show that these spectra are sufficiently different to cast doubt on the validity of the simple-ring-assignment approach. As such, our overarching objective is to determine a single, consistent approach for assigning Raman peaks, allowing us to apply Raman spectroscopy as a diagnostic of structure in the pre-crystalline synthesis gel.

Experiments on LTA, CHA, and Beyond: We synthesized silica LTA and CHA zeolites, as well as four other silica zeolites (AST, ITH, ITW, SOD) – all with 4-rings to determine the extent to which the framework structures around these 4-rings influence their Raman spectral signatures. Many of these zeolite syntheses required time-intensive syntheses of specific organic structure-directing agents (OSDAs). Raman spectra of all these materials were collected in collaboration with M. Timko and G. Tompsett at WPI, by dispersing several milligrams of calcined zeolite on a glass slide and employing a XploRa Raman microscope with a 785 nm laser line as the light source.

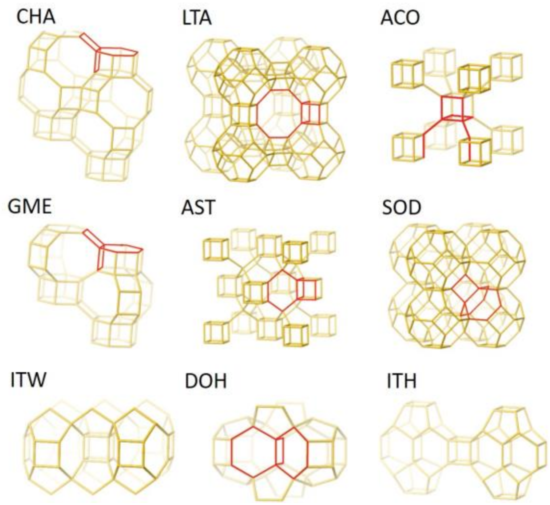

Fig 2. Structures of modeled zeolites; red bonds show "ring junctions" discussed below.

Modeling of LTA, CHA, and Beyond: We performed periodic DFT calculations on all the experimentally synthesized zeolites, as well as on ACO, DOH, and GME zeolites – all with 4-rings in different arrangements (Fig. 2). We used the VASP code with the PBE functional, ultrasoft pseudopotentials, a planewave energy cutoff of 480 eV, and K-point sampling appropriate to converge the energies and structures of each system. We computed normal modes and Raman intensities using Fonari and Stauffer's python script for computing derivatives of the polarizability, and constructed Raman spectra by summing Lorentzian peaks with 20 cm^{-1} widths.

Comparing Experiment and Theory: The PBE functional in DFT is known to slightly "underbind" systems, producing Si-O bond lengths and zeolite lattice parameters that are too large by a few %. We should otherwise expect good agreement between experiment and theory of Raman spectra of these silica zeolites. Figure 3 shows the comparisons for LTA and CHA zeolites, showing near quantitative agreement, with theory regularly red-shifted from experiment by around 30 cm^{-1}, consistent with PBE slightly underbinding the zeolite. Similar quality of agreement has been obtained for other zeolites (AST, ITH, ITW, SOD). The differences between the spectra for LTA and CHA – zeolites containing the same rings (4, 6, 8) – indicate that the environment in which rings vibrate in a given zeolite plays an important role in determining the nature of the Raman spectra.

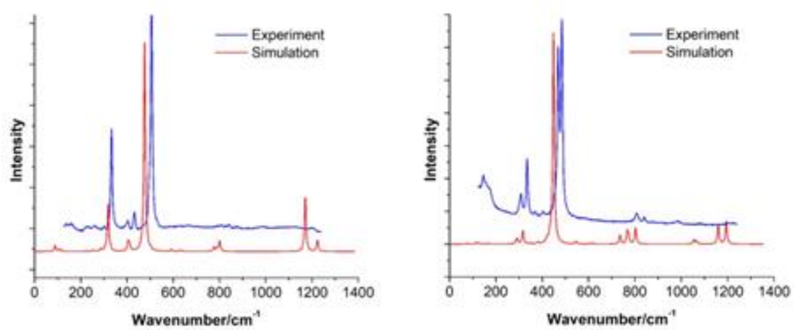

Fig 3. Experiment and modeling of Raman spectra of LTA (left) and CHA (right) showing sharp spectra and semi-quantitative agreement.

Assigning Raman Spectra for Silica Zeolites: Normal mode analyses allow the assignment of key peaks in the 300-600 cm^{-1} range, associated with zeolite ring-breathing modes. We sought an assignment method that goes beyond individual rings for the reasons stated above, but does not require unit cell symmetries as these are absent in the precursor gel. After investigating several assignment methods, we discovered that the Raman features could be understood through "edge-junctions" connecting three different rings in a given structure. For example, Fig. 2 shows in red the 4-4-6 edge junction in CHA, and the 4-4-8 edge-junction in LTA. Furthermore, the SOD zeolite only contains 4- and 6-rings configured in 4-4-6 junctions (Fig. 2), while LTA contains 4-4-6, 4-

4-8 and 6-6-8 edge junctions. This explains the single peak in the SOD Raman spectrum (not shown), and the three main peaks in the 200-700 cm^{-1} region of the LTA Raman spectrum (Fig. 3). This kind of analysis is novel, and integrates the previous three approaches of considering rings, Si-O-Si bridges, and composite building units such as double-4-rings.

We also investigated why the main peak in the Raman spectra in the range 400 – 500 cm^{--1} varies according to ACO ~ LTA > ITH > ITW > AST > CHA > GME > SOD > DOH. We investigated the role of the Si-O-Si bridge angle on the Raman frequency. We found a strong, linear anti-correlation between the Si-O-Si bond angle and the Raman frequency, considering angles in the range of 146-162^o. This suggests that the precise location of the main Raman feature in this spectral range (400 – 500 cm^{--1}) may pinpoint structural parameters beyond just the topological identification of rings that come together at a given location of the silica network.

Future Plans

We will extend our initial studies by investigating Raman spectra of zeolites including heteroatoms such as T = Al, Ge, and Zn, to determine if new correlations exist between Raman frequencies and Si-O-T angles. We will also study Raman spectra of zeolites containing OSDAs to determine how OSDAs influence vibrations of zeolites. These studies will enhance the diagnostic power of Raman spectroscopy for determining structure in silica gels leading to zeolites, to test whether rings and cages that form in the gel correlate with those in the eventual zeolite. We will also begin developing ex situ and in situ total X-ray scattering measurements to investigate medium-range order in solids formed during zeolite crystallization. We will also begin extending our signature “reaction ensemble Monte Carlo” technique to produce atomic-level models of precursor silica gel structures including heteroatoms and OSDAs. These approaches will provide data complementary data for identifying structural order at medium length scales leading to zeolite crystals.

References

1. Auerbach, S. M.; Karrado, K. A.; Dutta, P. K., *Handbook of Zeolite Science and Technology*. Marcel Dekker: New York, **2003**; p 1184.

2. Huber, G. W.; Corma, A., "Synthesis of Transportation Fuels from Biomass: Chemistry, Catalysts, and Engineering". *Chem. Rev.*, **2006,** *106*, 4044-4098.

3. J. G. Vitillo, B. Smit, L. Gagliardi, “Introduction: Carbon Capture and Separation,” *Chem. Rev*., **2017**, *117*, 9521-9523.

4. Auerbach, S. M.; Fan, W.; Monson, P. A., "Modelling the Assembly of Nanoporous Silica Materials". *International Reviews in Physical Chemistry,* **2014,** *34*, 35–70.

5. M. K. Wardani, *et al*., Highly Crystalline Mesoporous SSZ-13 Zeolite Obtained Via Controlled Post-Synthetic Treatment, *RSC Adv*., **2019**, *9*, 77-86.

6. P. K. Dutta, B. Del Barco, Raman Spectroscopy of Zeolite A: Influence of Silicon/Aluminum Ratio, *J. Phys. Chem*., **1988**, *92*, 354-357.

Publications

1. T. Wang, S. Luo, W. Fan, and S. M. Auerbach, "On Raman Spectra of All-Silica Zeolites: An Integrated Experiment and Modeling Study," JACS, submitted 2019.

Understanding reaction mechanisms in atomic layer deposition of metal oxides and sulfides

Stacey F. Bent
sbent@stanford.edu
Department of Chemical Engineering
Stanford University, Stanford, CA 94305

Program Scope

Atomic layer deposition (ALD) is a materials synthesis technique with potential to produce the precise, nanostructured materials needed in emerging energy conversion technologies. The fundamental nucleation and growth mechanisms of ALD can impact the properties of resultant thin film materials. The major goal of the project is to discover a framework of governing principles for ALD by performing fundamental studies to elucidate molecular-level reaction mechanisms and nucleation processes using both *in situ* and *ex situ* experimental tools complemented by theory. Our work is examining metal, metal oxide, metal sulfide, and ternary metal oxide ALD systems.

Recent Progress

Our recent results have helped expand the mechanistic understanding of binary and ternary metal oxide ALD and ALD of metal sulfides.

Mechanisms of ternary metal oxide ALD

The development of ALD processes for ternary and quaternary materials has become an emerging field in recent years due to applications requiring multicomponent thin films with precise thickness, uniformity and conformality. Our recent review of ternary and quaternary materials deposited by ALD reported more than 400 such systems to date.[3]

The ternary material, nickel-aluminum oxide (Ni-Al-O), has been studied for its potential use in applications ranging from sensors and electrocatalysts to electrochromics and hole-conducting materials. Despite its technological importance, ALD of Ni-Al-O ALD has not been previously reported. In this study, Ni-Al-O films are deposited by ALD using nickelocene/ozone and trimethylaluminum/water. While deposition of a wide range of compositions is achieved, non-ideal growth of the ternary material is observed. Nucleation studies performed to better understand the non-idealities observed in the ternary deposition reveal that Al uptake is greatly enhanced when Al_2O_3 ALD followed a NiO ALD cycle, while Ni uptake is hindered when NiO ALD follows an Al_2O_3 ALD cycle.

A model is developed to fit the experimental data using the conclusions about enhanced Al_2O_3 and attenuated NiO nucleation that was extracted from the nucleation studies. The model accurately predicts the general shape of both composition and growth per cycle (GPC) as a function of supercycle recipe (Figure 1).

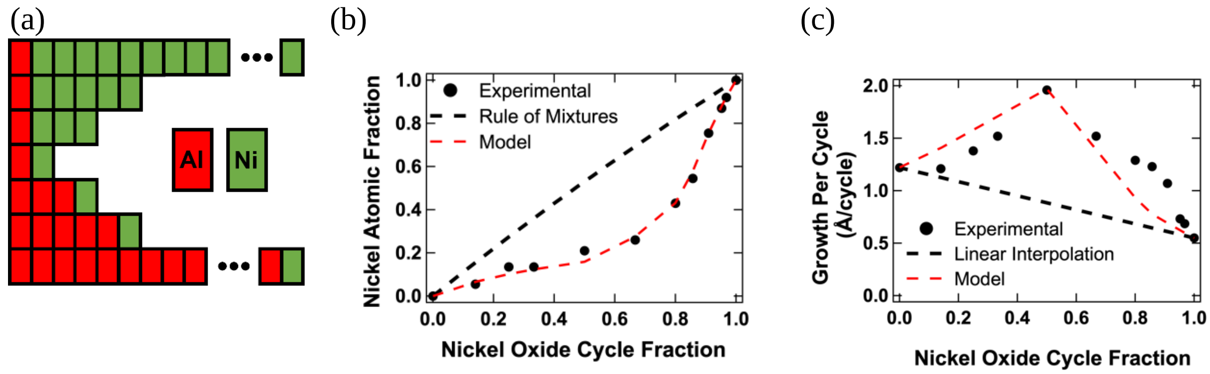

Figure 1: (a) Illustration of the supercycle recipe used to probe ternary growth behavior. Each block represents a full ALD cycle. Using the supercycle recipe scheme above, the composition (b) and GPC (c) of ternary films was measured as a function of nickel oxide cycle fraction. The black dashed line represents the predicted composition and GPC as a function of nickel oxide cycle fraction as described by the rule of mixtures. The red dashed line represents a fit to the experimental data for a model developed from nucleation studies.

Characterization of the deposited films reveals that Al-doping of NiO results in contraction of the NiO lattice, decreased crystallinity, and reduced density. The as-deposited films become completely amorphous at compositions <50% Ni. In addition, Al-doped NiO films deposited by ALD were tested as a hole-selective transport layer in lead-based perovskite solar cells. An Al doping of ~4% was found to improve power conversion efficiency of the perovskite-based devices over that of NiO.

Role of ozone in metal oxide ALD

Many metal oxide ALD processes rely on ozone as the oxidizing counter-reactant. Iron oxide ALD from metallocene precursors and ozone has been reported previously, but existing reports have been inconsistent in the growth rates and precursor exposures. Furthermore, none of the previous work explored saturation conditions thoroughly. We have explored the role of O_3 exposure in Fe_2O_3 ALD from *tert*-butylferrocene (TBF), and our results show that ozone plays a complex role in the ALD process and its exposure can be used to tune the resulting material properties.

Our work reveals that increasing ozone exposure leads to higher saturating growth rates, and that with higher ozone exposures more TBF is required to reach saturation (Figure 2a). Moreover, the thickness per cycle is greater than the roughly 2.3 Å reported thickness of a monolayer of Fe_2O_3, indicating that the process deposits more than one full monolayer of Fe_2O_3 per ALD cycle. The high growth rate and large precursor exposures required to reach saturation suggest that the growth mechanism of this process may be more involved than a simple surface-limited reaction that deposits a monolayer or less of material per cycle.

We propose a model for oxygen uptake into the film (Figure 2b), supported by x-ray spectroscopic and reflectivity measurements showing the presence of excess oxygen in the surface region of the film. In the model, oxygen species are iteratively taken up into the film from ozone and then withdrawn and consumed by TBF. Ozone exposure was also found to impact the crystallinity of the resulting films, and the dependence on ozone exposure can be used both to tune the phase between the pure γ and α phases of iron oxide and to control the orientation of crystalline domains.

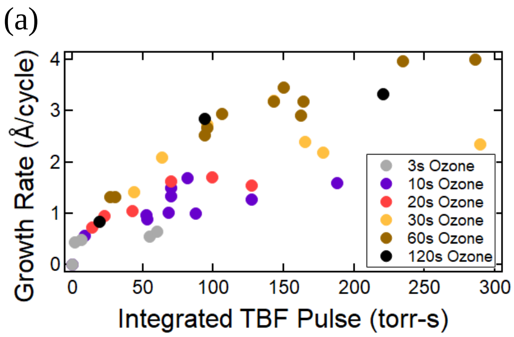

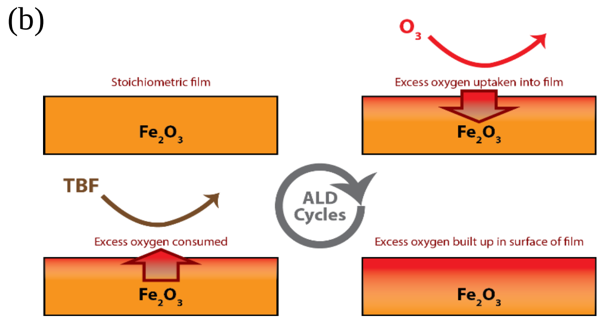

Figure 2. (a) Growth rate of Fe_2O_3 films as a function of t-butyl ferrocene (TBF) exposure for various ozone exposures. The saturating growth rates can be seen to increase with ozone exposure. Each data point represents one sample. (b) The proposed mechanism of Fe_2O_3 film growth during each ALD cycle, whereby each ozone exposure step introduces oxygen into the surface region of the film and each TBF exposure consumes oxygen from the film.

Activated ALD of metal oxides

Our studies on metal oxide ALD have recently uncovered an alternative mechanism by which the oxidizing counter-reactant can be activated. In particular, we show that some metal substrates have the ability to dissociate counter-reactants into the reactive species necessary to drive ALD. We demonstrate that the dissociation of O_2 on noble metal surfaces (e.g. Pt, Ir) enables ALD processes (e.g. Fe_2O_3 and NiO) which would otherwise require plasma activation of the oxygen. We name this "catalytically-activated ALD", and through this mechanism the metal at the substrate enables nucleation for an ALD reaction that would not ordinarily proceed.

The data show that using O_2 gas as co-reactant, ALD is achieved on the noble metal surface, while no deposition takes place on inert surfaces that do not dissociate oxygen (i.e. SiO_2, Al_2O_3, Au) (Figure 3a). The process is demonstrated for deposition of iron oxide and nickel oxide on platinum and iridium substrates. Characterization by *in situ* spectroscopic ellipsometry, transmission electron microscopy (Figure 3b), scanning Auger electron spectroscopy and x-ray photoelectron spectroscopy confirms the process, with linear ALD growth on the catalytic metal substrates and no deposition on inert substrates, even after 300 ALD cycles.

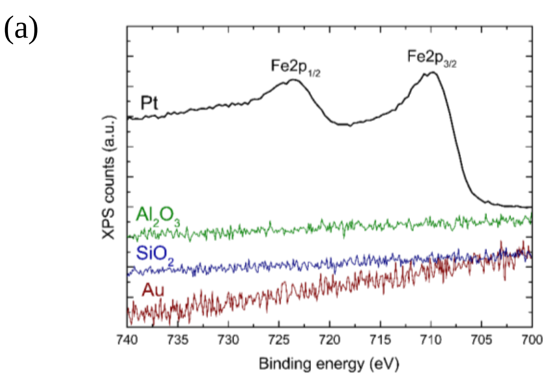

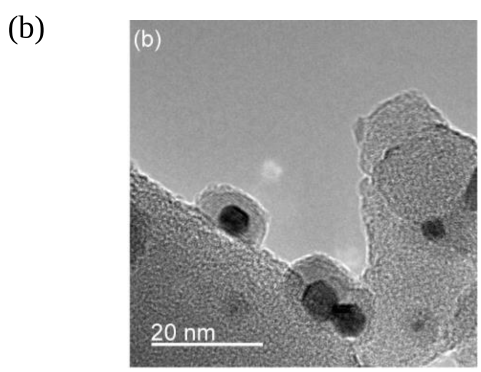

Figure 3. (a) X-ray photoelectron spectroscopy (XPS) scans showing the Fe_{2p} region after 300 ALD cycles of Fe_2O_3 on Pt, Au, SiO_2 and Al_2O_3 substrates using t-butyl ferrocene (TBF) and O_2. A clear Fe_{2p} signal is observed on Pt, but no Fe above the detection limit is detected on the catalytically inactive substrates. (b) Brightfield TEM image of Pt/Fe_2O_3 core/shell nanoparticles supported on SiO_2 nanospheres prepared by 50 cycles of Pt ALD followed by 50 cycles of Fe_2O_3 ALD from TBF/O_2.

Metal oxide ALD to decorate transition metal dichalcogenide materials

We have synthesized hybrid nanostructures comprised of ZnO nanocrystals decorating nanosheets and nanowires of MoS_2 prepared by ALD. We show that the concentration, size, and surface-to-volume ratio of the ZnO NCs can be systematically engineered by controlling both the number of ZnO ALD cycles and the properties and dimensions of the MoS_2 substrates, which are prepared by sulfurizing ALD MoO_3. The MoS_2 defect density and grain size are controlled by the sulfurization temperature of ALD MoO_3, and the ZnO nanocrystals in turn nucleate selectively at defect sites on MoS_2 surface and enlarge with increasing ALD cycle numbers. As the preparation temperature of the MoS_2 increases, larger grains with fewer grain boundaries of MoS_2 are obtained, resulting in a low concentration of ZnO nanocrystals due to fewer reactive nucleation sites (Figure 4). Application of this process to MoS_2 nanowires leads to hybrid nanostructures comprised of ZnO nanocrystals decorating the nanowires, as illustrated in Figure 4.

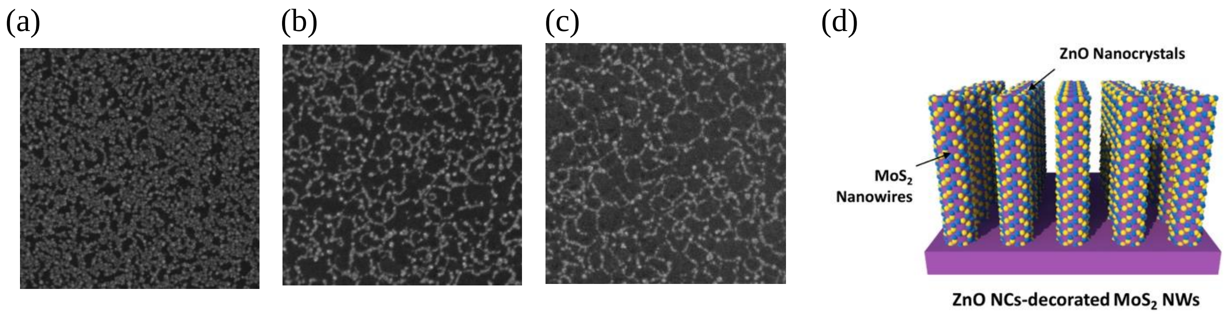

Figure 4. SEM images of 30 ALD ZnO cycles on three MoS_2 samples, from left to right on 600 °C-, 800 °C-, and 1000 °C-MoS_2. Right: Illustration of ZnO nanocrystal-decorated MoS_2 nanowire hybrid structures.

Future Plans

We plan to complete our studies of binary and ternary metal oxide ALD, including nickel and iron oxide-based films. Studies will investigate the role of the specific oxidizing species on the ALD process. We will also explore the relationship between growth conditions and film properties. Other studies will focus on ALD of metal sulfides, particularly MoS_2. We will finish our exploration of MoS_2 ALD, to understand the mechanisms of growth as well as the dependence of nucleation on the properties of the substrate.

In each of these studies, we will continue to deploy our custom-built ALD reactors both in our laboratory and at SSRL, applying both *in situ* and *ex situ* XRD, x-ray scattering measurements, IR, XPS and QCM.

Publications

1. "Area-selective atomic layer deposition of metal oxides on noble metals through catalytic oxygen activation," J. A. Singh, N. F. W. Thissen, W. H. Kim, H. Johnson, W. M. M. Kessels, A. A. Bol, S. F. Bent, and A. J. M. Mackus, *Chem. Mat*. **30** (2018) 663-670, 10.1021/acs.chemmater.7b03818.

2. “Thermal adsorption-enhanced atomic layer etching of Si_3N_4,” W. H. Kim, D. Y. Sung, S. Oh, J. Woo, S. K. Lim, H. J. Lee, and S. F. Bent, *J. Vac. Sci. Technol. A,* **36** (2018) 01B104, 10.1116/1.5003271

3. “Synthesis of doped, ternary, and quaternary materials by atomic layer deposition: a review,” A. J. M. Mackus*, J. R. Schneider*, C. MacIsaac, J. G. Baker, and S. F. Bent, *Chem. Mat.,* **31** (2019) 1142–1183, 10.1021/acs.chemmater.8b02878

4. “The role of aluminum in promoting of Ni-Fe-OOH electrocatalysts for the oxygen evolution reaction,” J. G. Baker, J. R. Schneider, J. A. Garrido Torres, J. A. Singh, A. J. M. Mackus, M. Bajdich, and S. F. Bent, *ACS Appl. Energy Mater.* **2** (2019) 3488-3499, 10.1021/acsaem.9b00265.

5. “Opportunities for atomic layer deposition in emerging energy technologies,” A. S. Asundi*, J. A. Raiford* and S. F. Bent, *ACS Energy Lett.* **4** (2019) 908−925, 10.1021/acsenergylett.9b00249.

6. “Enhancing nucleation in atomic layer deposition by pre-treatment with small organometallic molecules,” C. de Paula, L. Zeng, N. E. Richey, and S. F. Bent, submitted. ChemRxiv. Preprint. doi.org/10.26434/chemrxiv.8307572.v1

7. “Surface energy change of atomic-scale metal oxide thin films by phase transformation**,**” I.-K. Oh, L. Zeng, J.-E. Kim, J.-S. Park, K. Kim H. Lee, S. Seo, M. R. Khan, S. Kim, C. W. Park, J. Lee, B. Shong, Z. Lee, S. F. Bent, H. Kim, J. Y. Park, and H. B. R. Lee, submitted.

8. “Synthesis of a hybrid nanostructure of ZnO-decorated MoS_2 by atomic layer deposition,” I.-K. Oh, W.-H. Kim, L. Zeng, J. Singh, D. Bae, A. J. M. Mackus, J.-G. Song, S. Seo, B. Shong, H. Kim, and S. F. Bent, in preparation.

9. “Atomic layer deposition of nickel-aluminum oxide with ozone: mechanistic insights” J. G. Baker, J. R. Schneider, J. A. Raiford, and S. F. Bent, in preparation.

10. “ALD growth mechanisms of Fe_2O_3 using *tert*-butylferrocene and ozone,” J. R. Schneider, J. G. Baker, and S. F. Bent, in preparation.

Structure and transformation of highly stable vapor-deposited organic glasses

K. Bagchi, M. E. Fiori, M. D. Ediger
Department of Chemistry
University of Wisconsin-Madison, Madison, WI, 53706

Program Scope

Organic glasses prepared by physical vapor deposition (PVD) are useful and interesting materials that form the active layers in organic light emitting diodes (OLEDs). In contrast to glasses prepared by the traditional route of cooling a liquid, PVD glasses are often anisotropic. Using optical spectroscopy, x-ray experiments, and atomic force microscopy, we investigate three fundamental issues about PVD glasses with relevance both for their practical use and for our broader understanding of glasses: 1) How do PVD glasses lose their structure upon heating? This mechanism controls the thermal stability of PVD glasses used for organic electronics devices. 2) What is the structure of PVD glasses directly adjacent to the surface upon which the glass is deposited (the substrate)? The structure near the substrate influences device performance and the distance over which the substrate changes the structure is of fundamental interest. 3) Are co-deposited two-component PVD glasses homogeneous mixtures or partially phase separated? These results will be used to test the mechanism of PVD glass formation.

Recent Progress

Molecular layering in vapor-deposited Alq3 glasses: From the inception of OLED (organic light emitting diode) technology[1], Alq3 glasses have been used extensively in devices. With synchrotron grazing incidence wide angle x-ray scattering (GIWAXS), we discovered a tendency for molecular layering in vapor-deposited Alq3 glasses.[2] The tendency for layering manifests as an anisotropic scattering feature at ~ 0.7-0.8 Å^{-1}. This corresponds to a real space distance that is roughly equal to the diameter of an Alq3 molecule. We showed that the tendency for molecular layering can be controlled by varying the deposition temperature. Preparation at low substrate temperatures results in formation of "layered glasses" while isotropic glasses are created at higher substrate temperature. Remarkably, these structurally anisotropic glasses are optically isotropic as they exhibit nearly zero birefringence. Birefringence is a measure of P_2 molecular orientation. Our results show that while there is a tendency for molecular layering in vapor-deposited Alq3 glasses, the glasses exhibit isotropic molecular orientation as regards the P_2 function.

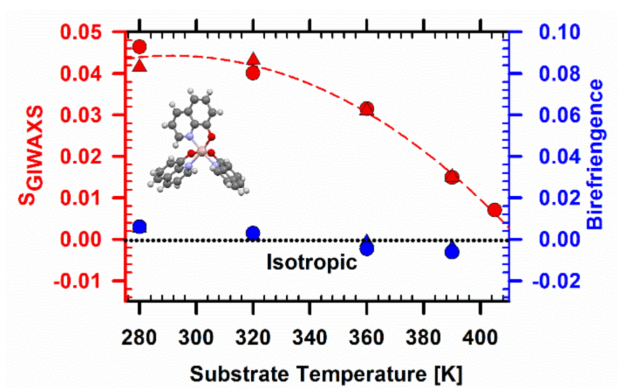

Figure. 1. The x-ray derived order parameter, S_{GIWAXS}, and the birefringence as a function of the substrate temperature during deposition for vapor-deposited Alq3 glasses. The molecular structure of Alq3 is shown as an inset.[2]

It has been shown previously that the orientational order of vapor-deposited glasses arises from equilibration towards the surface structure of the supercooled liquid (SCL) during vapor-deposition. This mechanism linking the surface structure of the equilibrium liquid to the bulk structure of the vapor-deposited glass has been called the “surface equilibration” mechanism.[3] Simulations performed by collaborators Jackson and de-Pablo allowed us to test this hypothesis for vapor-deposited Alq3 glasses. Consistent with the surface equilibration mechanism, molecular dynamics simulations of supercooled Alq3, reveal a tendency for surface layering. The surface equilibration mechanism hence explains the existence of layering in vapor-deposited glasses of Alq3. The tendency for layering is a feature commonly observed in vapor-deposited glasses; we expect our explanation of layering in Alq3 to be applicable to all these other glasses as well.

Bulk transformation: When heated above the glass transition temperature (T_g), thin films of stable glasses transform into the supercooled liquid (SCL) by growth fronts initiated at the free surface and/or substrate interface of the glass.[4] The bulk of the thin film maintains its packing from the deposition until it is reached by the SCL growth front. In contrast, liquid-cooled glasses transform into SCL homogeneously throughout the sample when they are heated above T_g. A second mechanism of transformation occurs in thick films of stable glasses. This mechanism has been observed in simulations[5] and detected experimentally[6, 7]. Simulations predict that SCL nucleates within the bulk of the stable glass and grows through the as-deposited glass.

Current work in the Ediger group seeks to directly observe the bulk nucleation and growth mechanism. Previous work has displayed that growth fronts of SCL in thin stable glasses can be inhibited by capping the interfaces of the film (the free surface and the substrate) with layers of a second stable glass with a higher T_g.[8, 9] In our work, we use TPD (T_g = 330 K) capped with Alq3 (T_g = 451 K) (Figure 1). When the capped TPD films are heated above $T_{g\ (TPD)}$, but below $T_{g\ (Alq3)}$, the TPD transforms into a SCL while the Alq3 layers remain glassy, as verified by spectroscopic ellipsometry measurements during annealing at $T_{g\ (TPD)}$ + 16 K. The ellipsometry data also show that the TPD does transform into a SCL, indicating that the Alq3 caps allow us to isolate the bulk transformation mechanism of TPD into a SCL. Figure 1 shows how the nucleation and growth process can be monitored with AFM.

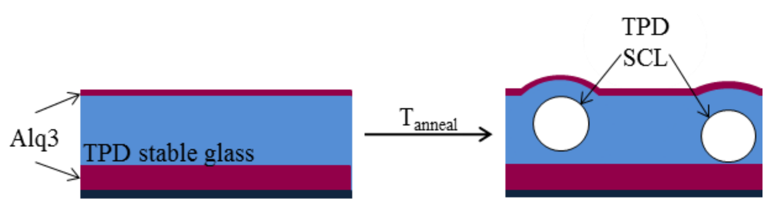

Figure 2. Scheme of TPD stable glass films capped at the free surface and the substrate with Alq3. When the layered films are heated above $T_{g\ (TPD)}$ and below $T_{g\ (Alq3)}$, the TPD will transform by the bulk mechanism into a SCL (shown in white on the right panel).

Multilayer films: Vapor-deposited glasses of small organic molecules are routinely used in OLED (organic light emitting diode) devices, which are composed of thin (< 50 nm) glassy layers of different organic semiconductors. However, much of the published work on vapor-deposited glasses of these materials has examined thick films (100-600 nm). Little is known about the structure of vapor-deposited glasses near an interface. Particularly relevant technologically is the structure at an organic-organic interface, which influences how efficiently charge is transported between different layers in an OLED device.

To investigate glass structure near an interface, we have deposited layers of Alq3 (T_g = 451 K) and DSA-Ph (T_g = 360 K) into films of stable glasses. Two architectures of films were initially studied (Figure 2). Both have the same molecular composition (58% Alq3 and 42% DSA-Ph), but they vary in the number of Alq3|DSA-Ph interfaces. Additionally, both architectures have 110 nm Alq3 on the silicon substrate to prevent any influence of the silicon interface. One set of films (the "trilayers") is made up of one bilayer of 300 nm Alq3 and 300 nm DSA-Ph, giving it two Alq3|DSA-Ph interfaces. The second set of films (the "multilayers") is composed of 30 bilayers of 10 nm Alq3 and 10 nm DSA-Ph, resulting in films with 61 Alq3|DSA-Ph interfaces. Because the films have the same composition and vary only in the number of organic-organic interfaces in the film, any differences in the structure or molecular orientation measured can be attributed to effects caused by Alq3|DSA-Ph interfaces.

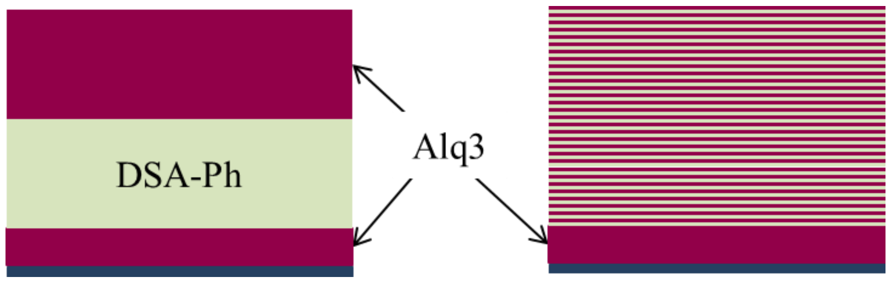

Figure 3. Alq3 and DSA-Ph layered glass films studied. *Left:* The trilayer film with two Alq3|DSA-Ph interfaces. *Right:* The multilayer film with 61 Alq3|DSA-Ph interfaces.

Birefringence is a robust and precise probe of molecular orientation. Alq3 glasses are optically isotropic[2]. For DSA-Ph, a negative birefringence indicates preferential horizontal orientation while a positive birefringence indicates vertical orientation[3]. We find the birefringence of DSA-Ph to be nearly equal in the multilayer and trilayer at all substrate temperatures (Figure 4). Furthermore, the birefringence of DSA-Ph in the layered films is the same as the birefringence of single layer of DSA-Ph deposited onto a silicon substrate. This indicates that the molecular orientation of the DSA-Ph in the 10 nm slabs is the same as it is in 300 nm thick DSA-Ph films. Any perturbation of the molecular orientation of DSA-Ph by the organic-organic interface must be much less than 10 nm. X-ray scattering measurements performed at SSRL support this result. Our work indicates that the presence of an interface perturbs glass packing over a length scale significantly less than 10 nm.

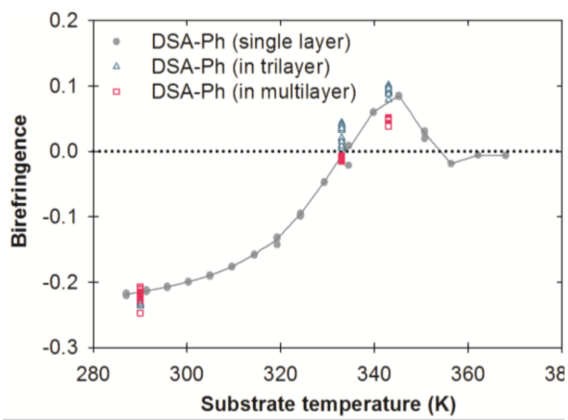

Figure 4. The birefringence of a single layer of DSA-Ph on silicon as a function of substrate temperature during deposition[3] is plotted in gray, and the birefringence of the DSA-Ph in the trilayers is plotted in teal triangles. The birefringence of the DSA-Ph in the multilayer films has been scaled to its composition and is plotted in pink squares.

Future Plans

Bulk transformation: We will try to observe the nucleation and growth of SCL bubbles within the bulk of the TPD stable glass using atomic force microscopy (AFM). Because the SCL of TPD is ~2% less dense than the as-deposited glass prepared at $T_{sub} = 0.85\ T_{g\ (TPD)}$,[3] the films will expand as they transform from a glass to a SCL. The regions of the TPD that have transformed into a SCL will be thicker than the surrounding as-deposited glass, and the increase in thickness will be monitored by AFM (Figure 1). Because growth fronts of TPD prepared at $0.85\ T_{g\ (TPD)}$ can propagate through films up to 2 microns thick, we expect that the nucleation sites SCL in the bulk transformation will be separated by >2 microns, making them easily observed by AFM.

Multilayer films: To further amplify the effects of organic-organic interfaces on glass packing, we will deposit films composed of 60 bilayers of 5 nm Alq3 and 5 nm DSA-Ph. We will also measure films composed of 50% Alq3 and 50% DSA-Ph deposited simultaneously, creating a mixed film. This film represents the limit of 'infinitely thin' layers.

Co-deposited PVD glass structure: X-ray scattering will be used to investigate whether co-deposited films phase segregate during deposition.

References

(1) C. W. Tang and S. A. VanSlyke, *Applied Physics Letters*, **1987**, 51, 913.
(2) K. Bagchi, N. E. Jackson, A. Gujral, C. Huang, M. F. Toney, L. Yu, J. J. de Pablo and M. D. Ediger, *J Phys Chem Lett*, **2018**, 10, 164.
(3) S. S. Dalal, D. M. Walters, I. Lyubimov, J. J. de Pablo and M. D. Ediger, *Proc Natl Acad Sci U S A*, **2015**, 112, 4227.
(4) S. F. Swallen, K. Traynor, R. J. McMahon, M. D. Ediger and T. E. Mates, *Phys Rev Lett*, **2009**, 102, 065503.
(5) R. L. Jack and L. Berthier, *J Chem Phys*, **2016**, 144, 244506.
(6) K. L. Kearns, M. D. Ediger, H. Huth and C. Schick, *The Journal of Physical Chemistry Letters*, **2009**, 1, 388.
(7) J. Rafols-Ribe, M. Gonzalez-Silveira, C. Rodriguez-Tinoco and J. Rodriguez-Viejo, *Phys Chem Chem Phys*, **2017**, 19, 11089.
(8) A. Sepulveda, S. F. Swallen and M. D. Ediger, *J Chem Phys*, **2013**, 138, 12A517.
(9) J. Rafols-Ribe, A. Vila-Costa, C. Rodriguez-Tinoco, A. F. Lopeandia, J. Rodriguez-Viejo and M. Gonzalez-Silveira, *Phys Chem Chem Phys*, **2018**, 20, 29989.

DOE sponsored publications(last two years):

(1) M. D. Ediger, J. De Pablo and L. Yu, *Acc. Chem. Res.*, **2019,** 52, 407.
(2) K. Bagchi, N. E. Jackson, A. Gujral, C. Huang, M. F. Toney, L. Yu, J. J. De Pablo and M. D. Ediger, *J. Phys. Chem. Lett.*, **2018**, 10, 164.
(3) Y. Qiu, L. W. Antony, J. M. Torkelson, J. J. De Pablo and M. D. Ediger, *J. Chem. Phys.*, **2018**, 149, 204503.
(4) N. Van Den Brande, A. Gujral, C. Huang, K. Bagchi, H. Hofstetter, L. Yu and M. D. Ediger, *Cryst. Growth Des.*, **2018**, 18, 5800–5807.
(5) Y. Qiu, S. S. Dalal and M. D. Ediger, *Soft Matter*, **2018**, 14, 2827–2834.
(6) A. Gujral, L. Yu and M. D. Ediger, *Curr. Opin. Solid State Mater. Sci.*, **2017**, 1.
(7) M. D. Ediger, *J. Chem. Phys.*, **2017**, 147, 210901.

(8) A. Gujral, S. Ruan, M. F. Toney, H. Bock, L. Yu and M. D. Ediger, *Chem. Mater.*, **2017**, 29, 9110–9119.
(9) Y. Chen, M. Zhu, A. Laventure, O. Lebel, M. D. Ediger and L. Yu, *J. Phys. Chem. B*, **2017**, 121, 2017.
(10) D. M. Walters, L. Antony, J. J. de Pablo and M. D. Ediger, *J. Phys. Chem. Lett.*, **2017**, 8, 3380–3386.

Program Title: Novel Synthesis of Quantum Epitaxial Heterostructures by Design

Principle Investigator: Chang-Beom Eom
Mailing Address: Room 2166 ECB, 1550 Engineering Drive, University of Wisconsin-Madison, Madison, WI 53706
E-mail: eom@engr.wisc.edu

Program Scope

Quantum materials such as unconventional superconductors, interfacial 2D electron gases (2DEGs), and multiferroics have been fertile ground for new discoveries. Our overarching goal is to develop novel synthesis routes that will create a new generation of epitaxial quantum thin film heterostructures for study of fundamental science and for development of new applications. These films can be of comparable or higher quality than available bulk single crystals, but more importantly film deposition conditions can be maintained far from equilibrium, so that metastable phases (nonexistent in nature) can be obtained by epitaxial stabilization of thin films. But these novel systems are usually sensitive to thin film heterostructure constraints, including interaction with the substrate, the difficulty in controlling point defects, and the challenge of forming atomically perfect interfaces.

Our hypothesis is that designing substrate interactions, controlling and identifying point defects, and working toward atomically perfect interfaces will reveal new phenomena and fundamental intrinsic properties of quantum materials arising from dimensionality, anisotropy, and electronic correlations. We have begun to implement some of these approaches, and have already demonstrated strain engineering of the Fe-based superconductor $BaFe_2As_2$, and made the first direct observation of the two-dimensional hole gas (2DHG) at an oxide interface. As a next step, we have developed a unique free-standing oxide stacked membrane fabrication technique to apply large dynamic strain, implemented a chemical pulsed laser deposition (CPLD), and begun to understand a route to new discoveries through control of highly perfect and defect free films and heterostructures. The **thrusts** of our proposed new work develop these advances, and expand into new materials systems:
(1) Novel CPLD Synthesis Route for oxide interface strain control, and oxide hole doping.
(2) Interface- and Strain engineered Fe-based superconductors

Recent Progress

Point Defect Control of Oxide-based Quantum Heterostructures

Point defects have played a major role in tuning the properties of materials over the last few decades. In quantum heterostructures based on complex oxides, however, the ability to control individual point defects continues to be challenging, due partially to non-stoichiometry issues in oxides. Here, we demonstrate the ability to tune point defects in oxide-based quantum heterostructure $LaAlO_3/SrTiO_3$ (LAO/STO), using a newly-developed chemical pulsed laser deposition (CPLD) growth technique. X-ray diffraction and Raman spectroscopy show that there is a wide process window of controlling the stoichiometry of STO without its structural change. Depth-resolved cathodoluminescence spectroscopy reveals that STO films grown at higher Titanium tetraisopropoxide (TTIP) flux has a higher ratio of antisite Ti/Sr vacancy with lower concentration of oxygen vacancies, which leads to higher electron mobility of two-dimensional electron gas at the interface of LAO/STO at low temperature, resulting in clear Shubnikov–de Haas oscillations. This result provides an essential part of the development of the next-generation complex oxide thin films and their heterostructures to investigate novel quantum phenomena.

We choose a LAO/STO heterostructure as a model system to demonstrate a point defect control of STO layer with a newly-developed chemical pulsed laser deposition (CPLD) growth technique. CPLD uses TTIP as a Ti source during laser ablation of a SrO target. The mechanism of CPLD growth for STO is related to that of hybrid MBE, where TTIP can only be adsorbed and decomposed to form STO on SrO-terminated surface, whereas it would be desorbed on TiO_2-termiated one. Using this technique, we were able to precisely tune point defects in STO.

We have grown homoepitaxial 25 u.c. $SrTiO_3$ thin films on (001) $SrTiO_3$ single crystal substrates. Figure 1a shows out-of-plane θ-2θ XRD patterns of $SrTiO_3$ films vs. TTIP inlet pressure. Peaks other than those from the single crystal substrate likely arise from cation off-stoichiometry, as the $SrTiO_3$ lattice parameter is highly sensitive to stoichiometry. The results indicate a stoichiometric $SrTiO_3$ growth window over a wide range of TTIP gas inlet pressure where $SrTiO_3$ film peaks overlap those of the $SrTiO_3$ substrate.

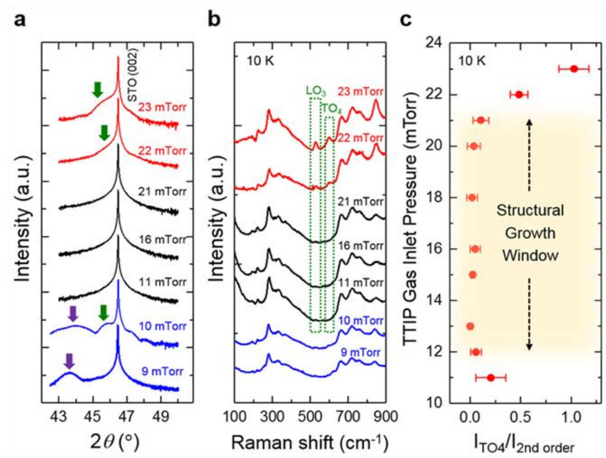

Figure 1. a, XRD patterns of $SrTiO_3$ films near (002) reflection. **b**, Raman spectra at 10 K. Data from Sr-rich, stoichiometric, Ti-rich $SrTiO_3$ (determined by XRD) films are represented in blue, black, red, respectively. **c**, Normalized TO_4 intensity in Raman spectra (**b**) as a function of TTIP inlet pressure. Yellow area is a stoichiometric growth window determined by Raman spectra at 10 K.

Variable-temperature Raman spectroscopy was performed to investigate signatures of inversion symmetry breaking due to point defects. $SrTiO_3$ is a cubic perovskite (space group Pm-3m) with 12 optical phonon modes. Because of odd modal symmetry with respect to the inversion center, 1st order Raman peaks are not present in the ideal $SrTiO_3$ structure. Point defects which break the inversion symmetry of $SrTiO_3$ can thus be detected by 1st order peaks in Raman spectra, *e.g*. the LO_3 or TO_4 modes. Raman spectrae of $SrTiO_3$ films measured at 10 K are shown in Fig. 2b. The intensity of the LO_3 and TO_4 peaks in Ti-rich $SrTiO_3$ films is higher outside the flux growth region of 11 to 21 mTorr, in agreement with the XRD stoichiometric growth process window.

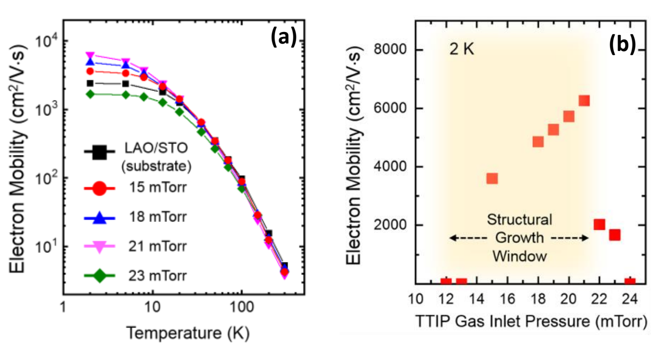

Fig. 2. (a) Electron mobility at the interface of $LaAlO_3/SrTiO_3$ substrate and $LaAlO_3$/MOPLD-grown $SrTiO_3/SrTiO_3$ substrate. TTIP gas inlet pressures of 15-23 mTorr were employed for growing $SrTiO_3$ films (b) $LaAlO_3$/ $SrTiO_3$ mobility at 2 K for various TTIP pressures.

Using the $SrTiO_3$ films as templates, epitaxial $LaAlO_3$ layers were grown on $SrTiO_3$ by conventional PLD to investigate the effect of point defects on 2DEG properties . The highest electron mobility of ~6,200 $cm^2/V{\cdot}s$ at 2 K (21 mTorr TTIP gas inlet pressure) (Fig. 2a) is substantially higher than the typical 2,400 $cm^2/V{\cdot}s$ without the TTIP process. The defect concentration inferred from the electron mobility monotonically decreases with increasing TTIP pressure within the structural growth window, as shown in Fig. 2b. We believe that point defect concentration varies within the structural growth window, resulting in the dramatic mobility enhancement.

We performed depth-resolved cathodoluminescence (DRCLS) to directly measure the point defects and their spatial distribution in STO films. Figure 3a shows DRCLS spectra of the LAO/STO samples with STO grown at 15 and 21 mTorr TTIP inlet pressure of. There is a clear difference in intensities between the 15 and 21 mTorr samples within the energy range from ~1.5

to ~3.4 eV when the spectra were normalized by the band gap (3.6 eV) energy. In Fig. 3b, relative point defect densities of Ti_{Sr}^{2+}, V_O^{2+} are plotted as a function of TTIP inlet pressures for the growth of STO films. As the TTIP inlet pressure is increased, the amount of Ti_{Sr}^{2+} is increased whereas the amount of V_O^{2+} is decreased. The electron mobility value measured at 2 K is again plotted in Fig. 3c for comparison. It is clear that lower concentration of V_O in STO is responsible for higher electron mobility at the interface of LAO/STO.

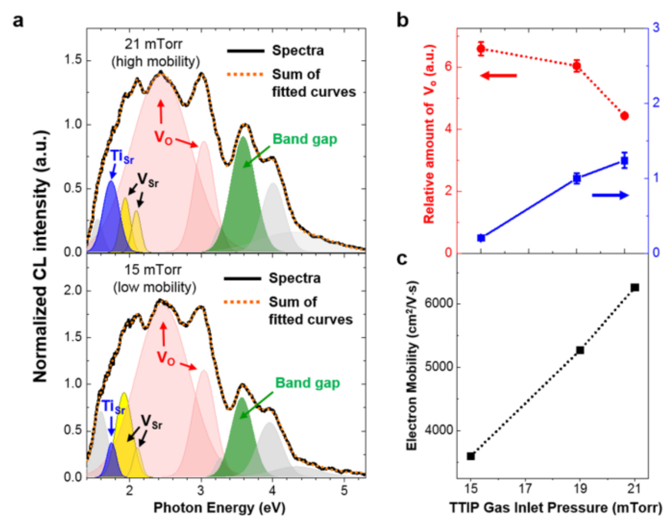

Fig. 3. (a) DRCLS Spectra of LAO 5 u.c./MOPLD-grown STO/ (001) STO substrate at 15, 21 mTorr TTIP gas inlet pressure. (b) Relative defect concentration of STO films as a function of TTIP gas inlet pressure during the growth, evaluated by summation of V_O^{2+} and V_O-R peak areas normalized with respect to the bandgap area near 3.6 eV. The relative ratio of Ti_{Sr}/V_{Sr} was evaluated by calculating the area of $Ti_{Sr}^{2+}/(V_{Sr}^{-}+V_{Sr}^{2-})$ (c) Electron mobility at 2 K in LAO/STO as a function of TTIP gas inlet pressure.

Since STO is one of the most widely used single crystals for growth of oxides, the point defect control by CPLD provides a way of making high quality STO for: (1) producing a template of STO on any substrate to integrate oxide in electronic (2) in principle because the quality of STO is superior that single crystals one can avoid buying expensive single crystals of STO, but rather producing them with CPLD.

Future Plans

(1) Novel CPLD Synthesis Route for advances in oxide films and heterostructures

We are continuing to develop a chemical pulsed laser deposition (CPLD) growth process that is showing dramatically lower concentration of point defects in complex oxide thin films. The higher quality epitaxial films and heterostructures described here remove several roadblocks that have limited the development of new science using quantum materials.

(2) Strain control of the $LaAlO_3/SrTiO_3$ interfacial two-dimensional electron gas

We will use our CPLD synthesis technique to understand the relation between point defect and electron gas properties, and to synthesize high-mobility electron gases to explore the effect of strain on fundamental aspects.

(3) Strain and Interface Engineered Unconventional Superconducting Quantum Heterostructures

Our new synthesis routes now allow exploration of strain- and electric-field dependent superconducting properties; such as (1) Giant strain control and investigation of the superconducting mechanism by lattice distortion and symmetry constraints in strain-engineered pnictides (2) the interaction of monolayer FeSe with strain- and interface engineered SrTiO3 films.

Publications (which acknowledge DOE support)

1. X. Yang, C. Vaswani, C. Sundahl, M. Mootz, L. Luo, J. H. Kang, I. E. Perakis, C. B. Eom & J. Wang, "Lightwave-driven gapless superconductivity and forbidden quantum beats by terahertz symmetry breaking" *Nature Photonics*, published on July 1, (2019)
2. X. Yang, X. Zhao, C. Vaswani, C. Sundahl, B. Song, Y. Yao, D. Cheng, Z. Liu, P. P. Orth, M. Mootz, J. H. Kang, I. E. Perakis, C.-Z. Wang, K.-M. Ho, C. B. Eom, and J. Wang,

"Ultrafast nonthermal terahertz electrodynamics and possible quantum energy transfer in the Nb_3Sn superconductor, *Phys. Rev. B* **99**, 094504 (2019)
3. Jiaxin Zhu, Jung-Woo Lee, Hyungwoo Lee, Lin Xie, Xiaoqing Pan, Roger A. De Souza, Chang-Beom Eom and Stephen S. Nonnenmann, "Probing vacancy behavior across complex oxide heterointerfaces" *Science Advances*, **5**, eaau8467 (2019)
4. D. Lee, B. Chung, Y. Shi, G. Y. Kim, N. Campbell, F. Xue, K. Song, S. Y. Choi, J. P. Podkaminer, T. H. Kim, P. J. Ryan, J. W. Kim, T. R. Paudel, J. H. Kang, D. A. Tenne, E. Y. Tsymbal, M. S. Rzchowski, L. Q. Chen, J. Lee, and C. B. Eom, "Isostructural metal-insulator transition" *Science* **362**, 1037 (2018).
5. J. H. Kang, L. Xie, Y. Wang, H. Lee, N. Campbell, J. Jiang, P. J. Ryan, D. J. Keavney, J. W. Lee, T. H. Kim, X. Pan, E. E. Hellstrom, D. C. Larbalestier, M. S. Rzchowski, Z. K. Liu, and C. B. Eom, "Control of Epitaxial $BaFe_2As_2$ Atomic Configurations with Substrate Surface Terminations" *Nano Letters* **18**, 6347 (2018).
6. T. Asaba, Z. Xiang, T.H. Kim, M. S. Rzchowski, C. B. Eom, and L. Li, "Unconventional Ferromagnetism in epitaxial (111) $LaNiO_3$" *Physical Review B* **98**, 121105 (2018).
7. T. Li, A. Lipatov, H. Lu, H. Lee, J. W. Lee, E. Torun, L. Wirtz, C. B. Eom, J. Íñiguez, A. Sinitskii, and A. Gruverman, "Optical Control of Polarization in Ferroelectric Heterostructures" *Nature Communications* **9**, 3344 (2018).
8. X. Yang, C. Vaswani, C. Sundahl, M. Mootz, P. Gagel, L. Luo, J. H. Kang, P. P. Orth, I. E. Perakis, C. B. Eom, and J. Wang, "Terahertz-light quantum tuning of a metastable emergent phase hidden by superconductivity" *Nature Materials* **17**, 586 (2018).
9. D. Lee, H. Wang, B. A. Noesges, T. J. Asel, J. Pan, J. W. Lee, Q. Yan, L. J. Brillson, X. Wu, and C. B. Eom, "Identification of a functional point defect in $SrTiO_3$" *Physical Review Materials* **2**, 060403(R) (2018).
10. D. T. Harris, N. Campbell, R. Uecker, M. Brützam, D. G. Schlom, A. Levchenko, M. S. Rzchowski, and C. B. Eom, "Superconductivity-localization interplay and fluctuation magnetoresistance in epitaxial $BaPb_{1-x}Bi_xO_3$ thin films" *Physical Review Materials* **2**, 041801(R) (2018).
11. Y. Y. Pai, H. Lee, J. W. Lee, A. Annadi, G. Cheng, S. Lu, M. Tomczyk, M. Huang, C. B. Eom, P. Irvin, and J. Levy, "One-Dimensional Nature of Superconductivity at the $LaAlO_3/SrTiO_3$ Interface" *Physical Review Letters* **120**, 147001 (2018).
12. H. Lee, N. Campbell, J. Lee, T. J. Asel, T. R. Paudel, H. Zhou, J. W. Lee, B. Noesges, J. Seo, B. Park, L. J. Brillson, S. H. Oh, E. Y. Tsymbal, M. S. Rzchowski, and C. B. Eom, "Direct observation of a two-dimensional hole gas at oxide interfaces" *Nature Materials* **17**, 231 (2018).
13. G. Cheng, A. Annadi, S. Lu, H. Lee, J. W. Lee, M. Huang, C. B. Eom, P. Irvin, and J. Levy, "Shubnikov–de Haas–like Quantum Oscillations in Artificial One-Dimensional $LaAlO_3/SrTiO_3$ Electron Channels" *Physical Review Letters* **120**, 076801 (2018).
14. H. Lu, D. Lee, K. Klyukin , L. Tao, B. Wang, H. Lee, J. Lee, T. R. Paudel, L. Q. Chen, E. Y. Tsymbal, V. Alexandrov, C. B. Eom, and A. Gruverman, "Tunneling Hot Spots in Ferroelectric $SrTiO_3$" *Nano Letters* **18**, 491 (2018).
15. S. Ryu, H. Zhou, T. R. Paudel, J. Irwin, J. P. Podkaminer, C. W. Bark, D. Lee, T. H. Kim, D. D. Fong, M. S. Rzchowski, E. Y. Tsymbal, and C. B. Eom, "In-situ probing of coupled atomic restructuring and metallicity of oxide heterointerfaces induced by polar adsorbates" *Applied Physics Letters* **111**, 141604 (2017).
16. M. Tomczyk, R. Zhou, H. Lee, J. W. Lee, G. Cheng, M. Huang, P. Irvin, C. B. Eom, and J. Levy, "Electrostatically tuned dimensional crossover in $LaAlO_3/SrTiO_3$ heterostructures" *APL Materials* **5**, 106107 (2017).

Exploiting Localized Thermal and Electric Field Gradients to Control Nanomaterial Phase and Composition in Far-From-Equilibrium Gas/Liquid Jet-Assisted E-Beam Deposition

Andrei G. Fedorov

Woodruff School of Mechanical Engineering, Georgia Tech, Atlanta, GA 30332-0405

Program Scope

Direct writing of nanoscale structures with focused electron beam induced processing (FEBIP) is a promising route to atom-by-atom growth of complex 3D nanostructures, but utility has been constrained by slow growth rates (largely due to low precursor density), a limited selection of non-carbonaceous precursors, and structural heterogeneity/porosity along with a lack of control over topology. As vividly stated in a recent review, electron/ion-beam based deposition methods have the potential for "full control of atomic arrangement and bonding in three dimensions"; yet the practical realization of this tantalizing possibility has been elusive, with only limited success confined to gas-phase precursors. [1] With DOE BES support, we are developing a family of multi-mode energized micro/nano-jet techniques as a method of local precursor delivery in an excited state, which aims to resolve both fundamental process control issues and to expand the range of useful precursors for FEBIP. Our ongoing program focuses on establishing a fundamental understanding of nanomaterials and meso-scale materials created under far from equilibrium conditions. Out-of-equilibria states for material nucleation and growth are established via thermally energized gas modulation of adatoms and electrokinetic separation of ionic precursors in liquid phase. In this report, we present fundamental advances on these two new methods, facilitated by the use of electrospray nano-jets and supersonic gas micro-jets, we pioneered for delivery of energized precursor molecules into a vacuum environment of the FEBIP chamber. The results of complementary experiments and multiscale modeling on high intensity thermal and electric field gradients associated with the energized multiphase jet delivery are presented leading to discovery of fundamental mechanisms of electron-precursor interactions and transport in the course of material synthesis with implications to FEBIP deposit growth rate, topology, phase and compositional purity. Energized micro/nano-jets provide unique capabilities for excitation of the far-from-equilibrium precursor-to-substrate molecular interactions, thus establishing a locally controlled deposition/etching/doping site for focused electron-beam induced processing (FEBIP). Not only this expands FEBIP to a wider range of precursor materials and new phase of synthesized nanomaterials, but also affords tuning of sticking coefficients and adsorption/desorption activation energies of participating molecules to controlling the deposition chemistry. The latter is especially critical for FEBIP on substrates, which are sensitive to doping such as graphene and other 2D materials, whose electronic properties change by adsorption of different molecules.

Recent Progress

We demonstrated the control of the material phase on the micron scale through a direct-write FEBIP process in an unenclosed liquid film. Nanoelectrospray as a mode of liquid phase introduction for FEBIP enables access to non-equilibrium solution states. [2] The potential bias of the electrospray jet (Fig. 1) has significant influence over the behavior of deposit growth and formation, determining the overall structure (granular vs. crystalline) of the deposit, and the formation of secondary (i.e. non-beam driven) deposited material. Positive nanoelectrospray of a metal salt with elementally exclusive metal cations (e.g. silver nitrate or cupric sulfate) in solution produces an excess of secondary deposited material in the form of metal nanoparticles. Nanoparticle formation in positive mode electrospray is attributed to the rapid increase in metal cation concentration due to desolvation and droplet fission processes. In contrast, negative nanoelectrospray produces an environment with an excess of non-metallic anions, and thus suppresses the formation of nanoparticles both within the electrospray droplets and within the liquid film. In addition, the presence of excess anions within the liquid bulk serves to shield metal cations from reaction with solvated electrons, limiting the rate of nucleation and growth of nanoparticles formed far from the point of beam impact. The absence of the excess of nanoparticles observed in positive electrospray is a key benefit of negative nanoelectrospray, where the

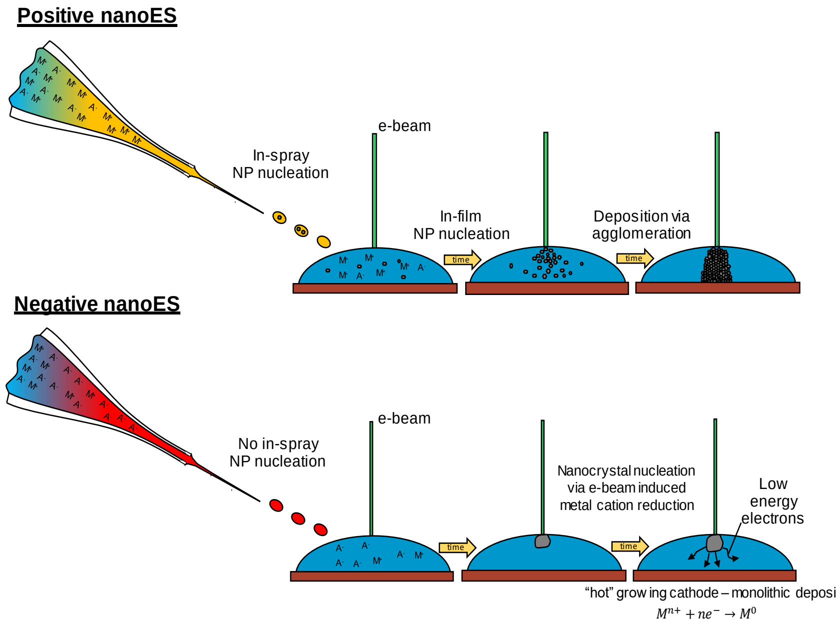

Fig. 1: (Top): Positive electrospray bias results in an excess of metal cations within the spray and film, resulting in nanoparticle formation both within the traveling droplets and the liquid film, forming a highly granular metal deposit. (Bottom): Negative electrospray bias results in an excess of anions paired with dissociated metal salt, suppressing the formation of nanoparticles to favor crystal growth via electrochemical reduction by solvated electrons.

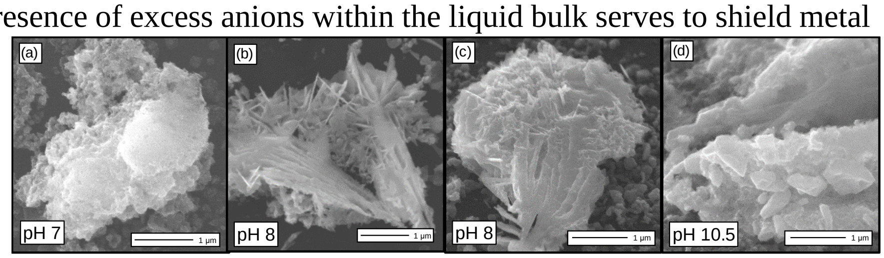

Fig. 2: Negative Mode NESA-FEBID silver deposits showing transition from NP agglomeration to crystalline monolith growth with an increasing solution pH by addition of sodium hydroxide (30 keV electron beam with a current of ~3.5 nA with a water solvent). (a) 1 mM AgNO3, pH 7, (b-c) 0.7 mM AgNO3, pH 8, (d) 0.7 mM AgNO3, pH 10.5. Deposit (a) features a primarily granular structure typical to deposits formed without an added base. Deposits (b-c) feature large-scale spike-like crystalline structures covering the surface of the deposit. Deposit (d) has large crystals on the scale of 0.5-1 μm embedded within the surface.

primary mode of deposit formation is instead beam-driven growth through electrochemical reduction of silver ions. First, a nanoparticle nucleates at the point of electron beam impact at the liquid/vacuum interface. Then the nanoparticle is charged by the beam, becoming the cathode in an electrochemical reaction, i.e., $M^{n+} + ne^- \rightarrow M^0$. The particle continues to grow due to electrochemical reduction of metal cations at the liquid/solid interface. The stationary growth of a single nanoparticle at the point of beam impact, rather than the agglomeration of nanoparticles, leads to the formation of crystalline deposits, rather than granular deposits (Fig. 2). Solution pH also plays a significant role, as elevating the pH from 8 to 10.5 via added sodium hydroxide significantly promotes the formation of crystalline deposits, as elevated pH increases the half-lifetime of solvated electrons in the boundary layer adjacent to the primary nucleate. [3]

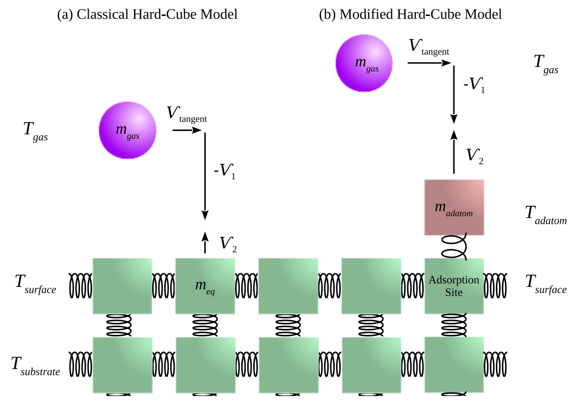

Fig. 3: The hard-cube model for adatom thermal state is based on the elastic binary collision between the impinging particle and the impingement site.

Modes of enhanced surface diffusion can be accessed *via* an externally applied energetic molecular beam that activates surface diffusion, not by bulk heating the surface, but by bringing adatoms into a state of strong thermal non-equilibrium with the surface. Since there is no technique to directly measure the adatom temperature without perturbing its intrinsic thermodynamic state, the only alternative is to rely on the predictions using a suitable model capturing the key physics of interactions and validated by comparison to carefully designed control experiments. To this end, the analytical hard-cube model was developed to include three interacting bodies such that the effective temperature of the middle body, the adatom, may be determined (Fig. 3). [4] The

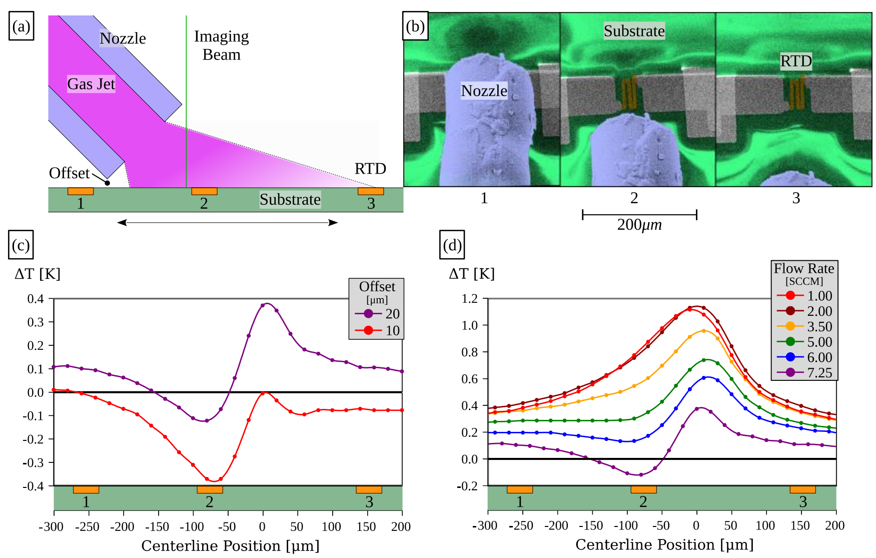

Fig. 4: (a) A schematic side-profile of the RTD lateral translation range illustrates how the RTD is positioned to collect thermal response data at different locations relative to the gas jet. (b) The SEM top-view follows the RTD as the substrate moves relative to the nozzle along the jet centerline position. The RTD thermal response (above the ambient equilibrium temperature when the jet is off) is collected for (c) a 7.25 ± 0.1 sccm oxygen gas jet with a 10μm and 20μm vertical offset between the nozzle tip outer diameter and the substrate and (d) an oxygen gas jet at various flow rates with a 20μm offset between the nozzle and the substrate. RTD temperature measurement uncertainty is ± 0.002K.

capability of the model in the prediction of temperature is verified by predicting complex heating and cooling surface profiles in response to gas jet impingement (Fig. 4), which can be used to bring the surface adsorbed precursor molecules into an excited thermodynamic state favorable for locally controlled nanofabrication by a supersonic inert gas jet FEBIP and shows an enhancement of the surface adsorbed precursor diffusion rate (and therefore the nanostructure growth rate) by 10X. Theoretical predictions reveal that a supersonic jet impingement, especially when it is thermal energized, can dramatically elevate the effective temperature of adatoms - bringing them into a state of thermal non-equilibrium with the surface with significant beneficial effects for FEBIP, such as enhanced growth rate, improved deposit morphology and structure, for many nanofabrication techniques that rely on the optimal state of the surface adsorbed precursor.[5]

Future Plans

Future work will focus on: (1) discovery of the reaction and growth pathways, resulting in formation of pure metal nanostructures with unique phases and crystalline structures by FEBIP from liquid-phase precursors under an influence of a strong local electric field; (2) discovery of new processing capabilities and fundamental understanding for the formation of e-beam patterned thin films via ion soft landing for locally-controlled electrochemical properties, and (3) establishment of experimentally-validated modeling framework for FEBIP enabled by controlled energy multi-phase precursor jets at a precisely controlled thermodynamic states. Collectively, these basic insights will not only bring about the fundamental understanding of coupled physical-chemical processes underlying new approaches to FEBIP, but will also enable new hypothesis generation and validation of new methods for improving the growth rate, resolution, and composition/phase control of FEBIP made nano/meso/micro-structures and synthesis of 3D-complex hierarchical materials and thin films with atomic scale control.

References

[1] Jesse et al., 2016. Directing matter: toward atomic-scale 3D nanofabrication, *ACS Nano*, **10**(6):5600.

[2] Fisher et al., 2015. Rapid electron beam writing of topologically complex 3D nanostructures using liquid phase precursor, *Nano Lett.*, **15**: 8385-8391.

[3] Fisher et al., 2018. Synthesis of crystalline metal nanomonoliths by e-beam reduction of negatively-electrified jets, *Materials Today Physics*, **5**: 87.

[4] Henry et al, 2019. Non-equilibrium adatom thermal state enables rapid nanomanufacturing, *Phys. Chem. Chem. Phys.*, **21**: 10449.

[5] Henry et al., 2016. High purity tungsten nanostructures via focused electron beam induced deposition with carrier-gas assisted supersonic jet delivery of organometallic precursors, *J. Phys. Chem. C*, **120** (19): 10584.

Publications

Henry, M., Kim, S., and Fedorov A. G Non-equilibrium adatom thermal state enables rapid additive nanomanufacturing, *Phys. Chem. Chem. Phys.*, **21**, 10449 - 10456 (2019).

Fisher, J., Kottke, P. A., and Fedorov A. G., Synthesis of crystalline metal nanomonoliths by e-beam reduction of negatively-electrified jets, *Materials Today Physics*, **5**, 87-92 (2018).

Johnson, G. E., Prabhakaran, V., Browning, N. D., Mehdi, B. L., Laskin, J., Kottke, P.A., and Fedorov, A. G., DRILL interface makes ion soft landing broadly accessible to energy science and applications, *Batteries & Supercaps*, 1 (3), 97-101 (2018).

Multi-Scale Simulation of Nanowire Growth in Solution

K. A. Fichthorn, PI
Department of Chemical Engineering
The Pennsylvania State University
University Park, PA, 16802

Program Scope

A significant challenge in the development of functional nanomaterials is understanding the growth of colloidal metal nanocrystals. From a practical perspective, a knowledge of how to synthesize selective metal nanocrystal sizes and shapes will be important in achieving a sustainable energy future. The science of shape-selective nanocrystal synthesis has been advancing at an increasingly rapid pace, with numerous recent reports of syntheses of various beneficial nanocrystal morphologies. Despite many successes, it is still difficult to achieve high, selective yields in most synthesis protocols. Many fundamental aspects of these complex syntheses remain poorly understood. Our research has focused on resolving the thermodynamic and kinetic mechanisms by which capping molecules and halides facilitate the growth of Ag and Cu seeds into nanocrystals. These studies rely on a collection of theoretical methods that has been developed in the Fichthorn group for quantifying kinetic nanocrystal shapes, characterizing solid-liquid interfacial free energies, and computing nanocrystal free energies via classical molecular dynamics (MD) simulations. In addition, quantum methods based on density functional theory (DFT) have been used.

Recent Progress

Five-fold twinned nanowires can be synthesized from various fcc metals *via* solution-phase methods. These anisotropic nanostructures can be grown with aspect ratios (AR) beyond 1000 and they possess unique electrical, optical, and mechanical properties that show promise for many applications (e.g., see ref. 1). Despite considerable interest in their synthesis and properties, the kinetic mechanisms that promote the high-AR growth of metal nanowires are not well understood.

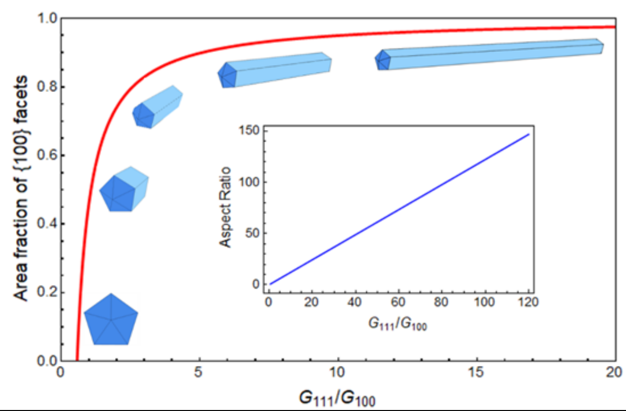

Figure 1. Nanowires at various relative linear facet growth rates. The inset shows the AR. {100} facets are light and {111} facets are dark.

The commonly assumed structure for five-fold twinned nanowires can be inferred from Fig. 1. Here, we see that these wires consist of ten {111} end facets and five {100} side facets. In experimental studies[2], it was suggested that the selective flux of Ag atoms/ions to the {111} ends relative to the {100} sides results in high-AR growth. This flux selectivity has been attributed to the facet-selective binding of capping molecules (*e.g.*, PVP, in the case of Ag nanowires[2]) to the {100} facets. While recent experiments[3] and theoretical studies based on DFT[4] confirm facet-selective binding of PVP to Ag(100), they also indicate that it is unlikely to be sufficient to produce nanowires.[5,6]

In Fig. 1, we show a kinetic Wulff construction that describes nanowire shapes for various linear facet growth rates G_i of the {111} ends and the {100} sides.[7] Here, we see that to achieve AR around 100 (seen in some experiments[1,2]), the flux to the {111} facet $G_{\{111\}}$ needs to be nearly 100 times larger than the flux to the {100} facet $G_{\{100\}}$. Our DFT-based calculations do not bear this out for Ag NW capped solely with PVP. In these studies[5,6], we found $G_{\{111\}}/G_{\{100\}} \approx 1.7$ - 2.0, which is sufficient to produce {100}-faceted nanocubes, but would lead to nanowires with AR around 2.

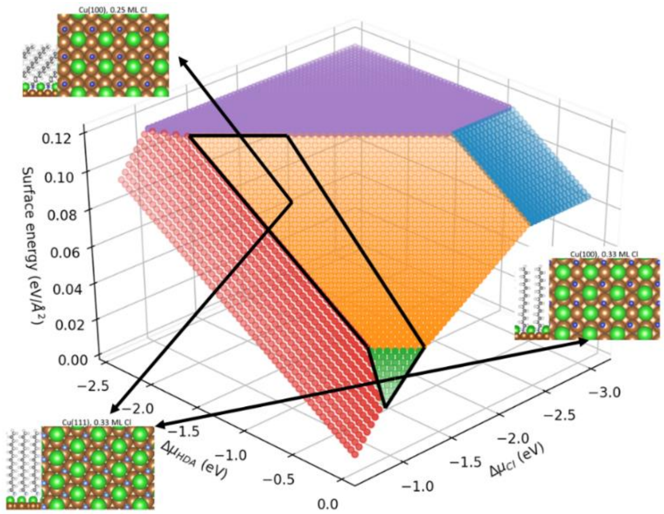

Figure 2. The surface energy of Cu(100) as a function of the Cl and HDA chemical potentials. The region outlined in black is where we predict nanowire formation. In this region, the Cl surface coverage on Cu(100) is either 0.25 ML (orange region) or 0.33 ML (green region) and the Cl surface coverage is 0.33 ML. The snapshots depict optimized HDA and Cl surface configurations from a side view (left) and a top-down view (right), in which only the Cl (green) and N (blue) atoms are shown. Dark blue N atoms are chemisorbed and light blue N atoms are physisorbed.

It is possible that the inadvertant introduction of halides could enhance nanowire growth for Ag, as Da Silva *et al.* found AR greater than 1000 in their studies of Ag nanowire growth in the presence of bromide.[1] In a joint theoretical and experimental study, we found evidence for a new mechanism by which both a capping agent, hexadecylamine (HDA), and Cl synergistically promote anisotropic growth of Cu nanowires.[8] Electrochemical measurements on Cu(111) and Cu(100) surfaces show that, in contrast to previous hypotheses, HDA does not selectively passivate Cu(100); it passivates both facets equally. However, the introduction of Cl^- in a narrow range of concentrations selectively disrupts the alkylamine monolayer on Cu(111), causing Cu to preferentially deposit onto {111} facets on the ends of the nanowires. DFT calculations show that HDA and Cl chemically adsorb to both Cu(111) and Cu(100) at sufficiently low Cl coverages and that HDA physically adsorbs at high Cl coverages. As in experiments, DFT calculations indicate there is a narrow, intermediate Cl coverage window, indicated in Fig. 2, where HDA chemisorbs to Cu(100), but physisorbs to Cu(111). Thus, anisotropic growth occurs via Cu atom addition to the less-protected {111} facets on nanowire end. However, Ag nanowires have been grown in the absence of halide.[1,2] Thus, a mechanism other than facet-selective ion deposition can be operative in producing nanowires. Here, we examine the possibility that this mechanism involves surface diffusion.

We consider the diffusion of Ag atoms on the surfaces of nanowire seeds and the possibility that their accumulation on the {111} facets can lead to the growth of seeds into nanowires. Fivefold twinned nanowires grow from decahedral seeds that are almost always depicted as shown in the lower left inset of Fig. 1. Seeds consist of five sub-units with {111} twin planes between each unti. The five-fold geometry is not space filling and there is strain associated with closing the gap. Our calculations based on an embedded-atom method potential for Ag indicate that a Marks-like decahedron is energetically favored for five-fold twinned Ag seeds. This structure is shown in Fig. 3. Such a structure relieves stress and is consistent with the rounded pentagonal nanowire cross sections observed in experiments.

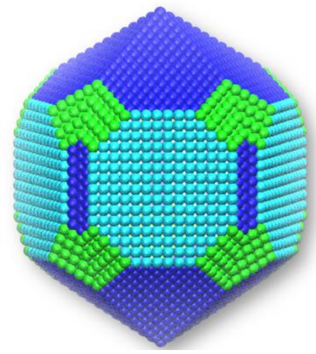

Figure 3. Predicted structure for a a five-fold twinned nanowire

Our MD simulations and energy minimizations indicate the strain distribution over the {111} facets of nanowire seeds induces heterogeneous atom aggregation and leads to atom trapping there. Using the climbing-image nudged-elastic band method, we calculated energy barriers for atoms to diffuse over the strained {111}, {100}, and {110} facets shown in Fig. 3. The major pathway for atoms to transit between the {111} and {100} facet is outlined in Fig. 4.

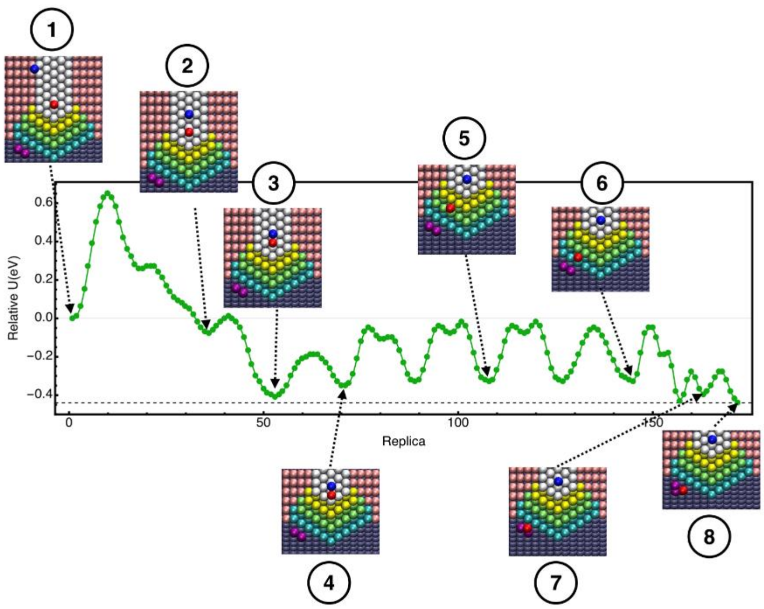

Figure 4. The energy profile for an atom to transit from the {100} facet (pink) to the {111} facet (violet) through the notch (white) and {110} facet (multi-colored).

We combined all of the elements discussed above: seed structure, nucleation, and diffusion to find mean-first passage times (MFPT) for inter-facet transport. We used the theory of absorbing Markov chains to compute MFPT. We find that the MFPT to go from a {111} to a {100} facet is significantly longer than the MFPT to go from a {100} to a {111} facet and also much longer than the experimental deposition time, indicating atom accumulation will occur on the nanowire ends. As the NW grow from seeds, the MFPT to go from {100} to {111} increases and reaches a point at which it equals and exceeds the deposition time. The length at which this point is reached is the length to which the nanowires will grow. We predict nanowire AR in the experimental range for experimentaly realizable deposition rates.

Future Plans

Many interesting studies are in the works. First, we are probing the cooperative roles of PVP and Cl in promoting Ag nanowire and nanocube growth. Preliminary studies indicate we will find similar trends to those in Fig. 2 for the Cu-Cl-HDA system. We are investigating the role of diffusion in promoting nanowire morphologies for the Cu-Cl-HDA system and preliminary calculations indicate that diffusion enhances nanowire growth beyond what we could expect from deposition. Finally, we have initiated studies of metal seed growth to understand how we might be able to influence seed growth trajectories and seed shapes, which critically determine final nanocrystal shapes.

References

1. Da Silva, R. R. *et al.* Facile Synthesis of Sub-20 nm Silver Nanowires through a Bromide-Mediated Polyol Method. *ACS Nano* **10**, 7892–7900 (2016).

2. Sun, Y., Mayers, B., Herricks, T. & Xia, Y. Polyol Synthesis of Uniform Silver Nanowires : A Plausible Growth Mechanism and the Supporting Evidence. *Nano Lett* **3**, 955–960 (2003).

3. Chen, Z., Chang, J. W., Balasanthiran, C., Milner, S. T. & Rioux, R. M. Anisotropic Growth of Silver Nanoparticles Is Kinetically Controlled by Polyvinylpyrrolidone Binding. *J. Am. Chem. Soc.* **141**, 4328–4337 (2019).

4. Al-Saidi, W. A., Feng, H. & Fichthorn, K. A. Adsorption of polyvinylpyrrolidone on Ag surfaces: Insight into a structure-directing agent. *Nano Lett.* **12**, (2012).

5. Qi, X., Balankura, T., Zhou, Y. & Fichthorn, K. A. How Structure-Directing Agents Control Nanocrystal Shape: Polyvinylpyrrolidone-Mediated Growth of Ag Nanocubes. *Nano Lett.* **15**, 7711–7717 (2015).

6. Balankura, T., Qi, X., Zhou, Y. & Fichthorn, K. A. Predicting kinetic nanocrystal shapes through multi-scale theory and simulation: Polyvinylpyrrolidone-mediated growth of Ag nanocrystals. *J. Chem. Phys.* **145**, (2016).

7. Qi, X., Chen, Z., Yan, T. & Fichthorn, K. A. Growth Mechanism of Five-Fold Twinned Ag Nanowires from Multiscale Theory and Simulations. *ACS Nano* **13**, 4647–4656 (2019).

8. Kim, M. J., Alvarez, S., Chen, Z., Fichthorn, K. A. & Wiley, B. J. Single-Crystal Electrochemistry Reveals Why Metal Nanowires Grow. *J. Am. Chem. Soc.* **140**, 14740–14746 (2018).

Publications

1. S.-H. Liu and K. A. Fichthorn, “Interaction of Alkylamines with Cu Surfaces: A Metal-Organic Many-Body Force Field”, *J. Phys. Chem. C* **121**, 22531-22541 (2017).

2. X. Qi and K. A. Fichthorn, “The thermodynamic influence of solution-phase additives in shape-controlled nanocrystal synthesis”, *Nanoscale* **9**, 15635-15642 (2017).

3. M. J. Kim, S. Alvarez, T. Yan, V. Tadepalli, K. A. Fichthorn, and B. J. Wiley, “Modulating the Growth Kinetics, Aspect Ratio, and Yield of Copper Nanowires with Alkylamines”, *J. Mater. Chem.* **30**, 2809–2818 (2018).

4. X. Qi, T. Balankura, and K. A. Fichthorn, **(Invited Feature Article)** “Theoretical perspectives on the influence of solution-phase additives in shape-controlled nanocrystal synthesis”, *J. Phys. Chem. C* **122**, 18785–18794 (2018).

5. T. Balankura, X. Qi, and K. A. Fichthorn, “Solvent effects on molecular adsorption on Ag surfaces: PVP oligomers”, *J. Phys. Chem. C* **122**, 14566–14573 (2018).

6. M. J. Kim, S. Alvarez, Z. Chen, K. A. Fichthorn, and B. J. Wiley, “Single-Crystal Electrochemistry Reveals Why Metal Nanowires Grow”, *J. Am. Chem. Soc.* **140**, 14740-14746 (2018).

7. Z. Chen, T. Balankura, K. A. Fichthorn, and R. M. Rioux, “Revisiting the Polyol Synthesis of Silver Nanocubes: Role of Chlorine in Silver Nanocube Formation”, *ACS Nano* **13**, 1849–1860 (2019).

8. X. Qi, Z. Chen, T. Yan, and K. A. Fichthorn, “Growth Mechanism of Fivefold-Twinned Ag Nanowires from Multiscale Theory and Simulations”, *ACS Nano* **13**, 4647–4656 (2019).

Fabricating Single Crystal Quantum Dot Solids

Tobias Hanrath,[1] Lena F. Kourkoutis,[1] Paulette Clancy[2] (1 Cornell University, 2 Johns Hopkins University)

Program Scope

This collaborative research program to aims to develop new fabrication techniques that enable the creation of single crystal quantum dot solids (QDS) with programmable symmetry and composition. Our approach towards that goal involves unique in-situ, multi-probe characterization techniques to gain deep insights into the fundamental relationship between processing conditions and nucleation and growth of QDS. The program integrates computational modeling and experiment to gain atomic-level insights into the underlying physical phenomena governing assembly and attachment and to guide development of optimized processing methods.

QDS promise tunable band structure through control of the quantum dot size and their coupling. The limiting factor in realizing these goals is structural disorder, which prevents carrier delocalization and limits the optoelectronic properties. Currently available fabrication methods yield polycrystalline QDS with poor control over crystal structure and small (~µm) grain sizes due to the complex interplay of particle diffusion, assembly, attachment and coupled fluid transport processes. The basic kinetic and thermodynamic factors governing the interplay of self-assembly and directed attachment are poorly understood; this knowledge gap defines a key motivation for the proposed work. We will discuss our approach to couple synthesis, modeling and advanced characterization by aberration corrected scanning transmission electron microscopy (STEM) to understand sources of this disorder and design strategies to overcome current limitations.

We hypothesized that QDS nucleation and growth processes can be rigorously controlled in small volumes of surface-patterned liquid droplets. Two principal goals of the proposed work are: (1) to establish fundamental principles that govern the formation of single crystal QDS in a confined liquid volume and (2) to understand and control the nature of the ‘epitaxial bond’ connecting the dots in the atomically coherent superlattice. We see the versatility of the methodologies developed in the project and the compatibility with existing device fabrication techniques as a key strength and anticipate that our work will likely spur additional advances in the synthesis and processing of 2D QDS as well as exploring their unique predicted electronic properties.

Recent Progress

We will discuss progress on three coordinated fronts: (i) fabrication of single QDS, (ii) structural analysis of QDS using advanced TEM methods, and (iii) computational simulations of epitaxial bridge formation.

Our goal to create QDS on the surface of confined liquid volumes lead us to investigate conditions under which QD suspensions could be ink-jet printed. We analyzed the hydrodynamic processes involved in jetting colloidal quantum dot suspensions on top of a patterned sessile droplet. Analysis of the modified Weber number (the ratio of the kinetic energy of the incoming droplet relative to the interfacial energy) provided guidance to key printing conditions such as jetting velocity and nozzle diameter. We identified an optimal solvent for the colloidal quantum dot suspensions which appropriate balance of volatility and viscosity; this solvent choice was informed by the in-situ X-ray scattering experiments of the quantum dot assembly.

We investigated how the formation of a quantum dot monolayer at the interface of two immiscible liquids is influenced by the coupled subprocesses of solvent spreading and evaporation. Notably, the process of forming a quantum dot assembly at a fluid-fluid interface involves several hydrodynamic complexities that have not been described (nor controlled) in previous reports in the literature. To address this knowledge gap, we performed a series of assembly experiments using the in-situ X-ray scattering chamber available at CHESS (Figure1). In-situ X-ray scattering experiments provided new insights into the complex interplay of solvent spreading and solvent evaporation. We discovered that the spreading of the bulk colloidal suspension is proceeded by the rapid spreading of a monolayer of quantum dots. Additionally, we explain how tuning the solvent parameters, such as volatility, surface tension and polarity, determines the mesoscale morphology of 2D superlattices on ethylene glycol.[1]

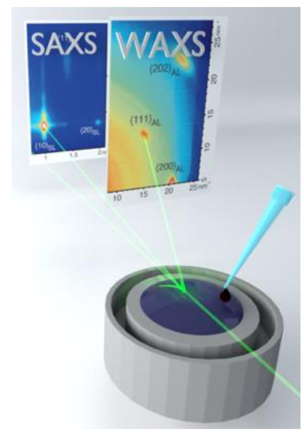

Figure 1: In-situ X-ray scattering provides insights into the dynamics forming QDS at a fluid interface.

Our analysis of the QDS structure demonstrated that orientational disorder of the nanocrystal atomic lattices plays an important role in the disorder of the superlattice. Atomic-resolution STEM images over large fields of view allow is to extract atomic lattice orientations across thousands of nanocrystals and quantify local lattice symmetries, showing a correlation between atomic lattice alignment between neighbors and local superlattice order (see Figure 2). Applying these techniques to a monolayer grain boundary, we see a striking difference between the sharp atomic lattice boundary and continuous deformation across the superlattice; this analysis supports the idea that the irreversibility of the oriented attachment process is a key element of the ultimate material structure. Coupling between the atomic lattice and the superlattice is a fundamental driver of film growth, and our results suggest nontrivial underlying mechanics, implying that simplified models of epitaxial attachment may be insufficient to understand DQS formation and disorder when oriented attachment and superlattice growth occur in concert [2].

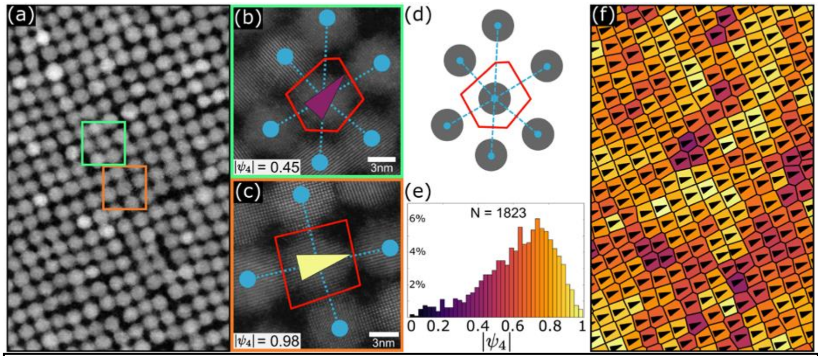

Figure 2: Local superlattice orientation and four-fold symmetry. (a) A HAADF-STEM image of a disordered, but approximately square, QDS. (b,c) structure order parameter ψ4 is calculated for each dot via their corresponding Voronoi cells, outlined in red. In comparatively ordered regions (c) the Voronoi cell is approximately square, while in more disordered regions (b) the cell perimeter is a less symmetric polygon. (d) More distant neighbors corresponding to shorter Voronoi cell edges are weighted less in the calculation of ψ4. (e) The magnitude of ψ4 quantifies the degree of local fourfold symmetry of the superlattice. (f) The Voronoi diagram corresponding to the image in (a), with the cells colored according ψ4 and the arrows indicating the direction of best fourfold symmetry determined from the complex argument of ψ4.

Computational progress on this project has been made on two fronts: (1) a concerted effort to create a new reactive force field that will model the kinds of molecular systems, like PbS and PbSe, that cannot currently be modeled by ubiquitous codes such as LAMMPS, nor by existing reactive force fields, like REAX-FF; (2) studying the mechanism by which bridges form between quantum dot building blocks. Our approach towards that goal applies the Simple Molecular Reactive Force Field (SMRFF) to accurately simulate interactions between quantum dots. This potential uses both reactive and non-reactive force fields to model interactions between particles at different interatomic distances: short-range interactions can be modeled by a reactive force field, such as the Morse or the Tersoff potential, smoothly connected to long-range interactions modeled by a superposition of the Lennard-Jones and Coulomb potentials. We have parametrized the force field using a diverse set of conformations of the initial PbS quantum dot building blocks. The simulations suggest that mechanism of bridge formation is sensitive to the nature of the force field that exists between particles. This places a premium on making sure that the force field is as accurate as possible, creating more impetus to finalize our reactive force field approach.

Future Plans

Having identified an 'operating window' in which colloidal quantum dot suspensions can be printed on top of immiscible sessile droplets, we will push forward to investigate how subsequent processing steps (i.e., introduction of chemical trigger to initial QD attachment) can be integrated. Whereas the relatively thin (~100µm) ethylene glycol droplet used in our initial inkjet printing studies are susceptible to mechanical instabilities upon impact from the inkjet printed colloidal quantum dot solutions, our current printing efforts focus on inkjet printing on

EG in custom-fabricated wells. We are investigating alternative fabrication methods including dip-pen deposition of the quantum dot suspension and the chemical trigger. To achieve better spatiotemporal control over the initiation of the structural transformation, we are currently investigated photoinitated amine trigger release.

With the characterization tools in place to track the structure of synthesized QDS, we will focus next on the effects of thermal annealing on connectivity and disorder. Using a MEMS based in-situ heating holder to control the temperature, annealing time and rate of heating we will directly image the evolution of the QDS. We will systematical probe processing conditions in order to maximize the benefits of annealing on the long range and local structure of the QDS films.

Moving beyond the initial parameterization of SMRFF for PbS quantum dots, we will have the foundation we need to conduct large-scale computational studies to comprehensively uncover the propensity and mechanism for systems that differ in the number of quantum dots (pairs, 4 in-plane dots, 9 full-shell dots), dot size, robustness to the regularity of the shape of the dots and the nature of the faceting, initial misalignment of the dots, and the existence of defects. In addition, given its sensitivity and impact on the outcomes, we will investigate the role of the force field to alter the outcomes of bridge formation. For direct comparison to experiments, we will also investigate the result of thermal annealing of the systems.

Publications

[1] D. Balazs, T. Dunbar, D.M. Smilgies, T. Hanrath, “*The dynamics of nanoparticle spreading and assembly at a fluid-fluid interface*”, submitted.

[2] A.R.C. McCray, B.H. Savitzky, K. Whitham, T. Hanrath, L.F. Kourkoutis, “*Orientational Disorder in Epitaxially Connected Quantum Dot Solids*”, submitted

Single Crystal growth via solid → solid transformation (SCGST) of glass

PI: Himanshu Jain and Co-PI: Volkmar Dierolf, Lehigh University, Bethlehem, PA USA

Program Scope

We are developing a new paradigm for fabricating single crystal in glass using solid → solid transformation. The selected compositions cannot be grown as single crystals using existing methods due to incongruent melting, decomposition upon heating to high temperature or phase transformation upon cooling. Previously, the proof-of-concept was demonstrated along with the discovery of a new class of solids, termed rotating lattice single (RLS) crystals, and introduction of the concept of 'lattice engineering'.

A phenomenological, working model has been proposed to explain the origin of lattice rotation, which needs verification. Further, key features and impact of SCGST and lattice rotation on properties remain unexplored/unexplained. To overcome this deficiency and to advance the distinctive attributes of such metastructures in practical applications, we have formulated four complementary working hypotheses: (A) SCGST is a widely applicable phenomenon, and not limited to congruently crystallizing glass compositions. (B) Rotation of lattice within RLS crystal represents dynamic equilibrium between the stresses arising from densification during SCGST and structural relaxation in the surrounding glass. (C) Although nucleation of crystal within the glass matrix is a random process, it should be possible to control the orientation of nuclei, hence of the desired crystal, by polarization or intensity profile of the laser. (D) SCGST imposes unique boundary conditions that allow the synthesis of single crystal architecture, which is otherwise very difficult or impossible to fabricate. In response to these questions and hypotheses, our goal is to investigate SCGST phenomenon and lattice rotation characteristics. The resulting information about the glass, the RLS crystal and the interfacial region in relation to local temperature and composition will help establish a comprehensive understanding suitable for guiding the fabrication of single crystal architecture of novel compositions and properties, which would not be feasible by the existing methods.

Recent Progress

During the current reporting period we have focused primarily on hypothesis (B), and to lesser extent on (A) and (C) to further characterize the lattice rotations within our RLS crystals. The most significant progress made in support of these hypotheses is summarized below:

(a) <u>Fundamental nature of lattice rotation within RLS crystal – *in situ* x-ray diffraction studies</u>

To understand the process of lattice formation that proceeds via solid→solid transformation, we have observed *in-situ* Sb_2S_3 crystal formation under x-ray irradiation. Here, an x-ray beam is used as the heating source to fabricate these crystal structures while Laue diffraction patterns are collected to characterize evolution of structure at the same time. Using this novel approach, we were able to observe the progression of crystallization of glass and track changes in orientation in real time. We found that during the initial growth of crystal dots, which are used as seed crystals for fabricating other crystal architectures, there is a small change in orientation of the crystal lattice until reaching the steady state where the seed crystal stops to rotate. This change in orientation is notably different from the constant rotation rate found in the crystal lines (see below).

From observations under static conditions, we see that diffraction begins with one spot until a second spot begins to emerge in its vicinity (Fig. 1). At the last diffraction pattern of the crystal dot, the diffraction pattern indexes as a single grain confirming we are creating single crystal seed. This evolution of a given Laue 'spot' supports the introduction and then polygonization of dislocation, leading to the formation of a low angle boundary within seed crystal. The small change in orientation is consistent with the small change in deviation angle observed from electron backscattered diffraction (EBSD) of the crystal dot. At the end of the crystal dot formation the diffraction peaks are elliptical, which suggests that there are still organized dislocations within the crystal structure.

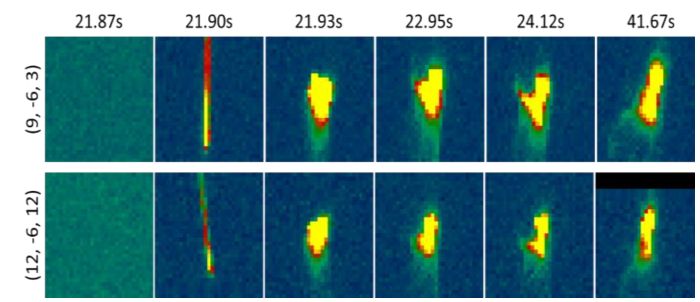

Figure 1: Evolution of two selected Laue reflections, (9,-6,3) and (12,-6,12) during seed crystallization. Time since the beginning of X-irradiation is indicated at the top.

To compare directly with laser-fabricated 1D RLS crystal lines, we replicated the procedure using the x-ray beam, starting from the previously formed dot seed crystal. In the transition from dot to line, the lattice evolves in a complex manner that introduces large errors in indexing. Thereafter, we observe a smooth rotation of the lattice in real time, in agreement with previously reported *ex-situ* observations, see Fig. 2. Since we observe this rotation as it occurs, we conclude that lattice rotation within RLS crystals arises during growth at temperature, and not afterward during cooling to ambient. We also note that the individual diffraction peaks are elliptical as with seed crystal, and not circular as expected from 'perfect' crystals. These results support the model that lattice rotation in RLS crystals arises from the presence of unpaired dislocations and small-angle boundaries.

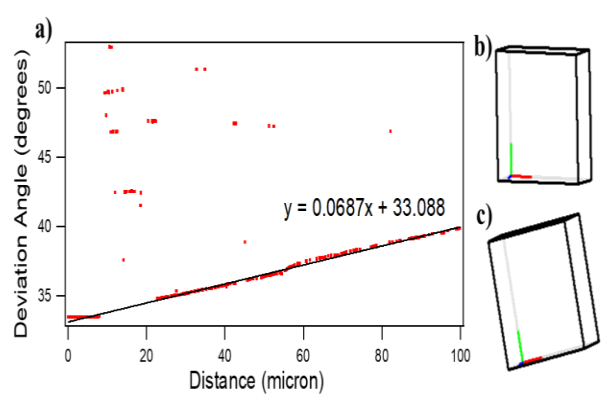

Figure 2: a) Plot of the deviation angle vs distance from the crystal seed. The equation of the linear fit is shown within the graph. b) Unit cell representation of the crystal orientation, [1, -26, 9], at the origin of the crystal line, 0 micron. c) Unit cell representation of the crystal orientation, [-1, -6, 3], at the end of the crystal line, 100 micron.

To directly verify that the lattice rotation in RLS crystals arises from the introduction of dislocations, we used transmission electron microscopy on an RLS crystal line that was previously characterized by EBSD. As seen in Fig. 3, edge dislocations of the same sign appear in the crystal, many of them are well aligned as in a low angle grain boundary. Using the Burgers vector for Sb_2S_3, a/2 = 0.565 nm and the spacing between dislocations, we estimated the rotation rate that would result from such dislocations. Thus, the rotation rate along growth direction was calculated to be 0.128°/μm. The EBSD result show the rotation rate as 0.11°/μm. This excellent agreement confirms that the lattice rotation is a manifestation of dislocations introduced regularly during single crystal growth via solid→solid transformation.

(b) Effect of laser polarization on the orientation of the lattice of RLS crystals

To establish if laser polarization has any influence on the orientation of lattice of RLS crystals, we performed laser-crystallization experiments using a spatial light modulator, SLM, that provides linearly polarized light. The SLM was used to modify the laser beam from its original Gaussian profile to rings of varying sizes to create larger crystal dots with a radially isotropic temperature profile; the only possible source of anisotropy is the polarization of laser. The crystal orientation deviation map shows that there is a rotation of the lattice, but it does not occur uniformly around the crystal dot. We also see that there is a maximum growth rate close to the direction of polarization, the y-direction, and minimum growth in the direction perpendicular to polarization, as seen in Fig. 4. A plausible explanation of this observation is that the alignment of the crystallization inducing electric field with the direction of crystal growth can lower the entropy of activation, creating an environment where it is easier for the crystal to nucleate and grow in that direction.

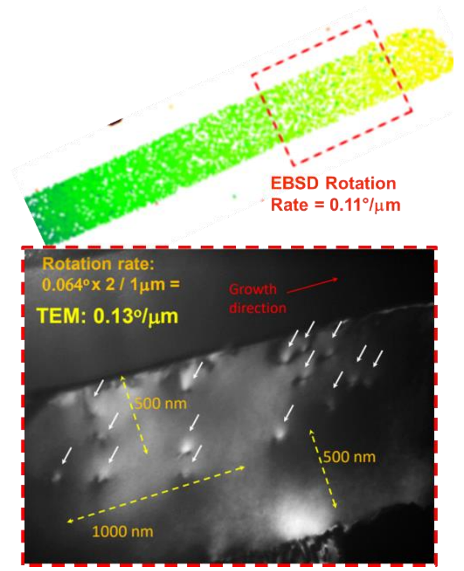

Figure 3: Above: Inverse pole figure of crystal section characterized by EBSD. Below: TEM image of the section of crystal identified by dashed red box. The white arrows point to individual dislocations.

The rotating lattice of the investigated crystals is the defining feature of what we now refer to as RLS crystals. Here, we see that when the growth rate is increased, there is a decreased rate of rotation; conversely at a decreased growth rate, we observe an increased rate of rotation. Therefore, if polarization can be used to control the relative growth rate of these structures it can help control the lattice rotation rate and increase their usefulness for applications.

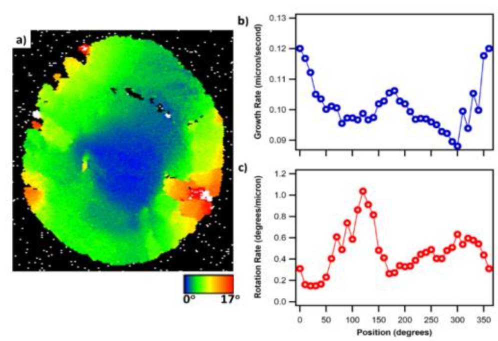

Figure 4: The single crystal dot #1 induced by the laser beam using the “ring” procedure on the surface of Sb_2S_3 glass: (a) Crystal orientation deviation (COD) map with reference to crystal orientation at the center of the dot. Graphs represent growth rate (b) and rotation rate (c) with respect to position from the center to the periphery of the dot, 0° corresponds to the top of the crystal dot.

(c) Atomistic simulation of SCGST

The control of orientation of laser fabricated single crystals remains a continuing challenge. It requires a detailed understanding of the nucleation process, which remains one of the most important problems of materials science. Accordingly, we have undertaken the task of atomistic simulation of the nucleation and growth of a crystal in glass. Since nucleation is a stochastic process and difficult to manage using currently available computational methods and resources, we have started our investigation into the nature of these processes in the vicinity of a well-defined crystal surface in the systems for which we already have experimental data. A better understanding of the glass/crystal interfacial structures is needed for elucidating the nucleation and crystal growth behaviors within the glass. Accordingly, *ab initio* Molecular Dynamics (AIMD) simulations are used to calculate the behaviors of crystalline/glassy Sb_2S_3

interface structures using Quantum Espresso and Vienna *ab initio* simulation packages. To begin, reliable structures of both crystal and glassy Sb_2S_3 have been obtained (see Fig. 5), as the basis for constructing crystal/glass interface. For this, slab models were used with applied periodic boundary in three dimensions. There is significant difference in the local structures of crystal and glass, for example, Sb in the former exists with coordination number (CN) 3 and 5 in equal concentration, while in the latter CN = 3, 4, 5 and 6 occur in relative abundance of 20.8%, 33.3%, 25.0% and 4.2%, with remaining in an under-coordinated state of CN = 1 or 2. To simulate crystallization of glass, we are determining the influence of one on the structure of the other by inserting a 3 Å vacuum layer. In this regard, the fraction of Sb in four-fold coordination would serve a simple parameter for following the evolution of disorder in glass towards crystalline order.

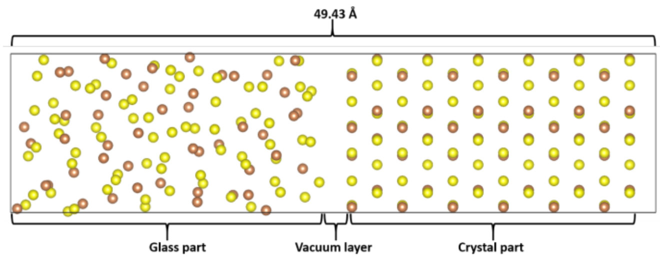

Figure 5. Schematic structure of initial generated Sb_2S_3 crystal/glass interface model. Brown: Sb; Yellow: S

Future Plans

For hypothesis (B) to further understand the rotating lattice, we plan to explore how the surface of our samples affect the rotating lattice. Learning how the surface can affect the rotation in our RLS crystals, we can further understand how to control the orientation. Previous experiments have shown that a 488 nm CW laser can create photo-expanded regions on the surface of our Sb-S-I glasses without crystallizing. To study these surface effects, we will create photo-expanded regions on the surface of our glass with the 488 nm laser. We will then switch to the traditionally used 639 nm laser to create crystal structures over these regions to determine if the change in surface topology creates changes in crystal orientation. We plan to characterize these crystals with EBSD.

We plan to continue our efforts with the *in situ* x-ray micro-diffraction experiments. We are currently conducting experiments using a collection rate of 30 frames per second at ALS. While this has been successful in exploring early crystal growth, it is not fast enough to explore nucleation characteristics. We are exploring x-ray diffraction beamlines at NSLS, to increase our time resolution to at least 100 frames per second. We plan to submit a proposal for commissioning time at there to explore these possibilities of performing our x-ray experiments with higher time resolution.

For hypothesis (C), we will form dot crystals with stationery CW laser on the surface of currently used chalcogenide glasses, but under external DC electric field. Initial tests show that application of field at the growth front could be a challenge if the glass matrix is readily polarized. Therefore, in parallel, we will investigate the effect of uniaxial compressive stress on crystal orientation.

Finally, we will advance atomistic simulations to model glass-crystal interface to yield z-density profile, pair distribution function and coordination number. These predictions will be compared with the measurement of structure using synchrotrons at NSLS and ALS. In line with Hypothesis (A), similar interface models will be constructed for Ge_xSe_{1-x} crystal/glass systems using AIMD due to lack of reliable empirical potentials for most of chalcogenide glass systems.

Publications

1. Fabrication of single crystal architecture in Sb-S-I glass: transition from dot to line
Dmytro Savytskii, Volkmar Dierolf, Nobumichi Tamura, Himanshu Jain
J. Non-cryst. Solids 501 (2018) 43-48. https://doi.org/10.1016/j.jnoncrysol.2017.12.007
(This publication was under review at the time of previous report. It was published subsequently and its complete citation is given here.)

2. Single Crystal Growth via Solid → Solid Transformation of Glass
H. Jain, D. Savytskii, V. Dierolf (Invited overview)
Trans Indian Inst Met (2019). https://doi.org/10.1007/s12666-019-01737-6

3. Influence of laser scanning rate on the structure of rotating lattice single crystal lines
Dmytro Savytskii, Volkmar Dierolf, Himanshu Jain
Cryst. Growth Des. Under review (2019)

Presentations at Conferences and Universities

1. (American Ceramic Society's 2019 Morey Award Lecture) H. Jain, "*The architectured glass*", International Congress on Glass and Ann. Meet. Glass & Optical Materials Div., Am. Ceram. Soc. Boston, MA, 2019 June.
2. C. Au-Yeung, C. Stan, B. Shaw, H. Jain, V. Dierolf, "*Characterization of rotating-lattice-single crystal growth on the surface of Sb_2S_3 chalcogenide glass via in situ observation*", International Congress on Glass and Ann. Meet. Glass & Optical Materials Div., Am. Ceram. Soc. Boston, MA, 2019 June.
3. E. Musterman*, C. Au-Yeung, V. Dierolf, H. Jain, "*Effects of Electric Field on the laser fabrication of Single Crystals of Ferroelectric Sb_2S_3 in $84Sb_2S_3$-$16SbI_3$ Glass*", International Congress on Glass and Ann. Meet. Glass & Optical Materials Div., Am. Ceram. Soc., Boston, MA, 2019 June.
4. (Invited colloquium) H. Jain, "*Driving ~perfect disorder to ~perfect order in solids*", Materials Science and Engineering Department, University of California, Davis, CA, 2019 May.
5. (Invited tutorial lecture) H. Jain, *"Hybrid Materials: Single Crystals in Glass*", First North American Summer School on Photonic Materials, University of Laval, Quebec City, Canada, 2019 June.
6. C. Au-Yeung, C. Stan, N. Tamura, H. Jain, V. Dierolf, *"In situ observation of Sb2S3 single crystal formation in glass by micro x-ray diffraction"*, American Physical Society March Meeting, Boson, MA, 2019 March.
7. C. Au-Yeung, C. Stan, H. Jain, V. Dierolf, *"In situ, real time observation of Sb2S3 crystal formation in Sb-S-I glass by micro x-ray diffraction"*, Gordon Research Seminar and Conference: Defects in Semiconductors, 2018 Aug.
8. (Invited colloquium) H. Jain, *"Driving ~perfect disorder to ~perfect order in solids"*, Department of Chemistry, Dalhousie University, Halifax, Nova Scotia, Canada, 2018 Dec.

9. (Invited talk) H. Jain, *"Fundamental Nature of the Light-Induced Restructuring and Modification of Properties of Glass*", Annual Meeting MRS: Symposium CM02: Structure–Property Relations in Non- Crystalline Materials, Boston, MA, 2018 Nov.
10. (Invited talk) V. Dierolf*, K. Veenhuizen, C. Au-Yeung, S. McAnany, L. Hoxha, K. Tafiti, B. Aitken, D. Nolan, D. Savytskyy, H. Jain, *"Laser Fabrication of Single Crystal within Glass—Influence of Polarization"*, Annual Meeting MRS: Symposium PM05: Electromagnetic Fields in Materials Synthesis-Far from Equilibrium Effects, Boston, MA, 2018 Nov.
11. (Invited talk) D. Savytskyy, A. Stone, K. Veenhuizen, C. Au-Yeung, S. McAnany, D. Nolan, B. Aitken, V. Dierolf, H. Jain*, *"Single crystal architecture in glass: Fabrication and unique characteristics"*, 13th International Conference on Solid State Chemistry, Pardubice, Czech Republic, 2018 Sep.
12. V. Dierolf, K. Veenhuizen, C. Au-Yeung, L. Hoxha, K. Tafiti, D. Savytskyy, S. McAnany, D. Nolan, B. Aitken, H. Jain, *"Crystal Lattice Engineering during Laser induced Single Crystal Growth*", 20th University Conference on Glass, State College, PA, 2018 Aug.
13. C. Au-Yeung, C. Stan, B. Shaw, H. Jain, V. Dierolf, *"In situ observation of Sb2S3 crystal formation in Sb2S3 glass by micro x-ray diffraction"*, 20th University Glass Conference, State College, PA, 2018 Aug.
14. D. Savytskyy, S. McAnany, M. Watanabe, V. Dierolf, H. Jain*, *"A dislocation based model of rotating-lattice single crystal growth on glass surface by CW-laser"*, 15th International Conference on the Physics of Non-Crystalline Solids & 4th European Society of Glass Conference, St. Malo, France, 2018 Jul.
15. (Invited talk) K. Veenhuizen, C. Au-Yeung, D. Savytskyy, S. McAnany, D. Nolan, B. Aitken, H. Jain, V. Dierolf, *"Crystal Lattice Engineering during Single Crystal Growth by Laser-induced Solid-Solid Conversion"*, Advanced Photonics 2018, Zurich, Switzerland, 2018 Jul.
16. (Invited poster) C. Au-Yeung, C. Stan, H. Jain, V. Dierolf, *"In situ, real time observation of Sb2S3 single crystal formation in Sb-S-I glass by micro x-ray diffraction."* Glass Summit 2018: Glass across Boundaries, Corning, NY, 2018 Jun.
17. (Invited talk) D. Savytskyy, C. Au-Yeung, S. McAnany, V. Dierolf, H. Jain*, *"Single crystal architecture in chalcogenide glasses"*, 21st International Symposium on Non-Oxide and New Optical Glasses (ISNOG), Quebec City, Canada, 2018 Jun.
18. C. Au-Yeung*, C. Stan, S. McAnany, D. Savytskyy, H. Jain, V. Dierolf, *"Growth of rotating-lattice-single crystal on the surface of Sb-S-I chalcogenide glass: mechanism and in situ observation"*, 21st International Symposium on Non-Oxide and New Optical Glasses (ISNOG), Quebec City, Canada, 2018 Jun.
19. (Invited talk) V. Dierolf*, K. Veenhuizen, C. Au-Yeung; S. McAnany, B. Aitken, D. Nolan, H. Jain, *"Crystal Lattice Engineering during Single Crystal Growth by Laser-induced Solid-Solid Conversion"*, 2018 Glass & Optical Materials Division Annual Meeting, San Antonio, TX, 2018 May.

20. C. Au-Yeung*, C. Stan, H. Jain, V. Dierolf, *"In situ observation of Sb2S3 crystal formation in Sb-S-I glass by micro x-ray diffraction"*, 2018 Glass & Optical Materials Division Annual Meeting, San Antonio, TX, 2018 May.
21. D. Savytskyy, V. Dierolf, N. Tamura, H. Jain*, *"Challenges of fabrication of single crystal architecture in glass: Transition from dot to line"*, 2018 Glass & Optical Materials Division Annual Meeting, San Antonio, TX, 2018 May.
22. (Invited talk) H. Jain*, *"Novel methods of glass restructuring for fabrication of devices by laser irradiation"*, 2018 Glass & Optical Materials Division Annual Meeting, San Antonio, TX, 2018 May.
23. (Invited talk) V. Dierolf, D. Savytskyy, *"Engineering the lattice of a single-crystal grown in glass, Engineering the lattice of a single-crystal grown in glass"*, 2017 Synthesis and Processing Science Principal Investigators' Meeting, Gaithersburg, MD, 2017 Nov.
24. (Poster) H. Jain, V. Dierolf, *"Laser Fabrication of Single Crystal Architecture in Glass of Noncongruent Composition"*, 2017 Synthesis and Processing Science Principal Investigators' Meeting, Gaithersburg, MD, 2017 Nov.
25. (Invited talk) D. Savytskyy, C. Au-Yeung, K. Veenhuizen, V. Dierolf, H. Jain, *"Engineering the lattice of single crystal grown in glass"*, 12th International Symposium on Crystallization in Glasses and Liquids (ISCGL), Segovia, Spain, 2017 Sep.
26. (Keynote/Plenary talk) D. Savytskyy, K. Veenhuizen, C. Au-Yeung, S. McAnany, B. Aitken, D. Nolan, V. Dierolf, H. Jain, *"Single crystal architecture in glass (SCAG): A new frontier of glass applications"*, XI Brazilian Symposium on Glass and Related Materials, Curitiba, Brazil, 2017 July.
27. (Invited seminar) V. Dierolf, *"Single crystal architecture in glass (SCAG): A new frontier of glass applications"*, Corning, NY, 2017 July.

Intercalation and High Pressure of Phosphorene - Pathways to Novel Materials and Physics

Jacek Jasinski, Conn Center for Renewable Energy Research, University of Louisville (PI)
Gamini Sumanasekera, Physics and Astronomy, University of Louisville (Co-PI)
Ming Yu, Physics and Astronomy, University of Louisville (Co-PI)

Program Scope

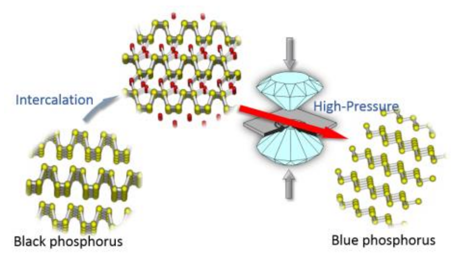

Fig. 1. Concept scheme of intercalation-induced phase transition with pressure.

Our preliminary studies have prompted the idea that intercalation followed by high pressure can lead to the transformation of black phosphorous to blue phosphorous. Intercalation can lead to the bond reorganization and thus lower the energy barriers for structural phase transitions. This offers new pathways for the synthesis of blue phosphorene, a new intriguing two-dimensional (2D) material, and creates an opportunity to explore novel physical phenomena in this and similar 2D systems. In order to expand the phase diagram space, we will combine the alkali metal (Li, Na, and K) intercalation of black phosphorous with high-pressure conditions (Fig. 1). The synergistic effects of intercalation and pressure on nanomaterials through computational modeling and *in-situ* monitoring and whether such effects can lead to new nanostructures, at atomic level, will be investigated. This research will have significant impacts on the fundamental understanding of physics associated with phosphorene and related 2D materials. It is expected that intercalation can significantly lower the pressure for the phase transformation from black phosphorous to theoretically predicted exotic blue phosphorous. This approach could offer pathways for the fabrication of blue phosphorene and also enable its fundamental studies to uncover novel physical phenomena in this predicted unique material. Theoretical calculations indicate that due to its unique electronic structure, blue phosphorene with varying stacking configurations may be a promising candidate as a BCS-superconductor after proper intercalation with alkali metals such as Li, Na, and K [1]. It may also exhibit the charge-density-wave (CDW) phase due to periodic distortion of the atomic lattice in this layered 2D material under proper intercalation and high pressure. Several layered transition metal dichalcogenides, including 1T-$TaSe_2$, 1T-TaS_2 and 1T-$TiSe_2$ are known to exhibit unusually high transition temperatures to different CDW phases [2]. Concerning the applications, it has been calculated that, energetically, blue phosphorus is nearly as stable as black phosphorus (with the binding energy difference < 2 meV/atom [3, 4]) and it also should be exfoliated easily to form new 2D structure, e.g. blue phosphorene. It has been

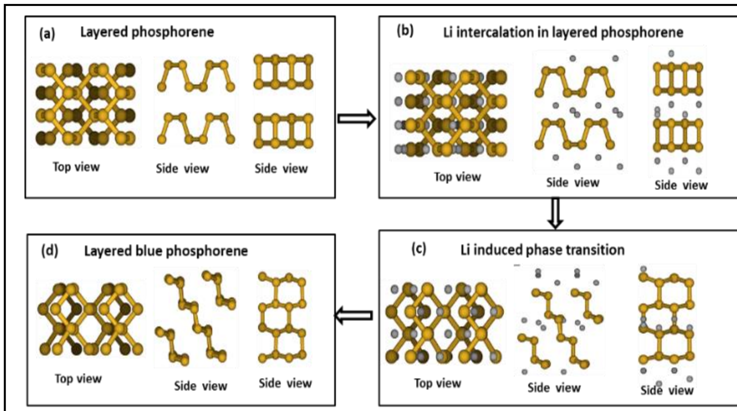

Fig. 2 Top and side views of (a) layered black phosphorene; (b) Li intercalation in the layered black phosphorene; (c) Li induced structural phase transition during the relaxation; and (d) layered blue phosphorene after Li removal, respectively. The arrows show the direction of the flow of the transition induced by the Li intercalation.

predicted that blue phosphorene has even a wider fundamental band gap (> 2 eV) compared to black phosphorene [4], layer-dependent tunable bandgap, semiconducting-semimetal transition under strain, possible high carrier mobility, and higher in-plane rigidity, making it a worthy contender in the emerging field of post-graphene 2D electronics [4].

Recent Progress

To understand the atomistic mechanism of the intercalation during the structural phase transition, we performed 'in situ' theoretical study to analyze the role played by Li atoms during Li intercalation on phosphorene considering a specific Li concentration and configuration $Li_{10}P_{16}$ (Fig. 2(b)). We found that under these conditions, the Li atoms on the top and bottom ridge of phosphorene slightly pull out nearby P atoms. Such that the particular P-P bonds between the valley and the ridge on the same layer broke and subsequently new P-P bonds between adjacent layers form. Such reconstruction together with the readjustment of some of the bonding angles leads to the rhombohedral structure with layers parallel to the (011) plane of the original orthorhombic structure (Fig.2 (c)). As a result, the puckered orthorhombic structure was automatically transformed to a buckled rhombohedral structure, indicating that the inserted Li atoms at those locations could act as 'catalysts' to drive the specific P atoms moving along specific directions, resulting bond breaking and forming, and subsequently, transforming layered black to layered blue phosphorene (Fig. 2 (d)). Interesting, we did not find such structure transformation if we insert K or Na with the same concentration and configuration (Fig. 3 (a) and (b)). It is clear that the bond lengths of K-K (~3.95 Å) and Na-Na (~3.45 Å) are larger than that of Li-Li (~2.85 Å), which might affect the interactions between K/Na and P and weaken their role as 'catalysts' to mediate the structure transformation on layered phosphorene. We are analyzing these results in terms of the attractive/repulsive interactions between Li and P/Li atoms, the charge transfer between Li and P atoms, the dislocations of particular P atoms during bonds breaking/forming process, and the change of the electronic band structure of the combined system along the transition path. Theoretical findings will be validated by experiments planned for the project. The experimental work focusses on the fabrication and characterization of black phosphorene, intercalation, and high-pressure experiments.

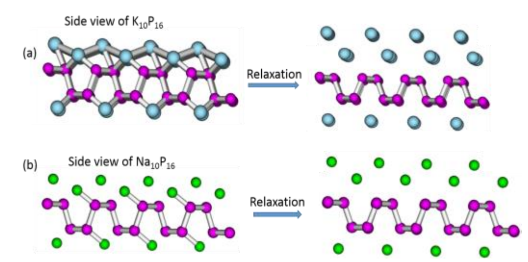

Fig. 3 (a) The initial (left) and the final (right) structures of $K_{10}P_{16}$. (b) The initial (left) and the final (right) structures of $Na_{10}P_{16}$. The pick, blue, and green dots denote P, K, and Na atoms, respectively.

Black phosphorus (BP) samples are synthesized using a short transport growth method [5]. Quartz glass ampules filled with tin

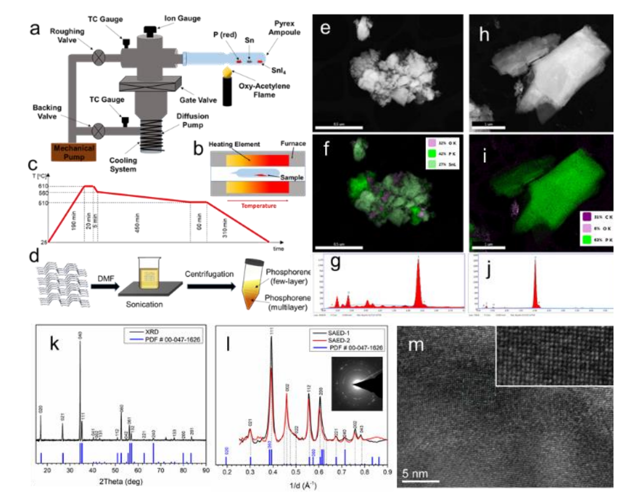

Fig. 4 (a-c) Schematic setup and conditions for the short transport growth method of BP. (d) Steps of liquid mechanical exfoliation of BP. (e-g) and (h-j) TEM-EDS elemental analysis of a poor- and high-quality BP sample produced in a single- and two-zone furnace, respectively. (k) XRD of BP powder and (l) SAED of BP flakes. (m) HRTEM of a single flake.

(Sn), tin iodide (SnI_4), and red phosphorus are evacuated to 10^{-6} Torr, sealed using an oxy-acetylene flame torch (Fig. 4a), and annealed in a quartz tube furnace (Fig. 4b) following the heating profile shown in Fig. 4c. The synthesis in a single zone furnace results in multiphase materials, composed of phosphorous and tin phosphide, (Fig. 4e-f. However, the use of a two-zone furnace and a well-defined temperature gradient yields high-quality BP samples (Fig. 4h-j, k-m). These materials are used for the systematic liquid phase exfoliation study. Crushed BP powders are suspended in solvent and are sonicated, followed by subsequent centrifuging for the separation into fraction of different number of layers (Fig. 4d). DMF and other solvents are tested for good control of the flake size and the number of layers.

Some of obtained phosphorene samples are also used for additional advanced studies. This includes a study where a field effect transistor (FET) structure was prepared with phosphorene as the conducting channel and its performance was evaluated upon exposure to different gases (H_2, N_2H_4, N_2O, air, and argon). The chemical doping effects lead to changes of transport properties. The observed changes show a strong gas sensing selectivity and are believed to originate from the gas-specific modulation of the Schottky barrier formed between the p-type phosphorene and aluminum contacts. The findings suggest that phosphorene is a highly attractive material for gas sensing applications. This research suggests also that devices fabricated from phosphorene must be studied carefully to fully understand how they behave under real working environments.

In another study, *in-situ* high-pressure Raman spectroscopy study of bilayer phoshorene were conducted at pressures up to 10 GaP (Fig. 5). The observed systematic shifting of A_g^1, B_{2g}, and A_g^2 Raman modes reflected the deformations in the structure and stiffness of the material. A substantial pressure-induced enhancement of the interactions between atoms for the out-plane mode A_g^1, mainly due to the directional nature of the lone pair of electrons and charge transfer, was observed. However, these interactions were weaker than those in BP. The study showed also a significant enhancement of the atomic interactions due to bond length for the in-plane mode B_{2g} along the zigzag direction. There is negligible effect on the in-plane mode A_g^2 along the armchair direction.

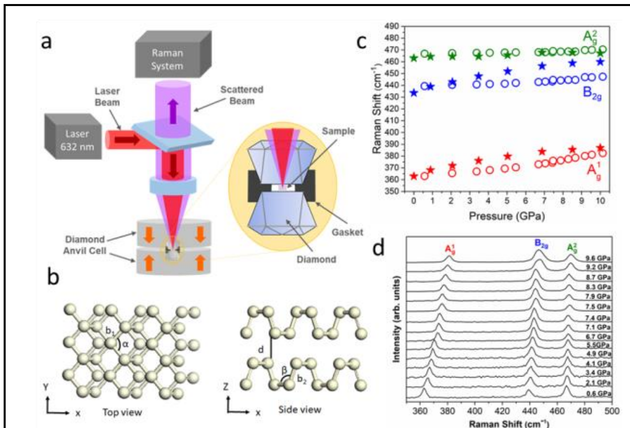

Fig. 5 (a) Schematic of the experimental setup used for *in-situ* high-pressure Raman spectroscopy. (b) Top and side view of the bilayer structure model. c) Comparison of high-pressure experimental (open circles) and theoretical (stars) Raman shifts for the three main modes. (d) High-pressure evolution of Raman spectra.

Future Plans

We have found that the Li intercalation with Li concentration 0.625 (i.e., $Li_{10}P_{16}$) and asymmetric configuration could lead to the structural transition from puckered orthorhombic to a buckled rhombohedral. In order to identify specific conditions for the structural transformation mediated by the alkali metal intercalation, we are surveying if there are other specific conditions and configurations for Li/Na/K intercalation such that the inserted alkaline atoms could induce the structural transformation from layered black to blue phosphorene. Based on the atomistic model provided above, we will perform a throughout computational MD modeling with various Li/Na/K configurations. We will consider the metal intercalation with (1) different Li/Na/K intercalation rates and (2) for a given rate, different Li/Na/K distributions in the interlayer space of black phosphorus (e.g., symmetric and asymmetric). Especially, we are interested in alkaline atoms at the specific ‘reactive centers’ to see how those atoms could lead to P atoms with specific dislocations and bond breaking on the same layer during dynamics process. All the intermediate states of the structural transformation will be monitored during the MD simulations and the relationships between metal and P atoms during the intercalation will be systematically analyzed.

Experimentally, we will continue optimizing the synthesis and exfoliation of BP for the good control of phosphorene flake size and its number of layers. Intercalation study with alkali metals and detailed characterization will also be conducted. This will include ex-situ measurements, as well as, the use of dedicated electrochemical cells (for Raman, XRD, and TEM) for in-situ monitoring of the structural evolution under different intercalation conditions. Intercalation experiments will help to validate theoretical findings and to prepare phosphorene samples for subsequent in-situ high-pressure study. During these experiments, flakes of pristine, intercalated, and de-intercalated phosphorene samples with different number of layers will be loaded to a DAC and Raman spectroscopy will be used for in-situ monitoring of structural changes and possible phase transitions in these materials under high-pressure conditions. Parallel high-pressure studies using a modulated nano/Å-indentation (MoNI/ÅI) method [6] are also planned in collaboration with Drs. Cellini and Riedo from New York University. The MoNI/ÅI measurements should help to validate DAC experiments and provide more data for better statistical analysis.

References

1. J.-J. Zhang and S. Dong, "Prediction of above 20 K superconductivity of blue phosphorus bilayer with metal intercalations", *2D Materials* 3, 035006, 2016.
2. G. Liu, B. Debnath, T. R. Pope, T. T. Salguero, R. K. Lake, and A. A. Balandin, "A charge-density-wave oscillator based on an integrated tantalum disulfide–boron nitride–graphene device operating at room temperature", *Nat. Nanotechnol.* 11, 845-850, 2016.
3. S. E. Boulfelfel, G. Seifert, Y. Grin, and S. Leoni, "Squeezing lone pairs: The A 17 to A 7 pressure-induced phase transition in black phosphorus", *Phys. Rev. B* 85, 014110, 2012.
4. Z. Zhu and D. Tománek, "Semiconducting layered blue phosphorus: a computational study", *Phys. Rev. Lett.* 112, 176802, 2014.
5. M. Köpf, N. Eckstein, D. Pfister, C. Grotz, I. Krüger, M. Greiwe, T. Hansen, H. Kohlmann, T. Nilges, “Access and in situ growth of phosphorene-precursor black phosphorus”, *J. Cryst. Growth* 405, 6-10, 2014.
6. F. Cellini, Y. Gao, E. Riedo. "Å-Indentation for non-destructive elastic moduli measurements of supported ultra-hard ultra-thin films and nanostructures", *Sci. Rep.* 9, 4075, 2019.

Publications

1. M. Akhtar, C. Zhang, M. Rajapakse, Md R. K. Musa, M.Yu, G. Sumanasekera, J. B. Jasinski, “Bilayer phosphorene under high pressure: in situ Raman spectroscopy", *Phys. Chem. Chem. Phys.* 21, 7298-7304, 2019.
2. A. Alruqi, R. Zhao, J. Jasinski, G. Sumanasekera, "Graphene-WS2 heterostructures by a lithography free method: their electrical properties", *Nanotechnology* 30, 275704, 2019.
3. A. Alruqi, R. Musa, R. Zhao, C. Zhang, J. Jasinski, M. Yu, G Sumanasekera, "Layer dependent hydrazine adsorption properties in few layer WS2", *J. Phys. Chem.* C, 2019.

Semiconductor Nanomembranes and Sheets: Compositions, Geometries, and Interfaces to Access New Functionalities

Max G. Lagally, University of Wisconsin-Madison, Madison WI-53706
Francesca Cavallo, University of New Mexico, Albuquerque, NM-87131

Program Scope

This new collaborative research program will leverage the unique attributes of inorganic nanomembranes (NMs)[1] to expand the palette of available compositions, geometries, and interfaces across energy-relevant materials. The effort, which involves both group IV- and III-V-based NMs, along with graphene and composites, will develop and understand methods to carry out synthesis and processing with precise control, and determine general process-structure-properties relationships for the targeted materials. We anticipate that our work will extend the NM platform into several unique directions.

Proposed work

This project is a new collaborative effort. Prior work by one of the collaborators is summarized in the Publications List appended. We choose here to discuss proposed research activities of the collaborative effort. Our work will focus on high-risk/high pay-off projects, described below.

1. NM-based materials for solid-state quantum computation.

We will engineer and characterize NM-based materials to support on-chip quantum computing. We focus on how to realize dissipation-less electrical transport and manipulation of spin and spin transport within widely available semiconductors, such as Si, Ge, and III-V compounds. Our work will extend over two directions as outlined below.

1.1 Synthesis and strain engineering of interfacial topological insulators. It has been theoretically predicted that appropriately engineered interfaces in epitaxial (111) oriented GaAs/Ge/GaAs structures may be able to drive Ge into a topologically insulating phase via the use of moderate strain (1-3%) and high intrinsic electric field (~10 MV/cm).[2] Motivated by these theoretical findings, we will grow and attempt to realize high electric field and moderate strain in GaAs/Ge/GaAs NM heterostructures that we will epitaxially grow using metalorganic vapor-phase epitaxy (MOVPE). Strain will be introduced by assembling the heterostructure NMs to polydimethylsiloxane (PDMS) spherical caps, as shown in Fig. 1. We will address the main synthesis, processing, and characterization challenges that relate to demonstrating interfacial topological states in GaAs/Ge/GaAs through these specific tasks:

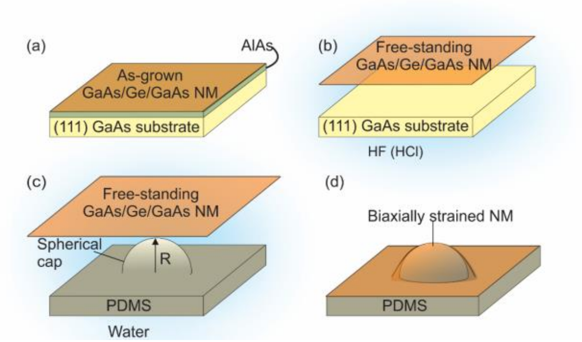

Figure 1. Synthesis of strain-engineered GaAs/Ge/GaAs via release and transfer of epitaxially grown NMs on PDMS substrates.

(i) realization of smooth and disorder-free Ge/GaAs and GaAs/Ge interfaces via epitaxial growth; (ii) isolation of the trilayer NM and its assembly to a textured compliant substrate;(iii) realization and characterization of static and dynamically tunable strain fields in the NM;(iv) characterization of topological edge states via gated magneto-transport measurements.

1.2 Controlled synthesis of screw dislocations in NMs. This work will explore controlled synthesis of screw dislocations (SDs) in semiconductor NMs. The thrust is motivated by recently reported findings that a SD in a crystalline semiconductor creates a unique form of 1D spin orbit coupling (SOC) along the dislocation core.[3] We will develop an approach to controlled synthesis of SDs that relies on overlaying a NM on either a bulk substrate or a NM of the same material and crystal orientation. We anticipate that the placement of the NM on a surface as shown in Fig. 2(a) will lead to the interfacial array shown in Fig. 2(b). We expect that annealing will foster propagation of SDs into the overlying NM, leading to the desired array on a suitable substrate to process spintronic devices.[3] We will characterize SOC in the fabricated materials by temperature-dependent measurements of magnetic susceptibility and by probing changes in the circularly polarized absorption in magnetic fields. We will correlate these results to high resolution transmission electron microscopy of the NMs that will provide insight on the crystalline structure of the material.

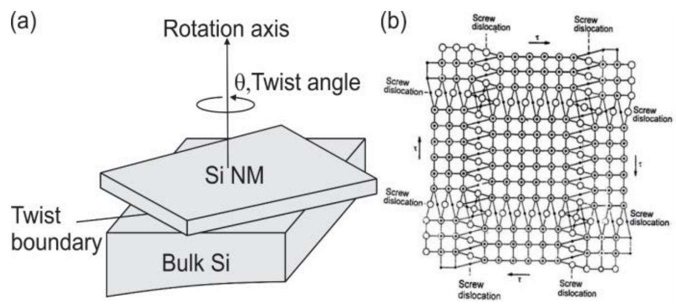

Figure 2. Si NM bonded to a bulk Si substrate with identical crystalline orientation (a) and expected interfacial structure at the atomic level (b).

Our effort will comprise the following tasks: *(i) high-yield synthesis of NM-substrate or NM-NM pairs with a controlled twist angle;(ii) thermal treatment of NM-substrate or NM-NM pairs; (iii) characterization of the structure and the magnetic properties of the NM.*

2. Synthesis and strain-engineering of GeSn NMs.

Using the NM platform, we will address the synthesis of GeSn with high Sn concentrations using the same approach that has allowed us to increase the amount of Ge in Si and the amount of Si in Ge for respectively Si-rich and Ge-rich SiGe alloy films. GeSn alloys hold great promise for the development of group-IV solid-state light emitters.[4]

Our approach leverages epitaxy on elastically relaxed (i.e., at natural lattice constants) GeSn NMs.[5] We will initially grow a GeSn thin film of the desired composition on a suitable sacrificial layer/substrate combination, with sufficiently small thickness to preserve pseudo-morphic growth.[5] The sacrificial layer will be then dissolved with a selective wet etch to release the GeSn NM. In the process, any strain that may have been present in the GeSn lattice is fully relaxed without the formation of any extended defect. Examples of sacrificial layers/substrate combinations that we will use in this work are AlAs/bulk GaAs and $In_{0.52}Al_{0.48}As$/bulk InP that allow incorporating up to 16% and 30 % Sn in a ~20 nm-thick pseudo-morphic GeSn NM, respectively.

Finally, we will bond the released NMs to a new carrier. We will utilize GeSn NMs bonded to rigid and planar hosts to template growth of thicker GeSn device layers.[4] NMs transferred to flexible polymeric films and mounted in a gas pressure cell[6], where strain and composition are fully decoupled from each other, will be used to explore the optoelectronic properties of GeSn. Major tasks within this effort will be: *(i) growth and isolation of GeSn NMs; (ii) subsequent growth of GeSn on relaxed GeSn NM substrates;(iii) characterization of the effect of decoupling composition and strain on the optoelectronic properties of GeSn NMs; (iv) determination of trade-off conditions between stretchability and thickness for GeSn NMs of various thicknesses and compositions.*

3. Graphene-based combinations.

We believe that the potential of combining graphene with other materials, particularly but not exclusively semiconductors has just begun to be explored. We will investigate new paradigms for synthesis of composites involving graphene as one layer to establish additional/enhanced electronic, thermal, and mechanical properties. Our effort will encompass the following tasks: *(i)Synthesis and characterization of graphene-Ge interfaces in 2D and 3D via direct growth and graphene release and transfer.* The objective is to generate understanding and predictive control of electrical transport in graphene/Ge by tailoring the chemistry and the geometry of the interface. We will compare process-structure-properties relationships of monolayer graphene grown on or transferred to a Ge NM[7-9] to determine the effect of the interface on electrical transport in the combination. This work expands on our highly interesting but controversial earlier work.[7] For this purpose we will use conventional structural characterization techniques in combination with gated magneto-transport measurements and multi-carrier analysis (e.g., maximum entropy spectrum analysis).[10] Additional studies will focus on planar Ge/graphene/Ge NMs and a variety of graphene/Ge interfaces in 3D geometries, such as rolled-up graphene/Ge NMs or graphene/Ge inverted funnels.

(ii) Synthesis and characterization of graphene-based interfaces for thermal transport. In this effort, we will fabricate composites in which one layer is graphene in order to investigate thermal transport through graphene/X interfaces. These measurements are relevant for thermal management in future devices that involve the use of graphene. We will focus on two promising systems for high-speed electronics, namely graphene/Ge and graphene/hBN.[7] The thermal measurements will be performed using a differential 3-omega technique on a measurement system that is highly sensitive to the thermal resistance of even a single-layer interface.[12]

Summary

The unifying theme in all the efforts described above is the synthesis and use of thin crystalline sheets (nanomembranes) to create new function, via the manipulation of strain, interfaces, and orientation, or the application of external stimuli (e.g., electric/magnetic fields, light, or heat).

References

1. Rogers, J. A.; Lagally, M. G.; Nuzzo, R. G., Synthesis, assembly and applications of semiconductor nanomembranes. *Nature* **2011,** *477* (7362), 45-53.
2. Zhang, D.; Lou, W. K.; Miao, M. S.; Zhang, S. C.; Chang, K., Interface-Induced Topological Insulator Transition in GaAs/Ge/GaAs Quantum Wells. *Phys Rev Lett* **2013,** *111* (15).
3. Hu, L.; Huang, H. Q.; Wang, Z. F.; Jiang, W.; Ni, X. J.; Zhou, Y. N.; Zielasek, V.; Lagally, M. G.; Huang, B.; Liu, F., Ubiquitous Spin-Orbit Coupling in a Screw Dislocation with High Spin Coherency. *Phys Rev Lett* **2018,** *121* (6).
4. Han, G.; Liu, M.; Zhang, Q.; Liu, Y.; Yan, J.; Cheng, B.; Hao, Y., Germanium-Tin Alloys: Applications in Microelectronics and Photonics. *J Nanoelectron Optoe* **2015,** *10* (1), 88-92.
5. Paskiewicz, D. M.; Tanto, B.; Savage, D. E.; Lagally, M. G., Defect-Free Single-Crystal SiGe: A New Material from Nanomembrane Strain Engineering. *ACS Nano* **2011,** *5* (7), 5814-5822.
6. Boztug, C.; Sanchez-Perez, J. R.; Sudradjat, F. F.; Jacobson, R. B.; Paskiewicz, D. M.; Lagally, M. G.; Paiella, R., Tensilely Strained Germanium Nanomembranes as Infrared Optical Gain Media. *Small* **2013,** *9* (4), 622-630.
7. Cavallo, F.; Delgado, R. R.; Kelly, M. M.; Perez, J. R. S.; Schroeder, D. P.; Xing, H. G.; Eriksson, M. A.; Lagally, M. G., Exceptional Charge Transport Properties of Graphene on Germanium. *ACS Nano* **2014,** *8* (10), 10237-10245.
8. Kazemi, A.; Vaziri, S.; Morales, J. D. A.; Fregonese, S.; Cavallo, F.; Zamiri, M.; Dawson, N.; Artyushkova, K.; Jiang, Y. B.; Brueck, S. J. R.; Krishna, S., Vertical Charge Transfer and Lateral Transport in Graphene/Germanium Heterostructures. *ACS Appl Mater Inter* **2017,** *9* (18), 15830-15840.
9. Delgado, R. R.; Jacobberger, R. M.; Roy, S. S.; Mangu, V. S.; Arnold, M. S.; Cavallo, F.; Lagally, M. G., Passivation of Germanium by Graphene. *ACS Appl Mater Inter* **2017,** *9* (20), 17630-17637.
10. Antoszewski, J.; Seymour, D. J.; Faraone, L.; Meyer, J. R.; Hoffman, C. A., Magnetotransport Characterization Using Quantitative Mobility-Spectrum Analysis. *J Electron Mater* **1995,** *24* (9), 1255-1262.
11. Navarro, M. X.; Delgado, R. R.; Lagally, M. G.; Kulcinski, G. L.; Santarius, J. F., Implantation of 30 keV Helium into Graphene-Coated Tungsten. *Fusion Sci Technol* **2017,** *72* (4), 713-718.
12. Schroeder, D. P.; Aksamija, Z.; Rath, A.; Voyles, P. M.; Lagally, M. G.; Eriksson, M. A., Thermal Resistance of Transferred-Silicon-Nanomembrane Interfaces. *Phys Rev Lett* **2015,** *115* (25).

Publications

1. "Dressed photon-orbital states in a quantum dot: Intervalley spin resonance", P. Scarlino, E. Kawakami, T. Jullien, D.R. Ward, D.E. Savage, M.G. Lagally, Mark Friesen, S.N. Coppersmith, M.A. Eriksson, and L.M.K. Vandersypen, Physical Review B 95, 165429 (2017). DOI: 10.1103/PhysRevB.95.165429.

2. "Passivation of germanium by graphene", R. Rojas Delgado, R.M. Jacobberger, S.S. Roy, V.S. Mangu, M.S. Arnold, F. Cavallo, and M.G. Lagally, ACS Applied Materials and Interfaces 9, 17629–17636 (2017) DOI: 10.1021/ACSami.7b03889.

3. "Extending the coherence of a quantum dot hybrid qubit", B. Thorgrimsson, D. Kim, Y.-C.Yang, L.W. Smith, C.B. Simmons, D.R. Ward, R.H. Foote, J. Corrigan, D.E. Savage, M.G. Lagally, M. Friesen, S.N. Coppersmith, and M.A. Eriksson, npj Quantum Information 3, Article number: 32 (2017); doi:10.1038/s41534-017-0034-2.

4. "Effects of charge noise on a pulse-gated singlet-triplet S – T_ qubit", Zhenyi Qi, X. Wu, D. R. Ward, J. R. Prance, Dohun Kim, John King Gamble, R. T. Mohr, Zhan Shi, D. E. Savage, M. G. Lagally, M. A. Eriksson, Mark Friesen, S. N. Coppersmith, and M. G. Vavilov, Phys. Rev. B96, 115305 (2017) DOI: 10.1103/PhysRevB.96.115305.

5. "Implantation of 30 keV Helium into Graphene-Coated Tungsten", M.X. Navarro, R.R. Delgado, M.G. Lagally, G.L. Kulcinski, and J.F. Santarius, Fusion Science and Technology 7, (2017). DOI: https://doi.org/10.1080/15361055.2017.1350481.

6. "Distinct nucleation and growth kinetics of amorphous $SrTiO_3$ on (001) $SrTiO_3$ and SiO_2/Si: A step towards new architectures", Yajin Chen, M. Humed Yusuf, Yingxin Guan, RB Jacobson, M.G. Lagally, S.E. Babcock, T.F. Kuech, and P.G. Evans, ACS Applied Mats. and Interfaces 9, 41034 (2017) DOI: 10.1021/ACSami.7b12978.

7. "Silicon Nanomembranes Incorporating Strain and Mixed Crystal Orientations", S.A. Scott, D.M. Paskiewicz, Chr. Deneke, Hyuk-Ju Ryu, D.E. Savage, M.A. Eriksson, and M.G. Lagally, ACS Applied Mats and Interfaces, 9, 42373-42382, (2017) DOI: 10.1021/ACSami.7b1429.

8. "Observation of large multiple scattering effects in ultrafast electron diffraction on single crystal silicon", I. Gonzalez Vallejo, G. Gall´e, B. Arnaud, S. A. Scott, M. G. Lagally, D. Boschetto, P.-E. Coulon, G. Rizza, F. Houdellier, D. Le Bolloc'h, and J. Faure, Phys. Rev. B97, 054302, (2018) DOI: 10.1103/PhysRevB.97.054302.

9. "Charge Transport in H-Terminated Si(001) Nanomembranes", W. Peng, M. Zamiri, S.A. Scott, F. Cavallo, J. Endres, I. Knezevic, M. A. Eriksson, and M. G. Lagally, Phys. Rev. Applied 9, 024037 (2018) DOI: 10.1103/PhysRevApplied.9.024037.

10. “A programmable two-qubit quantum processor in silicon”, T.F. Watson, S.G.J. Philips, E. Kawakami, D.R. Ward, P. Scarlino, M. Veldhorst, D.E. Savage, M.G. Lagally, Mark Friesen, S.N. Coppersmith, M.A. Eriksson, and L.M.K. Vandersypen, Nature 555, 633-637 (2018) doi:10.1038/nature25766.

11. “Strain Engineering and Mechanical Assembly of Silicon/Germanium Nanomembranes”, Qinglei Guo, Zengfeng Di, M.G. Lagally, and Yongfeng Mei, Materials Science and Engineering Reports R 128, 1-31 (2018) doi.org/10.1016/j.mser.2018.02.002.

12. "Valley dependent anisotropic spin splitting in silicon quantum dots" R. Ferdous, E. Kawakami, P.Scarlino, M. Nowak, D. Ward, D.E. Savage, M.G. Lagally, S. Coppersmith, Mark Friesen, M.A. Eriksson, L.Vandersypen, and R. Rahman, npj Quant. Inf. 4, 26 (2018); doi: https://doi.org/10.1038/s41534-018-0075-1.

13. “Optical properties of tensilely strained Ge nanomembranes”, R. Paiella and M.G. Lagally, Nanomaterials 8, 407 (2018) 407; doi:10.3390/nano8060407 (review).

14. “The critical role of substrate disorder in valley splitting in Si quantum wells”, S.F. Neyens, R.H. Foote, B. Thorgrimsson, T. J. Knapp, T. McJunkin, L.M.K. Vandersypen, P. Amin, N.K. Thomas, J.S. Clarke, D.E. Savage, M. G. Lagally, Mark Friesen, S.N. Coppersmith, and M.A. Eriksson, Appl. Phys. Letters 112, 243107 (2018); doi: 10.1063/1.5033447.

15. “Ubiquitous Ideal Spin-Orbit Coupling in Screw Dislocation of Semiconductors”, Lin Hu, Huaqing Huang, Zhengfei Wang, W. Jiang, Xiaojuan Ni, Y. Zhou, V. Zielasek, M.G. Lagally, Bing Huang, and Feng Liu, Phys. Rev. Letters 121, 066401 (2018) DOI: 10.1103/PhysRevLett.121.066401.

16. “Signatures of atomic-scale structure in the energy dispersion and coherence of a Si quantum-dot qubit”, J. C. Abadillo-Uriel, Brandur Thorgrimsson, Dohun Kim, L. W. Smith, C. B. Simmons, Daniel R. Ward, Ryan H. Foote, J. Corrigan, D. E. Savage, M. G. Lagally, M. J. Calderón, S. N. Coppersmith, M. A. Eriksson, Mark Friesen, Phys. Rev. B98 online 15 Oct (2018) DOI: 10.1103/PhysRevB.98.165438.

17. “Ultrawide strain-tuning of light emission from InGaAs nanomembranes”, X.W. Wang, X. R. Cui, A. Bhat, D. E. Savage, J. L. Reno, M. G. Lagally, and R. Paiella, Appl. Phys. Letters 113, 201105 (2018) doi: 10.1063/1.5055869.

18. “Wafer-scale alignment of semiconducting graphene nanoribbons on vicinal Ge(001) via chemical vapor deposition”, R. M. Jacobberger, E. Murray, M. Fortin-Deschenes, F. Göeltl, P. L. Levesque, D.E. Savage, C. Smoot, M.G. Lagally, R. Martel, O. Moutanabbir, M. Mavrikakis, and M.S. Arnold, Nanoscale 11, 4864 (2019); DOI: 10.1039/c9nr00713j.

19. “Interfacial thermal resistance in InAlAs/InGaAs superlattices”, G. R. Jaffe, S. Mei, C. Boyle, J. D. Kirch, D. E. Savage, D. Botez, L. J. Mawst, I. Knezevic, M. G. Lagally, and M.

A. Eriksson, ACS Applied Materials and Interfaces 11, 11970-11975 (2019); DOI: 10.1021/ACSami.8b17268.

20. “Benchmarking Gate Fidelities in a Si/SiGe Two-Qubit Device”, X. Xue, T.F. Watson, J. Helsen, D.R. Ward, D.E. Savage, M.G. Lagally, S.N. Coppersmith, M.A. Eriksson, S. Wehner, and L.M.K. Vandersypen, Physical Review X9, 021011 (2019); DOI: 10.1 103/PhysRevX.9.021011

21. “Passivation of Germanium Surfaces by Graphene: Growth Parameters and Surface Orientation”, R.M. Jacobberger, M.J. Dodd, M. Zamiri, A.J. Way, M.S. Arnold, and M.G. Lagally, ACS Applied Nanomaterials, in press.

22. “Outer Divertor Damage Characterization from Deuterium Plasma Bombardment in Graphene-Coated Tungsten in the C-2W Device”, M.X. Navarro, M. Zamiri, M.E. Griswold, G.L. Kulcinski, M.G. Lagally, and T. Tajima, Fusion Science and Technology, in press.

23. “Growth of High-Ge-Composition Ge/Six Ge1-x/Ge Trilayer Nanomembranes using Metal-Organic Vapor Phase Epitaxy”, O. Elleuch, A. Bhat, X.R. Cui, Y.X. Guan, K. Lekhal, S.A. Scott, M.G. Lagally, and T.F. Kuech, in preparation.

24. “High-Quality Graphene Membranes as a Coating for Polycrystalline Tungsten in Low-Energy Helium Plasma Exposures in the PISCES-A Facility”, M.X. Navarro, M. Zamiri, G.L. Kulcinski, M.G. Lagally, J. Santarius, O. Schmitz, R. Doerner, in preparation.

25. “High-Ge-content SiGe alloy single crystals using the nanomembrane platform”, A. Bhat, X Cui, Y.X. Guan, S.A. Scott, O. Elleuch, T.F. Kuech, and M.G. Lagally, in preparation.

Formation of Dirac and Topological States on Semiconductor Surface and Strain Engineering

Feng Liu
University of Utah

Program Scope

This project encompasses a comprehensive study of physical mechanisms that lead to formation of exotic quantum electronic states on semiconductor surfaces and explores a novel approach of strain engineering of such states. It covers four correlated research topics: (1) Mechanistic study of epitaxial growth of an overlayer of Dirac and topological states on semiconductor surfaces, which is atomically bonded but electronic isolated from the underlying substrates. (2) Self-assembled growth of topological states arising from non-conventional lattice symmetry in semiconductor surfaces. (3) Strain engineering of topological surface/edge states and topological nanomechanical architecture. (4) Nanostructured topological materials. The common theme of the proposed research is to understand a new class of "surface-based" 2D Dirac and topological materials chemically supported (i.e., non Van der Waals type) on a substrate. The theoretical studies will be done in collaboration with experiments including Prof. Lagally funded by the DOE-BES "Materials Synthesis and Processing" program.

We will employ a multiscale approach, combining several state-of-the-art theoretical and computational techniques, ranging from first-principles density-functional-theory (DFT) electronic structure calculations to semi-empirical tight-binding (TB) model Hamiltonian analyses and calculations and to classical molecular dynamics (MD) simulations. Specifically, surface equilibrium structure and associated energetics will be calculated by DFT and MD methods. Electronic band structure will be studied using both DFT and TB methods with the TB parameters fit to the DFT band structures in supercells of slab geometry to represent a surface. Band topology will be revealed by analyzing the bulk (thin film) Bloch wavefunctions and the topological surface (edge) states using DFT and TB bands and iterative Green's function and Wannier function method. In addition, DFT as well as classical MD simulations will be carried out to directly simulate topological nanomechanical architectures resulted from the strain induced bending of thin films to study strain engineered topological states and spin manipulation.

Our studies will significantly improve our fundamental understanding of physical origins of surface-based Dirac and topological states in solid material systems, in terms of lattice geometry, spin-orbit coupling (SOC), orbital composition and surface/interface interactions. It will open up a new route towards realizing topological quantum phases in a new class of surface-based 2D materials. It will foster a new field of research by taking the effect of stress/strain to new territories on topological order of materials, beyond strain engineering of self-assembled nanostructures and of electronic properties that we have studied in the past decade within the

DOE-BES program. We believe many of our theoretical findings will provide useful guidance for future experimental efforts in growing surface-based 2D materials as we propose, realizing novel topological phases, strain engineering of topological states and spin texture, and nanostructured topological materials. These studies have also technological impact on advancing electronic and optoelectronic materials for energy applications, to fulfill the mission of Department of Energy.

Recent Progress

During the last two years, we have published 43 journal papers fully or partially supported by this DOE grant, including 8 Physical Review Letters (**3 as Editor's Suggestion and 1 as Featured in Physics**), 3 Nano Letters, 1 Nature Communications, 1 ACS Nano; plus one invited review and one invited book chapter. Two postdoctoral research associates and three graduate students have been fully or partially supported by this DOE project. The PI gave 12 invited talks at national/international conferences, and 18 departmental colloquium/seminar presentations. Below is a brief summary of four topics of research achievements pertaining to this project.

(1) Quantum Spin Hall Effect and Spin Bott Index in Quasicrystal Lattice:[1,2] Despite the rapid progress in the field of the quantum spin Hall (QSH) effect, most of the QSH systems studied up to now are based on crystalline materials. Recently, we propose that the QSH effect can also be realized in quasicrystal lattices (QLs) (See Fig. 1). We show that the electronic topology of aperiodic and amorphous insulators can be characterized by a spin Bott index B_s. The nontrivial QSH state in a QL is identified by a nonzero spin Bott index $B_s = 1$, associated with robust edge states and quantized conductance. We further map out a topological phase diagram in which the QSH state lies in between a normal insulator and a weak metal phase due to the unique wave functions of QLs. Our findings not only provide a better understanding of electronic properties of quasicrystals but also extend the search of the QSH phase to aperiodic and amorphous materials that are experimentally feasible.

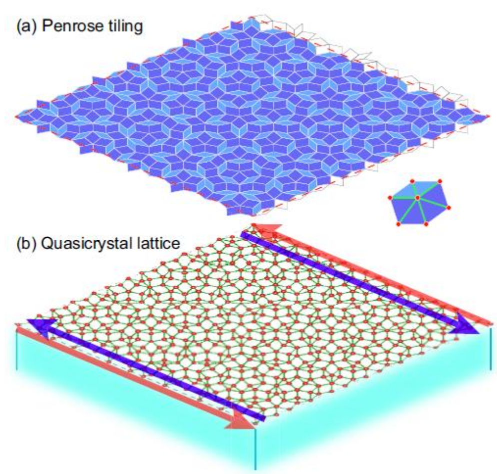

Fig. 1. (a) Penrose tiling of 521 vertices. The red dashed line marks a unit cell under periodic approximation. The inset shows the atomic orbitals on the vertices of rhombuses indicating nearest-neighbor hopping. (b) Illustration of a QSH state in a surface-based 2D QL. The red/blue arrows represent helical edge states with opposite spin polarizations.

Note: This work[1] was selected by PRL editor as "Editor's Suggestion" and published jointly with a PRB "Editor's Suggestion"[2] detailing the theory of Spin Bott index for defining the topology of aperiodic system. As a pleasant surprise, the PRB was converted from the originally submitted Supplementary Information for PRL upon referee and editor's kind recommendation.

(2) Ubiquitous Spin-orbit Coupling in a Screw Dislocation with High Spin Coherency:[3] We theoretically demonstrate that screw dislocation (SD), a 1D topological defect widely present in semiconductors, exhibits ubiquitously a new form of spin-orbit coupling (SOC) effect (see Fig. 2). Differing from the widely known conventional 2D Rashba-Dresselhaus (RD) SOC effect that typically exists at surfaces/interfaces, the deep-level nature of SD-SOC states in semiconductors readily makes it an ideal SOC. Remarkably, the spin texture of 1D SD-SOC, pertaining to the inherent symmetry of SD, exhibits a significantly higher degree of spin coherency than the 2D RD-SOC. Moreover, the 1D SD-SOC can be tuned by ionicity in compound semiconductors to ideally suppress spin relaxation, as demonstrated by comparative first-principles calculations of SDs in Si/Ge, GaAs, and SiC. Our findings therefore open a new door to manipulating spin transport in semiconductors by taking advantage of an otherwise detrimental topological defect.

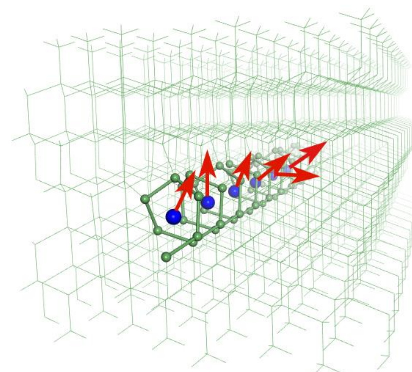

Fig. 2. A schematic diagram of screw dislocation (green balls) in crystal with rotating spin texture (red arrows) due to a ubiquitous SOC effect arising from breaking of local inversion symmetry.

Note: This work was selected by PRL editor as "Editor's Suggestion" and "Featured in Physics" with a nice Viewpoint written by Olena Gomonay in *Physics*, **11**, 78 (2018).

(3) Strain engineering of edge spin currents of quantum spin Hall insulators:[4,5] QSH system can exhibit exotic spin transport phenomena, mediated by its topological edge states. Recently we have demonstrated a new concept of bending strain engineering as an effective means to tune the spin transport properties of a QSH system.[4,5] We show that bending strain can be used to control the spin orientation of counter-propagating edge states of a QSH system to generate a non-zero spin current. This physics mechanism can be applied to effectively tune the spin current and pure spin current decoupled from charge current in a QSH ionsulator by control of its bending curvature. Furthermore, the curved QSH insulator can be achieved by the concept of topological nanomechanical architecture in a controllable way, as demonstrated by the material example of Bi/Cl/Si(111) nanofilm[4] and As-graphane[5] (Fig. 3). This concept of bending strain engineering of spins via topological nanomechanical

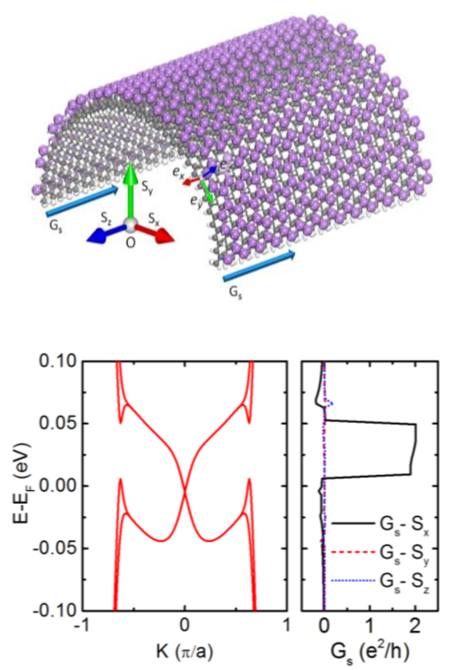

Fig. 3. Upper: A self-bent As-graphane, a curved 2D topological insulator. Lower left: Band structure of the bent As-graphane; lower right: Edge spin conductance.

architecture affords a promising route towards the realization of topological nano mechanospintronics.

Note: This work was highlighted in the DOE SC website (see screen shot on the right), as noted by the DOE Web editor: "The SC tweet about the highlight (https://science.energy.gov/bes/highlights/2017/bes-2017-12-f/) on bending materials was the **top tweet for the last week of December.**"

Future Plans

We plan to expand our current studies in the following areas:

(a) Develop new models for studying quantum materials
(b) Search for new inorganic and organic topological and quantum materials
(c) Continue exploring a new research direction in "topological phases in disordered systems, including quasi-crystalline materials" as recently initiated
(d) Explore different epitaxial growth routes towards formation of topological quantum phases on semiconductor surfaces, especially including studies of defects in topological phases
(e) Initiate a new research direction in flat-band materials
(f) Continue the efforts of experimental collaborations

References

1. "Quantum Spin Hall Effect and Spin Bott Index in a Quasicrystal Lattice", H. Huang and Feng Liu, *Phys. Rev. Lett.*, **121**, 126401 (2018). **Editor's Suggestion.**
2. "Theory of spin Bott index for quantum spin Hall states in nonperiodic systems", H. Huang and Feng Liu, *Phys. Rev. B.*, **98**, 12513, (2018). **Editor's Suggestion**.
3. "Ubiquitous Spin-Orbit Coupling in a Screw Dislocation with High Spin Coherency", L. Hu, H. Huang, Z. Wang, W. Jiang, X. Ni, Y. Zhou, V. Zielasek, M. G. Lagally, B. Huang and Feng Liu, *Phys. Rev. Lett*, **121**, 066401 (2018). **Editor's Suggestion, Featured in Physics.**
4. "Bending strain engineering in quantum spin Hall system for controlling spin currents", B. Huang, K-H Jin, B. Cui, F. Zhai, J. Mei and Feng Liu. *Nature Commun.*, **8**, 15850 (2017).
5. "Quantum Spin Hall Effect and Tunable Spin Transport in As-Graphane", L. Zhang, F. Zhai, K-H Jin, B. Cui, B. Huang, Z. Zhang, J. Lu and Feng Liu. *Nano Lett.*, **17**, 4359 (2017).

Publications

1. “Quantum Spin Hall Effect and Spin Bott Index in a Quasicrystal Lattice”, H. Huang and Feng Liu, *Phys. Rev. Lett*., **121**, 126401 (2018). **Editor's Suggestion.**
2. “Theory of spin Bott index for quantum spin Hall states in nonperiodic systems”, H. Huang and Feng Liu, *Phys. Rev. B*., **98**, 12513, (2018). **Editor's Suggestion**.
3. “Ubiquitous Spin-Orbit Coupling in a Screw Dislocation with High Spin Coherency”, L. Hu, H. Huang, Z. Wang, W. Jiang, X. Ni, Y. Zhou, V. Zielasek, M. G. Lagally, B. Huang and Feng Liu, *Phys. Rev. Lett*, **121**, 066401 (2018). **Editor's Suggestion, Featured in Physics.**
4. “Bending strain engineering in quantum spin hall system for controlling spin currents”, B. Huang, K-H Jin, B. Cui, F. Zhai, J. Mei and Feng Liu. *Nature Commun*., **8**, 15850 (2017).
5. “Quantum Spin Hall Effect and Tunable Spin Transport in As-Graphane", L. Zhang, F. Zhai, K-H Jin, B. Cui, B. Huang, Z. Zhang, J. Lu and Feng Liu. *Nano Lett*., **17**, 4359 (2017).
6. “Intrinsic Quantum Anomalous Hall Effect with In-Plane Magnetization: Searching Rule and Material Prediction”, Z. Liu, G. Zhao, B. Liu, Z. F. Wang, J. Yang, and Feng Liu, *Phys. Rev. Lett*. **121**, 246401 (2018). **Editor's Suggestion.**
7. “Significantly Enhanced Magnetoresistance in Monolayer WTe_2 via Heterojunction Engineering: A First-principles Study”, L. Hu, L. Kang, J. Yang, B. Huang and Feng Liu, *Nanoscale* **10**, 22231 (2018). **Nanoscale HOT Article Collection and Editor’s Choice: van der Waals heterostructures.**
8. “Pseudo Dirac nodal sphere semimetal”, J. Wang, Y. Liu, K-H Jin, X. Sui, L. Zhang, W. Duan, Feng Liu and B. Huang, *Phys. Rev. B*., **98**, 201112(R) (2018).
9. “Incident wavelength and polarization dependence of spectral shifts in β-Ga2O3 UV photoluminescence", Y. Wang, P. T. Dickens, J. B. Varley, X. Ni, E. Lotubai, S. Sprawls, F. Liu, V. Lordi, S. Krishnamoorthy, S. Blair, K. G. Lynn, M. Scarpulla and B. Sensale-Rodriguez, *Sci. Rep*. **8**, 18075 (2018).
10. “Cyano-Based Materials with Giant Optical Anisotropy and Second Harmonic-Generation Effect”, L. Kang, F. Liang, Z. Lin, F. Liu and B. Huang, *Inorg. Chem*. **57**, 15001 (2018).
11. “Black-hole horizon in the Dirac semimetal $Zn_2In_2S_5$”, H. Huang, K-H Jin and Feng Liu, *Phys. Rev. B*., **98**, 121110(R) (2018).
12. “Band gap reduction in van der Waals layered 2D materials via a de-charge transfer mechanism”, C. Zhang, H. Huang, X. Ni, Y. Zhou, L. Kang, W. Jiang, H. Chen, J. Zhang and Feng Liu. *Nanoscale*, **10**, 16759 (2018).
13. “Li doped kagome spin liquid compounds”, W. Jiang, H. Huang, J-W Mei and Feng Liu, *Phys. Chem. Chem. Phys*., **20**, 21693 (2018).
14. “Two Novel Deep-Ultraviolet Nonlinear Optical Crystals with Shorter Phase-Matching Second Harmonic Generation than $KBe_2BO_3F_2$: A First-Principles Prediction”, L. Kang, F. Liang, P. Gong, Z. Lin, Feng Liu and B. Huang, *Phys. Status Solodi RRL*, 1800276 (2018).
15. “Tunable topological semimetal states with ultraflat nodal rings in strained YN”, H. Huang, W. Jiang, K-H, Jin and Feng liu, *Phys. Rev. B* **98**, 045131 (2018).
16. “Intrinsic quantum anomalous hall effect in a two dimensional anilato-based lattice”, X. Ni, W. Jiang, H. Huang, K-H Jin and Feng Liu, *Nanoscale* **10**, 11901 (2018).
17. “Photoinduced nonequilibrium topological states in strained black phosphorus”, H. Liu. J. Sun, C. Cheng, Feng Liu and S. Meng, *Phys. Rev. Lett*. **120**, 237403 (2018).

18. “Prediction of two-dimensional nodal-line semimetals in a carbon nitride covalent network”, H. Chen, S. Zhang, W, Jiang, C. Zhang, H. Guo, Z. Liu, Z. Wang, Feng Liu and X. Niu, *J. Mater. Chem. A*, **6**, 11252 (2018).
19. “Pressure-induced organic topological nodal-line semimetal in the three-dimensional molecular crystal Pd(dddt)2”, Z. Liu, H. Wang, Z. F. Wang, J. Yang and Feng Liu, *Phys. Rev. B*. **97**, 155137 (2018).
20. “Light-Induced Type-II Band Inversion and Quantum Anomalous Hall State in Monolayer FeSe”, Z. F. Wang, Z. Liu, J. Yang and Feng Liu, *Phys. Rev. Lett*. **120**, 156406 (2018).
21. “Alloy Engineering of Topological Semimetal Phase Transition in $MgTa_{2-x}Nb_xN_3$”, H. Huang, K-H Jin and Feng Liu, *Phys. Rev. Lett*. **120**, 136403 (2018).
22. “Formation of a large gap quantum spin Hall phase in a 2D trigonal lattice with three p-orbitals”, C. Li, K-H Jin, S. Zhang, F. Wang, Y. Jia and Feng Liu, *Nanoscale* **10**, 5496-5502 (2018).
23. “Topological Electride Y_2C”, H. Huang, K-H, Jin, S. Zhang and Feng Liu, *Nano Lett*. **18**, 1972 (2018).
24. “Topological states in a two-dimensional metal alloy in Si surface: BiAg/Si(111)-4×4 surface”, X. M. Zhang, B. Cui, M. Zhao and Feng Liu, *Phys. Rev. B*, **97**, 085422 (2018).
25. "Kane Fermion in a Two-Dimensional π Conjugated Bis(iminothiolato)nickel Monolayer”, A. Wang, X. Zhao, M. Zhao, X. Zhao, Y. Feng and Feng Liu, *J. Phys. Chem. Lett*. **9**, 614 (2018).
26. “Prediction of large gap flat Chern band in a two-dimensional metal-organic framework”, N. Su, W. Jiang, Z. F. Wang and Feng Liu, *Appl. Phys. Lett*., **112**, 033301 (2018).
27. “Monte Carlo simulations of electrical percolation in multicomponent thin films with nano fillers”, X. Ni, C. Hui, N. Su, W. Jiang and Feng Liu, *Nanotechnology* **29**, 075401 (2018).
28. “Oxidation-promoted Interfacial Synthesis of Redox-active Bis(diimino)nickel Nanosheet", E. J. H. Phua, K-H Wu, K. Wada, T. Kusamoto, H. Maeda, J. Cao, R. Sakamoto, S. Sasaki, J-W. Mei, W. Jiang, Feng Liu and H. Nishihara, *Chem. Lett*., **47**, 2 (2018).
29. “Prediction of Ideal Topological Semimetals with Triply Degenerate Points in the NaCu3Te2 Family”, J. Wang, X. Sui, W. Shi, J. Pan, S. Zhang, Feng Liu, S.-H. Wei, Q. Yan, and B. Huang, *Phys. Rev. Lett.* **119**, 256402 (2017).
30. “Electronic and spin dynamics in the insulating iron pnictide $NaFe_{0.5}Cu_{0.5}As$”, S. Zhang, Y. He, J.-W. Mei, Feng Liu, and Z. Liu, *Phy. Rev B* **96**, 245128 (2017).
31. “Nanostructured topological state in bismuth nanotube arrays: inverting bonding–antibonding levels of molecular orbitals”, K-H Jin, S-H Jhi and Feng Liu, *Nanoscale*, **9**, 16638 (2017).
32. “Bis(aminothiolato)nickel nanosheet as a redox switch for conductivity and an electrocatalyst for the hydrogen evolution reaction", X. Sun, K. Wu, R. Sakamoto, T. Kusamoto, H. Maeda, X. Ni, W. Jiang, Feng Liu, S. Sasaki, H. Masunage and H. Nishihara. *Chem. Sci*., **8**, 8078 (2017).
33. “Multivalency-Driven Formation of Te-Based Monolayer Materials: A Combined First-Principles and Experimental study”,Z. Zhu, X. Cai, S. Yi, J. Chen, Y. Dai C. Niu, Z. Guo, M. Xie, Feng Liu, J. Cho, Y. Jia and Z. Zhang. *Phys. Rev. Lett*. **119**, 106101 (2017).
34. “Theoretical Discovery of a Superconducting Two-Dimensional Metal−Organic Framework”, X. Zhang, Y. Zhou, B. Cui, M. Zhao and Feng Liu. *Nano Lett*. **17**, 6166 (2017).
35. “Topological nodal-line semimetal in nonsymmorphic Cmce-phase Ag_2S”, H. Huang, K-H Jin and Feng Liu. *Phys. Rev. B* **96**, 115106 (2017).
36. “Atomically Abrupt Topological p−n Junction”, S. Kim, K-H Jin, B. Kho, B. Park Feng Liu J. Kim, H. Yeom. *ACS Nano*, **11**, 9671 (2017).

37. "Creation of half-metallic f-orbital Dirac fermion with superlight elements in orbital-designed molecular lattice", B. Cui, B. Huang, C. Li, X. Zhang, K-H Jin, L. Zhang, W. Jiang, D. Liu, and Feng Liu. *Phys. Rev. B* **96**, 085134 (2017).
38. "Spin fluctuation induced linear magnetoresistance in ultrathin superconducting FeSe films", Q. Wang, W. Zhang, W. Chen, Y. Xing, Y. Sun, Z. Wang, J. Mei, Z. Wang, L. Wang, X. Ma, Feng Liu, Q. Xue and J. Wang. *2D Mater.* **4**, 034004 (2017).
39. "Tuning interfacial spin filters from metallic to resistive within a single organic semiconductor family", J. Wang, A. Deloach, W. Jiang, C. M. Papa, M. Myahkostupov, F. N. Castellano, Feng Liu and D. B. Dougherty. *Phys. Rev. B*, **95**, 241410(R) (2017).
40. "Gapped Spin-1/2 Spinon Excitations in a New Kagome Quantum Spin Liquid Compound Cu3 Zn(OH)6FBr", Z. Feng, Z. Li, X. Meng, W. Yi, Y. Wei, J. Zhang, Y. C. Wang, W. Jiang, Z. Liu, S. Li, Feng Liu, J. Luo, S. Li, G.Zheng, Z. Y. Meng J. W. Mei and Y. Shi. *Chin. Phys. Lett.*, **34**, 7, 077502 (2017).
41. "π conjugation in the epitaxial Si(111)- ($\sqrt{3}\times\sqrt{3}$) surface: Unconventional "bamboo hat" bonding geometry for Si", W. Jiang, Z. Liu, M. Zhou, X. Ni and Feng Liu. *Phys. Rev. B*, **95**, 241405(R) (2017).
42. "Tensile strained gray tin: Dirac semimetal for observing negative magnetoresistance with Shubnikov–de Haas oscillations", H. Huang and Feng Liu. *Phys. Rev. B*, **95**, 201101(R) (2017).
43. "Pulse laser induced graphite-to-diamond phase transition: the role of quantum electronic stress", Z. F. Wang and Feng Liu. *Sci. Chi. Phys*., **60**, 026811 (2017).
44. "Computational design of two-dimensional topological materials", Z. F. Wang, K-H Jin and Feng Liu. WIREs Comput Mol Sci 2017, e1304. doi: 10.1002/wcms.1304. (**invited review**).
45. "Organic Topological Insulators" W. Jiang and Feng Liu, in World Scientific Reference on Spin in Organics, Chap 6, pp. 201-224 (2018) (**invited book chapter**).

Understanding the synthesis and new quantum phenomena of magnetic topological materials enabled by SCAN-based DFT calculations.

Zhiqiang Mao
Department of Physics, Pennsylvania State University, University Park, PA 16802
Jianwei Sun and Jiang Wei
Department of Physics an Engineering Physics, Tulane University, New Orleans, LA 16802

Program Scope

The 2D Dirac cone state in graphene as well as the recently-discovered quantum spin Hall (QSH) insulator in FeSe [1] and WTe_2 [2-4] monolayers imply that the introduction of non-trivial band topology to other 2D material systems may be an effective route to generate new quantum states with functional properties. This proposed research aims to discover novel 2D materials with topological quantum states through material synthesis and characterization. The specific interest of the proposed efforts is focused on ternary transition metal chalcogenides (TTMCs), including WHM (W=Zr/Hf/rare earth, H=Si/Ge/Sn/Sb, M=O/S/Se/Te)[5], MBX3 (M = Ni/Pd/Zn/Cd, B = P/Si/Ge, X =S/Se/Te) [6] and BaMX3 (M=V/Nb/Ta, X=S/Se)[7]. All these materials have been predicted to show topological quantum states in bulk and/or 2D thin layers, thus providing wonderful opportunities to explore new topological states in low dimensions. In this project, the PIs aim to develop a comprehensive strategy to grow the single crystals of those predicted topological materials through the integration of thermodynamic stability prediction by computation and experimental synthesis efforts. In addition to bulk single-crystal growth and characterization, the PIs also also explore the possibility of direct thin-film growth of topological semimetals using the vapor transport deposition method.

Recent Progress

We made significant progresses in several areas. First, we demonstrated it is effective to use the thermodynamic stability prediction by the DFT calculations to guide material synthesis. For example, $MnBi_2Te_4$ has recently been reported to be an intrinsic antiferromagnetic topological insulator and its 2D thin layers can realize the quantum anomalous Hall insulator and axion insulator [8-11]. However, the synthesis of this material has been extremely challenging, since it is a metastable phase. The co-PI Sun group revealed its thermodynamic stability through total energy calculations, which provides an important clue to the successful synthesis by the Mao group. Second, we have successfully synthesized single crystals of several other quantum materials and discovered new quantum phenomena in them, including bulk half-integer quantum Hall effect in $BaMnSb_2$, a tunable Weyl semimetal state induced by Rashba spin-orbit coupling in YSn_2 [12], high mobility surface state in ZrSiSe [13], and coexistence of superconductivity and non-trivial band-topology in $CaSn_3$ [14]. In addition, we have successfully constructed the new vapor transport growth system, which incorporated the induction heater to the vapor transport tube system, with the capability of heating source materials to 2000^{o}C. Such high temperature can generate high vapor pressures from sources with high melting points and should significantly increase the reaction rate in forming crystalline films on the substrate wafer.

- *Ab initio thermodynamics of 2D magnetic materials: a case study on $MnBi_2Te_4$*

Computational materials synthesis based on *ab* initio thermodynamics is playing an increasingly important role in discovery of novel materials that host interesting phenomena. Two dimensional magnetic materials (2DMM) are of particular interests as a playground of new physics and potential applications for various industries. However, *ab* initio description of 2DMM thermodynamics faces great challenges, due to the coexistence of different kinds of chemical bonds ranging from the strong covalent to weak van der Waals interaction as well as the coupling between charge, lattice, and spin degrees of freedom. As an illustration of such challenges, we investigated the metastability of a layered magnetic material $MnBi_2Te_4$[8-11], which hosts intrinsic quantum anomalous Hall effect, but is extremely difficult to synthesize. Using a combined *ab* initio-based approach that considers charge, lattice, and spin degrees of freedom, we calculated the temperature dependent formation free energy of $MnBi_2Te_4$ based on the reaction: Bi_2Te_3+MnTe=$MnBi_2Te_4$. We used a rescaled Monte Carlo method to treat the magnetic contribution and a combination of harmonic approximation and quasi-harmonic Debye model (QHA-Debye) to treat the vibrational contribution, all based on total energy calculations using the state-of-the-art SCAN+rVV10 density functional. We found $MnBi_2Te_4$ to be stable at high temperature but become unstable at low temperature, consistent with experiments. Magnetic coupling, van der Waals interaction, and anharmonicity, which usually have negligible contributions to thermodynamic stability of conventional bulk materials, but are intrinsic to 2DMM, are found to play delicate but vital roles in stabilizing $MnBi_2Te_4$ which might be general for 2DMM. These findings not only have assisted the Mao group in successfully growing high-quality $MnBi_2Te_4$ single crystals, but also could pave a way for future high throughput discovery of novel 2DMM.

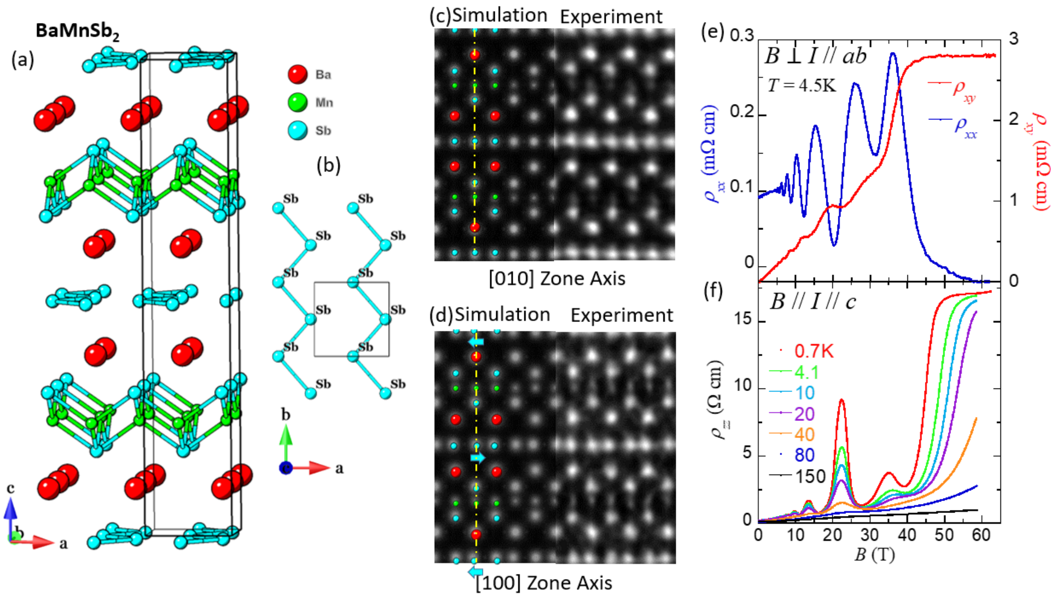

Figure 1: Bulk half integer quantum Hall effect observed in BaMnSb2: a) Crystal structure of $BaMnSb_2$. b) Top view of the Sb zig-zag chains which create quasi-2D Dirac fermions. (c) and (d) experimental and simulated STEM images along the [010] and [100] zone-axes, demonstrating the orthorhombic structure with the space group of I2mm. (e)longitudinal (ρ_{xx}) and Hall resistivity (ρ_{xy}); ρ_{xy} exhibit 3D half-integer quantum Hall effect. f) Out-of-plane resistivity (ρzz), the saturation of which below 20K demonstrates surface chiral metal (unpublished).

- *Bulk half-integer quantum Hall effect in a layered antiferromagnetic Dirac semimetal $BaMnSb_2$*

We have also expanded our efforts to explore some new layered topological materials relevant to our research goal. These efforts have led to discovery of half-integer quantum Hall effect (QHE) in bulk single crystals of a layered Dirac semimetal $BaMnSb_2$. QHE can give rise to plentiful exotic properties such as dissipationless edge transport and quasi-particles with fractional charges. Although the QHE is not generally expected for bulk materials due to the band dispersion along the magnetic field direction, bulk QHE has been observed in a few materials such as Cd_3As_2 [15], ZrTe5 [16]. We find a unique bulk half-integer QHE observed in $BaMnSb_2$. In the extreme quantum limit, its quantum Hall state is accompanied by two-dimensional chiral metal at the surface, which represents a novel quantum liquid, never observed in any other bulk single crystal materials. This finding establishes a promising experimental platform which not only provides access to 3D interacting topological states, but also offers opportunities to investigate the novel physics of 2D chiral metal. Mao and Sun have worked together on this project. The DFT calculations by Sun has enabled understanding of the crystal structure and electronic band structure of this material. We have prepared a manuscript for this work, which will be submitted in early July.

• *Unusual protection mechanism of the surface state in nodal-line semimetal ZrSiSe*
In topological semimetals, the bulk-edge correspondence principle results in a gapless edge mode when the symmetry group protecting the bulk bands' topology is unbroken on the surface. Such a topological surface state is considered as the fingerprint of the topological non-trivial bulk phase. Recently, a new type of surface state, the surface floating band, has been proposed in crystals with nonsymmorphic symmetry [17]. At the crystal surface where the nonsymmorphic symmetry is broken, the bulk bands' degeneracies are lifted, leaving an unusual surface band with trivial topology "floating" on top of the bulk. In the nano-flakes of nodal-line semimetal ZrSiSe, we have observed the surprising quantum oscillations arising from such a topological trivial surface band. Such a surface state remains robust with high mobility. This work has recently been submitted to Nature Nanotechnology.

•*Multiple topologically non-trivial bands in non-centrosymmetric YSn_2*
The square lattices formed by main-group elements such as Bi, Sb, Sn and Si in layered materials have attracted a lot of interest, since they can create rich topological phases. Recently, we have discovered the slightly distorted square lattice of Sn in a non-centrosymmetric YSn_2 generates multiple topologically non-trivial bands, one of which likely hosts nodal line and tunable Weyl semimetal state induced by the Rashba spin-orbit coupling and proper external magnetic field. The quasiparticles hosted by these bands are manifested by nearly zero mass and non-trivial Berry phases probed in quantum oscillations. The dHvA study also reveals YSn_2 has a complicated Fermi surface (FS), consisting of several 3D and one 2D pockets. Our first principle calculations show the point-like 3D pocket at Y point on the Brillouin zone boundary hosts the possible Weyl state. Our findings establish YSn_2 as a new interesting platform for observing novel topological phases and studying their underlying physics. This work has been published in PRB 98, 035117 (2018).

• *Thermodynamic stability prediction by the DFT calculations for the proposed materials*
The Sun group has been providing computational support for Mao and Wei to explain mechanisms behind materials properties and the synthesis and processing of the materials, and more importantly is to guide the experimental synthesis via (high-throughput) computations. Most of the target materials proposed in our proposal are indeed hypothetical compounds. The synthesis efforts may be much more efficient if we are able to predict the thermodynamic stability of the target materials by computation. The Sun group works closely with Mao and Wei groups and has

identified a group of material for synthesis among proposed materials. These efforts have recently led to a discovery of a new layered van der Waals material, which shows a magnetic order at 75K and be exfoliated to thin layers. This work is still on-going.

•*Enhanced chemical vapor deposition to grow thin films of complex topological materials*: *G*rowth of thin films of complex topological semimetals remain unexplored and is hindered by several obstacles related to the high melting points of precursors and complicated chemical reactions. We have explored the possibility of thin film growth with an enhanced chemical vapor deposition technique, in which induction heating is utilized to generate high vapor pressure of each precursor. We have constructed a new vapor transport growth system with an induction heater capable of reaching 2000^{o}C. Our preliminary growth efforts have successfully demonstrated growth of thin plates ofTa_2PdSe_6, a possible candidate of topological semimetal. Besides, simulation of the thin film growth dynamics has also been conducted to guide future growth efforts.

Future Plans

The Mao group will continue to synthesize and characterize those candidate materials predicted to be thermodynamic stable by Sun. In the current grant period, Sun has mostly focused on the WHM family. In the next grant period, Sun will complete thermodynamic stability evaluation for the other two materials systems, i.e. MBX_3 and AMX_3. In general, a more reliable prediction of the phase equilibrium temperature requires considerations of electron excitation, anharmonic treatment of phonon excitation, and more accurate methods for the treatment of magnon excitation. These issues will be addressed in the next grant period. For those materials synthesized successfully, the Mao group will perform various measurements to evaluate their topological fermion properties. The Wei group will explore their properties in 2D thin layers to discover new 2D topological quantum states. Moreover, Wei will also use the newly constructed CVT furnace to explore ZrSiS and ZrSiO thin film growth.

References

[1] Z. F. Wang et L., Nat. Mat. 15, 968 (2016).
[2] X. Qian, J. Liu, L. Fu, and J. Li, Quantum spin Hall effect in two-dimensional transition metal dichalcogenides, Science 346, 1344 (2014).
[3] S. Tang et al., , Nat Phys 13, 683 (2017).
[4] Z. Fei et al., Nat Phys 13, 677 (2017).
[5] Q. Xu et al., Phys. Rev. B 92, 205310 (2015).
[6] T. M. a. Y. M. Yusuke Sugita, arXiv:1704.00318 (2017).
[7] Q.-F. Liang et al., Phys. Rev. B 93, 085427 (2016).
[8] D. Zhang et al., ArXiv:1808.08014 (2018).
[9] J. Li et al., ArXiv:1809.07389 (2018).
[10] Y. Deng et al., arXiv:1904.11468 (2019).
[11] C. Liu et al., arXiv:1905.00715 (2019).
[12] Y.L. Zhu et al., Phys. Rev. B 98, 035117 (2018).
[13] Xue Liu et al., submitted to Nature Nanotechnology.
[14] Y.L. Zhu et al., Journal of Physics: Condensed Matter 31, 245703 (2019)
[15] C. Zhang et al., Nature. 565, 331–336 (2019).
[16] Tang et al., Nature. 569, 537 (2019).
[17] C. Zhang et al., Nature 565, 331 (2019)

Publications

[1] Multiple topologically nontrivial bands in noncentrosymmetric YSn_2,
Yanglin Zhu, Tiantian Zhang, Jin Hu, Jamin Kidd, David Graf, Xin Gui, Weiwei Xie, Mengze Zhu, Xianglin Ke, Huibo Cao, Zhong Fang, Hongming Weng, Zhiqiang Mao,
Physical Review B 98, 035117 (2018).

[2] Quantum oscillation evidence for a topological semimetal phase in ZrSnTe,
Jin Hu, Yanglin Zhu, Xin Gui, David Graf, Zhijie Tang, Weiwei Xie, Zhiqiang Mao,
Physical Review B 97, 155101 (2018).

[3] Emergence of intrinsic superconductivity below 1.17 K in the topologically non-trivial semimetal state of $CaSn_3$,
Yanglin Zhu, Jin Hu, F.N. Womack, David Graf, and P.W. Adams and Zhiqiang Mao,
Journal of Physics: Condensed Matter 31, 245703 (2019).

[4] Thermal Transport in Quasi-1D van der Waals Crystal $Ta_2Pd_3Se_8$ Nanowires: Size and Length Dependence,
Qian Zhang, Chenhan Liu, Xue Liu, Jinyu Liu, Zhiguang Cui, Yin Zhang, Lin Yang, Yang Zhao, Terry T Xu, Yunfei Chen, Jiang Wei, Zhiqiang Mao, Deyu Li,
ACS nano 12, 2634 (2018)

[5] Raman Spectroscopy, Photocatalytic Degradation and Stabilization of Atomically Thin Chromium Triiodide,
Dmitry Leonidovich Shcherbakov, Petr Stepanov, Daniel Weber, Yaxian Wang, Jin Hu, Yanglin Zhu, Kenji Watanabe, Takashi Taniguchi, Zhiqiang Mao, Wolfgang Windl, Joshua E Goldberger, Marc Bockrath, Chun Ning Lau.
Nano Letters 18, 4214 (2018).

[6] Dimensional reduction and ionic gating induced enhancement of superconductivity in atomically thin crystals of 2H-$TaSe_2$,
Yueshen Wu, Jiaming He, Jinyu Liu, Hui Xing, Zhiqiang Mao, Ying Liu,
Nanotechnology 30, 035702 (2018).

[7] Distinct Signatures of Electron-Phonon Coupling Observed in the Lattice Thermal Conductivity of $NbSe_3$ Nanowires,
Lin Yang, Yi Tao, Jinyu Liu, Chenhan Liu, Qian Zhang, Manira Akter, Yang Zhao, Terry T Xu, Ya-Qiong Xu, Zhiqiang Mao, Yunfei Chen, Deyu Li,
Nano letters 19, 415 (2019).

[8] Anisotropic ultraviolet-plasmon dispersion in black phosphorus,
Giuseppe Nicotra, Edo van Veen, Ioannis Deretzis, Lin Wang, Jin Hu, Zhiqiang Mao, Vito Fabio, Corrado Spinella, Gennaro Chiarello, Shengjun Yuan, Antonio Politano,
Nanoscale 10, 21918 (2018).

[9] Signature of quantum Griffiths singularity state in a layered quasi-one-dimensional superconductor,
Enze Zhang, Jinhua Zhi, Yi-Chao Zou, Zefang Ye, Linfeng Ai, Jiacheng Shi, Ce Huang, Shanshan Liu, Zehao Lin, Xinyuan Zheng, Ning Kang, Hongqi Xu, Wei Wang, Liang He, Jin Zou, Jinyu Liu, Zhiqiang Mao, Faxian Xiu,
Nature communications 9, 4656 (2018).

[10] Angle-dependent magnetoresistance as a sensitive probe of the charge density wave in quasi-one-dimensional semimetal Ta_2NiSe_7,
Jiaming He, Libin Wen, Yueshen Wu, Jinyu Liu, Guoxiong Tang, Yusen Yang, Hui Xing, Zhiqiang Mao, Hong Sun, Ying Liu.

Applied Physics Letters 113, 192401 (2018).
[11] Searching for topological Fermi arcs via quasiparticle interference on a type-II Weyl semimetal $MoTe_2$,
Davide Iaia, Guoqing Chang, Tay-Rong Chang, Jin Hu, Zhiqiang Mao, Hsin Lin, Shichao Yan, Vidya Madhavan,
npj Quantum Materials 3, 38 (2018)
[12] Thickness evolution of transport properties in exfoliated $Fe_{1+y}Te$ nanoflakes,
Tung-Wu Hsieh, Tao Zou, Jin Hu, Zhiqiang Mao, Pengpeng Zhang, Xianglin Ke,
Journal of Physics: Condensed Matter 30 (29), (2018).
[13] Electronic structure of Fe1.08Te bulk crystals and epitaxial FeTe thin films on Bi2Te3,
Fabian Arnold, Jonas Warmuth, Matteo Michiardi, Jan Fikáček, Marco Bianchi, Jin Hu, Zhiqiang Mao, Jill Miwa, Udai Raj Singh, Martin Bremholm, Roland Wiesendanger, Jan Honolka, Tim Wehling, Jens Wiebe, Philip Hofmann,
Journal of Physics: Condensed Matter 30, 065502 (2018).
[14] Lithium ion intercalation in thin crystals of hexagonal TaSe2 gated by a polymer electrolyte,
Yueshen Wu, Hailong Lian, Jiaming He, Jinyu Liu, Shun Wang, Hui Xing, Zhiqiang Mao, Ying Liu, Applied Physics Letters 112, 023502 (2018).
[15] Quantum oscillation and unusual protection mechanism of the surface state in nonsymmorphic semimetals.
Xue Liu, Chunlei Yue, Yanglin Zhu, Abin Joshy, Jinyu Liu, Ana M Sanchez, David Graf, Zhiqiang Mao, Jin Hu, Jiang Wei, submitted to Nature Nanotechnology.
[16] Chemical pressure effect on the optical conductivity of the nodal-line semimetals ZrSiY (Y = S, Se, Te) and ZrGeY (Y = S, Te),
J. Ebad-Allah, J. Fernández Afonso, M. Krottenmüller, J. Hu, Y. L. Zhu, Z. Q. Mao, J. Kuneš, and C. A. Kuntscher, Phys. Rev. B 99, 125154 (2019).
[17] Raman detection of hidden phonons assisted by atomic point defects in a two-dimensional Semimetal
Hui Yuan, Xieyu Zhou, Yan Cao, Qi Bian, Zongyuan Zhang, Haigen Sun, Shaojian Li, Zhibin Shao, Jin Hu, Yanglin Zhu, Zhiqiang Mao, Wei Ji & Minghu Pan,
npj 2D Materials and Applications 3, 12 (2019)

Long-range and short-range order as competing driving forces for synthesis of complex oxides

A Navrotsky, University of California–Davis
Grant number: DE-FG02-03ER46053

Program Scope:
Modern structural, thermodynamic and computational tools used together are discovering a wealth of complex intermediates in the synthesis, processing, use and degradation of complex oxide materials. The pyrochlore structure (ideal stoichiometry A_2B_2O) is an ordered superstructure of the basic fluorite aristotype (AO_2 or A_4O_8) with ordering of both cations and oxygen vacancies. Ordered, disordered and intermediate variants are often accessible under varying conditions. They possess different physical and optoelectronic properties, and are relevant to applications ranging from nuclear waste disposal to ionic conduction to catalysis. Structural and thermodynamic studies together elucidate the mechanisms, energetics and kinetics of disordering and annealing.

Recent Progress:
Pyrochlores can be amorphized by radiation and disordered by radiation and by grinding. Our recent structural studies by neutron scattering (which gives more information on ordering on the oxygen sublattice than attainable by X-ray methods) have been combined with calorimetric studies of energetics of formation and annealing of crystalline, disordered and amorphized pyrochlores of various compositions. The disordered and X-ray amorphous materials have in common large concentrations of short-range ordered domains with a weberite-like structure, representing an ordering scheme different from pyrochlore and intermediate in degree of order between the pyrochlore and disordered fluorite phases. On heating, the amorphous and disordered materials revert quickly near 800 °C to a structure with long-range pyrochlore ordering, but retain weberite-like short-range domains. These persist to at least 1200 °C. The energy released on heating to 1200 °C is only about half the total energy stored in the initial damaged samples, consistent with the persistence of short-range order and the decoupling of the kinetics of short- and long-range ordering.

Future Plans:
The implications of this complex energy landscape of order-disorder processes for the controlled synthesis of new materials in various complex oxide systems is being explored. We will continue investigations of pyrochlores, garnets and other phases. A different part of this program focuses on hybrid perovskites.

Publications:

"Formation and Dehydration Enthalpy of Potassium Hexaniobate," S. K. Sahu, L. A. Boatner, and A. Navrotsky, *J. Am. Ceram. Soc.*, 100, 304-311 (2017).

"A Correlation between Formation Enthalpy and Ionic Conductivity in Perovskite-Structured $Li_{3x}La_{0.67-x}TiO_3$ Solid Lithium Ion Conductors," X. Guo, P. S. Maram and A. Navrotsky; *J. Matl. Chem A*, 5, 12951-12957 (2017).

"Tunable Low-Density Palladium Nanowire Foams," D. Gilbert, E. Burks, S.V. Ushakov, P. Abellan, I. Arslan, T. Felter, A. Navrotsky, K. Liu, *Chem. of Matls., Chem. Mater.*, 29, 9814-9818 (2017).

"Thermochemistry of the Simplest Metal Organic Frameworks: Formates $[M(HCOO)_2] \cdot xH_2O$ (M = Li, Mg, Mn, Co, Ni, and Zn)," G. P. Nagabhushana, R. Shivaramaiah, and A. Navrotsky, *J. Chem. Therm.*, 118, 325-330 (2018).

"Energetics of Bulk Lutetium Doped $Ce_{1-x}Lu_xO_{2-x/2}$ Compounds," N. Yavo, G. Sharma, G. Kimmel, I. Lubomirsky, A. Navrotsky, O. Yeheskel, *J. Am. Ceram. Soc.,* 101, 3520-3526 (2018).

"Probing Disorder in Pyrochlore Oxides Using in situ Synchrotron Diffraction from Levitated Solids – A Thermodynamic Perspective," P.S. Maram, S.V. Ushakov, A. Navrotsky, *Sci. Rep.,* 8, 10658 (2018).

"High Resolution Thermochemical Study of Phase Stability and Rapid Oxygen Incorporation in $YBaCo_{(4-x)}ZnxO_{(7+\delta)}$ 114-Cobaltites," D. Tsvetkov, P.S. Maram, N. Tsvetkova, A. Zuev, A. Navrotsky, *J. Phys. Chem. A*, 122, 9597-9604 (2018).

"Structural and Thermodynamic Limits of Layer Thickness in 2D Halide Perovskites" C.M.M. Soe, G.P. Nagabhushana, R. Shivaramaia, H. Tsai, W. Nie, J.C. Blancon, F. Melkonyan, D.H. Cao, B. Traoré, L. Pedesseau, M. Kepenekian, C. Katan, J. Even, T.J. Marks, A. Navrotsky, A.D. Mohite, C.C. Stoumpos, M.G. Kanatzidis, *Proc. Natl. Acad. Sci.*, 116, 58-66 (2019).

"Thermodynamics of $Zn_xMn_{3-x}O_4$ and $Mg_{1-z}Cu_zCr_2O_4$ Spinel Solid Solutions," K. Lilova, G. Sharma, S. Hayun, D.P. Shoemaker, A. Navrotsky, *J. Mater. Res.*, In Press (2019).

"Enthalpies of Formation of the Solid Solutions of $Zr_xY_{0.5-x/2}Ta_{0.5-x/2}O_2$ ($0 \le x \le 0.2$ and $0.65 \le x \le 1$)," M. Lepple, K. Lilova, C. Levi, A. Navrotsky, *J. Mater. Res.*, Submitted (2019).

"Thermodynamic and Structural Evolution of Mechanically Milled and Swift Heavy Ion Irradiated $Er_2Ti_2O_7$ Pyrochlore," C.K. Chung, E. C. O'Quinn, J.C. Neuefeind, A.F. Fuentes, H. Xu, M. Lang, A. Navrotsky, *Acta Mater.*, Submitted (2019).

Synthesis and characterization of novel topological materials

Ni Ni

University of California, Los Angeles, Los Angeles, CA

Program Scope

Modern research of condensed matters devotes in understanding how properties of complex solids are determined by their structural and electronic degrees of freedom. Recently, since the discovery of protected surface state in bulk materials, band topology has emerged as a new organizing principle of states of matter. The entanglement of band topology and the spin, charge, orbital and lattice (SCOL) degrees of freedom have led to emergent phenomena, such as quantized anomalous Hall effect, colossal photovoltaic effect, etc. However, due to the lack of "ideal" topological materials where only minimum non-trivial nodal feature exists at the Fermi level, there are significant materials challenges facing the in-depth understanding of collective phenomena and excitations of topological materials, thus hindering the material discovery with favorable functionality arising from the non-trivial topology. The objective of this research is to design topological materials that lie at the edge of structural/magnetic instabilities, aiming at the discovery of "ideal" magnetic/superconducting topological materials and the in-depth understanding of the entanglement of band topology and SCOL degrees of freedoms through thermodynamic, transport, X-ray, and neutron measurements.

Recent Progress

1. Discovery of novel antiferromagnetic topological insulator with weal saturation field. Magnetic topological insulators (MTI), including Chern insulators with a Z-invariant and antiferromagnetic (AFM) topological insulators (TIs) with a Z_2-invariant, provide fertile ground for the exploration of emergent quantum phenomena such as the quantum anomalous Hall (QAH) effect, Majorana modes, the topological magnetoelectric effect, and the proximity

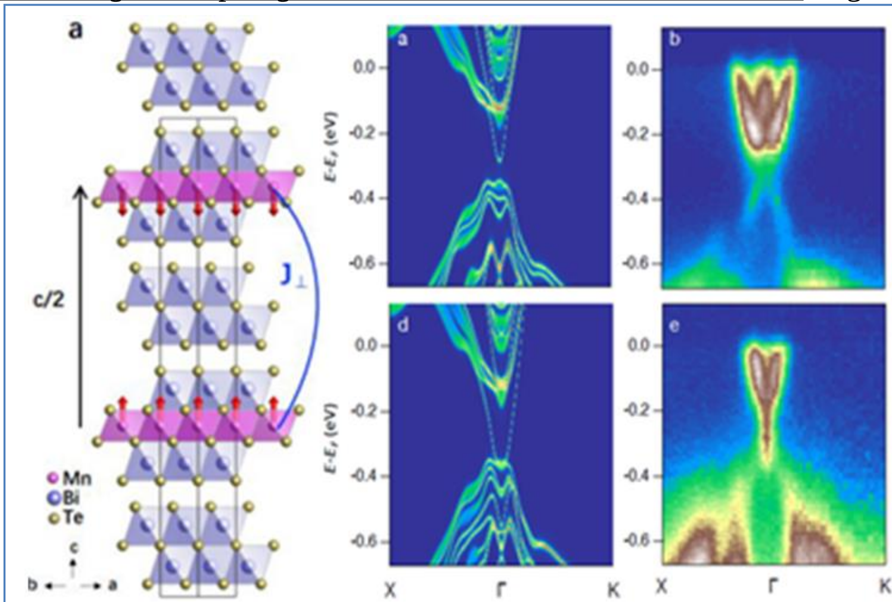

Figure 1: Crystal structure (**a**), DFT calculation (**b**) and angular-resolved photoemission spectroscopy (**c**) measurements of antiferromagnetic topological insulator $MnBi_4Te_7$.

effect. Although the QAH effect has been experimentally realized in magnetically doped topological insulator $Cr_{0.15}(Bi_{0.1}Sb_{0.9})_{1.85}Te_3$ thin films [1], it remains a challenge to realize the QAH effect at high temperatures. Recently $MnBi_2Te_4$ was discovered to be an intrinsic AFM TI [2]. In its two-dimensional (2D) limit [3], quantized Hall conductance originating from the topological protected dissipationless chiral edge states was realized in odd number of slab, a magnetic field of 12 T at 4.5 K or 6 T at 1.5 K, above which the AFM spins enter the forced ferromagnetic (FM) state [4].

How can we achieve the QAH effect at much lower magnetic fields in AFM TIs so that the associated emergent phenomena could be studied at more accessible conditions and the quantized Landau levels would not contaminate the QAH effect? Our recent work realized a bulk vdW material with a superlattice of alternating one [$MnBi_2Te_4$] and one [Bi_2Te_3] layers, as shown in Figure 1. This have paved a new avenue to achieve the QAH effect at low or even zero magnetic fields [5]. We showed that $MnBi_4Te_7$ is a Z_2 antiferromagnetic topological insulator with two distinct (001) surface states from [Bi_2Te_3] and [$MnBi_2Te_4$] termination, respectively. Strong FM fluctuations were observed above T_N (12 K). Due to its superlattice nature, in the two-dimensional limit, it serves as natural heterostructures. The extremely low out-of-plane saturation field ≈ 0.22 T makes it an ideal system to study the quantized anomalous Hall effect, quantum spin Hall effect and associated emergent phenomena.

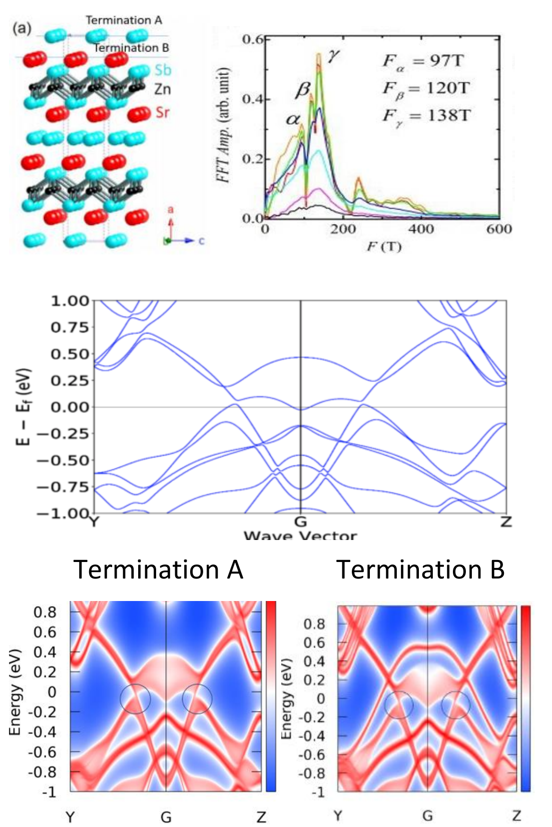

Figure 2: Crystal structure, quantum oscillation and DFT calculated bulk and surface band structures of $SrZnSb_2$ from two types of terminations.

2. Discovery of an ideal topological nodal line semimetal. Recently, the relativistic fermions hosted by square-net lattices of main group elements were found to have rich interplay with the magnetism in antiferromagnetic (AFM) material family of $AMnX_2$ (A=alkaline earth or rare earth elements, and X=Sb/Bi). $SrZnSb_2$ can be viewed as a nonmagnetic version of the $AMnX_2$ [6]. To examine the effect of magnetism on the existence of Dirac fermions in this group of mateirals, we have investigated quantum transport properties up to 35T for $SrZnSb_2$ which has a distorted square net of Sb. As seen in Fig. 2, we have observed de Haas–van Alphen (dHvA) oscillations in magnetic torque measurement starting from 5 T in $SrZnSb_2$. Our analysis reveals the nontrivial Berry phase accumulation and light effective masses of the quasiparticles in this system. The angular dependence of the de Haas van Alphen oscillations

further reveals that the Fermi surfaces are quasi 2D-like, similar to those in the $AMnX_2$ materials. Interestingly, our DFT calculation suggests this compound may serve as an ideal topological nodal line semimetal since the DFT band structure shows that we can tune the Fermi level so that only the nodal line feature exist at the G point in the reciprocal space. In collaboration with Dan Dessau's group on $SrZnSb_2$, ARPES measurement has been performed. The good agreement between ARPES experiment and DFT calculation indeed suggests the non-trivial topology and nodal line feature in $SrZnSb_2$. It also turned out that $(Sr_{1-x}La_x)ZnSb_2$ (x=0.1, 0.2, 0.25) single crystals can be made, where La doped electrons into the system, providing a tunable system to investigate the evolution of topological nodal line and drumhead surface state.

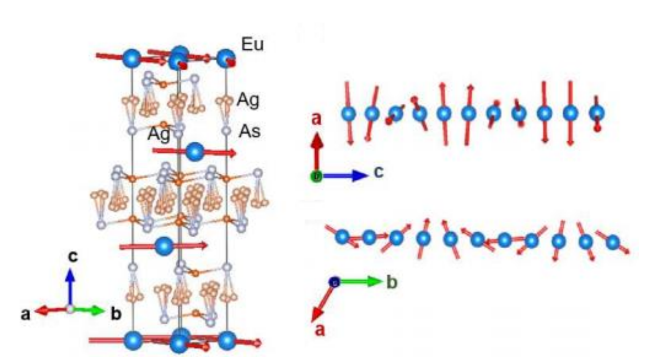

Figure 3: Crystal and magnetic structure of $EuAg_4As_2$.

3. The investigation of quasi-two-dimensional materials with structural/magnetic instability. Layered pnictide materials have provided a fruitful platform to study various emergent phenomena, including superconductivity, magnetism, charge density waves, etc. We performed transport, magnetic, single crystal X-ray and neutron diffraction measurements on AAg_4As_2 (A=Sr, Eu) [7,8]. We have revealed the Fermi surface topology and the strong coupling of magnetism and charge carriers. Both $SrAg_4As_2$ and $EuAg_4As_2$, show a nonmagnetic phase transitions emerge at around 110 K, likely associated with structural distortions. In $SrAg_4As_2$, quantum oscillations reveal small Fermi pockets with light effective masses. In $EuAg_4As_2$, noncollinear magnetism was revealed, as shown in Fig. 3, where two sets of superlattice peaks with the propagation vectors of q1 = ±(0,0.25,0.5) and q2 = ±(0.25,0,1) exist. Before the hexagonal Eu^{2+} sublattice enters into an incommensurate noncollinear antiferromagnetic state below 9 K with a propagation vector of (0,-0.1,0.12), a short-range antiferromagnetic order with reduced magnetic anisotropy takes place between 15 K to 9 K. The magnetic structure below 9 K is helical along the c axis and cycloidal along the b axis with a moment of 6.4 μ_B/Eu^{2+}.

4. Collaborations with various groups in this period. Our collaboration with Burch's group (Boston College) published on Nat. Mater. has demonstrated a colossal mid-infrared bulk photovoltaic effect in microscopic devices of TaAs which produces large photocurrent [11]. Our collaboration with Prasankumar's group (LANL) published on PRL has elucidated the relationship between the crystalline symmetry and the direction of the photocurrent [12].

Future Plans

We will continue our exploration and investigation on topological materials with structural/magnetic instabilities.

1. The existence of natural heterostructure $MnBi_{2n}Te_{3n+1}$ (n=1 to 4) family of alternating n[Bi_2Te_3] and [$MnBi_2Te_4$] makes this system great to investigate the effect of dimensionality and interlayer magnetic coupling on the band topology and magnetism. We will continue our investigation on the members with higher *n* numbers, aiming at discovering a FM natural heterostructure topological material.

2. By doping, intercalating and designing of new materials with the $MnBi_2Te_4$ building blocks, we will aim at the discovery of MTI with higher transition temperatures and natural heterostructure materials with alternating superconducting and topological magnetic layers.

3. In collaboration with Dan Dessau's group on $SrZnSb_2$, ARPES measurement will be performed on the $(Sr_{1-x}La_x)ZnSb_2$ (x=0.1, 0.2, 0.25) single crystals.

4. The TI material data base suggests that the sister compound of $SrAg_4As_2$, $SrAg_4Sb_2$ has nontrivial topology without structural distortion. As a comparison study, we will investigate $SrAg_4Sb_2$ and $EuAg_4Sb_2$ to reveal the role of topology and structural distortion in the transport properties.

5. We will explore chiral topological materials to investigate the effect of the chirality in the band topology.

References

[1] Chang, C.-Z. et al. Experimental observation of the quantum anomalous Hall effect in a magnetic topological insulator. Science 340, 167 (2013)

[2]Mikhail M. Otrokov, et al., Prediction and observation of the first antiferromagnetic topological insulator, arxiv: 1809.07389 (2019)

[3] Mikhail M. Otrokov, et al., Unique Thickness-Dependent Properties of the van der Waals Interlayer Antiferromagnet $MnBi_2Te_4$ Films, Phys. Rev. Lett. 122, 107202 (2019)

[4] Yujun Deng, et al., Magnetic-field-induced quantized anomalous Hall effect in intrinsic magnetic topological insulator $MnBi_2Te_4$, ArXiv:1904. 11468 (2019)

[5] Chaowei Hu, et al., A van der Waals antiferromagnetic topological insulator with weak interlayer magnetic coupling, arXiv:1905.02154 (2019), Nature Communication, Under review.

[6] Jinyu Liu, Eve Emmanouilidou, Jie Xing, David Graf and Ni Ni, Quantum oscillation studies of the Dirac state hosted by distorted Sb square net in $SrZnSb_2$, arXiv:1807.0254, under review, Phys. Rev. B, (2018)

[7] Bing Shen, Eve Emmanouilidou, Xiaoyu Deng, Alix McCollam, Jie Xing, Gabriel Kotliar, Amalia I. Coldea,and Ni Ni, Bing Shen, Eve Emmanouilidou, Xiaoyu Deng, Alix McCollam, Jie Xing, Gabriel Kotliar, Amalia I. Coldea, Ni Ni, Significant change in the electronic behavior associated with structural distortions in the monocrystalline $SrAg_4As_2$, Phys. Rev. B 98, 235130 (2018)

[8] Bing Shen, Chaowei Hu, Huibo Cao, Xin Gui, Eve Emmanouilidou, Weiwei Xie, and Ni Ni, Structural distortion and incommensurate noncollinear magnetism in $EuAg_4As_2$, arXiv:1809.07317, Phys. Rev. Mater., under review, (2018)

Publications

1. Eve Emmanouilidou, Huibo Cao, Peizhe Tang, Xin Gui, Chaowei Hu, Bing Shen, Junyi Wu, Shou-Cheng Zhang, Weiwei Xie, Ni Ni, Magnetic order induces symmetry breaking in the single crystalline orthorhombic CuMnAs semimetal, Phys. Rev. B 96, 224405 (2017)

   Work at UCLA was supported by the U.S. Department of Energy (DOE), Office of Science, Office of Basic Energy Sciences under Award No. DE-SC0011978. Work at ORNL s High Flux Isotope Reactor was sponsored by the Scientific User Facilities Division, Office of Basic Energy Sciences, DOE. The research at LSU was supported by the LSUstartup funding and Louisiana Board of Regents Research Competitiveness Subprogram under Contract No. LEQSF (2017-20)-RD-A-08. P.Z. and S.C.Z. acknowledge FAME, one of six centers of STARnet, a Semiconductor Research Corporation program sponsored by MARCO and DARPA. N.N. thanks Dr. Y. Wang for useful discussion

   Activity supported by this award: bulk sample growth, structure determination, bulk transport, thermodynamic and neutron measurements as well as data analysis.

2. Bing Shen, Eve Emmanouilidou, Xiaoyu Deng, Alix McCollam, Jie Xing, Gabriel Kotliar, Amalia I. Coldea,and Ni Ni, Bing Shen, Eve Emmanouilidou, Xiaoyu Deng, Alix McCollam, Jie Xing, Gabriel Kotliar, Amalia I. Coldea, Ni Ni, Significant change in the electronic behavior associated with structural distortions in the monocrystalline SrAg4As2, Phys. Rev. B 98, 235130 (2018)

   Work at UCLA was supported by the U.S. Department of Energy (DOE), Office of Science, Office of Basic Energy Sciences under Award Number DE-SC0011978. AIC acknowledges an EPSRC Career Acceleration Fellowship (EP/I004475/1). Part of this work was supported by HFML-RU/FOM and LNCMI-CNRS, members of the European Magnetic Field Laboratory (EMFL) and by EPSRC (UK) via its membership to the EMFL (grant no. EP/N01085X/1). Work at Rutgers was supported by the NSF DMREF program under the award NSF DMREF project DMR-1435918. NN would like to thank useful discussion with Gui Xin and Prof. Weiwei Xie.

   Activity supported by this award: bulk single crystal growth, structure determination, bulk transport, thermodynamic measurements and data analysis.

3. Eve Emmanouilidou, Jinyu Liu, David Graf, Huibo Cao, Ni Ni, Spin-flop phase transition in the orthorhombic antiferromagnetic topological semimetal Cu0.95MnAs, J. Magn. Magn. Mater. **469**, 570 (2019)

   Work at UCLA was supported by the U.S. Department of Energy (DOE), Office of Science, Office of Basic Energy Sciences under Award Number DE-SC0011978 and the NSF-MRI grant 1625776. Work at ORNL's High Flux Isotope Reactor was sponsored by the Scientific User Facilities Division, Office of Basic Energy Sciences, DOE.

Activity supported by this award: bulk single crystal growth, bulk transport, thermodynamic measurements and data analysis.

4. Jinyu Liu, Eve Emmanouilidou, Jie Xing, David Graf and Ni Ni, Quantum oscillation studies of the Dirac state hosted by distorted Sb square net in SrZnSb2, arXiv:1807.0254, under review, Phys. Rev. B, (2018)

   Work at UCLA was supported by DOE Award DESC0011978. The National High Magnetic Field Laboratory is supported by the National Science Foundation through NSF/DMR-1644779 and the State of Florida.

   Activity supported by this award: bulk single crystal growth, bulk transport, thermodynamic measurements and data analysis.

5. Bing Shen, Chaowei Hu, Huibo Cao, Xin Gui, Eve Emmanouilidou, Weiwei Xie, and Ni Ni, Structural distortion and incommensurate noncollinear magnetism in EuAg4As2, arXiv:1809.07317, Phys. Rev. Mater., under review, (2018)

Bing Shen and Chaowei Hu contributed equally. We thank Prof. Paul. C. Canfield for useful discussion. Work at UCLA was supported by the U.S. Department of Energy (DOE), Office of Science, Office of Basic Energy Sciences under Award Number DE-SC0011978. Work at ORNL's High Flux Isotope Reactor was sponsored by the Scientific User Facilities Division, Office of Basic Energy Sciences, DOE. The work at LSU was supported by Beckman Young Investigator (BYI) Program.

Activity supported by this award: bulk single crystal growth, bulk transport, thermodynamic measurements and data analysis.

6. Chaowei Hu, Xiaoqing Zhou, Pengfei Liu, Jinyu Liu, Peipei Hao, Eve Emmanouilidou, Hongyi Sun, Yuntian Liu, Harlan Brawer, Arthur P. Ramirez, Huibo Cao, Qihang Liu, Dan Dessau, Ni Ni, A van der Waals antiferromagnetic topological insulator with weak interlayer magnetic coupling, arXiv:1905.02154, Nature Communication, Under review, (2019)

   We thank Paul C. Canfield, Dr. Quansheng Wu, Suyang Xu, Filip Ronning and Chris Regan for helpful discussions, and Chris Jozwiak and Roland Koch at the Advanced Light Source for experimental help. Work at UCLA, the University of Colorado and UCSC were supported by the U.S. Department of Energy (DOE), Office of Science, Office of Basic Energy Sciences under Award Number DE-SC0011978, DE-FG02-03ER46066 and DESC0017862, respectively. Work at SUSTech was supported by the NSFC under Grant No. 11874195. HC acknowledges the support from US DOE BES Early Career Award KC0402010 under Contract DE-AC05- 00OR22725. This research used resources of the Advanced Light Source, which is a DOE Office of Science User Facility under contract no. DE-AC02-05CH11231.

Activity supported by this award: bulk single crystal growth, bulk transport, thermodynamic measurements and data analysis.

7. Gavin B. Osterhoudt, Laura K. Diebel, Xu Yang, John Stanco, Xiangwei Huang, Bing Shen, Ni Ni, Philip Moll, Ying Ran, Kenneth S. Burch, Colossal mid-infrared bulk photovoltaic effect in a type-I Weyl semimetal, Nature Materials 18, 471 (2019)

   Photocurrent experiments performed by G.O. and work done by K.S.B. were supported by the US Department of Energy (DOE), Office of Science, Office of Basic Energy Sciences under award no. DE-SC0018675. M.J.G. acknowledges support from the National Science Foundation, award no. DMR-1709987. L.K.D. was supported by a DAAD RISE fellowship. X.Y. and Y.R. acknowledge support from the National Science Foundation under grant no. DMR-1151440. Work at UCLA was supported by the US DOE, Office of Science, Office of Basic Energy Sciences under award no. DE-SC0011978. X.H. and P.J.W.M. were supported by the European Research Council (ERC) under the European Union's Horizon 2020 research and innovation programme (grant agreement no. 715730).

Activity supported by this award: bulk single crystal growth, bulk transport measurements and data analysis.

8. N. Sirica, R. I. Tobey, L. X. Zhao, G. F. Chen, B. Xu, R. Yang, B. Shen, D. A. Yarotski, P. Bowlan, S. A. Trugman, J. -X. Zhu, Y. M. Dai, A. K. Azad, N. Ni, X. G. Qiu, A. J. Taylor, R. P. Prasankumar, Tracking ultrafast photocurrents in the Weyl semimetal TaAs using THz emission spectroscopy, Phys. Rev. Lett., 122, 197401 (2019)

This work was performed at the Center for Integrated Nanotechnologies at Los Alamos National Laboratory (LANL), a U.S. Department of Energy, Office of Basic Energy Sciences user facility. N. S. and R. P. P. gratefully acknowledge the support of the U.S. Department of Energy through the LANL LDRD Program and the G. T. Seaborg Institute. D. Y. and J. X. Z. were supported by the Center for Advancement of Topological Semimetals, an Energy Frontier Research Center funded by the U.S. Department of Energy Office of Science, Office of Basic Energy Sciences, through the Ames Laboratory under its Contract No. DEAC02-07CH11358. R. I. T. was the recipient of the Los Alamos National Laboratory Rosen Scholar Award, supported by LDRD Grant No. 20180661ER. Work at U. C. L. A. was supported by the US DOE, Office of Science, Office of Basic Energy Sciences under Award No. DE-SC0011978.

Activity supported by this award: bulk single crystal growth, bulk transport measurements and data analysis.

9. Sihang Liang, Jingjing Lin, Satya Kushwaha, Jie Xing, Ni Ni, R. J. Cava and N. P. Ong, Experimental tests of the chiral anomaly magnetoresistance in the Dirac-Weyl semimetals Na3Bi and GdPtBi, Phys. Rev. X **8**, 031002 (2018)

The research was supported by the U.S. Army Research Office (Grant No. W911NF-16-1-0116) and a MURI award for topological insulators (No. ARO W911NF-12-1-0461). N. P. O. acknowledges support from the Gordon and Betty Moore Foundation's Emergent Phenomena in Quantum Systems Initiative through Grant No. GBMF4539. The growth and characterization of crystals were performed by S. K. and R. J. C., with support from the National Science Foundation (NSF MRSEC Grant No. DMR 1420541). Work at UCLA was supported by the U.S. Department of Energy (DOE), Office of Basic Energy Sciences, Award No. DE-SC0011978.

Activity supported by this award: bulk single crystal growth, bulk transport measurements and data analysis.

10. Xiao-Bo Wang, Xiao-Ming Ma, Eve Emmanouilidou, Bing Shen, Chia-Hsiu Hsu, Chun-Sheng Zhou, Yi Zuo, Rong-Rong Song, Su-Yang Xu, Gan Wang, Li Huang, Ni Ni*, Chang Liu*, Topological surface electronic states in candidate nodal-line semimetal CaAgAs, Phys. Rev. B 96, 161112(R) (2017)

We thank Ling-Yuan Kong, Bo-Qing Lv, Yao-Bo Huang, Ying Zou, and Hong Ding for useful discussions and technical support at the "Dreamline" beamline at SSRF. Work at SUSTech was supported by the National Natural Science Foundation of China (NSFC) (No. 11404160 and No. 11504159), the State Key Laboratory of Low-Dimensional Quantum Physics (No. KF201602), NSFC Guangdong (No. 2016A030313650), the Guangdong Innovative and Entrepreneurial Research Team Program (No. 2016ZT06D348), the Shenzhen Peacock Plan Team (No. KQTD2016022619565991), the Shenzhen Key Laboratory (No. ZDSYS20141118160434515 and No. ZDSYS20170303165926217), and the Technology and Innovation Commission of Shenzhen Municipality (No. JCYJ20150630145302240 and No. JCYJ20160531190254691). Work at UCLA was supported by the U.S. Department of Energy (DOE), Office of Science, Office of Basic Energy Sciences under Award No. DE-SC0011978.

Activity supported by this award: idea and bulk single crystal growth.

11. Xiaoqing Zhou, Qihang Liu, QuanSheng Wu, Tom Nummy, Haoxiang Li, Justin Griffith,Stephen Parham, Justin Waugh, Eve Emmanouilidou, Bing Shen, Oleg V. Yazyev, Ni Ni,Daniel Dessau, Coexistence of Tunable Weyl Points and Topological Nodal Lines in Ternary Transition-Metal Telluride TaIrTe4, Phys. Rev. B 97, 241102(R) (2018)

We acknowledge Dr. Y. D. Chuang, Dr. J. D. Denlinger and Dr. M. Hoesch for technical assistances in ARPES, Hao Zheng and Hengdi Zhao for technical assistance in structural determination. This work was carried out with the support of Diamond Light Source beamline I05 (proposal no. SI13406). This work was supported by the U.S. Department of Energy (DOE), Office of Science, Office of Basic Energy Sciences under Award Numbers DE-FG02-03ER46066 (University of Colorado) and DESC0011978 (UCLA). This work used resources of the National Energy Research Scientific Computing Center. The

Advanced Light Source is supported by DOE office of Science User Facility under contract No. DE-AC02-05CH11231. QSW and OY acknowledge support by the NCCR Marvel.

Activity supported by this award: bulk sample growth, bulk transport measurements and data analysis.

12. Shu Cai, Eve Emmanouilidou, Jing Guo, Xiaodong Li, Yanchuan Li, Ke Yang, Aiguo Li, Qi Wu, Ni Ni, Liling Sun, Observation of superconductivity in the pressurized Weyl semimetal candidate TaIrTe4, Phys. Rev. B 99, 020503(R) (2019)

    We thank Dr. Li Zhang for helpful discussions on our highpressure XRD data. The work in China was supported by the National Key Research and Development Program of China (Grants No. 2017YFA0302900, No. 2016YFA0300300, and No. 2017YFA0303103), the NSF of China (Grants No. 11427805, No. U1532267, and No. 11604376), and the Strategic Priority Research Program (B) of the Chinese Academy of Sciences (Grant No. XDB25000000). The work at UCLA was supported by the U.S. Department of Energy (DOE), Office of Science, Office of Basic Energy Sciences under Award No. DE-SC0011978.

    Activity supported by this award: bulk single crystal growth, bulk transport measurements and data analysis.

13. Jin Hu, Su-Yang Xu, Ni Ni, Zhiqiang Mao, Electronic Transport and quantum oscillation of Topological Semimetals, arXiv:1904.04454, to appear at Annual Reviews of Materials Research. (2019)

    JH is supported by the U.S. Department of Energy (DOE), Office of Science, Office of Basic Energy Sciences under Award DE-SC0019467. ZQM is supported by the US National Science Foundation under grant DMR1707502. NN is supported by the U.S. Department of Energy (DOE), Office of Science, Office of Basic Energy Sciences under Award Number DE-SC0011978. We thank Prof. Antony Carrington from Bristol University for the informative discussions on the effective mass for multifrequency oscillations.

    Activity supported by this award: literature research and manuscript writing.

14. Antonio L. Levy, Andrei B. Sushkov, Fengguang Liu, Bing Shen, Ni Ni, Howard D. Drew, Gregory S. Jenkins, Optical evidence of the chiral magnetic anomaly in Weyl semimetal TaAs, arXiv: 1810.05660 (2018) Phys. Rev. Lett., Under review.

    Work at UCLA was supported by the U.S. Department of Energy (DOE) under Award Number de-sc0011978. A. B. Sushkov and H. D. Drew were supported by DOE de-sc0005436 grant, A. L. Levy, G.S. Jenkins and H. D. Drew were supported by NSF DMR-1610554. F. G. Liu was supported by China Scholarship Council No. 201508340005.

Activity supported by this award: bulk sample growth, bulk transport measurements and data analysis.

15. Jennifer Coulter, Gavin B. Osterhoudt, Christina A. C. Garcia, Yiping Wang, Vincent Plisson, Bing Shen, Ni Ni, Kenneth S. Burch, Prineha Narang, Uncovering Electron-Phonon Scattering and Phonon Dynamics in Type-I Weyl Semimetals, arXiv:1903.07550 (2019)

    This work was supported by the DOE Photonics at Thermodynamic Limits Energy Frontier Research Center under Grant No. de-sc0019140. Analysis and measurements performed by G.B.O. and work done by K.S.B. was supported by the U.S. Department of Energy (DOE), Office of Science, Office of Basic Energy Sciences under Award No. de-sc0018675. Raman experiments by Y.W. and V.P. were supported by the National Science Foundation through grant DMR-1709987. This research used resources of the National Energy Research Scientific Computing Center, a DOE Office of Science User Facility supported by the Office of Science of the U.S. Department of Energy under Contract No. DE-AC02-05CH11231, as well as resources at the Research Computing Group at Harvard University. J.C. recognizes the support of the DOE Computational Science Graduate Fellowship (CSGF) under Grant No. DE-FG02-97ER25308. C.A.C.G. is supported by the NSF Graduate Research Fellowship Program. Work at UCLA was supported by the U.S. Department of Energy (DOE), Office of Science, Office of Basic Energy Sciences under Award Number de-sc0011978. J.C. and G.B.O. contributed equally to this work.

    Activity supported by this award: bulk single crystal growth, bulk transport measurements and data analysis.

16. M. Mehdi Jadidi, Mehdi Kargarian, Martin Mittendorff, Yigit Aytac, Bing Shen, Jacob C. König-Otto, Stephan Winnerl, Ni Ni, Alexander L. Gaeta, Thomas E. Murphy, H. Dennis Drew, Optical Control of Chiral Charge Pumping in a Topological Weyl Semimetal, arXiv:1905.02236 (2019) Nature Physics, Under review.

    Work at UCLA was supported by the U.S. Department of Energy (DOE), Office of Science, Office of Basic Energy Sciences under Award Number de-sc0011978. M. K. acknowledges the support from the Sharif University of Technology under Grant No. G690208.

    Activity supported by this award: bulk single crystal growth, bulk transport measurements and data analysis.

17. Yu-Jie Hao, Pengfei Liu, Yue Feng, Xiao-Ming Ma, Eike F. Schwier, Masashi Arita, Shiv Kumar, Chaowei Hu, Rui'e Lu, Meng Zeng, Yuan Wang, Zhanyang Hao, Hongyi Sun, Ke Zhang, Jiawei Mei, Ni Ni, Liusuo Wu,Kenya Shimada, Chaoyu Chen, Qihang Liu, Chang Liu, Gapless surface Dirac cone in antiferromagnetic topological insulator MnBi2Te4, arXiv: 1907.03722 (2019), submitted to PRL

We thank Jieming Sheng, Yue Zhao, Haizhou Lu, Jianpeng Liu, Weiqiang Chen and Dapeng Yu for discussions. ARPES experiments were performed with the approval of the Hiroshima Synchrotron Radiation Center (HSRC), Hiroshima, Japan under Proposal Nos. 19AG014 and 19AG004. Work at SUSTech was supported by the National Natural Science Foundation of China (NSFC) (Nos. 11504159 and 11874195), NSFC Guangdong (No. 2016A030313650), the Guangdong Innovative and Entrepreneurial Research Team Program (Nos. 2016ZT06D348 and 2017ZT07C062), the Shenzhen Peacock Plan Team (No. KQTD2016022619565991), the Shenzhen Key Laboratory (No. ZDSYS20170303165926217), and the Technology and Innovation Commission of Shenzhen Municipality (Nos. JCYJ20150630145302240 and KYTDPT20181011104202253). Work at UCLA was supported by the U.S. Department of Energy (DOE), Office of Science, Office of Basic Energy Sciences under Award Number DE-SC0011978.

Activity supported by this award: bulk single crystal growth.

Fundamentals of Spark-Plasma Sintering: Rapid and Ultra-Rapid Materials Consolidation and Joining

PI: Prof. E. Olevsky, San Diego State University

Program Scope

The main project idea is the analysis of the spark plasma sintering (SPS – Fig. 1) physical basis at multiple scales specifically exploring the role of electric current in the acceleration of mass transport and with an emphasis on ultra-rapid materials consolidation and joining. Thereby the project specifically addresses the following issues: (I) The development of a new constitutive model for spark-plasma sintering, taking into account the role of electric current in the acceleration of mass transport. (II) The development of a comprehensive multi-scale SPS modeling framework incorporating the elaborated SPS-specific constitutive model. (III) The development of a new Flash Hot Pressing (Flash SPS) processing technique. (IV) Exploring SPS capabilities for joining (including direct seamless bonding) of ceramic and metallic materials.

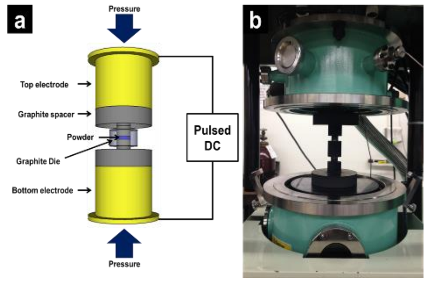

Fig. 1 (a) Schematic representation of SPS process, (b) SPS tooling before an experiment.

Recent Progress

The impact of the electric current on sintering is revealed by introducing the three heating modes during spark plasma sintering enabling the different electric current density flowing into the electrically conductive powders under the same temperature [1]. The experimental evidence of the electric current effect on sintering is demonstrated by the determination of the electric current related constitutive parameters obtained from the three heating modes (Figs. 2,3).

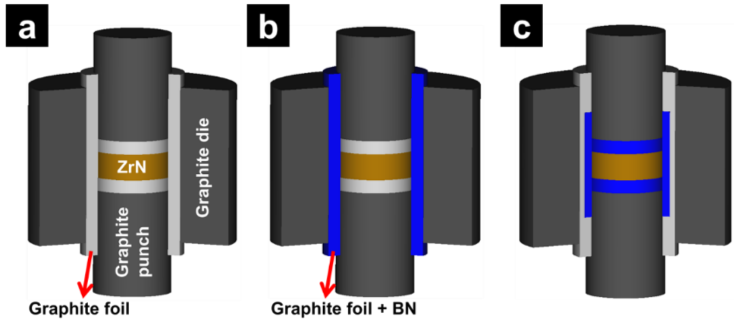

Fig. 2 Schematics of spark plasma sintering setup enabling the different current density flow into ZrN powders. Black, gray, gold and blue color indicate the graphite component, graphite paper, ZrN, and boron nitride.

The enhancement of the dislocation motion and the reduction of the flow stress under the electric current passage are experimentally proven by the ex-situ mechanical strength tests and using the X-ray diffraction results analyzed by the modified Williamson-Hall equation.

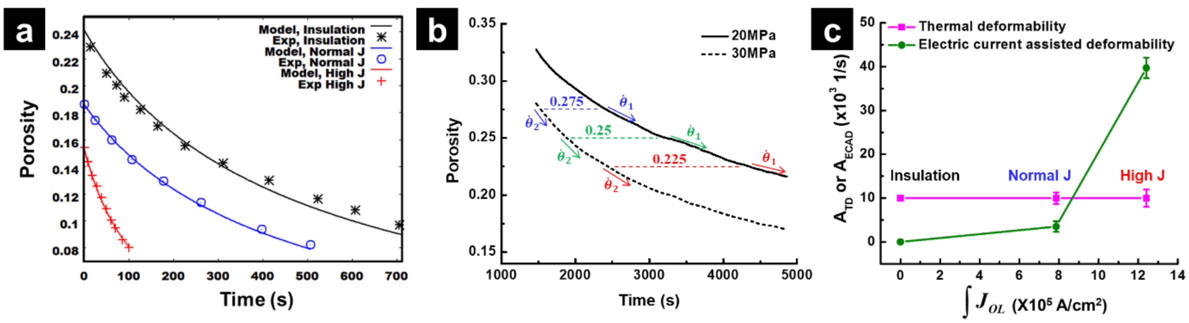

Fig. 3 (a) Experimental porosity evolution curves of ZrN specimens processed by three SPS modes fitted by Eq. (2). (b) Porosity evolution of ZrN under 20 MPa (solid line) and 30 MPa (dashed line) at 1500 ºC, $\dot{\theta}$_1 and $\dot{\theta}$_2 indicate the densification rate for 20 MPa and 30 MPa case at specified porosity levels (θ = 0.225, 0.25 and 0.275) (c) Comparison of calculated ATD (thermal deformability) and AECAD (electric current assisted deformability) of ZrN for 3 SPS modes based on the fitting results.and boron nitride.

Mo nanopowders are synthesized by ball milling and the following hydrogen reduction of MoO3 powders. The densification mechanism of Mo nanopowders during spark plasma sintering (SPS) is analyzed by the combination of the regression of the experimental data on regular SPS and on the SPS multistep pressure dilatometry based on the continuum theory of the sintering. The Mo mirror with 400 nm average grain size and 93% relative density is fabricated by the SPS. The performance of the mirrors made from a single crystal Mo and from the hydrogen-reduced sintered Mo nanopowder is discussed (Figs. 4,5). The microstructure and optical properties of the mirrors are characterized before and after plasma exposure, and no substantial degradation of the reflectivity was observed [2,3].

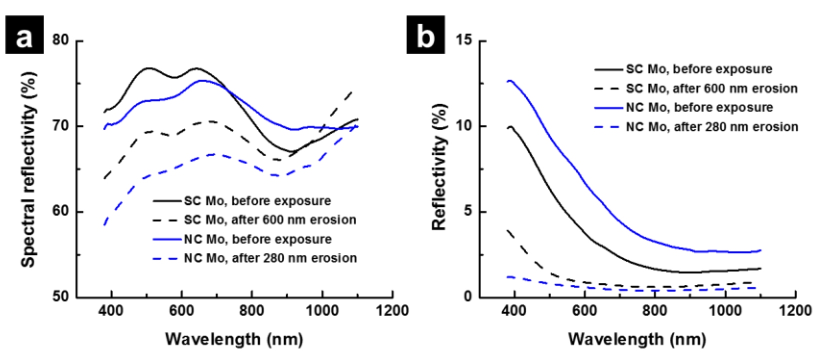

Fig. 4. (a) Specular reflectivity of single crystal (SC) and nanocrystal (NC) Mo before and after plasma exposure (45° illuminations and 45° collection), (b) Diffuse reflectivity of SC and NC Mo and (45° illuminations and 35° collection).

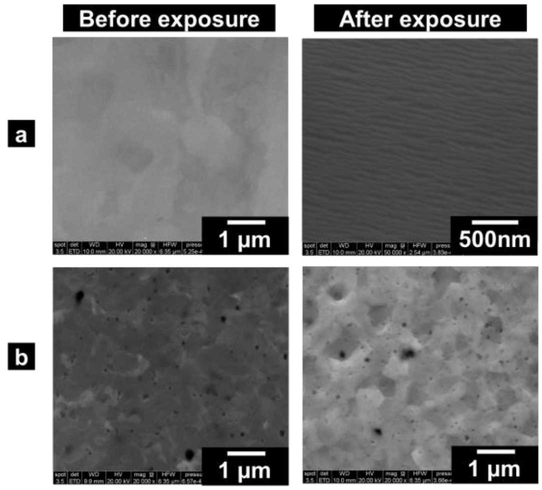

Fig. 5. SEM images of (a) single crystal (SC) and (b) nanocrystal (NC) Mo before (left) and after (right) plasma exposure.

The densification mechanism of conductive powders is revealed by comparing the electric current-assisted spark plasma sintering (SPS) of ZrN powder with conventional hot pressing (HP) carried out with the same powder and under the same pressure and temperature [4]. To determine the actual temperature inside ZrN powder, a sacrificial thermocouple is directly inserted into the powder during the SPS process. The spatial distribution of the electric current passing through the powder is calculated using the finite element modeling (Fig. 6).

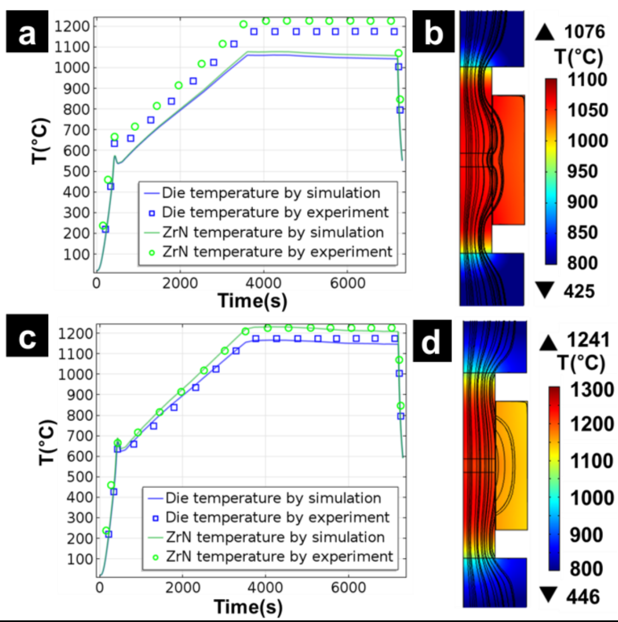

Fig. 6. Experimentally measured and FEM-simulated temperatures of ZrN powder and graphite die during SPS thermal cycle (a) without contact resistance, (c) with electrical and thermal contact resistance. FEM simulation map of the temperature and electric current flow at the end of the holding time (b) without contact resistance, (d) with electrical and thermal contact resistance. SPS at 1100 °C under 60 MPa and 10 °C/min was used.

The porosity-interparticle neck area geometrical relationship is applied to estimate the electric current density inside the powder volume subjected to SPS. For the first time, by taking into account the explicit influence of the electric current effect on the SPS densification mechanism, the constitutive equations describing the electric current-assisted hot pressing of powders are developed [4]. The densification mechanism of ZrN is determined by the inverse regression of the new SPS constitutive equations and by utilizing the experimental results on ZrN powder consolidation with and without the participation of the electric current effect (Fig. 7).

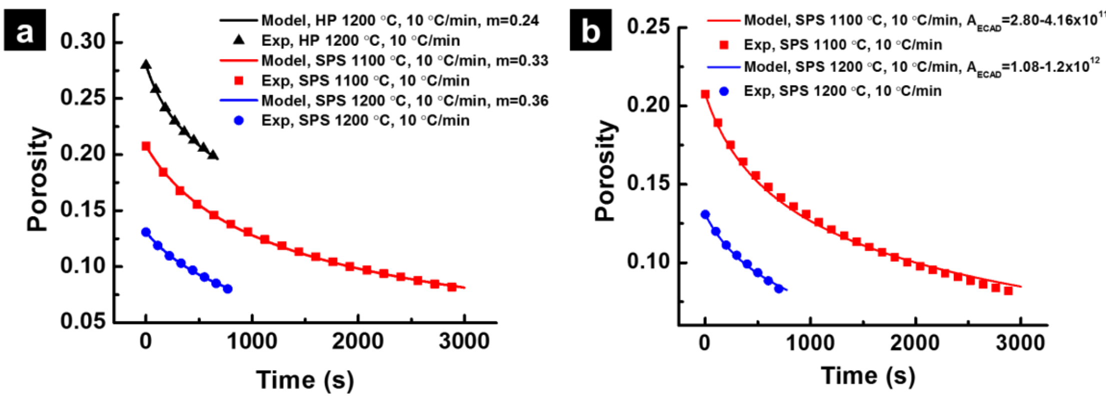

Fig 7. (a) Experimental porosity evolution curves of ZrN specimens processed by HP or SPS fitted by constitutive equation developed in [3], (b) experimental porosity evolution curves of ZrN specimens processed by SPS fitted by constitutive equation developed in [3] (Black triangle: HP with 1200 °C and 10 °C/min, red square: SPS with 1200 °C and 10 °C/min, and blue circle: SPS with 1200 °C and 10 °C/min). Applied compaction pressure was a 60 MPa. Detailed fitting parameters are shown in Ref. [3].

Future Plans

In accord with the proposed plan, the following activities will be carried out:

The continuation of the analysis of the SPS physical basis at multiple scales specifically exploring the role of electric current in the acceleration of mass transport and with an emphasis on the conditions of controlled non-equilibrium.

References

1. G. Lee, C. Manière, J. McKittrick, E.A. Olevsky, Electric current effects in spark plasma sintering: From the evidence of physical phenomenon to constitutive equation formulation, Scripta Mater., 170, 90-94 (2019)
2. G. Lee, C. Manière, J. McKittrick, R. Doerner, D. Nishijima, A. Gattuso, T. Abrams, D. Thomas, C. Back, E.A. Olevsky, Consolidation of Molybdenum nanopowders by spark plasma sintering: Densification mechanism and first mirror application, J. Nuclear Mater., 516, 354-359 (2019)

3. G. Lee, C. Manière, J. McKittrick, A. Gattuso, C. Back, E.A. Olevsky, Oxidation effects on spark plasma sintering of molybdenum nanopowders, J. Amer. Ceram. Soc., 102 , 801-812 (2019)
4. G. Lee, E.A. Olevsky, C. Manière, A. Maximenko, O. Izhvanov, C. Back, J. McKittrick, Effect of electric current on densification behavior of conductive ceramic powders consolidated by spark plasma sintering, Acta Mater., 144, 524-533 (2018)

Publications (the 2-year list of publications)

Book

E. A. Olevsky and D. V. Dudina, Field-Assisted Sintering: Science and Applications, Springer Nature IP, ISBN 978-3-319-76031 5, 425p. (2018)

Papers in refereed journals

1. G. Lee, C. Manière, J. McKittrick, E.A. Olevsky, Electric current effects in spark plasma sintering: From the evidence of physical phenomenon to constitutive equation formulation, Scripta Mater., 170, 90-94 (2019)
2. G. Lee, C. Manière, J. McKittrick, A. Gattuso, C. Back, E.A. Olevsky, Oxidation effects on spark plasma sintering of molybdenum nanopowders, J. Amer. Ceram. Soc., 102 , 801-812 (2019)
3. G. Lee, C. Manière, J. McKittrick, R. Doerner, D. Nishijima, A. Gattuso, T. Abrams, D. Thomas, C. Back, E.A. Olevsky, Consolidation of Molybdenum nanopowders by spark plasma sintering: Densification mechanism and first mirror application, J. Nuclear Mater., 516, 354-359 (2019)
4. C. Manière, G. Lee, J. McKittrick, E.A. Olevsky, Energy efficient spark plasma sintering: Breaking the threshold of large dimension tooling energy consumption, J. Amer. Ceram. Soc., 102, 706-716 (2019)
5. C. Manière, E. Torresani, E.A. Olevsky, Simultaneous Spark Plasma Sintering of Multiple Complex Shapes, Materials, 12, 557 (2019)
6. Y. Shan, X. Wei, X. Sun, E. Torresani, E.A. Olevsky, J. Xu, Effect of heating rate on properties of transparent aluminum oxynitride sintered by spark plasma sintering, J. Amer. Ceram. Soc., 102 (2), 662-673 (2019)
7. C. Manière, S. Chan, E.A. Olevsky, Microwave sintering of complex shapes: From multiphysics simulation to improvements of process scalability, J. Amer. Ceram. Soc., 102 (2), 611-620 (2019)
8. D. Giuntini, R.K. Bordia, E.A. Olevsky, Feasibility of in situ de-agglomeration during powder consolidation, J. Amer. Ceram. Soc., 102, 628-643 (2019)

9. X. Wei, O. Izhvanov, C. Back, C.D. Haines, D.G. Martin, K.S. Vecchio, E.A. Olevsky, Spark plasma sintering of structure-tailored ultra-high temperature components: First step to complex net-shaping, J. Amer. Ceram. Soc., 102 (2), 548-558 (2019)
10. C. Manière, G. Lee, T. Zahrah, E.A. Olevsky, Microwave flash sintering of metal powders: From experimental evidence to multiphysics simulation, Acta Mater., 147, 24-34 (2018)
11. G. Lee, E.A. Olevsky, C. Manière, A. Maximenko, O. Izhvanov, C. Back, J. McKittrick, Effect of electric current on densification behavior of conductive ceramic powders consolidated by spark plasma sintering, Acta Mater., 144, 524-533 (2018)
12. Y. Shan, X. Sun, B. Ren, H. Wu, X. Wei, E.A. Olevsky, J. Xu, J. Li, Pressureless sintering of highly transparent AlON ceramics with CaCO3 doping, Scripta Mater., 157, 148-151 (2018)
13. C. Manière, S. Chan, G. Lee, J. McKittrick, E.A. Olevsky, Sintering dilatometry based grain growth assessment, Results in Physics, 10, 91-93 (2018)
14. A.L. Maximenko, E.A. Olevsky, Pore filling during selective laser melting-assisted additive manufacturing of composites, Scripta Mater., 149, 75-78 (2018)
15. R. Yamanoglu, I. Daoud, E.A. Olevsky, Spark plasma sintering versus hot pressing–densification, bending strength, microstructure, and tribological properties of Ti5Al2.5Fe alloys, Powder Metal., 1-9, 1743-2901 (2018)
16. J. Rechtin, E. Torresani, E. Ivanov, E. Olevsky, Fabrication of Titanium-Niobium-Zirconium-Tantalium alloy (TNZT) bioimplant components with controllable porosity by spark plasma sintering, Materials, 11, 181 (2018)
17. C. Manière, E. Saccardo, G. Lee, J. McKittrick, A. Molinari, E.A. Olevsky, Swelling negation during sintering of sterling silver: An experimental and theoretical approach, Results in Physics 11, 79-84 (2018)
18. C. Manière and E. A. Olevsky, Porosity Dependence of Powder Compaction Constitutive Parameters: Determination Based on Spark Plasma Sintering Tests, Scripta Mater. , 141, 62-66 (2017)
19. C. Manière, G. Lee, E. A. Olevsky, All-materials-inclusive flash spark plasma sintering, Nature Sci. Reports,7, 15071 (2017)
20. X. Wei, J. Rechtin, and E. A. Olevsky, Fabrication of all-solid-state lithium-ion batteries via spark plasma sintering, Metals, 7, 372 (2017)
21. R. Bordia, S.J. Kang, E.A. Olevsky, Current understanding and future research directions at the onset of the next century of sintering science and technology, J. Am. Ceram. Soc., 100, 2314-2335 (2017)
22. C. Manière, T. Zahrah, E.A. Olevsky, Inherent heating instability of direct microwave sintering process: Sample analysis for porous 3Y-ZrO 2, Scripta Mater., 128, 49-52 (2017)
23. C. Manière, T. Zahrah, E.A. Olevsky, Fully coupled electromagnetic-thermal-mechanical comparative simulation of direct vs hybrid microwave sintering of 3Y-ZrO2, J. Am. Ceram. Soc., 100, 2439-2450 (2017)

24. X. Wei, A.L. Maximenko, C. Back, O. Izhvanov, E.A. Olevsky, Effects of loading modes on densification efficiency of spark plasma sintering: sample study of zirconium carbide consolidation, Phil. Mag. Lett., 97, 265-272 (2017)
25. C. Manière, G. Lee, E.A. Olevsky, Proportional integral derivative, modeling and ways of stabilization for the spark plasma sintering process, Results in Physics, 7, 1494-1497 (2017)
26. C. Manière, T. Zahrah, E.A. Olevsky, Fluid dynamics thermo-mechanical simulation of sintering: Uniformity of temperature and density distributions, Appl. Therm. Eng., 123 603–613 (2017)
27. Y. Shan, X. Wei, X. Sun, J. Xu, Q. Qin, E.A. Olevsky, Highly infrared transparent spark plasma sintered AlON ceramics, J. Mater. Res., 32, 3279-3285 (2017)

Integrated Development of Scalable Materials Platforms for Topological Quantum Information Devices

Vlad Pribiag, University of Minnesota (Principal Investigator)
Paul Crowell, University of Minnesota (Co-Investigator)
Sergey Frolov, University of Pittsburgh (Co-Investigator)
Noa Marom, Carnegie Mellon University (Co-Investigator)
Chris Palmstrøm, University of California Santa Barbara (Co-Investigator)

Topological excitations such as Majorana fermions provide unique pathways to fault-tolerant quantum computing. Recent progress in this direction has been enabled by proximity effects between non-superconducting materials and superconductors; however, further breakthroughs leading to topological quantum computation require developing new material systems that integrate semiconductors not only with superconductors, but also with epitaxial ferromagnets or antiferromagnets. Currently, Majorana devices based on semiconductors require application of an external magnetic field to induce spin splitting and open a helical gap – necessary to realize an odd-parity topological superconductor. However, the presence of this magnetic field limits the robustness of topological properties (by weakening the induced superconductivity). Moreover, the stringent requirements on its orientation with respect to the device greatly restrict the scalability of Majorana-based quantum information systems. A promising path forward is to realize Majorana modes without an applied magnetic field by closely integrating epitaxially-grown ferromagnets or antiferromagnets with semiconductors and superconductors. The goals of our inter-disciplinary effort are to develop novel one- and two-dimensional materials platforms, and to leverage them to discover novel topological excitations and demonstrate topological quantum systems with novel functionality. Ultimately, we aim to use these new materials platforms to demonstrate robust topological properties of Majorana modes. This talk will provide a brief overview of the motivations behind and approaches towards these goals, and summarize our current progress.

Transport Characterization and First-Principles Calculations of Low-Dimensional Magnet-InSb Structures

Vlad Pribiag, University of Minnesota (Principal Investigator)
Paul Crowell, University of Minnesota (Co-Investigator)
Sergey Frolov, University of Pittsburgh (Co-Investigator)
Noa Marom, Carnegie Mellon University (Co-Investigator)
Chris Palmstrøm, University of California Santa Barbara (Co-Investigator)

Program Scope

Topological excitations such as Majorana fermions provide unique pathways to fault-tolerant quantum computing. Recent progress in this direction has been enabled by proximity effects between non-superconducting materials and superconductors; however, further breakthroughs leading to topological quantum computation require developing new material systems that integrate semiconductors not only with superconductors, but also with epitaxial ferromagnets or antiferromagnets. Currently, Majorana devices based on semiconductors require application of an external magnetic field to induce spin splitting and open a helical gap – necessary to realize an odd-parity topological superconductor. However, the presence of this magnetic field limits the robustness of topological properties (by weakening the induced superconductivity). Moreover, the stringent requirements on its orientation with respect to the device greatly restrict the scalability of Majorana-based quantum information systems. A promising path forward is to realize Majorana modes without an applied magnetic field by closely integrating epitaxially-grown ferromagnets or antiferromagnets with semiconductors and superconductors. We propose an inter-disciplinary effort that will combine materials synthesis with in-situ characterization and device fabrication, integrated with a computational approach based on lattice matching, genetic algorithm (GA) optimization, and machine learning. Having developed novel one- and two-dimensional materials platforms, we will then leverage them to discover novel topological excitations and to demonstrate topological quantum systems with novel functionality. Ultimately, we aim to use these new materials platforms to demonstrate robust topological properties of Majorana modes. This includes detection of the non-local nature of Majorana modes, and more ambitiously, measurement-based braiding. Importantly, our approach will be compatible with large-area scalability to form two-dimensional arrays of non-Abelian qubits. Thus, if successful, the proposed research has the potential to greatly advance topologically-protected quantum information processing.

Recent Progress (Details on growth progress and plans will be presented in a separate poster by Chris Palmstrøm)

<ins>Transport Experiments:</ins> Pribiag and Crowell (U. Minnesota), together with Frolov (U. Pittsburgh) have undertaken research into ferromagnet-InSb nanowire-ferromagnet (FM-NW-FM) structures using Fe and CoFe. At U. Minnesota, the focus has been on FM-NW-FM structures using Fe, which form quantum point-contacts with magnetic contacts. Conductance measurements (U. Minnesota) as a function of gate voltage demonstrate quasi-one-dimensional transport: electrons

enter nanowires from FM reservoirs as quantized transverse modes and the quantized conductance provides evidence of 1D ballistic transport (Figure 1). Moreover, we also observed Fabry-Pérot interference patterns in the devices. This is a direct consequence of the quantum wave properties of the e lectrons, as they form quasi-bound states in the nanowires because of potential barriers near the FM-NW interfaces. To investigate the magnetic properties of electron transport in the FM-NW-FM structures we performed magneto-resistance measurements. At high back-gate voltage, where nanowires are more conductive, we can observe spin valve-like hysteretic magnetoresistance dips. Bias (Figure 2) and contact-spacing dependence (not shown) showed that the MR ratio decreased with higher bias and longer spacing. This indicates spin transport across the NW. At lower back-gate voltage, in the few quantum modes regime, the magnetoresistance we observe two kinds of hysteretic features: spin valve-like magnetoresistance and spin-filtering. We

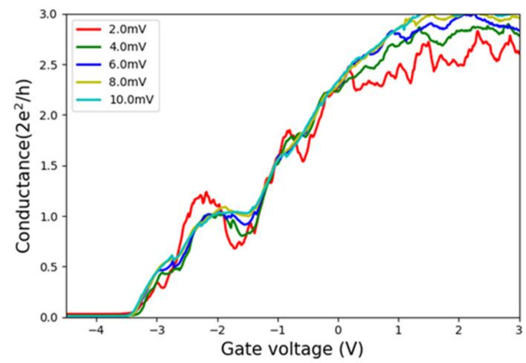

Figure 1: Evidence of ballistic transport in a FM-NW-FM structure with 200 nm spacing between the FM contacts.

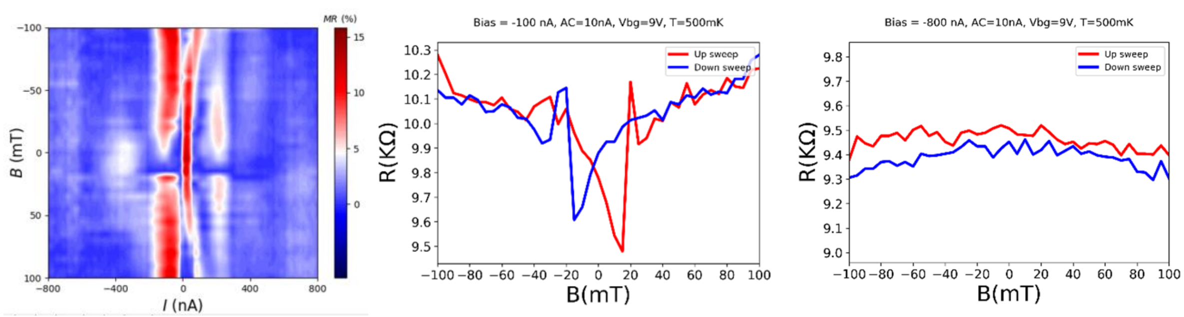

Figure 2: (left) 2D map of magneto-resistance (*MR*) vs. current bias (*I*) and magnetic field (*B*) through a FM-NW-FM structure in the many-modes regime. (center) cut showing pronounced hysteretic *MR* at low bias. (right) cut showing that hysteresis vanishes at higher bias.

ascribe the latter to spin-dependent quantum interference in the NW. At low gate voltages, the Fermi wavelength is large, leading to stronger quantum interference effects. Electrons in the semiconductor NW acquire a phase as they propagate through the NW and a phase-shift when they are reflected at the NW-FM interface. Spin splitting due to Zeeman effects and Rashba spin-orbit coupling leads to different phases for the two spin species, affecting the quantum transmission probability for each spin, this forming a spin-filter device. To better understand the effects of the local spins on the MR, we have been performing micro-magnetic simulations using the Mumax package. In parallel, we have also been exploring ways to reduce the curvature of the FM near the interface with the NW (due to the shape of the NW) by using a planarization process. This will be an important task going forward.

In parallel, Frolov (U. Pittsburgh) has been focusing on developing NW-FM InSb-CoFe devices in various configurations. Starting with an InSb nanowire, CoFe contacts were fabricated in the spin-valve configuration. 3D micromagnetic simulations (OOMF) developed in collaboration with U. Minnesota suggest that contacts of 100-400 nm width and 20-50 nm thickness are in the single domain regime. Hysteretic magnetoconductance behavior was observed. Subsequently, non-local spin valve geometry was developed, with four contacts on a single InSb nanowire (two ferromagnetic CoFe and two non-magnetic Ti/Au contacts). It was observed that hysteretic magnetoconductance is strongly dependent on the setting of the voltage on the back gate which is the doped silicon substrate separated by 300 nm of thermal oxide. The amplitude and the sign of the hysteresis can be controlled by the gate, contrary to typical spin-valve behavior in diffusive semiconductor systems. Furthermore, hysteretic signals were observed even when current was passed between the two normal contacts flowing past the ferromagnetic contacts. A hypothesis has emerged that the hysteresis is due to dipolar coupling of stray magnetic fields from the ferromagnetic contacts to the nanowire, amplified by the large effective g-factor of InSb (the shape of the FM contacts employed at U. Pittsburgh is different from that used at U. Minnesota, like resulting in larger stray field effects). To test this, CoFe contacts were fabricated without etching the InSb oxide layer, i.e. in the same geometry but without any electrical contact to the nanowire. This confirmed that stray fields are the likely origin of the hysteretic behavior for the magnet shape used in Pittsburgh. Following this, effort has shifted to improving the stray field configuration to maximize the effect. This work is currently underway.

First-principle calculations**:** In the Marom group, we made a breakthrough for InAs/Al interface, which will help us explore interfaces involving InSb. Previous studies show that only MBJ and hybrid functionals could predict a correct band gap for InAs, while GGA and GGA+U fail to do so. However, we proved that GGA+U does work with a certain combination fo U values and it is much faster than MBJ and hybrid functionals. We successfully utilize a machine learning technique, Bayesian Optimization,to find a pair of U values for InAs which could be used in GGA+U method. The Bayesian Optimization itself is very suitable for finding unknown U values, it takes only 1 hr to get the U values compared to the 70 hrs with grid search method. The U we choose is -4 eV for In's p orbital and -9 eV for As's p orbital. The band structure is similar to the result of MBJ (Fig. 3) and it opens a band gap around 0.35 eV compared to experimental gap 0.41 eV and MBJ gives a gap of 0.6 eV.

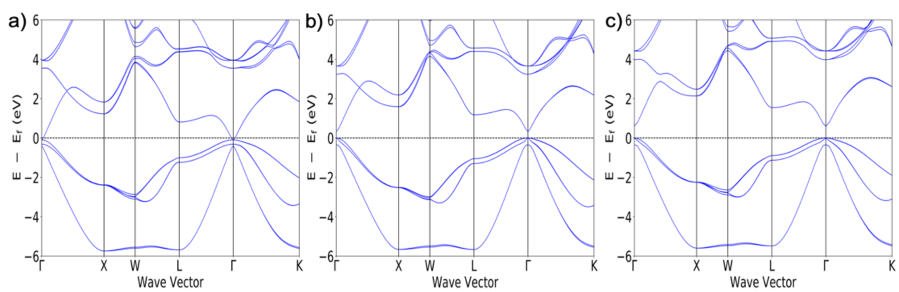

Figure 3: The band structure of InAs with GGA, GGA+U, MBJ in a), b), c), respectively

We also built a SnSe(111)/EuS(111) interface and a SnTe(111)/CaTe(111) with and without vacuum space, and compared their bands by VASP. A nontrivial topological surface state is found in Γ near the Fermi level for model 1. However, we found that this topological surface states on top and bottom are both broken in model 2 where the SnSe(111) is in contact with EuS(111) in both surfaces. In this case, we observed a gap of 20 meV is induced for the surface state. The Dirac cone on top is well preserved, but the Dirac cone on bottom which is in contact with EuS(111) is broken, resulting in a gap of 20 meV, same value as model 2. We believe this is caused by the magnetic proximity effect of EuS, since we observed a magnetic penetration for the first Se(-0.27 μB) and Sn (-0.07μB) atoms at bottom, while the pure SnSe shows a nonmagnetic properties. We are comparing these results with another SnTe/CaTe interface in order to compare the behavior of a magnetic interface to a non-magnetic one. Models related to SnTe(111)/CaTe(111) show that a topological surface state of SnTe can also be found in the Γ near the Fermi level. After calculating the band structure of SnTe(111) contacting with CaTe(111) on both sides, where CaTe is a non-magnetic semiconductor, we found that the Dirac cone is well preserved. We also studied the band structure where SnTe(111) only contacts CaTe(111) on one side. We find that the Dirac cone is also intact in this case. Comparing to SnSe(111)/EuS(111) interface, the non-magnetic CaTe layers do not break the topological surface states of the slab, which further proves the impact of magnetic effect on the topological surface states.

Future Plans

In Minnesota, the Crowell group will be focused on measurements of the tunneling anisotropic magnetoresistance (TAMR) using both DC magnetotransport and microwave rectification. After starting with prototype samples based on Fe, Co and Heusler alloys ($Co_2Mn_{1-x}Fe_xSi$) on GaAs, epitaxial samples will be prepared on $In_xGa_{1-x}As$ and InSb substrates. In addition to measuring the TAMR as a proxy for the strength of the interfacial spin-orbit coupling, the information on interfacial magnetism will be used to improve the InSb nanowire devices.

The Pribiag group will also transition from ex-situ to in-situ prepared interfaces, investigating InSb and InAs nanowire devices onto which Palmstrøm will have deposited FM and AFM materials. These will be selective-area growth wires and bottom-up wires prepared with the help of in-situ cleaning of the interface.

Going forward, stray fields from micromagnets can be used in the future to create local Zeeman splitting of InSb states and create Majorana zero modes without the use of external global fields. In the immediate future, the Frolov group will transition to fabricating superconducting and ferromagnetic contacts onto the same nanowire.

So far, the Marom group has been working on developing DFT methods to treat semiconductors, such as InAs and InSb, which erroneously come out metallic with standard DFT methods (e.g. the PBE functional), as shown for InAs in Figure 3a. Marom is currently developing a machine learning method for finding the optimal Hubbard U parameter in a GGA+U approach by Bayesian optimization. Her group has some promising results with an objective function that is only based on reproducing the band gap obtained by more accurate methods (namely the HSE hybrid functional), as shown in Figure 3b. This method works well for InAs and InSb and reproduces band structures obtained by HSE and MBJ (Figure 3c). However, it does not work well for other materials, such as EuS, because it reproduces the correct band gap but distorts the band structure. In the near term, the plan is to develop a more sophisticated objective function that also considers other features of the band structure, then apply these to the materials interfaces listed in Table 1 of our proposal.

Publications

None – new grant.

Project Title: Using Crystallization to Control Filler Dispersion and Vice Versa in Polymer Nanocomposites

PI:
Linda Schadler, Mechanical Engineering Department, University of Vermont
Sanat Kumar, Department of Chemical Engineering, Columbia University
Brian Benicewicz, Department of Chemistry and Biochemistry, University of South Carolina

Program Scope

To achieve the full promise of nanoparticle filled polymers, control over both filler organization and polymer morphology is required. Recent work demonstrated that there is a critical crystallization rate below which, nanoparticles will align in the interlamellar regions of semicrystalline polymers. This project explores the fundamental principles behind tailoring the organization of fillers by varying filler / matrix compatibility, filler diffusivity, and matrix molecular weight. A second component will focus on organizing fillers in the melt to alter matrix crystalline morphology. This abstract focuses on the former. Molecular dynamics (MD) simulations on a coarse-grained model were performed to study the effect of the particle size on the critical crystallization velocity in the nanoparticle limit. Experimentally, we successfully align layers of nanoparticles in the interlamellar spaces in poly(ethylene oxide) (PEO) through isothermal crystallization. We have explored the impact of graft density, graft molecular weight, and crystallization rate on this response. To achieve this same alignment in a broadly used engineering polymer, we developed the first method for grafting olefins to nanoparticles with control over both graft density and molecular weight. We have found that the degree of filler-matrix compatibility leads to a competition between filler organization and filler agglomeration leading to interlamellar alignment at low molecular weight, and larger scale alignment in higher molecular weight systems. While the nanoparticles are ordered by the crystallization process, they are still templated by the spherutlitic nature of the semicrystalline morphology. We go beyond beyond this limitation, and created one-dimensionally ordered NP structures, by using zone annealing to create elongated spherulites along the flow direction.

Key Recent Progress

(1) A new synthetic technique developed for linear polyethylene grafted chains on nanoparticles. A range of graft densities and molecular weights were achieved. This is exciting because of the potential impact for all nanofilled polyethylene, as well as the fundamental goals achieved in this project.
(2) The balance between repulsive and attractive interactions has been studied via molecular dynamics (MD) simulations on a coarse-grained model molecular dynamics (MD) simulations on a coarse-grained model. The critical growth velocity can be determined with the balance force. Using a more detailed model is necessary to capture the experimental

behavior of critical velocity, including incorporating the role of temperature gradients at the crystallization fronts.

(3) Linear nanoparticle organization in interlamellar spaces has been achieved within PMMA-g-silica Nanoparticle/PEO systems. Tuning the grafting density of PMMA chains on the silica can varying the uniformity of the nanoparticle dispersion, as predicted by the phase diagram by Kumar et al. SAXS patterns of melted composites shown difference in dispersions across a range of NP loadings.

(4) Successful good dispersion of C18 modified silica particles in high density polyethylene (HDPE) was achieved through solvent mixing. By controlling the rate of crystallization, we can tailor the organization of the nanofillers. The particles either organize in the interlamellar, interfibrillar, and interspherulitic zones. The result depends on the balance between nanoparticle aggregation, nanoparticle diffusivity and crystallization organization.

(5) Zone melting process was developed to create a melt front that provides more specific control over growing morphology. The uniformity of the zone annealing thermal processing history imparts unidirectional alignment of NPs in the direction of translation. Ongoing efforts to quantify the anisotropy involve calculating the Hermans orientation function for different positions along the samples.

(6) The impact of the morphology on mechanical and dielectric properties was investigated for both PEO and HDPE systems using DMA and dielectric spectroscopy. The effects of multiscale ordering can enhance the resulting modulus to the original neat polymer with relatively small amounts of filler and can balance the crystallinity effect on permittivity to optimize the dielectric properties of the polymer nanocomposite.

(7) Organization of PE grafted silica nanoparticles in the HDPE melt with preliminary impact on the crystallization behavior of the HDPE matrix were studied. Controlling the initial dispersion of nanoparticles in the melt state can significantly alter the confinement seen by the crystallization matrix. This has dramatic effects on the crystallization rate, crystallization morphology, and in turn the mechanical reinforcement or permittivity difference. Continued work has been done to study more drastic changes in the crystallization from controllably aggregated systems.

Future Plans

(1) Correlate the Hermans orientation function to the invariant calculation in order to get a more complete picture of the extent and direction of NP alignment in the zone annealing and isothermal crystallization experiments. Model the scattering profiles with Percus-Yevick structure factors to gain a deeper understanding of the physical parameters within our system.

(2) Judiciously integrate our experimental results with coarse-grained MD simulations to understand the physical phenomena that control the morphology of nanoparticle organization through crystallization.

(3) Tailor the compatibility of the nanoparticle with the HDPE matrix using bimodal grafted ligands with controlled grafting density to balance the inter nanoparticle interactions and nanoparticle diffusion rate. Develop a map of spherulitic growth velocity of silica/HDPE systems vs. isothermal crystallization to understand the mechanism of nanoparticle diffusivity and crystallization growth on nanoparticle alignment. For select nanofiller organizations, the mechanical and dielectric properties will be studied.

(4) Tune the surface ligands (such as grafting chain length, grafting density etc.) on nanofillers to tailor the enthalpic and entropic driving forces to develop the assembly of PE-grafted nanoparticles in HDPE matrices in the melt. Develop a morphology map (sheets, strings, uniform distribution, small clusters, aggregations) based on grafted brush/matrix Mw ratio and grafting density. Analyze how these morphologies can affect the matrix crystallization behavior in turn. The effects of fillers organization as well as crystalline morphology on mechanical and dielectric properties will be analyzed.

References

[1] A.J. Lovinger, C.C. Gryte, The Morphology of Directionally Solidified Poly(ethylene oxide) Spherulites, Macromolecules. 9 (1976) 247–253. doi:10.1021/ma60050a014.

[2] J. Blechinger, R. Herrmann, D. Kiener, F.J. García-García, C. Scheu, A. Reller, C. Bräuchle, Perylene-Labeled Silica Nanoparticles: Synthesis and Characterization of Three Novel Silica Nanoparticle Species for Live-Cell Imaging, Small. 6 (2010) 2427–2435. doi:10.1002/smll.201000762.

[3] D. Zhao, V. Gimenez-Pinto, A.M. Jimenez, L. Zhao, J. Jestin, S.K. Kumar, B. Kuei, E.D. Gomez, A.S. Prasad, L.S. Schadler, M.M. Khani, B.C. Benicewicz, Tunable Multiscale Nanoparticle Ordering by Polymer Crystallization, ACS Cent. Sci. 3 (2017) 751–758. doi:10.1021/acscentsci.7b00157.

[4] P. Akcora, H. Liu, S.K. Kumar, J. Moll, Y. Li, B.C. Benicewicz, L.S. Schadler, D. Acehan, A.Z. Panagiotopoulos, V. Pryamitsyn, V. Ganesan, J. Ilavsky, P. Thiyagarajan, R.H. Colby, J.F. Douglas, Anisotropic self-assembly of spherical polymer-grafted nanoparticles, Nat. Mater. 8 (2009) 354–359. doi:10.1038/nmat2404.

[5] S.K. Kumar, N. Jouault, B. Benicewicz, T. Neely, Nanocomposites with Polymer Grafted Nanoparticles, Macromolecules. 46 (2013) 3199–3214. doi:10.1021/ma4001385.

Publications

1. Pribyl, J., Benicewicz, B., Bell, M., Wagener, K., Ning, X., Schadler, L., Jimenez, A. and Kumar, S., 2019. Polyethylene Grafted Silica Nanoparticles Prepared via Surface-Initiated ROMP. *ACS Macro Letters*, 8, pp.228-232.
2. Pribyl, J., Benicewicz, B., 2019. Surface and Particle Modification via RAFT Polymerization: An Update. *Handbook of RAFT Polymerization* (invited chapter). Weinheim: Wiley-VCh (submitted).

3. Ning, N., Chittigori, J., Li, Y., Horner, G., Ullal C. and Schadler L, 2019. Photophysical Property Enhancement of Perylene Dye Molecules Using Nanoparticle Encapsulation Strategies for Luminescence Converter of Hybrid LED. *Journal of Colloid and Surface Interface Science* (submitted).
4. Jimenez, A., Krauskopf, A., Perez-Camargo, R., Zhao, D., Pribyl, J., Jestin, J., Benicewicz, B., Muller, A.J., Kumar, S.K. Effects of Hairy Nanoparticles on Polymer Crystallization Kinetics, *Macromolecules* (submitted).

Using Interfaces to Create Strongly-Coupled Magnetic-Ferroelectrics

Darrell G. Schlom[1], Craig J. Fennie[2], David A. Muller[2]

[1]Department of Material Science and Engineering, Cornell University, Ithaca, New York 14853

[2]School of Applied and Engineering Physics, Cornell University, Ithaca, New York 14853

Program Scope

Our objective is to create a ferromagnetic ferroelectric that can be deterministically switched between symmetry equivalent states using an electric field. The electric-field switching of a magnetization between 180° symmetry equivalent states has not been demonstrated in any material. The required coupling between ferroelectric and ferromagnetic domains allowing such switching is a missing feature in most multiferroics and is key to advancing the field both scientifically and technologically. Starting at the level of electrons and atoms our goal is to rationally design complex oxide heterostructures and interface-materials with this targeted emergent behavior. This is not a matter of simply optimizing material parameters, but rather begins with understanding a mechanism to control the interplay between the diverse microscopic degrees of freedom prevalent in complex oxides in order to achieve this desired behavior, and ends with the design of new material realizations. These realizations are in turn created with atomic-layer precision, structurally assessed to see that they are the intended realization, and finally their relevant properties are measured. In this program we will develop the scientific ideas necessary to apply this design paradigm to the creation of multiferroics with unprecedented coupling between ferroelectric and magnetic order parameters, i.e., strongly-coupled magnetic-ferroelectrics.

Recent Progress

Using a combination of theory and experiment, we discovered the world's first material that is simultaneously ferrimagnetic and ferroelectric at room temperature.[1] Materials that exhibit simultaneous order in their electric and magnetic ground states hold tremendous promise for enabling electrical control of magnetism. Such materials are, however, exceedingly rare as a consequence of the competing requirements for ferroelectricity and magnetism and until recently $BiFeO_3$ was the only material with this functionality at room temperature.[2-5] Unfortunately, $BiFeO_3$ is a slightly canted *anti*ferromagnet so the spontaneous magnetization of $BiFeO_3$ at room temperature is quite small (0.04±0.02 Bohr magnetons per iron atom).[6-9]

We recently discovered a means to hierarchically construct a single-phase multiferroic where ferroelectricity and strong magnetic ordering are coupled near room-temperature.[1] This involves a combination of interface engineering, epitaxial stabilization, polarization doping, and symmetry breaking. Starting with hexagonal $LuFeO_3$, a metastable geometric ferroelectric[10] with the greatest known planar rumpling, individual extra monolayers of FeO were introduced during growth to construct formula-unit-thick layers of ferrimagnetic $LuFe_2O_4$ within the $LuFeO_3$ matrix, more specifically, $(LuFeO_3)_m/(LuFe_2O_4)_1$ superlattices. Note that the stable polymorph of $LuFeO_3$ has a centrosymmetric perovskite structure in which the iron coordination polyhedron is an octahedron. As inversion symmetry precludes ferroelectric behaviour, the stable polymorph of $LuFeO_3$ is unwanted. We used epitaxial stabilization to achieve the desired hexagonal ferroelectric polymorph of $LuFeO_3$, where the iron coordination polyhedron is a trigonal bipyramid, by growing it on (111) YSZ.[11] Fabricating $(LuFeO_3)_m/(LuFe_2O_4)_1$ superlattices involves interface engineering. Cross-sectional TEM images of these superlattices shown in the figure below illustrate the severe rumpling imposed by the neighbouring $LuFeO_3$ that drives the ferrimagnetic $LuFe_2O_4$ into a simultaneously ferroelectric state, while also

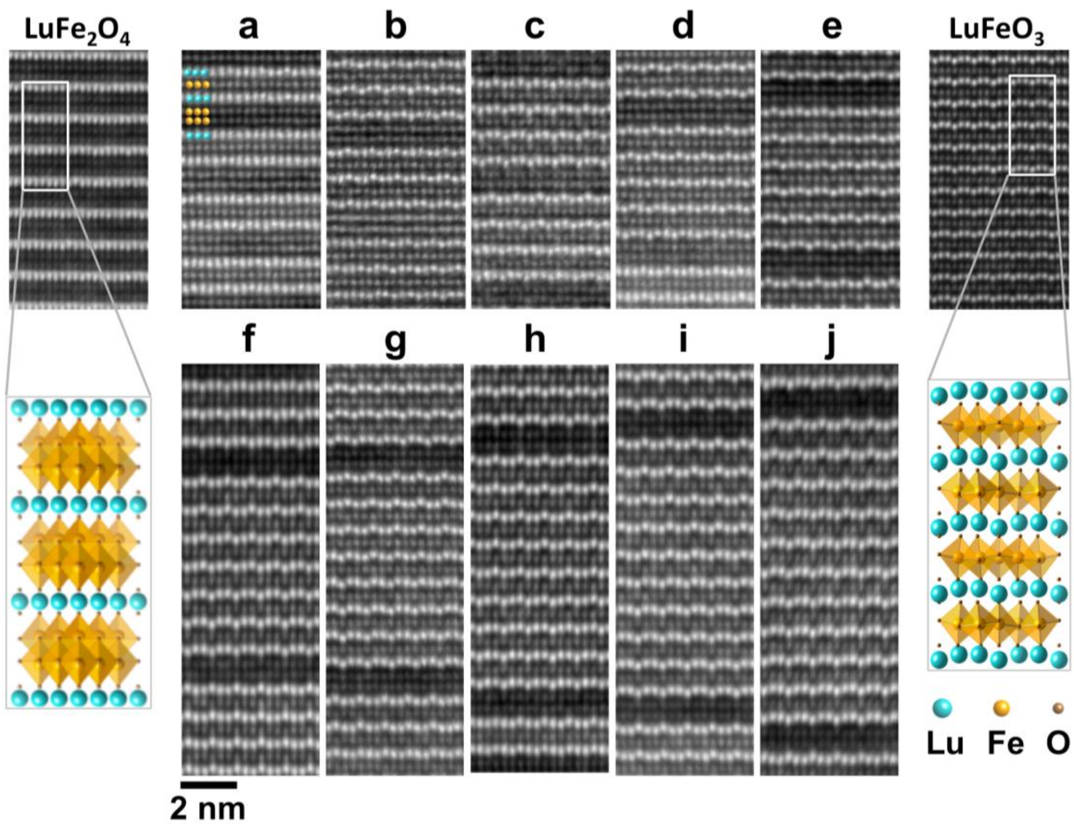

Creating an atomic-level composite between a ferrimagnet and a geometric ferroelectric. Alternating layers of the ferrimagnet $LuFe_2O_4$ (the crystal structure of which is shown at the left) and the geometric ferroelectric $LuFeO_3$ (shown at the right) were made by MBE. (a)-(j), Cross-sectional high-angle annular dark field scanning transmission electron microscopy (HAADF-STEM) images of $(LuFeO_3)_m/(LuFe_2O_4)_1$ superlattices with m=1 to 10. The severe rumpling imposed by the $LuFeO_3$ drives the ferrimagnetic $LuFe_2O_4$ into a simultaneously ferroelectric state, while also reducing the $LuFe_2O_4$ spin frustration. This increases the magnetic transition temperature to 281 K for $(LuFeO_3)_9/(LuFe_2O_4)_1$ shown in (i). Lu, Fe and O atoms are coloured turquoise, yellow and brown, respectively, in the crystal structures. (After Ref. 1) reducing the $LuFe_2O_4$ spin frustration. This rumpling increases the magnetic transition temperature significantly—from 240 K for $LuFe_2O_4$ to 281 K for $(LuFeO_3)_9/(LuFe_2O_4)_1$. Note that the rumpling from the $LuFeO_3$ imposes a local distortion on the neighbouring $LuFe_2O_4$—one that removes the mirror symmetry that the $LuFe_2O_4$ layers would otherwise have—and in so doing enables the $LuFe_2O_4$ to become simultaneously ferromagnetic and ferroelectric. As no macroscopic strain is involved, this rumpling is distinct from strain engineering. Importantly, in these superlattices the ferroelectric order couples to the ferrimagnetism, enabling electrical control of magnetism at 200 K.[1]

Our result demonstrates a design methodology for creating higher-temperature magnetoelectric multiferroics. The key aspect of this design methodology is to combine a frustrated magnetic system with a geometric ferroelectric that rumples it. In this case $LuFe_2O_4$ is the frustrated ferromagnetic and $LuFeO_3$ is the geometric ferroelectric. When brought into intimate atomic contact, the geometric ferroelectric distorts the ferrimagnet reducing its frustration. This reduced frustration leads to a higher magnetic ordering temperature of the ferrimagnet and is an example of how ferroelectricity can enhance magnetism. Though rare, that magnetism can be strengthened by ferroelectricity has been predicted[12] and seen in other systems[13] and is desired for producing superior multiferroics. Ongoing DOE-SISGR work has shown the possibility to create other related superlattices, with the possibility to enhance the magnetic ordering temperature through the introduction of ferrimagnetic spinels (for example, $CoFe_2O_4$) while seeking to maintain the ferroelectric coupling.

Future Plans

We have submitted a renewal proposal to depart from designing and creating multifunctional materials that are interesting/useful for their ground-state, *insulating* properties (i.e., the multiferroics we have worked on up to now) and apply our materials-by-design approach to identify new*, low-symmetry metallic* materials*:* non-centrosymmetric metals, which may also lack time-reversal symmetry. By doing so, we will greatly expand our toolset for designing materials that can enable future energy-efficient spin-based memory or logic devices.

References

1 J.A. Mundy, C.M. Brooks, M.E. Holtz, J.A. Moyer, H. Das, A.F. Rébola, J.T. Heron, J.D. Clarkson, S.M. Disseler, Z. Liu, A. Farhan, R. Held, R. Hovden, E. Padgett, Q. Mao, H. Paik, R. Misra, L.F. Kourkoutis, E. Arenholz, A. Scholl, J.A. Borchers, W.D. Ratcliff, R. Ramesh, C.J. Fennie, P. Schiffer, D.A. Muller, and D.G. Schlom, "Atomically Engineered Ferroic Layers Yield a Room-Temperature Magnetoelectric Multiferroic," *Nature* **537** (2016) 523–527.

[2] J. Wang, J.B. Neaton, H. Zheng, V. Nagarajan, S.B. Ogale, B. Liu, D. Viehland, V. Vaithyanathan, D.G. Schlom, U.V. Waghmare, N.A. Spaldin, K.M. Rabe, M. Wuttig, and R. Ramesh, "Epitaxial $BiFeO_3$ Multiferroic Thin Film Heterostructures," *Science* **299** (2003) 1719–1722.
[3] A.A. Belik, S. Iikubo, K. Kodama, N. Igawa, S.-I. Shamoto, S. Niitaka, M. Azuma, Y. Shimakawa, M. Takano, F. Izumi, and E. Takayama-Muromachi, "Neutron Powder Diffraction Study on the Crystal and Magnetic Structures of $BiCoO_3$," *Chem. Mater.* **18** (2006) 798–803.
[4] M.-R. Li, U. Adem, S.R.C. McMitchell, Z. Xu, C.I. Thomas, J.E. Warren, D.V. Giap, H. Niu, X. Wan, R.G. Palgrave, F. Schiffmann, F. Cora, B. Slater, T.L. Burnett, M.G. Cain, A.M. Abakumov, G. van Tendeloo, M.F. Thomas, M.J. Rosseinsky, and J.B. Claridge, "A Polar Corundum Oxide Displaying Weak Ferromagnetism at Room Temperature," *J. Am. Chem. Soc.* **134** (2012) 3737–3747.
[5] M.J. Pitcher, P. Mandal, M.S. Dyer, J. Alaria, P. Borisov, H. Niu, J.B. Claridge, and M.J. Rosseinsky, "Tilt Engineering of Spontaneous Polarization and Magnetization above 300 K in a Bulk Layered Perovskite," *Science* **347** (2015) 420–424.
[6] H. Béa, M. Bibes, A. Barthélémy, K. Bouzehouane, E. Jacquet, A. Khodan, J. P. Contour, S. Fusil, F. Wyczisk, A. Forget, D. Lebeugle, D. Colson, and M. Viret, "Influence of Parasitic Phases on the Properties of $BiFeO_3$ Epitaxial Thin Films," *Appl. Phys. Lett.* **87** (2005) 072508.
[7] J. Dho, X. Qi, H. Kim, J.L. MacManus-Driscoll, and M.G. Blamire, "Large Electric Polarization and Exchange Bias in Multiferroic $BiFeO_3$," *Adv. Mater.* **18** (2006) 1445–1448.
[8] T. Zhao, A. Scholl, F. Zavaliche, K. Lee, M. Barry, A. Doran, M.P. Cruz, Y.H. Chu, C. Ederer, N.A. Spaldin, R.R. Das, D.M. Kim, S.H. Baek, C.B. Eom, and R. Ramesh, "Electrical Control of Antiferromagnetic Domains in Multiferroic $BiFeO_3$ Films at Room Temperature," *Nat. Mater.* **5** (2006) 823–829.
[9] J.F. Ihlefeld, A. Kumar, V. Gopalan, D.G. Schlom, Y.B. Chen, X.Q. Pan, T. Heeg, J. Schubert, X. Ke, P. Schiffer, J. Orenstein, L.W. Martin, Y.H. Chu, and R. Ramesh, "Adsorption-Controlled Molecular-Beam Epitaxial Growth of $BiFeO_3$," *Appl. Phys. Lett.* **91** (2007) 071922.
[10]. Ederer, C. & Spaldin, N. A. Magnetoelectrics: A new route to magnetic ferroelectrics. *Nat. Mater.* **3,** 849–851 (2004).
[11]. Bossak, A. A. *et al.* XRD and HREM studies of epitaxially stabilized hexagonal orthoferrites $RFeO_3$ (R = Eu−Lu). *Chem. Mater.* **16,** 1751–1755 (2004).
[12] C.J. Fennie and K.M. Rabe, "Magnetic and Electric Phase Control in Epitaxial $EuTiO_3$ from First Principles," *Phys. Rev. Lett.* **97** (2006) 267602.
[13] J.H. Lee, L. Fang, E. Vlahos, X. Ke, Y.W. Jung, L.F. Kourkoutis, J-W. Kim, P.J. Ryan, T. Heeg, M. Roeckerath, V. Goian, M. Bernhagen, R. Uecker, P.C. Hammel, K.M. Rabe, S. Kamba, J. Schubert, J.W. Freeland, D.A. Muller, C.J. Fennie, P. Schiffer, V. Gopalan, E. Johnston-Halperin, and D.G. Schlom, "A Strong Ferroelectric Ferromagnet Created by means of Spin-Lattice Coupling," *Nature* **466** (2010) 954-958.

Publications

1. W. Wang, J.A. Mundy, C.M. Brooks, J.A. Moyer, M.E. Holtz, D.A. Muller, D.G. Schlom, and W. Wu, "Visualizing Weak Ferromagnetic Domains in Multiferroic Hexagonal Ferrite Thin Film," *Physical Review B* **95** (2017) 134443.
2. J.A. Mundy, J. Schaab, Y. Kumagai, A. Cano, M. Stengel, I.P. Krug, D.M. Gottlob, H. Doğanay, M.E. Holtz, R. Held, Z. Yan, E. Bourret, C.M. Schneider, D.G. Schlom, D.A. Muller, R. Ramesh, N.A. Spaldin, and D. Meier, "Functional Electronic Inversion Layers at Ferroelectric Domain Walls," *Nature Materials* **16** (2017) 622–627.
3. N.F. Quackenbush, H. Paik, M.E. Holtz, M.J. Wahila, J.A. Moyer, S. Barthel, T.O. Wehling, D.A. Arena, J.C. Woicik, D.A. Muller, D.G. Schlom, and L.F.J. Piper, "Reducing Orbital Occupancy in VO_2 Suppresses Mott Physics while Peierls Distortions Persist," *Physical Review B* **96** (2017) 081103.
4. L. Xie, L.Z. Li, C.A. Heikes, Y. Zhang, Z.J. Hong, P. Gao, C.T. Nelson, F. Xue, E. Kioupakis, L.Q. Chen, D.G. Schlom, P. Wang, and X.Q. Pan, "Giant Ferroelectric Polarization in Ultrathin Ferroelectrics via Boundary-Condition Engineering," *Advanced Materials* **29** (2017) 1701475.
5. M.E. Holtz, K. Shapovalov, J.A. Mundy, C.S. Chang, Z. Yan, E. Bourret, D.A. Muller, D. Meier, and A. Cano, "Topological Defects in Hexagonal Manganites: Inner Structure and Emergent Electrostatics," *Nano Letters* **17** (2017) 5883−5890.
6. Z. Chen, Z. Chen, Z.Q. Liu, M.E. Holtz, C.J. Li, X.R. Wang, W.M. Lü, M. Motapothula, L.S. Fan, J.A. Turcaud, L.R. Dedon, C. Frederick, R.J. Xu, R. Gao, A.T. N'Diaye, E. Arenholz, J.A. Mundy, T. Venkatesan, D.A. Muller, L.-W. Wang, J. Liu, and L.W. Martin, "Electron Accumulation and Emergent Magnetism in $LaMnO_3/SrTiO_3$ Heterostructures," *Physical Review Letters* **119** (2017) 156801.
7. J. Schaab, S.H. Skjærvø, S. Krohns, X. Dai, M.E. Holtz, A. Cano, M. Lilienblum, Z. Yan, E. Bourret, D.A. Muller, M. Fiebig, S.M. Selbach, and D. Meier, "Electrical Half-Wave Rectification at Ferroelectric Domain Walls," *Nature Nanotechnology* **13** (2018) 1028–1034.
8. H. Boschker, T. Harada, T. Asaba, R. Ashoori, A.V. Boris, H. Hilgenkamp, C.R. Hughes, M.E. Holtz, L. Li, D.A. Muller, H. Nair, P. Reith, X.R. Wang, D.G. Schlom, A. Soukiassian, J. Mannhart, "Ferromagnetism and Conductivity in Atomically Thin $SrRuO_3$," *Physical Review X* **9** (2019) 011027.
9. R. Ramesh and D.G. Schlom, "Creating Emergent Phenomena in Oxide Superlattices," *Nature Reviews Materials* **4** (2019) 257–268. (Cover Image)
10. S. Das, Y.L. Tang, Z. Hong, M.A.P. Gonçalves, M.R. McCarter, C. Klewe, K.X. Nguyen, F. Gómez-Ortiz, P. Shafer, E. Arenholz, V.A. Stoica, S.-L. Hsu, B. Wang, C. Ophus, J.F. Liu, C.T. Nelson, S. Saremi, B. Prasad, A.B. Mei, D.G. Schlom, J. Íñiguez, P. García-Fernández, D.A. Muller, L.Q. Chen, J. Junquera, L.W. Martin, and R. Ramesh, "Observation of Room-Temperature Polar Skyrmions," *Nature* **568** (2019) 368–372.

Probing the solidification of quasicrystals through joint experiment and simulation

Ashwin J. Shahani and Sharon C. Glotzer, University of Michigan, Ann Arbor, MI 48109

Program Scope

The long-term objective of this project is to identify the fundamental processes underlying the *self-assembly of quasicrystals*. For instance, how do clusters of atoms in the liquid phase organize themselves into a quasiperiodic lattice during solidification? What types of defects does the growing quasicrystal possess? Finally, how do these structural defects influence the growth shapes of the quasicrystals? Resolving these open questions requires a tight collaboration between experiment and simulation. In particular, **Shahani's** team is harnessing *in situ* dynamic transmission electron microscopy together with synchrotron-based X-ray imaging to peer into the growth dynamics of quasicrystals, covering a broad range of length scales and solidification pathways. In parallel, **Glotzer's** team is performing large-scale molecular dynamics simulations of quasicrystal growth using their massively parallel, GPU-enabled, open source HOOMD-blue software package. On the basis of the experiments and simulations (see **Fig. 1**), the collaborative team will advance a self-consistent theory of quasicrystal formation.

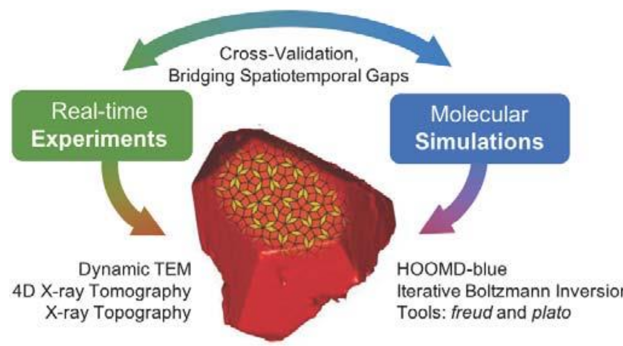

Fig. 1. *Overview of program*, showing the superposition of experimental data (*e.g.*, solid-liquid interfaces, in red) and simulation data (*e.g.*, tiling model, in yellow).

Recent Progress

Through synchrotron X-ray "live" imaging, **Shahani's** team has had the unique opportunity to capture the growth and equilibrium shapes of decagonal[1] and icosahedral[2] quasicrystals in a liquid. We have also compared the growth dynamics of a quasicrystal and its periodic approximant, finding significant differences between the two despite their similar structural motifs.[†] We have since turned our attention to the problem of growth interactions between quasicrystals. When the nucleation rate is relatively high, the nuclei ('seeds') may impinge on one another (*via* 'hard collisions'). Under ordinary circumstances, a grain boundary is formed between the two crystals. However, we recently observed through X-ray tomography that this may instead lead to the formation of single quasicrystals, devoid of dislocations, see **Fig. 2**. That is, the bicrystal relaxes into a single-crystal state. We expect that

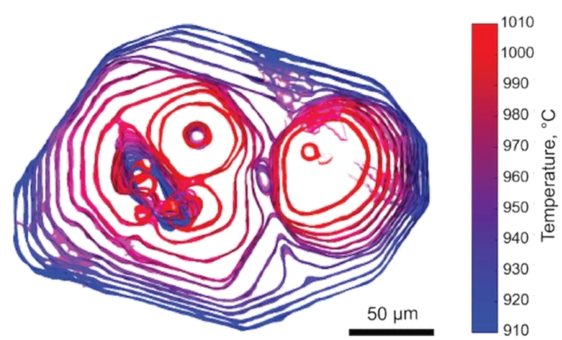

Fig. 2. *Isochrones of solid-liquid interfaces during crystallization.* At early stages (red) in growth, multiple QC particles can be observed; at longer times (blue) these particles impinge on each other and grow into a single QC with ten facets.

phasonic defects — that are unique to quasicrystals — may help distribute the coherency stresses, thereby suppressing dislocations. To determine if this hypothesis is correct, **Glotzer's** team developed a model describing a decagonal quasicrystal and used this force field to investigate two grains growing together, mimicking the experimental conditions as closely as possible. Our preliminary results match those of the experiments – namely, the absence of a grain boundary upon collision. Current efforts are directed towards extracting the phasonic strain field (where the crystals meet) by lifting the particles onto the four-dimensional hypercube lattice. In addition, we are deriving analytic data on the trajectory of every single atom using machine learning, which may provide a more direct and detailed view of phason flips. By varying the simulation conditions (*e.g.*, temperature and seed misorientation) and quantifying the particle dynamics in this manner, we can determine under what conditions the phason flips are dominant and single crystals are formed.

Future Plans

Shahani's team will conduct dynamic transmission electron microscopy (DTEM) studies of *quasicrystal nucleation and growth under far-from-equilibrium conditions* at Lawrence Livermore National Laboratory (LLNL). We have been granted access to LLNL in summer 2019. This instrument has the unique capability to monitor irreversible transformations down to nm and ns in space and time, respectively, which is a considerably finer resolution compared to synchrotron X-ray tomography. The DTEM experiments will be done in the 'movie-mode' configuration; that is, one ns (or fs) laser beam will trigger the melting of a thin film of quasicrystal composition while the second laser beam will generate the electron bunches (10^9 electrons) for subsequent TEM imaging and/or diffraction, see schematic in **Fig. 3**. The time-resolved images will provide clues of the origin of quasiperiodicity — one of the fundamental puzzles in the field of crystal growth — and determine whether classical or non-classical nucleation theories[3] apply. For instance, it may be found that the formation of the critical nucleus is correlated to icosahedral clusters in the fluid. If this is indeed the case, then it is interesting to consider whether the clusters have any properties that make them favorable hosts for quasicrystal nuclei, a question that can be readily answered using **Glotzer's** particle simulation toolkit.

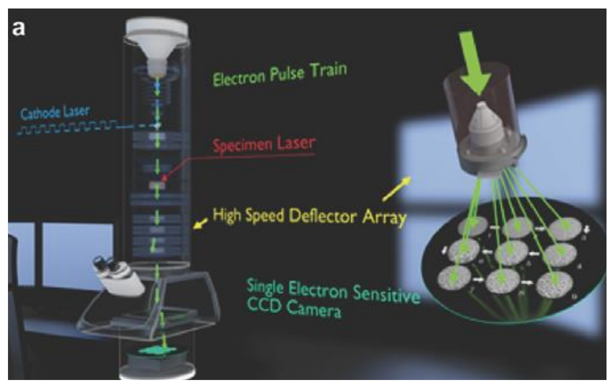

Fig. 3. *Schematic of DTEM*, in which one laser generates the electron pulses (green) for imaging while a second laser (red) provides the melting stimulus.

References

1. I. Han, X. Xiao, and A.J. Shahani, *Sci. Rep.* **7**, 17407 (2017).
2. N. Senabulya, I. Han, X. Xiao, and A.J. Shahani, *Scripta Mater.* **146**, 218-221 (2018).
3. P.J. Smeets, A.R. Finney, W.J. Habraken, F. Nudelman, H. Friedrich, J. Laven, J.J. De Yoreo, P.M. Rodger, and N.A. Sommerdijk, *Proc. Natl. Acad. Sci.* **114**, E7882-E790 (2017).

Publications

†□ I. Han, X. Xiao, H. Sun, and A.J. Shahani, *Acta Cryst. A* **75**, 281-296 (2019).

New inorganic compounds in shallow energy landscapes

Daniel P. Shoemaker, Materials Science and Engineering Department and Materials Research Laboratory, University of Illinois at Urbana-Champaign

Program Scope

The major goals of this project are to investigate rapid in situ materials discovery and kinetics, and understand how to interface the process with computational methods. Our project is demonstrating that the paths we take to make new materials can be made many times faster, and more hypothetical materials can be experimentally screened when we can watch reactions in real-time.

At the heart of our project is the ability to conduct materials synthesis with in-situ diffraction in-house, as a method of screening for new materials and understanding the kinetic barriers to compound formation. We began with trial systems in the Fe—Si—S and Fe—S systems to uncover routes to octahedral iron semiconductors.[1] The current goal is discover new phases while also developing mechanisms to probe relevant mechanisms that appeared in initial studies. Throughout the project, opportunities to interface enthalpy calculations and known kinetic data are crucial to leveraging our data for more efficient synthesis.

Recent Progress

Discovery of semiconducting sulfides: The grand challenge of synthesizing bulk materials by predictive design remains outstanding because the experimental thermodynamic and kinetic factors that influence synthesizability can quickly become intractable, even for well-known systems. Nevertheless, predictions that are sufficiently benchmarked by large amounts of quality data should have *predictable rates of success*. A coarse predictor, such as the synthesizability of a compound based on its bonding energy E as determined by density functional theory (DFT), has a success probability P less than 1. However, when a search space returns enough plausible hits N such that $NP > 1$, there should be a fertile ground. In this project, we found that multiple phase spaces without exotic elements obey this rule, and we present a family of previously undescribed zinc-based semiconductors, all

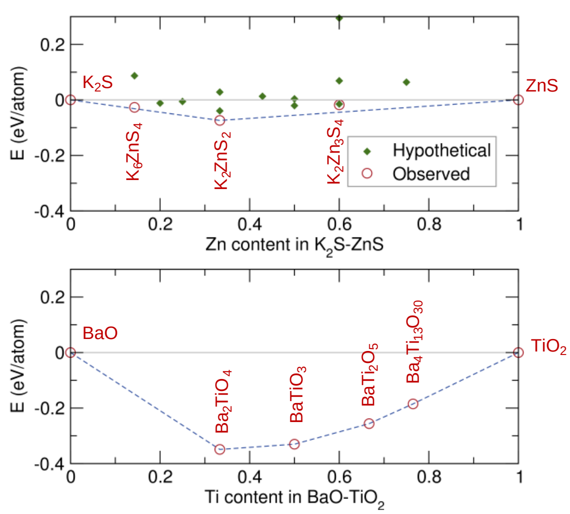

Figure 1. On top, DFT-derived enthalpies for ternary compounds along the K_2S-ZnS pseudobinary reveal many metastable crystal structures alongside the observed phases, all of which are extremely close ("flat") in energy. A comparison can be made to that of a deep ternary, the BaO—TiO_2 system at bottom.

of which exhibit known structure types and indicate the possibility of many such phases hiding in easily-accessible phase space.

We operate under the assumption that all predictions (e.g. bond energies E from DFT) are proxies for the Gibbs free energy G, which can only be approximated since it arises from the actual enthalpy and entropy of all compounds, which are many-body problems. While it may seem disheartening that G for a particular material cannot be predicted, a set of E approximations can return valuable information about the propensity to form new or metastable phases in a particular phase space.

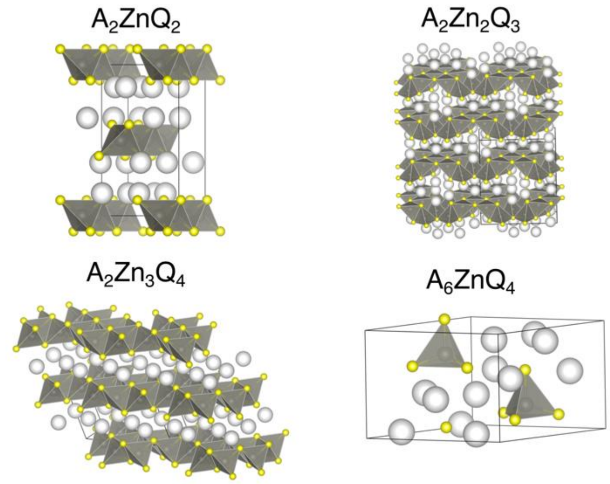

Figure 2. Structures of the new ternary zinc chalcogenide compounds A–Zn–Q with stoichiometry A_2ZnQ_2, $A_2Zn_2Q_3$, A_6ZnQ_4, and $A_2Zn_3Q_4$. The alkali metal, zinc and chalcogen are shown in white, gray and yellow respectively.

We begin with candidate structures in the A–Zn–Q systems where A = Na or K and Q = S or Se, and use a straightforward chemical substitution algorithm from Materials Project to generate candidate materials that exhibit known structure types.[2] The T = 0 K enthalpy is approximated using DFT-LDA for all the compounds, most of which we do not expect to be observed experimentally. The representative plot for the K—Zn—S system is shown in Figure 1, top. Two things should be noted here. First, the plots contain multiple polymorphs of certain compositions, indicating that the algorithm finds many plausible structures. Second, there are multiple phases with $\Delta E < 0.01$ eV/atom versus the end members, which is ten times smaller than a typical DFT "error bar" on E. This means that these landscapes are very flat; *i.e.* there are multiple compounds at multiple compositions that are plausibly stable.

These results validate our hypothesis that compound prediction is best performed statistically, and that high numbers of prospective phases are the best indicators of regions of phase space where new compounds are likely to form. The K_2S—ZnS system can be compared to a well-known system such as BaO—TiO_2, (Figure 1, bottom) which is a much deeper energy well.

We have isolated the new compounds $Na_2Zn_2S_3$, Na_2ZnSe_2, Na_6ZnSe_4, K_2ZnS_2, $K_2Zn_3S_4$, K_2ZnSe_2, and $K_2Zn_3Se_4$. Structures are shown in Figure 2. We have also verified the existence of additional compounds $Na_2Zn_3S_4$, K_6ZnS_4, $Na_2Zn_2Se_3$, and $K_2Zn_2S_3$. All these compounds are comprised of Zn tetrahedrally coordinated by S, but they vary in connectivity of these motifs from 0-D (isolated tetrahedra) to 2-D (sheets of edge-sharing tetrahedra). The UV-vis absorption spectra are shown for the selenides in Figure 3. More detailed studies of the optoelectronic behavior of these highly anisotropic compounds are underway.

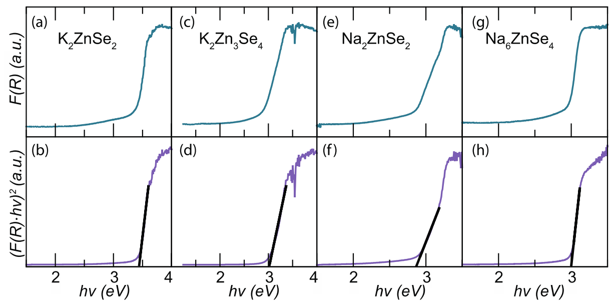

Figure 3. UV-Vis data for a selection of new alkali zinc selenides reveal band gaps between 3.0-3.5 eV.

Similar ternary zinc chalcogenides have shown interesting properties such as the Eu(II) activated Sr_2ZnS_3 phosphor, which possesses strong yellow emission and can be excited in the wide range by near-UV and blue light.[3] Similarly, Mn-activated Ba_2ZnS_3 is an important red phosphor material.[4] Ba_2ZnSe_3 has been evaluated for visible-light-responsive photocatalytic materials.[5] $Cs_2Zn_3Se_4$ and $Cs_2Zn_3Te_4$ have been predicted as potential p-type transparent conducting materials.[6] $BaTiS_3$ was recently shown to have giant optical anisotropy for use in linear and non-linear optics.[7]

Probing reactions in liquids: Experimental exploration of flat and complex energy landscapes often occurs in liquids and fluxes. We have used in-situ X-ray scattering to study flux reactions to great effect, and continue to do so as part of this project. Reactions in liquids represent a tremendous advantage in their flexible chemistry but pose distinct challenges in their small volume fraction of product. We commissioned a new proof-of-concept setup for energy-dispersive X-ray diffraction (EDXRD) of solvothermal reactions at the Advanced Photon Source (APS) beamline 6-ID, shown in Figure 4. This setup uses a large solvent-compatible oven with excellent temperature uniformity, which is the typical full-size oven that is used for ex-situ solvothermal reactions. This

Figure 4. Left: A custom-built class-A convection oven for reproducible solvothermal reactions, with beam ports on each side, in place at Advanced Photon Source beamline 6-ID for energy-dispersive X-ray diffraction (EDXRD) of Cu_4O_3 formation in ethanol-DMF. Right: The reaction tube inside the oven, with beam port on left marked by a square of Kapton and mylar tape.

setup was designed to study the formation of Cu_4O_3, a metastable oxide. In Figure 5, an hours-long data collection of the growth of Cu_4O_3 from copper nitrates in an ethanol-dimethylformamide (DMF) mixed solvent is shown. Unlike our previous ex-situ work examining the formation of this compound ex situ,[7] we see formation of Cu_4O_3 in less than an hour at 130°C. As part of our work understanding the formation mechanisms of this phase, we discovered a copper-ethylenediamine (en) complex [Cu(en-N)(en-N,N′)$_2$]$(NO_3)_2$ with a totally new five-fold copper coordination, which was accepted as a cover article in *CrystEngComm*.

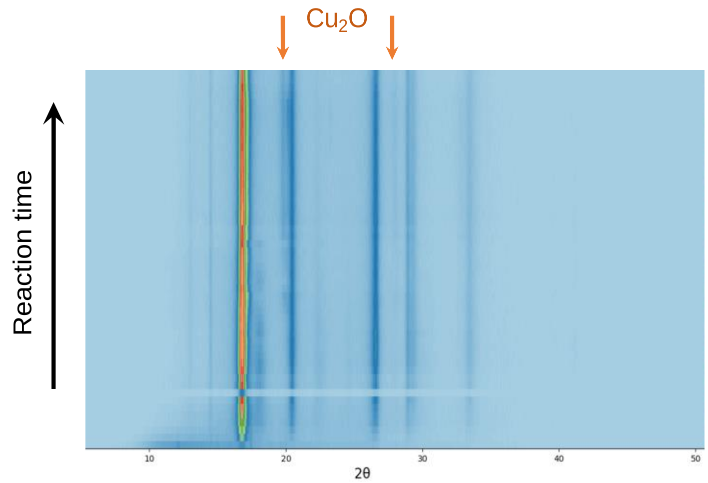

Figure 5. In situ EDXRD data of Cu_4O_3 formation, plotted with equivalent 2θ for Mo-Kα X-rays. Most peaks are Cu_4O_3, indicating fast formation that was totally unexpected after our ex situ trials. Some slow and minor conversion to Cu_2O (weak peaks arrowed) is evident. Total reaction time shown is 11 h.

Future Plans

Detailed electronic spectra are being calculated to understand the possible optoelectronic applications of the alkali zinc oxides. Further optimization of the search process is under way to understand how to apply this flatness criterion to understudied phase spaces. We found that probing the Cu_4O_3 reaction with EDXRD was effective when product was in the beam, but locating the product can be challenging due to lack of contrast when viewed with hard X-rays. Further optimization of the data collection parameters (beam intensity, spot size, and rastering) will establish best practices probing for a wide variety of reaction chemistries.

Flux reactions, while not discussed in this abstract, are amenable to the discovery of compounds in “flat” reaction spaces and can benefit for EDXRD studies. We performed encapsulated flux reactions of sulfur-rich Ba—Fe—S samples in situ at (APS) beamline 17-BM. Further technique development (pre-reaction amorphization, machine-learning pattern deconvolution) will be a valuable step toward disentangling diffraction data that contain many competing unknown phases.

References

1. Z. Jiang, *et al. J. Mater. Chem. C.* **5** 5709-5717 (2017)
2. G. Hautier, *et al. Inorg. Chem.* **50** 656–663 (2011)
3. V. Petrykin *et al. Chem. Mater*. **22** 5800–5802 (2010)
4. A. Vecht, *et al. J. Electrochem. Soc.* **121** C94–C94 (1974)
5. M. Zhou, *et al. Inorg. Chem*. **55** 12783–12790 (2016)
6. H. Shi, *et al. Phys. Rev. B* **90** 184104 (2014)
7. Z. Jiang, *et al. Chem. Mater*. **28** 3080-3089 (2016)

Publications

1. Z. Jiang, A. Ramanathan, D. P. Shoemaker. In situ Identification of Kinetic Factors that Expedite Inorganic Crystal Formation and Discovery. *J. Mater. Chem. C.* **5** 5709-5717 (2017)

2. R. D. McAuliffe, D. P. Shoemaker. Inflexible stoichiometry in bulk pyrite FeS_2 as viewed by in situ and high-resolution X-ray diffraction. *Acta Cryst. B* **74** 1-9 (2018)

3. J. Sharma, Z. Jiang, A. Bhutani, P. Behera, D. P. Shoemaker. A unique copper coordination structure with both mono- and bi-dentate ethylenediamine ligands. *CrystEngComm* **21** 2711-2711 (2019)

Exploring and Embracing Heterogeneity in Atomically Thin Energy Materials

Peter Sutter, Dept. of Electrical & Computer Engineering, University of Nebraska-Lincoln, Lincoln, NE 68588 (psutter@unl.edu); Eli Sutter, Dept. of Mechanical & Materials Engineering, University of Nebraska-Lincoln, Lincoln, NE 68588 (esutter@unl.edu)

Program Scope

Atomically thin semiconductors offer extraordinary opportunities for the manipulation of charge carriers, many-body optical excitations, quantum light emitters, and non-charge based quantum numbers. Confinement and reduced dielectric screening in these two-dimensional (2D) materials give rise to large characteristic energies so that many-body and quantum effects are important even at room temperature. Optical excitations in extended homogeneous areas have been investigated intensely, albeit mostly focusing on a limited set of materials, particularly transition metal dichalcogenides. Much less understood are light-matter interactions for other classes of 2D semiconductors, as well as effects that arise in heterogeneous materials, either near naturally occurring defects, impurities, edges and grain boundaries, or as a result of intentional interface formation in heterostructures. Addressing such systems experimentally involves significant challenges: *Understanding the atomistic growth mechanisms* of 2D semiconductors, so that novel systems with designed properties, specific 'imperfections', or controlled interfaces can be realized; and *probing of local excitations* at scales that match the relevant (nanometer) length scales in heterogeneous materials. Here, we address these challenges by harnessing quantitative *in-situ* microscopy to study the growth of 2D and layered semiconductors and heterostructures, combined with local spectroscopic measurements of quasiparticles excited at the nanometer scale. An integral part of the research is the development of novel experimental approaches, both for *in-situ* microscopy of synthesis and nanoscale spectroscopy. Experiments are guided and analyzed *via* computations of structure, chemistry, and excitation spectra. The particular materials focus is on group IV chalcogenides, a family of less explored 2D/layered semiconductors whose diversity in crystal structure and properties promises a fundamental understanding of novel classes of materials that meet core 21st century technology needs.

Recent Progress

Group IV monochalcogenides (*MX*; *M*: Sn, Ge; *X*: S, Se) are anisotropic 2D/layered compound analogues of black phosphorus/phosphorene. In bulk form, these semiconductors have long been considered for energy conversion applications (*e.g.*, photovoltaics) and showed exceptional characteristics, such as record thermoelectric performance. Recent calculations predicted a number of intriguing properties for single-layer group IV monochalcogenides, including large exciton binding energies, high carrier mobility, strain-tunable band offsets and

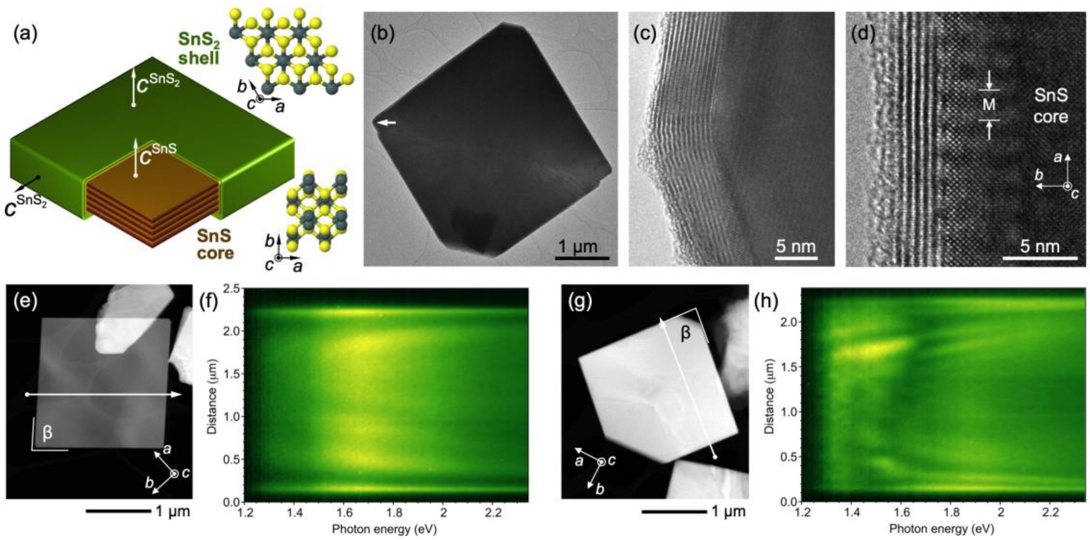

Figure 1: Wrap-around core-shell structures of layered crystals. (a) Schematic of SnS-SnS_2 core-shell crystals formed spontaneously by phase separation during growth. **(b)** TEM image of a typical µm-scale core-shell structure. **(c)** High-resolution TEM image showing a corner (arrow in (b)) with a layered SnS_2 shell tightly wrapped around the SnS core. **(d)** High-resolution image of the unconventional perpendicular interface between core and shell. 'M': Interlayer moiré pattern between van der Waals stacked SnS and SnS_2. **(e)-(f)** STEM image and hyperspectral CL linescan of a thin (45 nm) core-shell heterostructure. **(g)-(h)** STEM image and hyperspectral CL linescan of a thicker (80 nm) core-shell structure.

charge separation in lateral heterostructures, selective valley polarization, and coupled ferroelectricity and -elasticity up to above room temperature.

The controlled synthesis of few-layer and 2D group IV monochalcogenides, required to explore the unique properties of these materials, is a major challenge. To establish fundamental synthesis approaches for ultrathin *MX* crystals, we carried out extensive *in-situ* microscopy of SnS growth on van der Waals (vdW) substrates.[1] The results showed an unusual imbalance between strong adsorption on SnS nuclei and negligible sticking on the surrounding substrate, which favors vertical growth and complicates the synthesis of large ultrathin crystals. Using alternative ('reactive') vdW substrates and novel synthesis strategies, we were able to realize high quality few-layer SnS and GeS and identify their thickness-dependent properties. A comparison of shapes developed during growth and sublimation established that the typical crystal habits observed for SnS and related monochalcogenides are kinetic growth shapes rather than equilibrium (Wulff) shapes. This insight can guide the design of approaches for achieving particular shapes of SnS and related layered crystals.[2] *In-situ* electron microscopy identified the thermal stability and sublimation pathways of layered GeS, and demonstrated that GeS flakes self-encapsulate in a thin, sulfur-rich amorphous GeS_x shell during growth. In contrast to exfoliated GeS, which rapidly degrades when exposed to air, synthetic GeS flakes protected by GeS_x shells show no signs of chemical attack and remain stable in air for extended time periods.[3] Photoluminescence spectroscopy showed tunable bandgaps due to out-of-plane quantum confinement in GeS flakes below 100 nm thickness. Cathodoluminescence (CL) spectroscopy with nanoscale excitation showed interfacial charge transfer due to a type II heterojunction between the crystalline core and amorphous shell. Finally, locally excited CL provided

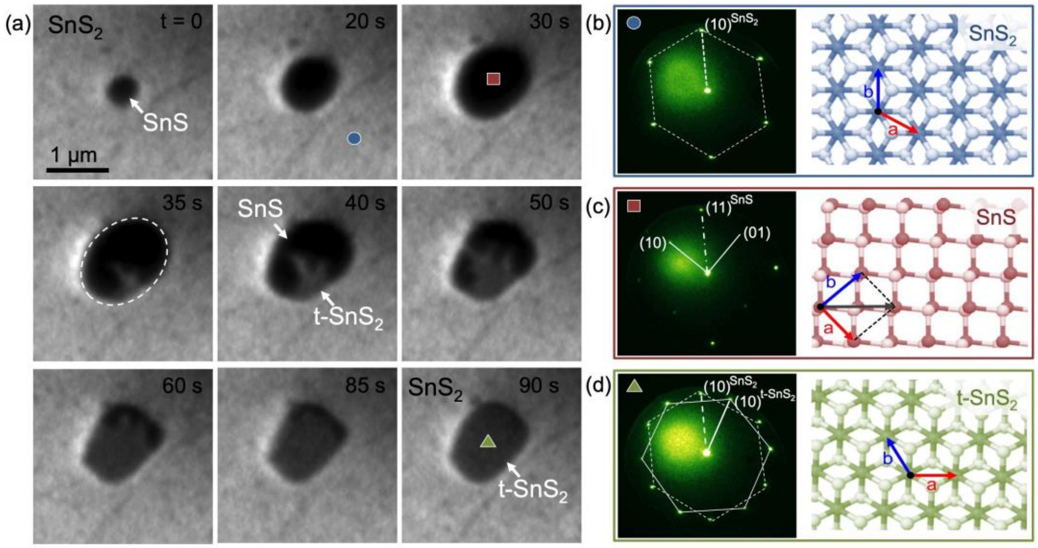

Figure 2: Synthesis of twisted van der Waals heterostructures. (a) Real-time low-energy electron microscopy during SnS growth on SnS_2, showing the spontaneous transformation of a SnS nucleus into twisted t-SnS_2. **(b)-(d)** Diffraction analysis of the competing surface phases and their orientation: SnS_2 substrate (b); initial SnS nuclei, azimuthally aligned with the SnS_2 substrate (c); and ultrathin 30° twisted t-SnS_2, formed by S-incorporation into the SnS intermediate (d).

measurements of the minority carrier diffusion length in p-type GeS, which is on par with the largest diffusion lengths reported for layered chalcogenide semiconductors.

A unique aspect of group IV chalcogenides is the existence of stable layered crystal phases with different chalcogen content, *i.e.*, MX, M_2X_3, and MX_2, and the facile reversible transformation between these phases by control of the chalcogen chemical potential. The structurally distinct and essentially immiscible phases present rich opportunities for exploring self-organization phenomena involving phase-separation and -conversion of layered crystals. SnS growth from mixed precursors containing S-rich minority phases causes the spontaneous formation of novel wrap-around core-shell structures, in which a phase separated single-crystalline SnS core is enclosed in a few-layer SnS_2 shell (Fig. 1).[4] STEM-CL spectroscopy with nanometer-scale excitation shows anisotropic carrier separation at type II core-shell hetero-interfaces, where holes and electrons are transferred to the SnS core and SnS_2 shell, respectively. Extreme infrared sensitization in light harvesting to photon energies significantly below the fundamental bandgaps of both constituent semiconductors is realized due to spatially indirect absorption at the abundant interfaces of the wrap-around core-shell structures.

VdW heterostructures between azimuthally misaligned (‘twisted’) layers have attracted considerable interest due to emergent optoelectronic and many-body correlation phenomena that arise in twist-moiré patterns. However, twisted heterostructures have been realized primarily by mechanical stacking of exfoliated crystals and no scalable synthesis methods offering twist control exist to date. Using group IV chalcogenides as model systems, we obtained fundamental insight into novel approaches for growing twisted vdW heterostructures. Real-time microscopy during the growth of ultrathin SnS on SnS_2 showed a striking transformation, in which initial

SnS nuclei with fixed azimuthal orientation relative to the substrate incorporate additional sulfur and spontaneously convert to few-layer SnS_2 (Fig. 2).[5] Importantly, the resulting t-SnS_2 does not adopt the equilibrium aligned (0°) stacking with the underlying SnS_2 support, but its orientation (30° twisted) is determined by the intermediate SnS crystal. These findings point to a general strategy in which a sacrificial intermediate phase is employed to realize twisted vdW heterostructures by bottom-up synthesis. While the above approach readily provides large twist angles, obtaining controlled small interlayer twists presents additional challenges. We identified a novel architecture, van der Waals nanowires – implemented using layered GeS as a model system – in which small interlayer twists arise spontaneously during growth.[6] Eshelby twist causes a chiral structure of the layered GeS nanowires so that the in-plane crystal axes progressively rotate and layers in adjacent turns of the helix naturally form a twist moiré pattern. The axial rotation and the twist moiré are tunable via the nanowire diameter. Our combined findings demonstrate novel approaches toward the scalable fabrication of vdW structures with defined twist angles, for which interlayer moirés are realized either at planar interfaces or on helical paths along layered nanowires.

Future Plans

Combining *in-situ* microscopy of synthesis processes and nanometer-scale optoelectronic probes creates unique opportunities for exploring the controlled synthesis and emerging phenomena in atomically thin energy and quantum materials. By understanding the fundamental growth processes, we can identify synthesis protocols for ultrathin group IV chalcogenide semiconductors and test theoretical predictions of their properties, *e.g.*, strongly bound excitons and ferroelectricity/elasticity. Focusing on these materials, we already demonstrated the spontaneous formation of a rich set of unconventional heterostructures. We will further systematically explore phase-conversion and -separation phenomena to realize novel heterostructure architectures and establish their interfacial light-matter interactions using local CL spectroscopy and mapping. By addressing these and other emerging phenomena, such as single photon emission and controlled valley polarization, we will realize the overarching goals of this program: A fundamental understanding of the ways in which defects, edges, and judiciously placed interfaces affect the interactions between light and many-body excitations, and its translation into robust materials platforms that harness imperfections for new functionality in energy conversion or quantum information processing.

References

[1] P. Sutter and E. Sutter, ACS Appl. Nano Mater. **1**, 3026 (2018).
[2] E. Sutter, J. Wang, and E. Sutter, Chem. Mater. **31**, 2563 (2019).
[3] E. Sutter, B. Zhang, M. Sun, and P. Sutter, in review (2019).
[4] P. Sutter, J.Wang, and E. Sutter, Adv. Mater., DOI: 10.1002/adma.201902166 (2019).
[5] P. Sutter, R. Ibragimova, H.-P. Komsa, B.A. Parkinson, and E. Sutter, in review (2019).
[6] P. Sutter, S. Wimer, and E. Sutter, Nature **570**, 354–357 (2019).

Publications

1. H. Qin, X. Chen, J. Li, P. Sutter, and G. Zhou, *Atomic-Step Induced Local Non-Equilibrium Effects on Surface Oxidation*, Journal of Physical Chemistry C **121**, 22846 (2017). [**DOI:** 10.1021/acs.jpcc.7b07321]
2. P. Sutter, H.-P. Komsa, A.V. Krasheninnikov, Y. Huang, and E. Sutter, *Defect Generation During Structural Transformations of Layered Tin Dichalcogenides*, Applied Physics Letters **111**, 262102 (2017). Highlighted in AIP *Scilight*, DOI: /10.1063/1.5020516. [**DOI:** 10.1063/1.5007060]
3. B. Maughan, P. Zahl, P. Sutter and O. L. A. Monti, *Configuration-Specific Electronic Structure of Strongly Interacting Interfaces: TiOPc on Cu(110)*, Physical Review B **96**, 235133 (2017). [**DOI:** 10.1103/PhysRevB.96.235133]
4. Y. Huang, E. Sutter, and P. Sutter, *Thick Layered Semiconductor Devices with Water Top-Gates: High On-Off Ratio Field-Effect Transistors and Aqueous Sensors*, ACS Applied Materials & Interfaces **10**, 23198 (2018). [**DOI:** 10.1021/acsami.8b05932]
5. P. Sutter and E. Sutter, *Growth Mechanisms of Anisotropic Layered Group IV Chalcogenides on van der Waals Substrates for Energy Conversion Applications*, ACS Applied Nano Materials **1**, 3026 (2018). Cover of ACS Applied Nano Materials. [**DOI:** 10.1021/acsanm.8b00660]
6. P. Sutter, C. Argyropoulos, and E. Sutter, *Germanium Sulfide Nano-Optics Probed by STEM-Cathodoluminescence Spectroscopy*, Nano Letters **18**, 4576 (2018). [**DOI:** 10.1021/acs.nanolett.8b01840]
7. P. Sutter, S. Wimer, and E. Sutter, *Chiral Twisted van der Waals Nanowires*, Nature **570**, 354 (2019). [**DOI:** 10.1038/s41586-019-1147-x]
8. E. Sutter, J. Wang, and E. Sutter, *Nanoparticle-Templated Thickness Controlled Growth, Thermal Stability, and Decomposition of Ultrathin Tin Sulfide Plates*, Chemistry of Materials **31**, 2563 (2019). [**DOI:** 10.1021/acs.chemmater.9b00177]
9. P. Sutter, J. Wang, and E. Sutter, *Wrap-Around Core‑Shell Heterostructures of Layered Crystals*, Advanced Materials (2019) [**DOI:** 10.1002/adma.201902166]
10. P. Sutter, R. Ibragimova, H.-P. Komsa, B.A. Parkinson, and E. Sutter, *Self-Organized Twist-Heterostructures via Aligned van der Waals Epitaxy and Solid-State Transformations*, in review (2019).
11. E. Sutter, B. Zhang, M. Sun, and P. Sutter, *Few-Layer Germanium (II) Sulfide: Synthesis, Structure, Stability, and Optoelectronics*, in review (2019).

Spin Coating Epitaxial Semiconductors

Jay A. Switzer

Department of Chemistry & Materials Research Center

Missouri University of Science and Technology

Rolla, MO 65409-1170

jswitzer@mst.edu

Program Scope

Our work focuses on using solution methods such as electrodeposition to produce epitaxial films of semiconductors, optical materials, and catalysts. Epitaxy is the growth of crystals whose orientation is determined by their crystalline substrate (*1*, *2*). Epitaxy can produce thin films with atomic perfection that rivals that of single crystals as well as metastable phases (such as body-centered cubic Ni on Fe and face-centered cubic Fe on Cu), superlattices, quantum wells, and strained-layer architectures with tunable properties (*2*). Although epitaxial growth is usually constrained to ultrahigh vacuum or high temperatures by techniques such as molecular beam epitaxy, chemical vapor deposition, and liquid-phase epitaxy, it was first demonstrated in aqueous solution in 1836 when Frankenheim showed that sodium nitrate crystals could be grown epitaxially on a freshly cleaved calcite substrate (*3*). In 1950, Johnson also used aqueous solution to grow NaCl crystals epitaxially on single-crystal Ag (*4*). Other examples of solution-based deposition of epitaxial films are hydrothermal processing (*5*), chemical bath deposition (*6*-*8*), and electrodeposition (*9*-*11*). Each of these solution methods has limitations. Hydrothermal processing requires high temperature and pressure, chemical bath deposition requires specific reactions to occur at the substrate surface, and electrodeposition requires conducting or semiconducting substrates.

Recent Progress

Spin-coated films, such as photoresists for lithography or perovskite films for solar cells, are either amorphous or polycrystalline. Here, we show that epitaxial films of inorganic materials such as $CsPbBr_3$, PbI_2, ZnO, and NaCl can be deposited onto a variety of single crystal and single-crystal-like substrates by simply spin coating either solutions of the material or precursors to the material. The out-of-plane and in-plane orientation of the spin-coated films is determined by the substrate. The thin stagnant layer of supersaturated solution produced during spin coating promotes heterogeneous nucleation of the material onto the single-crystal substrate over homogeneous nucleation in the bulk solution, and ordered anion adlayers may lower the activation energy for nucleation on the surface. The method can be used to produce functional materials such as inorganic semiconductors or to deposit water-soluble materials such as NaCl that can serve as growth templates.

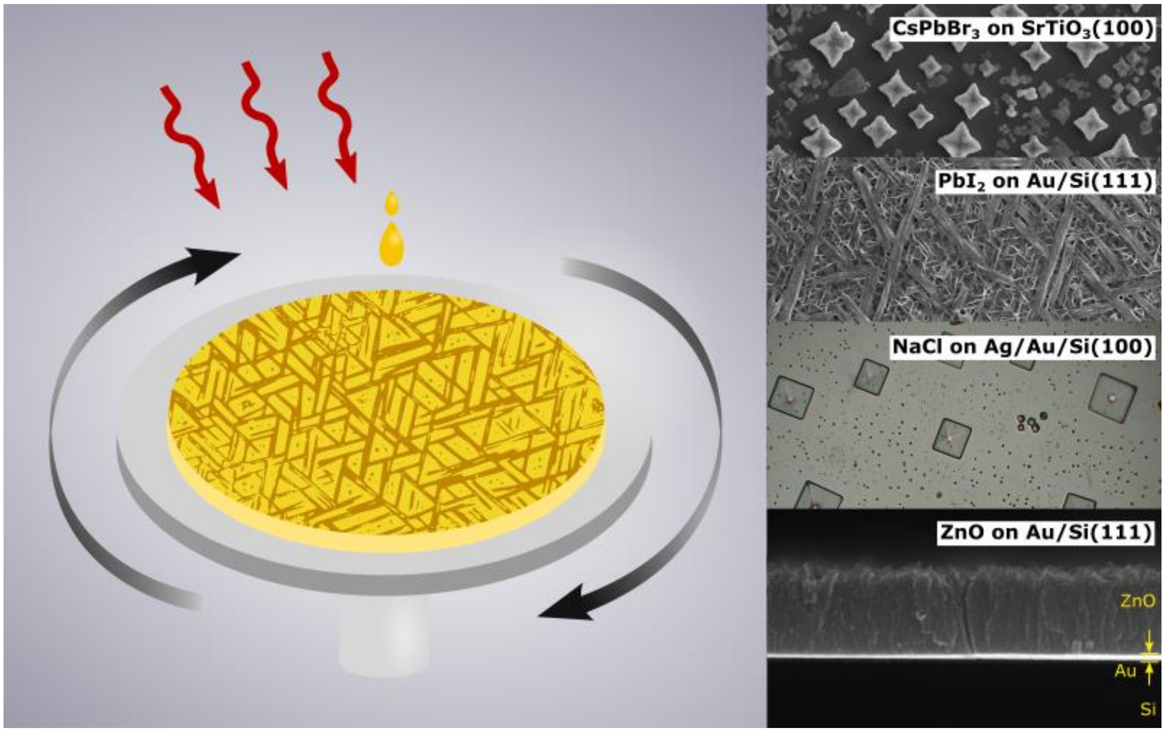

Fig. 1. A new spin on epitaxy. Left : spin-coating scheme. Right : micrographs of spin-coated $CsPbBr_3$, PbI_2, NaCl, and ZnO on single crystal and single-crystal-like substrates.

Future Plans

1. Spin coating epitaxial semiconductors for photovoltaics.
    a. Can we spin coat epitaxial metal sulfides?
    b. Construct perovskite solar cell – need electron and hole conducting layers.
    c. Minimize electron-hole recombination?
2. Chiral Surfaces.
    a. Chiral catalysis (e.g., oxidation of L and D dopa) and chiral crystallization on Au(643) and on Au(111) with cysteine self-assembled monolayers.
3. Topotactic conversion of metal oxides and halides to epitaxial metal chalcogenides.

References

1. G. B. Stringfellow, Epitaxy. *Rep. Prog. Phys.* **45**, 469-529 (1982).
2. E. G. Bauer *et al.*, Fundamental issues in heteroepitaxy—A Department of Energy, Council on Materials Science Panel Report. *J. Mater. Res.* **5**, 852-894 (1990).

3. M. L. Frankenheim, Uber die Verbindung vershiedenartiger Kristalle. *Ann. Phys.* **113**, 516-522 (1836).
4. G. W. Johnson, Some Observations on the Epitaxy of Sodium Chloride on Silver. *J. Appl. Phys.* **21**, 1057-1062 (1950).
5. D. Andeen, L. Loeffler, N. Padture, F. F. Lange, Crystal chemistry of epitaxial ZnO on (111) $MgAl_2O_4$ produced by hydrothermal synthesis. *J. Cryst. Growth* **259**, 103-109 (2003).
6. M. Froment, M. C. Bernard, R. Cortès, B. Mokili, D. Lincot, Study of CdS Epitaxial Films Chemically Deposited from Aqueous Solutions on InP Single Crystals. *J. Electrochem. Soc.* **142**, 2642-2649 (1995).
7. S. Sengupta *et al.*, Chemical epitaxy and interfacial reactivity in solution deposited PbS on ZnTe. *J. Mater. Chem. C* **4**, 1996-2002 (2016).
8. O. Friedman, D. Korn, V. Ezersky, Y. Golan, Chemical epitaxy of CdSe on GaAs. *CrystEngComm* **19**, 5381-5389 (2017).
9. R. Liu, A. A. Vertegel, E. W. Bohannan, T. A. Sorenson, J. A. Switzer, Epitaxial electrodeposition of zinc oxide nanopillars on single-crystal gold. *Chem. Mater.* **13**, 508-512 (2001).
10. R. Liu, F. Oba, E. W. Bohannan, F. Ernst, J. A. Switzer, Shape control in epitaxial electrodeposition: Cu_2O nanocubes on InP(001). *Chem. Mater.* **15**, 4882-4885 (2003).
11. N. K. Mahenderkar *et al.*, Epitaxial lift-off of electrodeposited single-crystal gold foils for flexible electronics. *Science* **355**, 1203-1206 (2017).

Publications over last two years resulting from work supported by the DOE project

1. N. K. Mahenderkar, Q. Chen, Y.–C. Liu, A. R. Duchild, S. Hofheins, E. Chason, and J. A. Switzer, "Epitaxial lift-off of electrodeposited single-crystal gold foils for flexible electronics," *Science* **355**, 1203-1206 (2017).

2. Q. Chen and J. A. Switzer, "Photoelectrochemistry of Ultrathin, Semitransparent, and Catalytic Gold Films Electrodeposited Epitaxially onto n-Silicon(111)," *ACS Appl. Mater. Interfaces* **10**, 21365-21371 (2018).

3. M. V. Kelso, J. Z. Tubbesing, and J. A. Switzer, "Epitaxial Electrodeposition of Chiral Metal Surfaces on Silicon(643)," *J. Am. Chem. Soc.* **140**, 15812-15819 (2018).

4. C. M. Hull and J. A. Switzer, "Epitaxial Electrodeposition of Copper(100) onto Silicon(100) and Lift-off of Single-Crystal-Like Cu(100) Foils," *ACS Appl. Mater. Interfaces* **10**, 38596-38602 (2018).

5. Q. Chen and J. A. Switzer, "Electrodeposition of nanometer-thick epitaxial films of silver onto single-crystal silicon wafers," *J. Mater. Chem. C* **7**, 1720-1725 (2019).

6. M. V. Kelso, N. K. Mahenderkar, Q. Chen, J. Z. Tubbesing, and J. A. Switzer, "Spin coating epitaxial films," *Science* **364**, 166-169 (2019).

Elucidating the Morphological Instability Mechanisms During Electrodeposition of Active Metals

Ming Tang, Department of Materials Science and NanoEngineering, Rice University

Program Scope

The overarching goal of this project is to understand how a group of metals with relevance to batteries develop unstable growth morphology during electrodeposition, a process important for the functionality of batteries. These metals include alkali metals (e.g. lithium, sodium and potassium) and zinc, which have high atomic mobility and reactivity with electrolytes. While they are attractive electrode candidates for the next-generation rechargeable batteries, the prevalent formation of highly non-uniform electroplating morphologies presents a major barrier to their successful application by causing rapid capacity fading and internal shorting of the batteries. This project focuses on examining two hypotheses on the mechanism of unstable growth during electrodeposition of such systems by using on zinc as a model system, namely: I) A stress-related morphological instability mechanism generally operates in this group of active metals; II) The complex mossy structure of electroplated active metals results from a stress-driven nucleation and defect-mediated growth process. Accordingly, the project has three specific objectives: 1) Investigate the relation between plating stress and morphology, 2) Characterize the microstructure of mossy electrodeposits, 3) Model stress-enhanced morphological instability phenomena.

Recent Progress

I. Effect of plating stress on zinc electroplating morphology

Similar to our previous finding in lithium[1], we discovered that plating stress also plays a significant role in initiating mossy structure in zinc electrodeposition, which provides strong support to our Hypothesis I that a common stress-induced morphological instability mechanism operates in the active metal group (alkali elements, Zn, Cd). We conducted comparative study of electroplating zinc on soft vs hard substrates to examine the effect of plating stress on deposition morphology. As shown in Figure 1a, surface profile measurement reveals the periodic wrinkling pattern of soft substrate after zinc deposition, which confirms the presence of compressive stress in zinc during electroplating. The measured wrinkle periodicity agrees well with the small deformation theory. After wrinkling, residual stress in zinc plated on soft substrate is relieved to lower level. Under

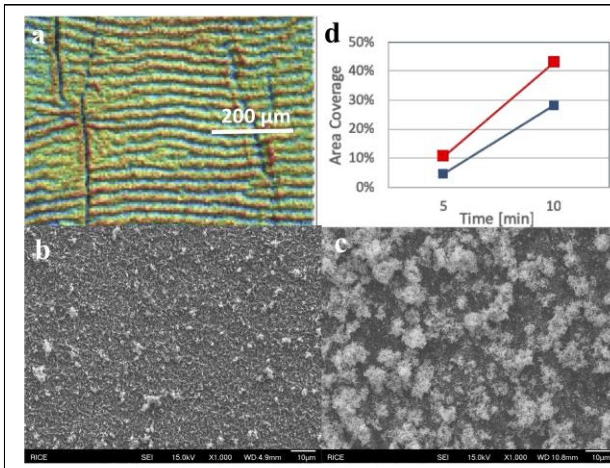

Fig. 1 Zinc electrodeposition on soft vs hard substrate. a) Wrinkle pattern on soft substrate after zinc plating. **b) & c)** Morphology of zinc deposit on soft (b) and hard (c) substrate after plating at 10 mA/cm^2 for 5 min. **d)** Area coverage of mossy zinc on soft (blue line) vs hard (red line) substrate.

otherwise the same condition, zinc plating on soft substrate (Figure 1b) exhibits ~50% fewer mossy zinc deposits (bright regions) than on hard substrate without stress relaxation (Figure 1c), in both number count and area coverage. The difference persists with increasing plating time. The observed difference provides evidence that plating stress does contribute to the nucleation of zinc mossy structure and its elimination can suppress the mossy growth.

II. Microstructure characterization of zinc mossy structure

We performed the first detailed TEM characterization of individual zinc filaments (Fig. 2a) in the mossy deposits, with the goal to identify the filament growth direction and defects present. The zinc filaments are found to grow along the <210> axis (Fig. 2b, c). A surprising finding is that that the filaments are single-crystalline in nature despite the presence of topological defects such as kinks and branch points. This is proven by the continuous lattice fringes across the kink (Fig. 2b) and the single diffraction pattern of the branching point of the filament (Fig. 2d inset). We note that these observations are remarkably similar to the recent cryo-TEM characterization of kinked single-crystalline filaments in lithium mossy structure[2]. The similarity between the filament structures of electroplated lithium and zinc provides further support to the existence of a universal morphological instability mechanism among active metals.

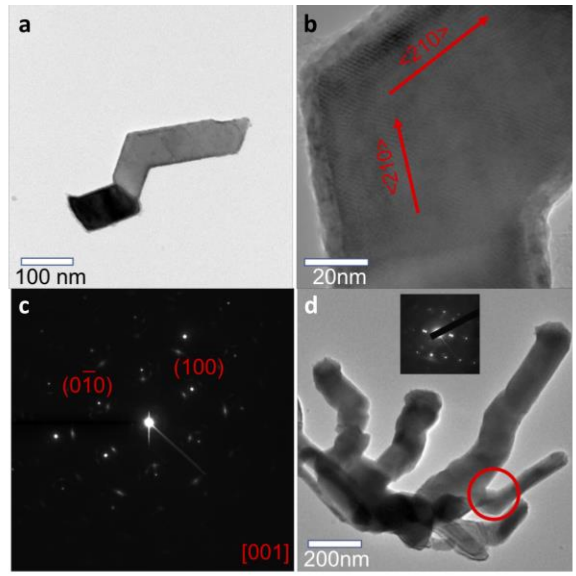

Fig. 2 TEM characterization of zinc filaments. a) TEM image of a kinked filament from mossy zinc structure. b) Same zinc filament at higher resolution, with defect visible at the kink. c) Selected area diffraction (SAD) confirms that the filament grows along <210>. The weak diffraction pattern belongs to surface zinc oxide. d) TEM image of a branched zinc filament. SAD of the circled region shows reveals only one diffraction pattern (inset), confirming the single crystallinity of the branched filament.

In addition to characterization at the single filament level, we applied FIB/SEM to reconstruct the mossy zinc's filament network structure. We developed a novel pre-FIB sample preparation procedure, in which PMMA is spin coated onto electroplated zinc surface and penetrates into the pore space inside mossy zinc under capillary force, followed by cross-linking PMMA. Compared to conventional pore filling by gas-deposited carbon or Pt, this method can achieve a much higher degree of pore filling, which significantly enhances the contrast of filaments (Figure 3a) and eliminates potential reconstruction artifacts due to the presence of residual voids within mossy zinc. Using the approach, several individual mossy zinc structures have been reconstructed to reveal their internal microstructure for the first time. One example is shown in Figure 3b. Analysis of topological and statistical features of reconstructed mossy zinc shows that zinc filaments frequently branches or bifurcates during the unstable mossy growth, see Figure 3c. This contributes to the fast growth kinetics of the mossy structure. Notably, the average filament length between two neighbor branch points displays no or only slight increase with electroplating time, Figure 3d, which suggests that filament branching is a steady state process. Currently, the detailed topological and geometrical information obtained from FIB/SEM reconstruction provides valuable guidance to the development of a kinetic model of mossy zinc growth process.

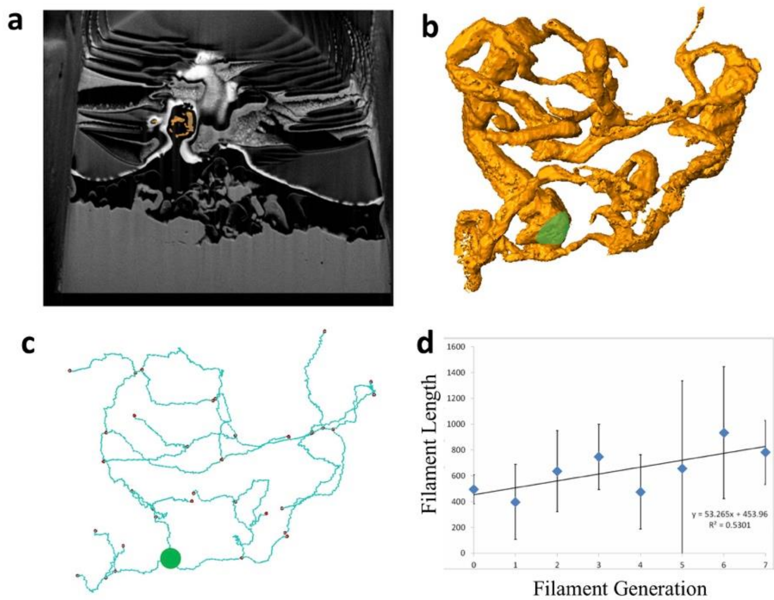

Fig. 3 FIB/SEM reconstruction of mossy zinc. **a)** SEM image of a FIB-ed cross section of zinc moss (medium bright color) filled with PMMA (dark) and covered by a 20nm gold layer (bright). **b)** A reconstructed zinc moss, which is highlighted in orange in a). **c)** Skeletonized view of the reconstructed mossy structure in b), with its base marked by the green circle. Red dots represent 3-way branch points or end points of the filaments. **d)** Zinc filament length between two neighbor branching points as a function of the filament generation, defined as the number of branch points between the filament and mossy structure base.

III. Modeling of stress-induced morphological instability in electrochemical processes

In addressing Objective 3, progress was made in understanding the effect of stress on morphological evolution in the broad context of electrochemical processes relevant to energy storage. As a prelude to the study of stress-induced unstable growth in electrodeposition, which involves the interplay between stress, surface reaction and mass transfer, we first considered a related but simpler phenomenon of stress-induced instability in electrochemical ion intercalation in battery compounds. Through this exercise, we aim to develop the necessary theoretical tools for studying the more involved phenomena in electroplating. Using linear stability analysis, we show that an initially flat ion intercalation front moving inside a battery compound during (dis)charge can become morphologically unstable driven by the misfit stress between ion-rich and ion-poor regions. We term this phenomenon as the "inverted Grinfeld instability" for its close analogy to the classical Asaro-Tiller-Grinfeld instability[3] in epitaxially strained thin film growth, Figure 4a. We further studied such interface instability in phase-field simulation (Figure 4b), which shows excellent agreement with the linear stability analysis in predicting the early-stage growth kinetics of interface perturbation, Figure 4c. An interface stability map (Figure 4d) is constructed to reveal the conditions (particle size, applied overpotential, interface location) under which the intercalation front can maintain its stability. A notable finding is that enhancing ion diffusion can stabilize the intercalation front against perturbation, which is contrary to the role diffusion typically plays in promoting interface instability in other processes such as solidification.

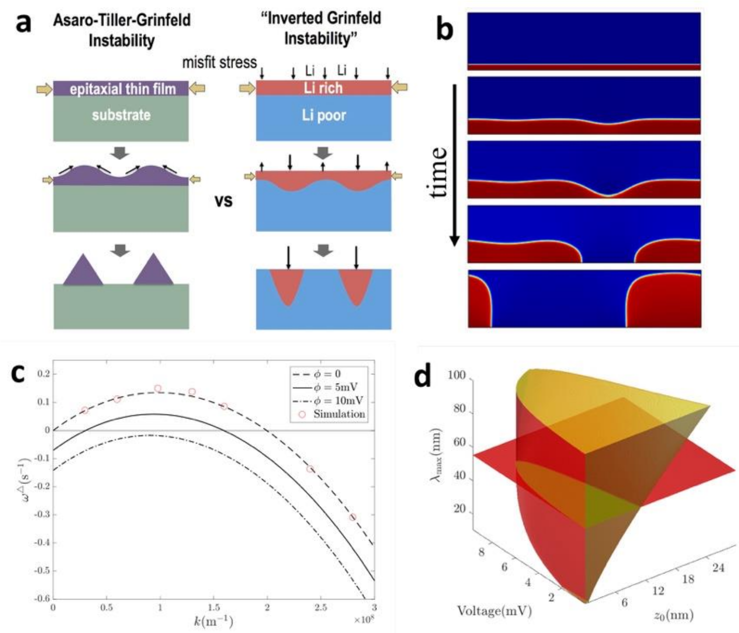

Fig. 4 Stress-induced ion intercalation front instability in battery compounds. a) Analogy between Asaro-Tiller-Grinfeld instability in epitaxial thin film growth and stress-induced ion intercalation front instability in battery compounds. **b)** Phase-field simulation of intercalation front instability when a Li-rich phase (red) advances in a Li-poor (blue) particle. **c)** Growth exponent vs wave vector of interface perturbation predicted by linear stability analysis (lines) agrees well with phase-field simulation (red circles). **d)** Interface stability map in the parameter space of particle size, applied overpotential and interface distance to particle surface. Interface is unstable in the shaded region.

Future Plans

1) Towards Objective 1, we will apply the multi-beam optical stress sensor (MOSS) technique to perform in-situ plating stress measurement to determine the correlation between stress evolution and the onset of unstable zinc plating behavior. Zinc electrodeposition experiments on soft vs hard substrate will be expanded to a wide range of plating current density and time to establish a preliminary zinc plating morphology map.

2) Towards Objective 2, in addition to continuing FIB/SEM reconstruction and analysis of mossy zinc structure, we will initiate an effort to perform in operando nanotomography reconstruction in collaboration with beamline scientists at NSLS-II beamline 18-ID. High-resolution TEM characterization will focus on analyzing the locations and types of defects (e.g. grain boundary) in the mossy structure.

3) Towards Objective 3, we will extend the linear stability theory of ion intercalation in battery compounds to the electroplating process and analyze the conditions under which stress can initiate the nucleation of filamentary or mossy structure. A macroscopic kinetic model of mossy growth process will be developed and validated by FIB/SEM reconstruction and measurements of mossy zinc size as a function of time.

References

1 Wang, X. *et al.* Stress-Driven Lithium Dendrite Growth Mechanism and Dendrite Mitigation by Electroplating on Soft Substrates. *Nature Energy* **3**, 227-235 (2018).
2 Li, Y. *et al.* Atomic structure of sensitive battery materials and interfaces revealed by cryo–electron microscopy. *Science* **358**, 506-510 (2017).
3 Asaro, R. J. & Tiller, W. A. Interface Morphology Development during Stress-Corrosion Cracking 1. Via Surface Diffusion. *Metall Trans* **3**, 1789 (1972).

Publications

- L. Hong, K. Yang, M. Tang, A Mechanism of Defect-Enhanced Phase Transformation Kinetics in Lithium Iron Phosphate Olivine, NPJ Computational Materials, under review.
- J. Zhang, F. Wang, V. Shenoy, M. Tang, J. Lou, Towards Controlled Synthesis of 2D Crystals by Chemical Vapor Deposition (CVD), Nature Materials, under review.

Experimental and Computational Studies of Crystal Nucleation in Composition Gradients

Timothy P. Weihs, Department of Materials Science, Hopkins Extreme Materials Institute, Johns Hopkins University

Michael L. Falk, Department of Materials Science, Department of Mechanical Engineering, Department of Physics and Astronomy, Hopkins Extreme Materials Institute, Johns Hopkins University

Program Scope

The major goals of the project are to develop a predictive model of crystallization that incorporates composition gradients and is applicable to a large range of metallic systems which form both stochiometric and non-stochiometric compounds. This model will expand the extant thermodynamics-based theories, and will lay groundwork to improve the general understanding and predictive capabilities of the role that gradients play in phase formation, glass formability and stability. To that end, we use Molecular Dynamics simulations and both isothermal and isochronal nanocalorimetric experiments on amorphous phases with controlled composition gradients to validate and improve the classical nucleation model or develop new kinetic theories more applicable in the regimes of interest.

Recent Progress

Phase selection through nucleation in composition gradients in multi-layer materials, interpreted by Desré's theory [1], offers opportunities for materials and device engineering. To examine the controlling and fundamental mechanisms experimentally, we completed and analyzed DC nanocalorimetry studies of Cu/Zr amorphous films with controlled composition gradients using isochronal heating (Fig. 1). This expanded the dataset for nucleation temperatures within this system and underscored the need for isothermal investigations. Characterization methodologies for these amorphous films were honed as well. More recently we commenced fabrication of amorphous films of a second binary system, aluminum-zirconium (Al/Zr), and characterized the as-deposited composition gradients in these films. However, there appear to be challenges in depositing persistent sharp gradients in this binary system that did not occur in Cu/Zr system.

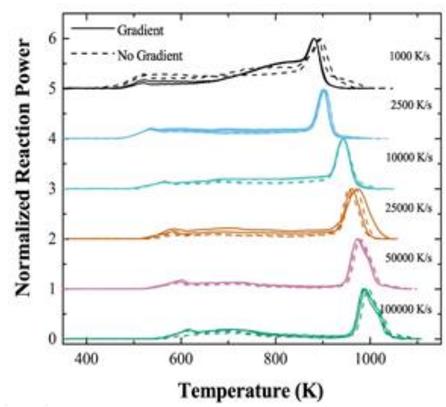

Figure 1: Isochronal reaction power vs temperature for Cu-Zr amorphous thin films with average composition equivalent to the $Cu_{10}Zr_7$ phase, showing no evidence of the gradient impacting nucleation temperature.

To complement our existing DC nanocalorimetry methods, we developed the capability to use alternating current (AC) controlled nanocalorimetry for low heating rate and isothermal investigations. During this process, we uncovered issues with voltage-controlled AC nanocalorimetry, and we identified the causes of these issues with helpful insight from Prof. Joost Vlassak at Harvard University. We implemented the required hardware for current-controlled AC nanocalorimetry, along with the requisite software development, expedited by useful discussions with our collaborator, Dr. Karsten Woll at Karlsruhe Institute of Technology.

Working with Dr. Woll and his group, we performed in situ synchrotron microdiffraction and nanocalorimetric experiments on Al-Zr based multilayer samples to identify variations in phase formation sequences as a function of heating rate.

We identified challenges for our in situ TEM nanocalorimeter experiments regarding sensor and sample holder designs, and we are designing and building alternate sensors and sample holders. Specifically, the current nanocalorimeter sensor requires electrical contacts be made on either side of the sensor, thereby requiring contacts inside the polepiece of the TEM. This was acceptable in designing holders for much older TEMs (such as the instrument upon which the DTEM at LLNL was based), but for modern TEMs with small-pole pieces it is either challenging or impossible. The new design pulls the contact pads out of the pole piece and is compatible with the highest resolution and most capable modern TEMs.

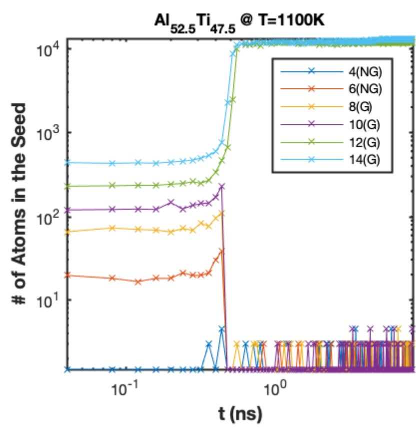

Figure 2: Plot of embedded intermetallic seed size versus time with initial seed radius = 4, 6, 8, 10, 12, and 14Å at around 23% undercooling (T = 1100K) in $Al_{52.5}Ti_{47.5}$, where 'G' represents growth, and 'NG' represents no growth. Only 1 of multiple independent runs at each seed radius is shown.

To provide atomistic level studies of the process, independent brute force MD simulation were performed. For simulations of nucleation we found that it is essential to choose model systems that have a relatively simple intermetallic crystal structure and relatively fast intermetallic nucleation rate due to the limited length- and time- scales accessible to MD. Thus, we first screened multiple compounds (Table 1) by simulating growth of an embedded intermetallic seed from super-cooled melts at selected temperatures and compared the observations with those for the Ni/Al system. MD simulation of the growth of the $Cu_{10}Zr_7$ compound proved difficult due to its complicated intermetallic crystal structure and slow growth kinetics. The AlTi phase crystalizes as quickly as NiAl with some 'HCP' structure evident in the 'FCC' structure, which is likely due to stacking faults. Since the 50/50 compound sits on a phase boundary at lower temperatures, $Al_{52.5}Ti_{47.5}$ is more suitable for further studies in binary systems with composition gradients. The Al/Zr system exhibited a slow growth rate for the Al_2Zr and Al_3Zr compounds, though as a line compound, Al_2Zr is still within our interests due to its smaller critical nucleus size than Al_3Zr. Thus, Table 2 outlines investigations in $Al_{52.5}Ti_{47.5}$ and Al_2Zr in MD simulations. The melting temperatures in the MD studies were estimated by simulating competition between coexisting crystal and liquid phases, separated by a flat interface. We also applied the survival probability test method to estimate critical nucleus size at selected undercooling (Fig. 2) [2]. Both $Al_{52.5}Ti_{47.5}$ and Al_2Zr exhibit lower melting points and larger critical nuclei than AlNi.

Table 1: Summary of binary alloy compounds studied in growth simulations with embedded spherical intermetallic seed (initial radius =15 Å) at 1200K/1100K.

Binary System	Compounds	Structure Type in CNA	Growth w/ an Embedded Seed
Ni/Al	NiAl @ 1200K	BCC	Quick
Al/Ti	AlTi @ 1200K	FCC/HCP	Quick with negligible stacking fault
	$Al_{52.5}Ti_{47.5}$ @ 1100K	FCC/HCP	Quick with 1/3 stacking fault

Al/Zr	Al_2Zr @ 1200K	ICO on Al (w/ noise)	Slow
	Al_3Zr @ 1200K	FCC	No growth w/ critical nucleus radius R_c>15Å
Ni/Zr	NiZr	Lack of effective order parameter to identify the crystal structure	N/A
Cu/Zr	$Cu_{10}Zr_7$	Lack of effective order parameter to identify the crystal structure	N/A

Table 2: Summary of melting points and critical nucleus radii in selected binary alloy compounds.

Binary Compound	Melting Point in MD (K)	Critical Nucleus Radius (Å) at Undercoolings		
		23%	**35%**	**50%**
NiAl	1825±5	7±1	5±1	1±1
Al_2Zr	1425±5	11±1	7±1	7±1
$Al_{52.5}Ti_{47.5}$	1505±5	7±1	<6	<6

Using MD simulations we previously demonstrated the suppression of nucleation by steep composition gradients in the Ni/Al system at small undercoolings. This is in qualitative agreement with Desré [2]. The applicability of Desré's model depends on two conditions: (1) knowledge of the composition and temperature dependence of the interfacial energy, and (2) applicability of classical nucleation theory (CNT) at deep undercooling. We developed calculation methods for the interfacial free energy between an amorphous phase and an intermetallic phase using the capillary fluctuation method (CFM) [3-5] . We demonstrated in the Ni/Al system that the interfacial free energy at the melting point has a strong composition dependence (Fig. 3), which we will incorporate into the nucleation model.

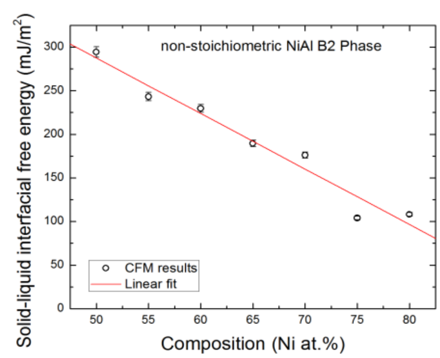

Figure 3: (a) Solid-liquid interfacial free energy at melting point as a function of composition for the non-stoichiometric NiAl B2 compound

Future Plans

The key experimental focus will be on implementation of isothermal *in situ* nanocalorimetric experiments to assess nucleation rates in composition gradients. Complementing these experiments, we will perform cross-sectional TEM characterization of the nuclei that form. Due to the computational challenges for the Cu/Zr system that we experienced during this reporting period, we will perform the isothermal experiments on both Cu/Zr and Al/Zr or Al/Ti, unless the latter systems prove to be significantly more complicated experimentally than Cu/Zr. Early experiments on Al/Zr suggest that fabricating a sharp gradient which persists at or above room temperature may be challenging, thus Al/Ti will be simultaneously investigated and we will investigate how the fabrication could be altered or optimized. Other key steps to these experiments are the final development of current-controlled AC nanocalorimetry, implementation of an alternative nanocalorimeter design compatible with modern TEMs, and final development of a TEM holder for that design.

Moving forward, we have several computational/theoretical issues to address. For good glass formers such as Cu/Zr, it is very difficult to investigate direct nucleation events using MD. Whether the reason for this is primarily thermodynamic or kinetic remains unclear. In addition, the model systems used in MD simulations rarely yield strict line compounds, i.e. nucleation on MD time scales is far easier to achieve for intermetallic compounds for which there is a broad composition range. This might pose some issues in direct comparison with experiments where choices of compounds are also constrained technically. We will continue to explore other glass forming model systems that enable direct amorphous-intermetallic nucleation for comparison with experiments. Another challenge is finding suitable order parameters to distinguish atoms in the intermetallic phases from those in the amorphous phase. In addition to common neighbor analysis, we will investigate more efficient order parameter algorithms, for example, revised bonded common neighbor analysis. Methodologies to remove statistical noise from the data at elevated temperatures are also being developed.

The experiments are typically performed at deep undercoolings (~50%) due to the fact that we are heating from room temperature where composition gradients can be fabricated for physical experiments (on nanocalorimeters) rather than by cooling from the melt where sharp gradients do not exist. At these deep undercoolings, the applicability of CNT remains questionable. The critical nucleus size might be too small for nucleation to be the rate-limiting mechanism. Even if nucleation barriers persist at these deep undercoolings, analyzing nuclei by applying a geometrically idealized model is problematic (Fig. 4) [6]. While we continue extending our previous computation of thermodynamic quantities into deep supercooling regime, we will also investigate alternative theoretical frameworks for deep undercooling conditions, the role of the composition gradient on the kinetics of crystal growth, and the potential for the occurrence of spinodal decomposition.

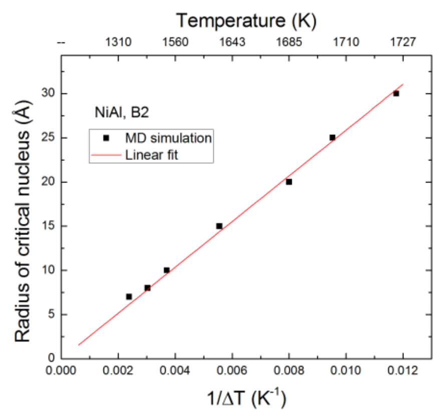

Figure 4: Radius of critical nucleus as a function of undercooling for the NiAl B2 compound.

References

1. Desré, P.J. and A.R. Yavari, Physical Review Letters, 1990. **64**(13): p. 1533-1536.
2. Yi, P., M.L. Falk, and T.P. Weihs, The Journal of Chemical Physics, 2017. **146**(18): p. 184501.
3. Hoyt, J.J., M. Asta, and A. Karma, Physical Review Letters, 2001. **86**(24): p. 5530.
4. Asta, M., J.J. Hoyt, and A. Karma, Physical Review B, 2002. **66**(10): p. 100101.
5. Wu, L.-K., et al., Rare Metals, 2018. **37**(7): p. 543-553.
6. Sosso, G.C., et al., Chemical Reviews, 2016. **116**(12): p. 7078-7116.

Publications

Shane Q. Arlington, Feng Yi, David LaVan, Timothy P. Weihs. *A nanocalorimetric study of the effect of composition gradients on crystallization in amorphous Cu-Zr thin films* (2019). AIP Advances, 9, 035324. https://doi.org/10.1063/1.5080312.

Predictive models for 2D materials synthesis, examples of practical relevance

Boris I. Yakobson, MSNE Department, Rice University

Program Scope

The discovery of novel physics in graphene has ignited the interest and expanded the scope of research worldwide, to the extended family of 2D-materials "beyond graphene." This raised several broader compelling questions about the ways of making such monoatomic layers. The exfoliation from natural bulk precursors is not scalable. On the other hand, their synthesis through chemical vapor deposition involves complex gas-solid chemistry works empirically, but still lacks theoretical understanding and sentient design. Hence, our general goal is to develop state-of-the-art multiscale models of 2D-layers on substrates and of atomistic mechanisms of their nucleation and growth. We aim to explore how a sentient choice of a substrate, interacting at just the right level with the commencing nucleus, can facilitate the growth of planar materials forms, even for compositions currently unavailable. The primary set of materials for our project includes those of already established great interest: graphene, hexagonal boron nitrogen, and transition metal dichalcogenides. We will also investigate the nucleation and growth of emergent or even hypothetical 2D materials: borophene, phosphorene, stanene, silicene. The impact of this project could be enormous by leading to an efficient synthesis of materials with novel desired properties. It will impact fundamental studies in this field, as well as permit various applications in devices, energy utility, and production, of commercial and defense significance.

Recent Progress

The last decade was marked by the unprecedented growth of the family of 2-dimensional (2D) materials – not only theoretically predicted but practically synthesized – with most of them possessing interesting novel properties. The rapid progress in this relatively new field brings closer a promise of the future 2D electronics. Yet the transition from the purely scientific research to the industrial applications demands the fundamental understanding of the materials properties and growth mechanisms. On the example of the three important groups of 2D materials, hexagonal boron nitride (h-BN), transitional metal dichalcogenides (TMDs) and borophene, we would discuss recent progress in the field with the emphasis on its practical relevance.

The synthesis of the large-scale and high-quality monocrystals of 2D materials is the first obstacle for their industrial use. Unlike graphene, for which variety of methodologies were successfully realized, many other materials (such as h-BN and TMDs) possess lower symmetry, which on commonly used low-index surfaces of substrates leads to nucleation of mutually inverted islands, merging into polycrystals replete with grain boundaries. On vicinal substrate surfaces, such growing pieces were observed to orient alike, and very recently, this effect enabled the growth of large single crystal h-BN [1]. Using first-principles calculations on various surfaces of Cu and Ni as representative catalytic substrates, we confirm that h-BN would preferentially nucleate docked to the step with N-passivated zigzag edge without evidence of any surface epitaxy [2].

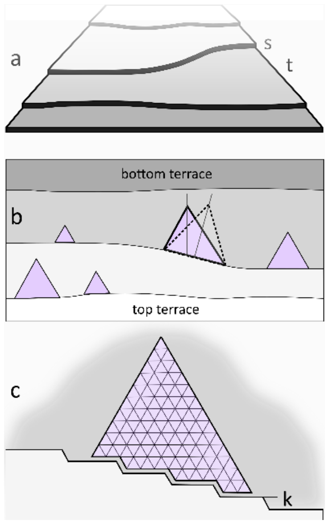

Figure 1. (a) Perspective view of a vicinal surface with unidirectional steps. (b) Top view of the nucleating 2D islands docked to the steps; the one shown as the dashed-line triangle is tilted, to follow the step curve. (c) Close-up view of a meandering step, composed of sparse kinks and “1D terraces” of principal direction, to which the h-BN nuclei are docked. [2]

Theoretically, in case of well-aligned steps, this would result in co-oriented islands of growing material avoiding anti-parallel orientation and consequently grain boundaries. In practice, however, steps on vicinal surfaces are commonly curved or even meandering at higher temperatures used for the growth of h-BN (Fig.1). Presence of misaligned segments of steps should lead to misorientation in growing islands, yet considered at the atomistic level curved steps consist of series of parallel 1-D terraces separated by kinks, allowing islands to nucleate on aligned terraces. Presence of kinks though can lead to stress concentration and ultimately the creation of defects if dimensions of kinks on substrate steps do not match those for growing material. This introduces the additional requirement of kink complementarity for the successful growth of monocrystalline materials on vicinal surfaces. We formulate a criterion for choosing promising substrates for growth of h-BN through a selection of substrate material, surface, and step directions. We suggest (110) surface with steps along [-112] for Cu, Pt, Ir, and Ni to be the most promising substrates in agreement with recent experimental success on (110) Cu surface. While our investigation was carried out on the example of h-BN, the developed approach is suitable for the consideration of other materials without inversion symmetry, such as TMDs.

While the growth of single crystal TMDs remains of great importance, the high variability of this class of materials opens a new aspect of this 2D semiconductors. Similar structure and variability of various TMDs – MoS_2 and WSe_2, for example – allows for the creation of alloys that, in turn, enables a bandgap modulation as been shown earlier [3]. Furthermore, the thermal annealing of such alloys results in the creation of the atomically sharp electronic junctions (Fig.2) [4]. Direct synthesis of sharp interfaces is generally challenging as the creation of alloys is entropically favored. As was previously shown on the examples of classic III-V semiconductors, an increased number of components in the system can result in the introduction of the miscibility gap. Consequently, in such systems, alloys became metastable at certain compositions, and phase transition towards now stable heterostructure can be induced with thermal treatment (see Fig.2 right). Using the phase diagram from the reciprocal solution model, we demonstrate the existence of the miscibility gap in quarternary Mo/W-S/Se TMD systems that is further confirmed by experimental observations.

The diversity of TMDs is further increased by the existence of two phases: the ground state 2H and the metastable 1T. On the example of WSe_2 and MoS_2 nanoribbons, we demonstrate the possibility to switch the stability of the two phases in TMD nanoribbons [5]. We found that at

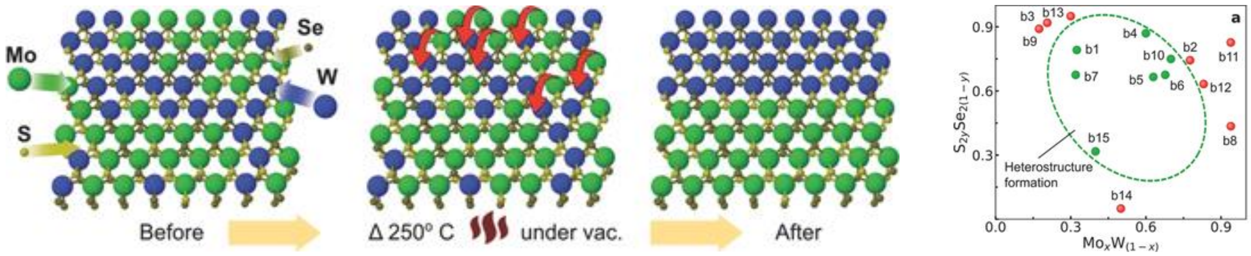

Figure 2. Schematic diagram showing the main steps for heterostructure formation in the quaternary alloys. Left to right: Following the CVD growth, transition metals preferentially segregate under annealing, forming a lateral heterostructure. Right: Various compositions of quaternary alloys indicating the compositions which transform into heterostructure. [4]

narrow width 1T phase is favored over 2H due to higher coordination of edge metal atoms in 1T phase than in the 2H phase and an interesting electronic reconstruction of 1T lattice in the ribbon interior. The edge configuration of the 1T phase diminishes the dangling bonds on edge and thereby enhances the stability of TMD nanoribbons. Our findings emphasize the importance of edges in determining the structures of 2D TMDs and are crucial for their future scientific studies and potential applications.

Another promising 2D material – borophene, or 2D boron – is characterized by a very high structural variability. Borophene can be thought of as a triangular boron lattice with the inclusion of vacancies or hollow hexagons (HHs). The concentration of such vacancies can vary between 0 (triangular lattice) to 1/3 (hexagonal lattice). The vast number of possible HH arrangements underlies the polymorphic nature of borophene and necessitates direct HH imaging to identify its atomic structure definitively. The use of CO-functionalized atomic force microscopy allowed visualization of structures corresponding to boron-boron covalent bonds confirming the $v_{1/5}$ and $v_{1/6}$ borophene models [6]. Using this methodology, we assemble a borophene phase diagram, including a transition from rotationally commensurate to incommensurate phases at high growth temperatures, thus corroborating the chemically discrete nature of borophene. Furthermore, $v_{1/6}$ and $v_{1/5}$ phases were found to intermix and accommodate line defects in each other with structures that match the constituent units of the other phase [7]. First principle calculations show that these line defects energetically favor spatially periodic self-assembly that gives rise to new borophene phases, which ultimately blurs the distinction between borophene crystals and defects. This phenomenon is unique to borophene as a result of its high in-plane anisotropy and energetically and structurally similar polymorphs.

Lastly, to illustrate the variability of growth processes within 2D materials, we demonstrate the mechanism of recently observed borophene growth on Au (111) that significantly differs from all other substrates. Unlike previously studied growth on Ag substrates, boron diffuses into Au at elevated temperatures and segregates to the surface to form borophene islands as the substrate cools [8]. The *ab initio* modeling shows the process of the interstitial boron diffusion into the Au lattice that facilitates such a mechanism. Our first principle calculations show that borophene synthesis also modifies the surface reconstruction of the Au (111) substrate, resulting in a trigonal network that templates growth at low coverage. As the concentration of boron increases, nano-templating breaks down and larger borophene islands emerge. The borophene grown on Au (111) possesses a metallic electronic structure, suggesting various potential applications.

Future Plans

The rise of scientific interest towards borophene inevitably motivates us to investigate it in more details. Consideration of the borophene nucleation process as well as its growth on various substrates can provide valuable insights into the borophene-substrate interaction and allow more general understanding of how such interaction aids the formation of 2D boron sheets vs. 3D structure. Furthermore, this approach would assist in resolving the still outstanding question of the post-growth separation from the substrate through the optimization of the strength of the substrate interaction. Additionally, consideration of the heterostructures and junctions between borophene and other 2D materials may prove to be of high importance for practical use in the future. Another promising element of the future nano-electronics, transition metal dichalcogenides, remain high on our priority list. Unlike borophene, TMDs do not require a catalyst for the growth with most of the reactions happening in the gas phase where we focus our interest and would perform detailed analysis to determine reaction mechanisms and possible ways to optimize them for more efficient and controlled synthesis. Lastly, our investigation into monocrystalline growth of the hexagonal boron nitride, material attracting significant attention in recent years as a convenient 2D insulator, based on interaction with the steps and terraces on the surface of the substrate would continue.

References

1. L. Wang, X. Xu, L. Zhang et al. "Epitaxial growth of a 100-square-centimetre single-crystal hexagonal boron nitride monolayer on copper." *Nature* **2019**, 570, 9195.
2. K.V. Bets, N. Gupta, and B.I. Yakobson. "How the Complementarity at Vicinal Steps Enables Growth of 2D Monocrystals." *Nano Letters* **2019**, 19(3), 2027.
3. S. Susarla, A. Kutana, J.A. Hachtel et al. "Quaternary 2D transition metal dichalcogenides (TMDs) with tunable bandgap." *Advanced Materials* **2017**, 29(35), 1702457.
4. S. Susarla, J.A. Hachtel, X. Yang et al. "Thermally Induced 2D Alloy-Heterostructure Transformation in Quaternary Alloys." *Advanced Materials* **2018**, 30 (45), 1804218.
5. W. Zan, Z. Zhang, Y. Yang et al. "Width-dependent phase crossover in transition metal dichalcogenide nanoribbons." *Nanotechnology* **2018**, 30 (7), 075701.
6. X. Liu, L. Wang, S. Li et al. "Geometric imaging of borophene polymorphs with functionalized probes." *Nature Communications* **2019**, 10 (1), 1642.
7. X. Liu, Z. Zhang, L. Wang et al. "Intermixing and periodic self-assembly of borophene line defects." *Nature Materials* **2018**, 17, 783-788.
8. B. Kiraly, X. Liu, L. Wang et al. "Borophene Synthesis on Au (111)." *ACS Nano* 2019, 13(4), 3816.

Publications, past 2 years

1. X. Liu, L. Wang, S. Li, M.S. Rahn, B.I. Yakobson, and M.C. Hersam. "Geometric imaging of borophene polymorphs with functionalized probes." *Nature Communications* **2019**, 10 (1), 1642.
2. B. Kiraly, X. Liu, L. Wang, Z. Zhang, A.J. Mannix, B.L. Fisher, B.I. Yakobson, M.C. Hersam, and N.P. Guisinger. "Borophene Synthesis on Au (111)." *ACS Nano* 2019, 13(4), 3816.
3. K.V. Bets, N. Gupta, and B.I. Yakobson. "How the Complementarity at Vicinal Steps Enables Growth of 2D Monocrystals." *Nano Letters* **2019**, 19(3), 2027.
4. X. Tian, J. Duan, Y. Wei, N. Feng, X. Wang, Z. Gong, Y. Du, and B.I. Yakobson. "Modulating Blue Phosphorene by Synergetic Codoping: Indirect to Direct Gap Transition and Strong Bandgap Bowing." *Advanced Functional Materials* **2019**, 29 (11), 1808721.
5. W. Zan, Z. Zhang, Y. Yang, X. Yao, S. Li, and B.I. Yakobson. "Width-dependent phase crossover in transition metal dichalcogenide nanoribbons." *Nanotechnology* **2018**, 30 (7), 075701.
6. S. Susarla, J.A. Hachtel, X. Yang, A. Kutana, A. Apte, Z. Jin, R. Vajtai et al. "Thermally Induced 2D Alloy-Heterostructure Transformation in Quaternary Alloys." *Advanced Materials* **2018**, 30 (45), 1804218.
7. X. Liu, Z. Zhang, L. Wang, B.I. Yakobson, and M.C. Hersam. "Intermixing and periodic self-assembly of borophene line defects." *Nature Materials* **2018**, 17, 783-788.
8. A.J. Mannix, Z. Zhang, N.P. Guisinger, B.I. Yakobson, and M.C. Hersam. "Borophene as a prototype for synthetic 2D materials development." *Nature Nanotechnol.* **2018**, 13 (6), 444-450.
9. S.N. Shirodkar, E.S. Penev, and B.I. Yakobson. "Honeycomb boron: alchemy on aluminum pan?" *Science Bulletin* **2018**, 63(5), 270-271.
10. J. Zhou, J. Lin, X. Huang, Y. Zhou, Y. Chen, J. Xia, H. Wang et al. "A library of atomically thin metal chalcogenides." *Nature* **2018**, 556 (7701), 355.
11. I.V. Vlassiouk, Y. Stehle, P.R. Pudasaini, R.R. Unocic, P.D. Rack, A.P. Baddorf, I.N. Ivanov et al. "Evolutionary selection growth of two-dimensional materials on polycrystalline substrates." *Nature materials* **2018**, 17, 318.
12. Z. Zhang, E.S. Penev, and B.I. Yakobson. "Two-dimensional boron: structures, properties and applications." *Chemical Society Reviews* **2017**, 46 (22), 6746-6763.
13. Z. Zhang, S.N. Shirodkar, Y. Yang, and B.I. Yakobson. "Gate-Voltage Control of Borophene Structure Formation." *Angewandte Chemie* **2017**, 129 (48), 15623-15628.
14. H. Yu, N. Gupta, Z. Hu, K. Wang, B.R. Srijanto, K. Xiao, D.B. Geohegan, and B.I. Yakobson. "Tilt grain boundary topology induced by substrate topography." *ACS Nano* **2017**, 11 (9), 8612-8618.
15. C. Zhang, J. Sha, H. Fei, M. Liu, S. Yazdi, J. Zhang, Q. Zhong et al. "Single-atomic ruthenium catalytic sites on nitrogen-doped graphene for oxygen reduction reaction in acidic medium." *ACS Nano* **2017**, 11 (7), 6930-6941.
16. J. Lei, A. Kutana, and B.I. Yakobson. "Predicting stable phase monolayer Mo_2C (MXene), a superconductor with chemically-tunable critical temperature." *Journal of Materials Chemistry C* **2017**, 5 (14), 3438-3444.
17. Y. Yang, Z. Zhang, E.S. Penev, and B.I. Yakobson. "B_{40} cluster stability, reactivity, and its planar structural precursor." *Nanoscale* **2017**, 9 (5), 1805-1810.

The Role of the Surface Chemistry of Precursors in Growing Thin Solid Films

Francisco Zaera
Department of Chemistry, University of California, Riverside, CA 92521
Email: zaera@ucr.edu

i) Program Scope

The general objective of our project is to develop a molecular-level understanding of the thermal reactions that the organometallic compounds used for atomic layer deposition (ALD) follow on surfaces. ALD is one of the dominant technologies for the growth of nanometer-sized conformal films in many industrial applications. In microelectronics in particular, ALD can be used for the growth of diffusion, adhesion, and protection barriers and of metal interconnects, structures that are central to the buildup of diodes, transistors, and other elements within integrated circuits. More recently, the applications of ALD has been extended to areas related to energy production and use such as solar cells and photovoltaics, batteries, fuel cells, and catalysts and photocatalysts. All these processes require the deposition of isotropic films on complex topographies under mild conditions and with monolayer control. ALD is particularly suited to all those uses, but many questions concerning the underlying surface chemistry need to be answer to improve performance. Our mechanistic studies of ALD reactions are being pursued with the aid of surface-sensitive techniques such as X-ray photoelectron (XPS), low-energy ion scattering (LEIS), temperature programmed desorption (TPD), and infrared (IR) spectroscopies.

ii) Recent Progress

We have identified a number of key issues relevant to the behavior of common organic ligands used to make ALD precursors. At the beginning, the work financed by this grant has focused primarily on the chemistry of copper precursors, a metal used in microelectronics applications. In recent years we have expanded that work to also include the deposition of other transition metals, with emphasis on films of interest in catalysis, batteries, fuel cells, and other energy applications.

Our studies with copper have illustrated the difficulties that may be encountered when selecting metalorganic compounds of late transition metals for ALD and other chemical vapor deposition (CVD) processes. In particular, it is worth realizing that the precursors for CVD and ALD are often designed and chosen based on their known thermal chemistry from inorganic chemistry studies, taking advantage of the vast knowledge developed in that field over the years. Although a good first approximation, this approach can lead to wrong choices, because the reactions of these precursors at gas-solid interfaces can be quite different from what is seen in solution. For one, solvents often aid in the displacement of ligands in metalorganic compounds, providing the right dielectric environment, temporarily coordinating to the metal, or facilitating multiple ligand-complex interactions to increase reaction probabilities; these options are not available in the gas−solid reactions associated with CVD and ALD. Moreover, solid surfaces act as unique "ligands", if these reactions are to be viewed from the point of view of the metalorganic complexes used as precursors: they are bulky and rigid, can provide multiple binding sites for a single reaction, and can promote unique bonding modes, especially on metals, which have delocalized electronic structures. The differences between the molecular and surface chemistry of CVD and ALD precursors can result in significant variations in their reactivity, ultimately leading to unpredictable properties in the newly grown films. In collaboration with the groups of Professors Sean Barry (Carleton University) and Andrew Teplyakov (University of Delaware), we have recently published a perspective in *Accounts of Chemical Research* where we discuss some of the main similarities and differences in chemistry that CVD/ALD precursors follow on surfaces when contrasted against their known behavior in solution, with emphasis on our own work but also referencing other key contributions [1]. Our approach is unique in that it combines expertise from the inorganic, surface science, and quantum-mechanics fields to better understand the mechanistic details of the chemistry of CVD and ALD processes and to identify new criteria to consider when designing CVD/ALD precursors. Analogies in terms of the chemistry of ligands have been drawn between metalorganic discrete compounds and the reaction of organic ligands on surfaces (Figure 1). A useful set of initial observations and conclusions was discussed, but more research is needed from the scientific community to be able to derive a more comprehensive picture.

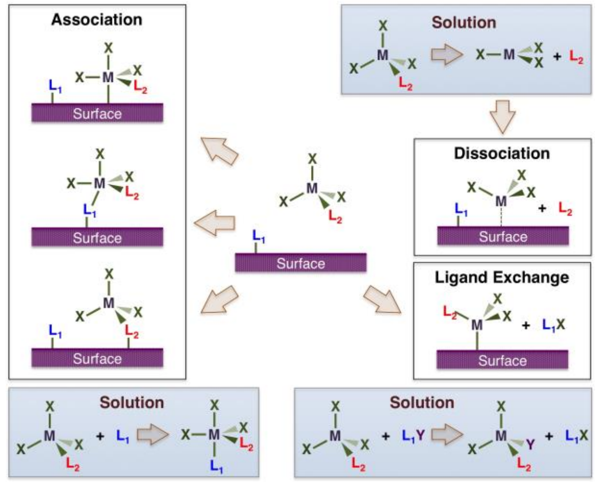

Figure 1. The surface chemistry of precursors for ALD and CVD viewed from an inorganic, ligand-based,

Within the last couple of years of this project, our research on copper amidinates as precursors for the deposition of metallic Cu films was culminated with the design of a fourth-generation copper metalorganic compound, Cu(I)-2-(tert-butylimino)-5,5-dimethyl-pyrrolidinate. On the basis of our previous surface science studies with similar acetamidinate, guanidinate, and iminopyrrolidinate complexes, it was concluded that the high (and undesirable) reactivity of these when adsorbed on metal surfaces is due to the lability of their C−N bonds, which can be triggered by β-hydrogen elimination steps. Accordingly, a ligand was designed without any available hydrogen atoms at these positions. The result is a much more stable reactant (Figure 2) [2]. Temperature-programmed desorption (TPD) experiments indicated that dehydrogenation from the new compound on Ni(110) starts only at 450 K, an increase of about 200 K in comparison with any of the earlier-generations ALD precursors. TPD and X-ray photoelectron spectroscopy (XPS) data were used to establish the details of the decomposition mechanism of the ligands, which appears to be initiated by the scission of the iminopyrrolidine C−N bond. Many byproducts are produced, including HCN, N_2,

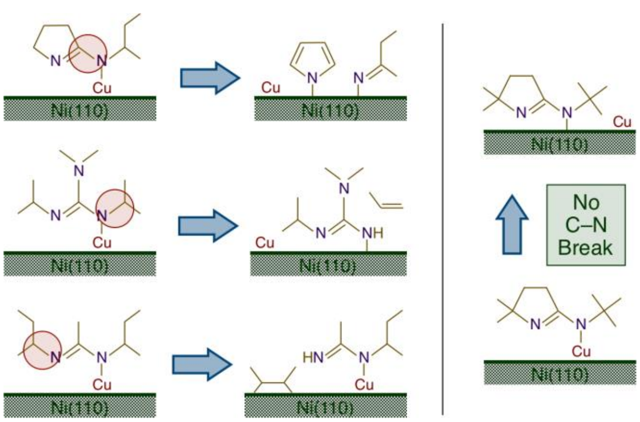

Figure 2. Mechanistic depiction of the initial decomposition step of imidinate ligands in ALD/CVD metal precursors.

iso-butene, and possibly pyrroline and other olefins such as pentenes. However, all of that occurs at relatively high temperatures, leaving an acceptable temperature window for the use of this complex for the deposition of copper films. An increased stability of the new ligands in our new copper ALD precursor was also observed on SiO_2 thin films, attesting to the generality of our conclusions. We suggest that our methodology for the rational design of this ALD precursor, based on studies of its surface chemistry, can be easily extended to other cases.

More recently, we have extended our mechanistic studies to other metals and to other ligands. One direction of our work has been to characterize the surface chemistry of cyclopentadienyl ligands, with focus on the ALD process developed for the deposition of platinum films using trimethyl(methylcyclopentadienyl)platinum(IV) ($MeCpPtMe_3$). The chemistry of that precursor and its reactivity with oxygen were characterized by using XPS [3]. The uptake of the $MeCpPtMe_3$ ALD precursor was found to be self- limiting between 525 and 625 K, but to lead to multilayer deposition at 675 K. The adsorbed species display a C:Pt ratio of approximately 5:1, suggesting that all methyl moieties are lost upon activated bonding to the surface but that the methylcyclopentadienyl group remains coordinated to the adsorbed Pt atoms. Oxygen treatment of that surface leads to the complete removal of the carbon-containing species from the surface and to the formation of a thin NiO film. Further dosing with $MeCpPtMe_3$, in the next ALD cycle, fully reduces that NiO film to metallic Ni(0) and adds more Pt to the surface. However, no Pt film buildup was seen after several ALD cycles. Angle-resolved XPS data suggested that the deposited Pt migrates below the NiO that forms during the O_2 exposures and possibly alloys with the metallic Ni substrate at that stage.

Because $MeCpPtMe_3$ is difficult to activate initially on surfaces, the use of external excitations sources to facilitate that first step was tested. The use of gas-phase electron-impact activation in particular was probed [4], in an analogous way as we had reported in the past for a similar Mn precursor [5] (Figure 3). Uptake enhancements of more than one order of magnitude were calculated from XPS data. On the basis of the measured C:Pt ratios, the surface species were estimated to mainly consist of MeCpPt moieties, likely because of the prevalent formation of $[MeCpPtMe_{x-n}H]^+$ ions after gas-phase ionization (as determined by mass spectrometry and recently corroborated by using static secondary-ion mass spectroscopy). Counterintuitively, more extensive adsorption was observed on thick SiO_2 films than on the native thin SiO_2 film that forms on Si(100) wafers, despite the former having virtually no surface OH groups. The adsorption of MeCpPt fragments on silicon oxide surfaces was determined by density functional theory (DFT) calculations to be highly exothermic and to favor attachment to Si−O−Si bridge sites.

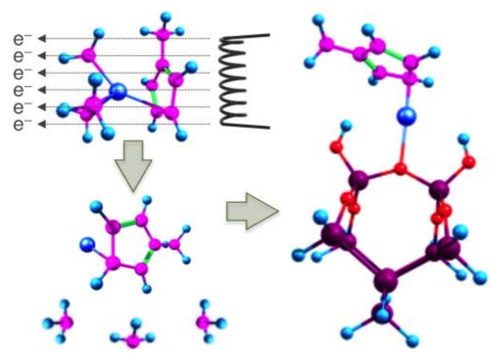

Figure 3. Schematic depiction of the gas-phase electron-impact excitation approach developed to facilitate the adsorption of cyclopentadienyl ALD precursors.

For ruthenium deposition, the thermal chemistry of tris(2,2,6,6-trameth-yl-3,5-heptanedionato)-ruthenium(III) ($Ru(tmhd)_3$) single-crystal surfaces was characterized on Ni(110) by using a combination of TPD, XPS, and reflection−absorption infrared spectroscopy (RAIRS) [6]. Additional characterization of the surface chemistry of the protonated ligand, Htmhd, was evaluated as well for reference. It was found that the molecularly adsorbed ruthenium compound reacts readily by approximately 310 K, loosing its ligands to both the gas phase and the surface as the central ion is reduced to its Ru^0 metallic state. The diketonate ligand, now bonded to the nickel surface, starts to decompose at around 400 K and generates gas-phase carbon monoxide and molecular hydrogen in TPD peaks at 435 K, and more extensive decomposition is seen at 535 K, yielding 2,2-dimethyl-3-oxopentanal, isobutene, ketene, and carbon monoxide, and also carbon dioxide and molecular hydrogen at slightly higher temperatures (Figure 4). The XPS data corroborate the early reduction of the metal center and the losses of carbon- and oxygen-containing adsorbates to the gas phase, and the RAIRS traces show similar chemistry followed by the Ru complex and the free ligand, both converting via an initial decarbonylation step and a subsequent loss of the terminal tert-butyl groups. The early decomposition of the ligand on the metal surface points to potential problems with the clean deposition of metal films using diketonate complexes, but the ease with which those ligands are displaced from the central ion suggests that there is a potential for low-temperature film deposition chemistry under specific circumstances.

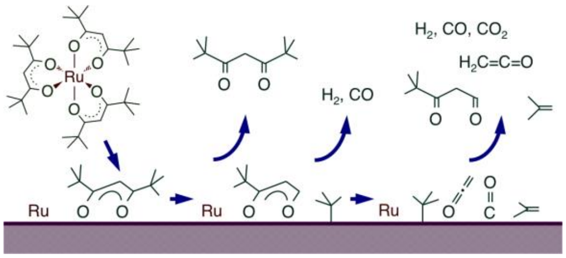

Figure 4. Reaction mechanism for the decomposition of Ru diketonate precursors.

iii) Future Plans

In the near future, we plan to continue exploring the surface chemistry of precursors viable for film deposition of transition metal films. Our choice of systems to explore is guided by two parallel goals:

1. We aim to study the deposition of materials of interest to applications in energy-related problems, including catalysis, batteries, fuel cells, and others. Our immediate next target will be the deposition of nickel, which is useful to promote the hydrogenation or reforming of carbon dioxide.
2. We also search for general trends in the surface chemistry of common ligands used for ALD/CVD precursors. We have been targeting three families of multiply coordinate ligands: amidinates, cyclopentadienyls, and diketonates.

iv) References

[1] S. T. Barry, A. V. Teplyakov, F. Zaera, Acc. Chem. Res. 51 (2018) 800-809.
[2] B. Chen, J. P. Coyle, S. T. Barry, F. Zaera, Chem. Mater. 31 (2019) 1681-1687.
[3] C. Lien, H. Sun, X. Qin, F. Zaera, Surf. Sci. 677 (2018) 161-166.
[4] C. Lien, M. Konh, B. Chen, A. V. Teplyakov, F. Zaera, J. Phys. Chem. Lett. 9 (2018) 4602-4606.
[5] H. Sun, X. Qin, F. Zaera, J. Phys. Chem. Lett. 3 (2012) 2523-2527.
[6] X. Qin, F. Zaera, J. Phys. Chem. C 122 (2018) 13481-13491.

v) Publications Sponsored by This DOE Grant, 2018-2019

1. Seán T. Barry, Andrew V. Teplyakov, and Francisco Zaera, The Chemistry of Inorganic Precursors during the Chemical Deposition of Films on Solid Surfaces, *Acc. Chem. Res.*, **51(3)**, 800-809 (2018).

2. Xiangdong Qin and Francisco Zaera, Chemistry of Ruthenium Diketonate Atomic Layer Deposition (ALD) Precursors on Metal Surfaces, *J. Phys. Chem. C*, **122(25)**, 13481-13491 (2018). INVITED, Prashant V. Kamat Festschrift

3. Clinton Lien, Huaxing Sun, Xiangdong Qin, and Francisco Zaera, Platinum Atomic Layer Deposition on Metal Substrates: A Surface Chemistry Study, *Surf. Sci.* **677**, 161-166 (2018). INVITED, Special Issue entitled "Unraveling Surface Structure and Chemical Pathways: In Honor of Jan Hrbek"

4. Clinton Lien, Mahsa Konh, Bo Chen, Andrew Teplyakov, Francisco Zaera, Gas-Phase Electron-Impact Activation of Atomic Layer Deposition (ALD) Precursors: $MeCpPtMe_3$, *J. Phys. Chem. Lett.*, **9**, 4602-4606 (2018).

5. Zhihuan Weng, Zhi-hui Chen, Xiangdong Qin, and Francisco Zaera, Sub-Monolayer Control of the Growth of Oxide Films on Mesoporous Materials, *J. Mater. Chem. A*, **6**, 17548-17558 (2018).

6. J. Guerrero-Sánchez, Noboru Takeuchi, and Francisco Zaera, Density Functional Theory Study of the Surface Adsorption and Dissociation of Copper(I) Acetamidinates on Cu(110) Surfaces, *J. Phys. Chem. C*, **123(7)**, 4341-4348 (2019).

7. Bo Chen, Jason P. Coyle, Seán T. Barry, and Francisco Zaera, Rational Design of Metalorganic Complexes for the Deposition of Solid Films: Growth of Metallic Copper with Amidinate Precursors, *Chem. Mater.*, **31**, 1681-1687 (2019).

8. Yunxi Yao, Jonathan Guerrero-Sánchez, Noboru Takeuchi, and Francisco Zaera, Coadsorption of Formic Acid and Hydrazine on Cu(110) Single-Crystal Surfaces, *J. Phys. Chem. C*, **123**, 7584-7593 (2019). INVITED, Hans-Joachim Freund and Joachim Sauer Festschrift

Atomic-scale mechanism of unidirectional oxide growth

Guangwen Zhou
Department of Mechanical Engineering, State University of New York, Binghamton, NY 13902

Program Scope

Acquiring the ability to manipulate the microscopic processes of surface oxidation of metals represents a vast field of basic scientific interest because of its huge technological implications ranging from mitigating corrosion damage to increasing fuel efficiency. This project therefore encompasses an atomic-scale study of the fundamental principles in controlling the surface oxidation from the initial stage of oxygen surface chemisorption to subsequent oxide formation. A combination of *in situ* experiments and theoretical modeling is employed to elucidate the interplay between kinetic and thermodynamic aspects of the surface oxide formation, where the thermodynamics governs the phase stability conditions while kinetic process contributes to the stabilization of the oxide film. Based on the structure and chemistry measurements of the oxide films formed under a wide range of environmental conditions and coordinated density-functional theory and first-principles thermodynamics modeling, three critical issues are addressed, i) tune oxide nucleation and selective oxidation of metallic alloys, ii) tailor oxide growth, structural ordering and polymorph transitions, iii) elucidate the structure dynamics of the oxide/metal interface and its role in guiding the oxide growth and atomic structure evolution. The long-term goal of the research is to establish the fundamental knowledge in oxide thin film design to produce new material systems in a controlled manner.

Recent Progress

More than 70 % of the elements in the periodic table are metals, signifying that a wealth of metal oxides with various properties and functionalities could be fabricated. Particularly, oxide nanowires represent an important class of quasi-one-dimensional (1D) nanomaterials and have received broad interest because of the possibility of tuning their functionalities by size, shape, stoichiometry, phase, atomic termination and defects. Oxidation induced oxide nanowire formation has received considerable attention for its technical simplicity and large-scale growth possibility with high crystalline quality[1-4]. Contrary to its technical simplicity, however, the mechanism underlying the oxide nanowire growth has not been resolved to date although the oxide whisker formation during the oxidation of metals was observed frequently back in 1950s[5-9]. Precise nanocrystal growth with controlled size, shape, and functionalities requires a fundamental knowledge of the growth mechanism, thereby allowing manipulation of the growth process. Growth kinetics plays a key role in controlling the morphology, shape, and facets of nanocrystals. In bulk or ensemble systems, crystal growth proceeds through the nucleation and growth processes and the kinetic understanding is developed around the statistical averaging of these two convoluted processes. Thus, many key aspects of the crystal growth may be buried in these entangled events and cannot be resolved directly. Among the leading challenges is the ability to disentangle these events via visualizing complex growth processes under in situ conditions.

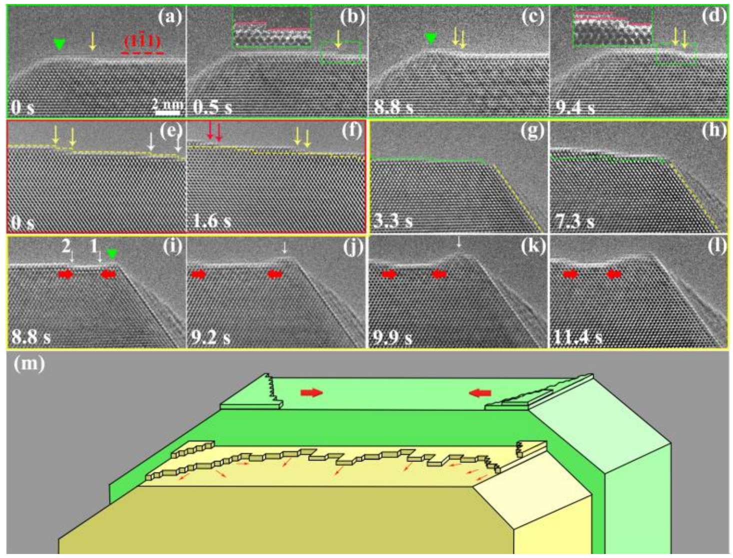

Fig. 1: *In situ* TEM imaging of the unidirectional growth of a bi-crystal at the atomic scale during the oxidation of Cu at 400 °C and in ≈ 0.5 Pa of O_2 flow. (a-d) Time sequence of HRTEM images showing the nucleation of monoatomic layers at the top-left corner of the tip. (e, f) Sequential HRTEM images showing the layer-over-layer, step-flow growth of atomic planes on the tip in the middle region. (g-l) Sequential HRTEM images showing the nucleation of atomic layers in the top-right corner region of the nanowire tip and their lateral propagation via the step-flow growth toward the left side. (m) Schematic illustrations of the nucleation and growth process of atomic layers at the nanowire tip.

Transmission electron microscopy (TEM) has evolved dramatically in recent years and the development of environmental TEM enables disentangling nucleation and growth kinetics through atomically resolved imaging of the dynamic evolution of the local atomic configurations at the vapor-solid and solid-solid interfaces. By employing a dedicated environmental TEM equipped with an image corrector and a differential pumping system, we demonstrate *in situ* TEM visualization of the growth of oxide nanowires during the oxidation of copper, which provides significant new insight into the rather complex kinetic process underlying the directional crystal growth. By introducing reactive gases into the sample region while simultaneously monitoring the structure changes at the atomic scale, we monitor the growth of individual CuO nanowires by directly imaging the nucleation and growth of atomic layers at the growing end of CuO nanowires formed by heating metallic Cu in an O_2 gas flow (Fig. 1). We describe a nanowire growth mechanism, driven by an axial bi-crystal boundary along the length of the nanowire. The self-propagation of atomic steps at the nanowire tip with adatoms supplied through the bi-crystal boundary diffusion enables one-dimensional crystal growth. The observed step-flow propagation of atomic layers from the nanowire tip toward the root direction further confirms the bicrystal boundary diffusion mechanism for the nanowire growth. The dynamic visualization of the oxide growth at the atomic scale demonstrates the remarkable ability of bi-crystal boundaries to direct the unidirectional growth of crystals.

Together with density-functional theory calculations (DFT), we further show that the asymmetry in the corner-crossing barriers promotes the unidirectional oxide growth by hindering the transport of Cu ions from the nanowire tip to the sidewall facets (Fig. 2). We expect broader applicability of our results in manipulating the growth of nanostructured oxides by controlling the bicrystal boundary structure that favors anisotropic diffusion for unidirectional, one-dimensional crystal growth for nanowires or isotropic diffusion for two-dimensional platelet growth.

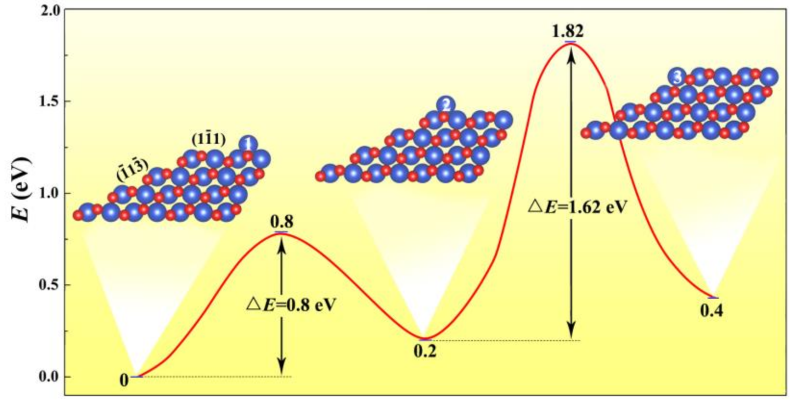

Fig. 2: DFT computed minimum energy path for the diffusion of a Cu adatom on the CuO (1$\bar{1}$1) tip terrace from site 1 to 2 and then to site 3 on the ($\bar{1}$1$\bar{3}$) side wall. Blue and red balls represent Cu and O atoms, respectively.

Future Plans

We will continue the in-situ microscopy and spectroscopy experiments with coordinated modeling to address a number of critical issues including the dynamics of metal/oxide interfaces, charge transfer between surface adsorbates and underlying metal atoms, tuning the surface reaction dynamics by manipulating the surface structure of intermetallic compounds, and the interplay between surface and subsurface in modulating the surface reaction dynamics.

(i) Misfit dislocations are usually generated at heterointerfaces that join dissimilar materials involving lattice mismatch. Such interface defects play a key role in various interfacial phenomena including adhesion, mass transport, and phase transformation. However, directly probing misfit dislocation dynamics has been a major challenge due to the experimental inaccessibility of buried interfaces. We will overcome this issue by employing environmental TEM to observe the dynamic evolution of misfit dislocations during H_2-induced Cu_2O reduction at the epitaxial Cu_2O/Cu interface. Our preliminary in-situ TEM observations at the atomic scale and in real time show that the interfacial reaction proceeds via step flow in a stop-and-go manner, by which the $Cu_2O \rightarrow Cu$ transformation is pinned at the core of misfit dislocations and then become unpinned after the dislocation core climbs to the adjacent lattice plane of the oxide. We will continue the study for potentially manipulating the way that buried interfaces can affect the mass transport and interfacial transformation.

(ii) Measuring the charge transfer between adsorbates and metal surfaces. Charge transfer reactions constitute one of the broadest classes of chemical processes such as photosynthesis, corrosion and catalysis reactions. Oxygen chemisorption on metallic surfaces represents a model reaction for understanding the metal-to-ligand and ligand-to-metal charge transfer processes. Measuring charging transfer is experimentally challenging but important to understanding the nature of chemical bonding. Our preliminary study showed the unique capability using a combination of X-ray photoelectron spectroscopy (XPS) and Auger electron spectroscopy in measuring the electron transfer associated with the chemisorption of oxygen on Cu surfaces. We will continue the study with more systematic measurements along with DFT modeling of the experimental results.

(iii) Intermetallic compounds exhibit unique and tunable surface reactivity towards oxygen, carbon, and hydrogen that is of significant interest to the heterogeneous catalysis community. Using NiAl(100) as a model system, we will study how the control in the surface composition and structure of the intermetallic compounds can enable fine control over reactions that involve C-O, O-H, O-O bond cleavage or formation. In-situ LEEM will be employed to monitor the surface reaction dynamics of NiAl(100) with CO, CO_2, H_2O and O_2 with complementary measurements by LEED on surface structure and AP-XPS on surface chemistry.

(iv) Surface and subsurface are commonly considered as separate entities because of the difference in the bonding environment and are often investigated separately due to the experimental challenges in differentiating the surface and subsurface effects. However, the physical and chemical functionalities of the oxides are often intimately controlled by the interplay between the surface and subsurface states. Detailed insight into such surface-subsurface interactions is needed for better understanding of the fundamental features of the reactivity and for the design of efficient catalysts. Unfortunately, deconvoluting the subsurface and surface effects has been a major challenge, and the subsurface and surface effects are therefore often investigated separately. To overcome this change, we will employ environmental TEM to dynamically resolve the atomic structural changes in both the surface and deeper regions of the CuO lattice in response to hydrogen induced surface reactions. Our preliminary results show that the hydrogen-CuO surface reaction results in structural oscillations in the deeper region of the CuO lattice below the surface via cycles of ordering and disordering of oxygen vacancies in the subsurface. We will continue the study by developing an in-depth understanding of the reaction pathway and atomistic origin underlying the propagation of the reaction dynamics into the deeper region of the bulk.

References:

1. Jiang, X.; Herricks, T.; Xia, Y, *Nano Letters 2*, 1333 (2002).
2. Kolmakov, A.; Moskovits, M., *Annual Review of Materials Research 34*, 151 (2004).
3. Comini, E.; Baratto, C.; Faglia, G.; Ferroni, M.; Vomiero, A.; Sberveglieri, G., *Progress in Materials Science 54*, 1 (2009).
4. Zhang, Q.; Zhang, K.; Xu, D.; Yang, G.; Huang, H.; Nie, F.; Liu, C.; Yang, S., *Progress in Materials Science 60*, 208 (2014).
5. Compton, K.; Mendizza, A.; Arnold, S., *Corrosion 7*, 327 (1951).
6. Takagi, R., *Journal of the Physical Society of Japan 9*, 162 (1954).
7. Takagi, R., *Microscopy* **1955,** *3* (1), 18-20.
8. Arnold, S.; Koonce, S. E., *Journal of Applied Physics 27*, 964 (1956).
9. Takagi, R., *Journal of the Physical Society of Japan 12*, 1212 (1957).

Publications in the Last Two Years

1. Y.G. Zhu, D.X. Wu, Q.Q. Liu, J.T. Sadowski, G.W. Zhou, "*Hydrogen induced clustering of metal atoms in oxygenated metal surfaces*", **Journal of Physical Chemistry C 123**, 11662-11670 (2019)
2. L.F. Zou, C.M. Yang, Y.K. Lei, D. Zakharov, J.M.K. Wiezorek, D. Su, Q.Y. Yin, J. Li, Z.Y. Liu, E.A. Stach, J.C. Yang, L. Qi, G.F. Wang, G.W. Zhou, "*Facilitating dislocation nucleation through atomic segregation*", **Nature Materials 17**, 56-63 (2018)
3. L.L. Luo, M. Su, P. Yan, L.F. Zou, D. Schreiber, D. Baer, Z.H. Zhu, G.W. Zhou, Y. Wang, S. Bruemmer, Z. Xu, C. Wang, "*Atomic origins of water-vapour-promoted alloy oxidation*", **Nature Materials** 17, 514-518 (2018)
4. D.X. Wu, Q.Q. Liu, J. Li, J. Sadowski, G.W. Zhou, "*Visualizing Reversible Two-Dimensional Phase Transitions in Oxygen Chemisorbed Layers*", **Journal of Physical Chemistry C** 122, 28233-28244 (2018)
5. J.Y. Wang, C.R. Li, Y.G. Zhu, J.A. Boscoboinik, G.W. Zhou, "*Insight into the Phase Transformation Pathways of Copper Oxidation: from Oxygen Chemisorption on the Clean Surface to Multi-Layer Bulk Oxide Growth*", **Journal of Physical Chemistry C** 122, 26519-26527 (2018)
6. X.B. Chen, D.X. Wu, L.F. Zou, Q.Y. Yin, H.L. Zhang, D.N. Zakharov, E.A. Stach, G.W. Zhou, "*In situ atomic-scale observation of inhomogeneous oxide reduction*", **Chemical Communications** 54, 7342-7345 (2018)
7. L.F. Zou, W.A. Said, Y. Lei, Z. Liu, J. Li, L. Li, Q. Zhu, D. Zakharov, E.A. Stach, J,C. Yang, G.F. Wang, G.W. Zhou, "*Segregation induced order-disorder transition in Cu(Au) surface alloys*", **Acta Materialia 154**, 220-227 (2018)
8. H.L. Zhang, L.L. Luo, X.B. Chen, G.W. Zhou, "*Tailoring the formation of textured oxide films via primary and secondary nucleation of oxide islands*", **Acta Materialia** 156, 266-274 (2018)
9. L.F. Zou, J. Li, D. Zakharov, E.A. Stach, G.W. Zhou, "*In situ atomic-scale imaging of the metal/oxide interfacial transformation*", **Nature Communications 8**, 307 (2017)
10. L.F. Zou, J. Li, D. Zakharov, W.A. A. Saidi, E.A. Stach, G.W. Zhou, "*Atomically visualizing elemental segregation induced surface restructuring*", **Journal of Physical Chemistry Letters** 8, 6035-6040 (2017)
11. D.X. Wu, J. Li, G.W. Zhou, "*Oxygen adsorption at heterophase boundaries of the oxygenated Cu(110)*", **Surface Science 666**, 28-43 (2017)
12. H.L. Qin, X.D. Chen, J. Li, P. Sutter, G.W. Zhou, "*Atomic-step-induced local nonequilibrium effects on surface oxidation*", **Journal of Physical Chemistry C 121**, 22846-22853 (2017)

This page is intentionally blank.

Author Index

This page is intentionally blank.

This page is intentionally blank.

Participant List

This page is intentionally blank.

Name	Organization	Email Address
Archer, Lynden	Cornell University	laa25@cornell.edu
Arnold, Michael	University of Wisconsin, Madison	michael.arnold@wisc.edu
Auerbach, Scott	University of Massachusetts, Amherst	auerbach@umass.edu
Bent, Stacey	Stanford University	sbent@stanford.edu
Bozovic, Ivan	Brookhaven National Laboratory	bozovic@bnl.gov
Cavallo, Francesca	University of New Mexico	fcavallo@unm.edu
Chambers, Scott	Pacific Northwest National Laboratory	sa.chambers@pnnl.gov
Chen, Xi	Oak Ridge National Laboratory	chenx@ornl.gov
Clancy, Paulette	Johns Hopkins University	pclancy3@jhu.edu
Crowell, Paul	University of Minnesota	crowell@umn.edu
De Yoreo, Jim	Pacific Northwest National Laboratory	James.deyoreo@pnnl.gov
Dierolf, Volkmar	Lehigh University	vod2@lehigh.edu
Du, Yingge	Pacific Northwest National Laboratory	yingge.du@pnnl.gov
Dudney, Nancy	Oak Ridge National Laboratory	dudneynj@ornl.gov
Ediger, Mark	University of Wisconsin, Madison	ediger@chem.wisc.edu
Eom, Chang-Beom	University of Wisconsin, Madison	eom@engr.wisc.edu
Falk, Michael	Johns Hopkins University	mfalk@jhu.edu
Fan, Wei	University of Massachusetts, Amherst	wfan@ecs.umass.edu
Fedorov, Andrei	Georgia Institute of Technology	agf@gatech.edu
Fichthorn, Kristen	Pennsylvania State University	fichthorn@psu.edu
Geohegan, David	Oak Ridge National Laboratory	geohegandb@ornl.gov
Gersten, Bonnie	US Department of Energy	bonnie.gersten@science.doe.gov
Hanrath, Tobias	Cornell University	th358@cornell.edu
Jain, Himanshu	Lehigh University	h.jain@lehigh.edu

Jasinski, Jacek	University of Louisville	jacek.jasinski@louisville.edu
Kaspar, Tiffany	Pacific Northwest National Laboratory	tiffany.kaspar@pnnl.gov
Kramer, Matthew	AMES Laboratory	matthewjosephkramer@gmail.com
Kumar, Sanat	Columbia University	sk2794@columbia.edu
Lagally, Max	University of Wisconsin, Madison	lagally@engr.wisc.edu
Lang, Maik	University of Tennessee	mlang2@utk.edu
Li, Donsheng	Pacific Northwest National Laboratory	dongsheng.li2@pnnl.gov
Liu, Feng	University of Utah	fliu@eng.utah.edu
Liu, Jun	Pacific Northwest National Laboratory	jun.liu@pnnl.gov
Mao, Zhiqiang	Pennsylvania State University	zim1@psu.edu
Navrotsky, Alexandra	University of California, Davis	anavrotsky@ucdavis.edu
Ni, Ni	University of California, Los Angeles	nini@physics.ucla.edu
Olevsky, Eugene	San Diego State University	eolevsky@sdsu.edu
Palmstrom, Chris	University of California, Santa Barbara	cpalmstrom@ece.ucsb.edu
Pribiag, Vlad	University of Minnesota	vpribiag@umn.edu
Schadler Feist, Linda	University of Vermont	Linda.Schadler@uvm.edu
Schlom, Darrell	Cornell University	schlom@cornell.edu
Sennett, Michael	US Department of Energy	michael.sennett@science.doe.gov
Shahani, Ashwin	University of Michigan	shahani@umich.edu
Shoemaker, Daniel	University of Illinois	spshoema@illinois.edu
Sun, Jianwei	Tulane University	jsun@tulane.edu
Sushko, Peter	Pacific Northwest National Laboratory	peter.sushko@pnnl.gov
Sushko, Maria	Pacific Northwest National Laboratory	maria.sushko@pnnl.gov
Sutter, Eli	University of Nebraska, Lincoln	esutter@unl.edu
Sutter, Peter	University of Nebraska, Lincoln	psutter@unl.edu

Switzer, Jay	Missouri University	jswitzer@mst.edu
Tang, Ming	Rice University	mt20@rice.edu
Tringides, Michael	Iowa State University/Ames Laboratory	mctringi@iastate.edu
Wei, Jiang	Tulane University	jwei1@tulane.edu
Weihs, Timothy	Johns Hopkins University	weihs@jhu.edu
Xiao, Kai	Oak Ridge National Laboratory	xiaok@ornl.gov
Yakobson, Boris	Rice University	biy@rice.edu
Yu, Ming	University of Louisville	m0yu0001@louisville.edu
Zaera, Francisco	University of California	zaera@ucr.edu
Zangari, Giovanni	University of Virginia	gz3e@virginia.edu
Zhou, Guangwen	State University of New York, Binghamton	gzhou@binghamton.edu